[redacted]

Westinghouse Non-Proprietary Class 3

[redacted]

Westinghouse Energy Systems

Westinghouse Non-Proprietary Class 3

[redacted]

Westinghouse Energy Systems

WCAP 14293

AP600
LOW-PRESSURE INTEGRAL SYSTEMS TEST AT OREGON STATE UNIVERSITY TEST ANALYSIS REPORT

JULY 1995

TABLE OF CONTENTS

TABLE OF CONTENTS (Continued)

TABLE OF CONTENTS (Continued)

TABLE OF CONTENTS (Continued)

NOTE: Shaded sections are not included in this revision of the report. They will be included in the next revision.

LIST OF TABLES

LIST OF TABLES (Continued)

LIST OF FIGURES

ACRONYMS

ADS	automatic depressurization system
APEX	advanced plant experiment facility at OSU
ASME	American Society of Mechanical Engineers
BAMS	break and ADS measurement system
CCT	condensate collection tank
CD ROM	compact disk read-only memory
CMT	core makeup tank
CRP	condensate return pump
CVS	chemical and volume control system
DAS	data acquisition system
DEG	double-ended guillotine
DP	differential pressure transmitter
DVI	direct vessel injection
FMM	magnetic flow meter
GSM	general scaling methodology
H2TS	hierarchical two-tiered scaling analysis
HPS	heated phase switch
HX	heat exchanger
IRWST	in-containment refueling water storage tank
LAN	local area network
LCS	lower containment sump
LDP	level differential pressure
LOCA	loss-of-coolant accident
LRGMS	large main steam
MSS	main steam system
NSS	nonsafety systems
OSU	Oregon State University
PC	personal computer
PIRT	phenomena identification ranking table
PPIRT	plausible phenomena identification ranking table
PQP	project quality plan
PRHR	passive residual heat removal
PT	pressure transducer
PWR	pressurized water reactor
PXS	passive core cooling system
RCP	reactor coolant pump
RCS	reactor coolant system
RNS	normal residual heat removal system
RV	reactor vessel
SASM	severe accident scaling methodology
SBLOCA	small-break loss-of-coolant accident
SCR	silicon-controlled rectifier
SG	steam generator
SGS	steam generator system
VI	virtual instrumentation

ACKNOWLEDGMENTS

The authors express their appreciation for the extensive discussions and inputs obtained from the key designer of the test facility, Mr. L.K. Lau, and the developer of the scaling analyses, Prof. J.N. Reyes.

SUMMARY

The Oregon State University (OSU) test facility is a 1/4-height, reduced-pressure simulation of the AP600 nuclear steam supply system and the AP600 passive safety features. A series of design-basis events were simulated at OSU to obtain data for verification and validation of the computer models used for the safety analysis of AP600.

The purpose of this report is to describe the analysis of the test data, to describe the thermal-hydraulic behavior of the test facility, to identify the phenomena observed in the tests and the relationship to the phenomena identification ranking table (PIRT), and to demonstrate, through mass and energy balances, the applicability of the OSU tests for computer model verification and validation.

1.0 INTRODUCTION

This report describes the analysis of the Oregon State University (OSU) test data that will be used to validate the AP600 safety analysis computer codes. The test data report for the OSU tests is given in *AP600 Low-Pressure Integral Systems Test at Oregon State University, Final Data Report,* WCAP-14252[1] which describes the test facility, the valid instrumentation, and the test facility performance for the different experiments. This report will examine, in additional detail, the thermal-hydraulic behavior of the test facility and the phenomenon observed in the experiments, as identified in the phenomena identification ranking table (PIRT), Table 1.3-1. This analysis will aid the computer code validation activities.

The OSU test facility is a 1/4-height, reduced-pressure model of the AP600 and its passive emergency core cooling systems. The test facility includes the reactor coolant system (RCS), steam generators, passive core cooling system (PXS), automatic depressurization system (ADS), and nonsafety injection systems, such as normal residual heat removal system (RNS) and chemical and volume control system (CVS), in the Radiation Center at the University in Corvallis, Oregon. The test facility, fabricated completely from austenitic stainless steel designed for normal operation at 450°F and 400 psig, was scaled using the hierarchical two-tiered scaling analysis (H2TS) method developed by the U.S. Nuclear Regulatory Commission (NRC). Simulated piping breaks were tested in the hot leg, cold leg, pressure balance line between the cold leg and the core makeup tank (CMT), and the direct vessel injection (DVI) line. Decay heat that scaled to 3 percent of the full power (about 2 minutes after shutdown) was supplied by electrically heated rods in the reactor vessel. Simulated accidents were programmed by the control system to proceed automatically. About 850 data channels were recorded by the data acquisition system (DAS) and downloaded to compact disks for subsequent data reduction and plotting. The OSU test facility was specifically designed to examine the small-break loss-of-coolant accident (SBLOCA) periods as well as the long-term cooling aspects of the AP600 passive safety systems.

1.1 Background

AP600 is a 600 MWe Westinghouse advanced reactor designed to enhance plant safety with accident mitigation features that, once actuated, depend only on natural forces, such as gravity and natural circulation, to perform all required safety functions.

The AP600 primary system is a two-loop design. Each loop contains one hot leg, two cold legs, and one steam generator (SG) with two canned motor reactor coolant pumps (RCPs) attached directly to the SG outlet channel head. The passive safety systems comprise the following:

- Two full-pressure core makeup tanks (CMTs) that provide borated makeup water to the primary system at any pressure.
- Two accumulators that provide borated water to the reactor vessel if the primary pressure $\leq$ 700 psia.
- A passive residual heat removal (PRHR) heat exchanger (HX), comprised of a C-shaped tube bundle submerged in the in-containment refueling water storage tank (IRWST), that can remove heat from the primary system at any pressure.
- The automatic depressurization system (ADS), which is comprised of a set of valves connected to the pressurizer steam space and the two hot legs. The valves connected to the pressurizer vent to the IRWST through a sparger. The valves connected to the hot leg vent to the containment. These valves are opened sequentially to provide controlled depressurization of the primary system.
- An IRWST that provides a large source of core cooling water, which drains by gravity after the ADS has actuated.
- A passive containment cooling system (PCS) that utilizes the AP600 steel containment shell to transfer heat to the environment (ultimate heat sink). The PCS was not directly included in the OSU experiments, however, the containment circulation of condensed liquid back to the IRWST or sump was simulated for selective tests.

In reviews of the AP600, the U.S. Nuclear Regulatory Commission (NRC) identified several concerns regarding the performance of the AP600 passive safety systems. Those concerns include the following:

- Possible high-pressure passive safety system interactions that could retard cooling of the core.
- Possible active system/passive system interaction that could retard cooling of the core.

- The dependence on small temperature differences resulting in small density differences, which then are responsible for driving heads for recirculating flows.

- The effects of code accuracy in predicting long transients in which the driving heads for flow in the system are small.

- The behavior of the primary system and the containment during the long-term cooling phase of the transient; specifically, the reduced driving heads for flow from the sump and the resulting pressure drops in the primary system that could reduce venting and increase steam binding of the system at low pressure.

The OSU test facility was specifically designed to model the AP600 transients so that the NRC concerns could be addressed.

The OSU test facility is a facility constructed specifically to investigate the AP600 passive system characteristics. The facility design models the detail of the AP600 geometry, including the primary system, pipe routings, and layout for the passive safety systems. The primary system consists of one hot leg and two cold legs, with two active pumps and an SG for each of the two loops. There are two CMTs, each connected to a cold leg of one primary loop. The pressurizer is connected to the other primary loop, as in the AP600 plant design. Gas-driven accumulators are connected to the direct vessel injection (DVI) lines. The discharge lines from a CMT and one of the two IRWST and reactor sump lines are connected to each DVI line. The two independent lines of each stage of ADS 1, 2, and 3 are modeled by one line containing an orifice. Two-phase flow from ADS 1-3 is separated in a swirl-vane separator, and liquid and vapor flows are measured to obtain the total flow rate. The separated flow streams are then recombined and discharged into the IRWST through a sparger. Thus, mass and energy flow from the ADS into the IRWST are preserved.

The period for simulation included not only IRWST injection, but also IRWST draining and sump injection to simulate the long-term cooling mode of the AP600. The time scale for the OSU test facility is about one-half; that is, the sequence of events occurred about twice as fast in the test facility as in the AP600.

To model the long-term cooling aspects of the transients, two-phase flow from the break was separated in a swirl-vane separator, and the liquid and vapor portions of the total flow were measured. The liquid fraction of the flow was discharged to the reactor sump, as in the AP600 plant. The vapor was discharged to the atmosphere, and the equivalent liquid flow was capable of being added to the IRWST and sump to simulate the condensate return from passive containment. A similar approach was also used for the two ADS-4 valves on the hot legs. The two-phase flow was separated in a swirl-vane separator, the two stream flows were measured, the liquid phase was discharged into the reactor sump while the vapor phase was discharged to the atmosphere, and the liquid equivalent was capable of being added to the IRWST and sump. The IRWST, reactor sump, and separators could be

pressurized to simulate containment pressurization following a postulated loss-of-coolant accident (LOCA).

Prior to the performance of matrix tests, and to provide benchmark data on facility behavior for the computer code analysis, a series of cold, low-pressure and hot, high-pressure pre-operational tests were performed to characterize the OSU facility, to demonstrate proper operation of the facility, to ensure that piping/component parameters properly matched the AP600 plant. The matrix tests discussed in Section 3 were developed to examine the AP600 passive safety system performance in mitigating the effects of design-basis events (DBEs). Events that were evaluated include LOCAs ranging from 1-in. diameter equivalent to the double-ended guillotine (DEG) break of an 8-in. DVI line. A large-break LOCA was also simulated.

1.2 Test Objectives

The OSU facility was designed and constructed to specifically examine the long-term cooling performance of the AP600 passive safety systems and their interaction with the nonsafety related active systems. The range and types of tests investigated in the OSU test facility covered the ranges and phenomena expected for the SBLOCA and long-term cooling transients. The data from the experiments is to be used to validate the safety analysis computer codes used to analyze the AP600.

To cover the range of conditions for the long-term cooling transient, tests were performed modeling as large a break as possible to rapidly depressurize the facility so that decay power would be at a high value when long-term cooling began. Also, experiments were performed with conditions that would result in a hot IRWST and sump when the primary system transitioned into long-term cooling. Both conditions maximized the production of core steam to be vented through the ADS-4 valves to maintain sump injection.

A detailed scaling analysis was developed for the OSU experiments to relate the scaled-pressure and reduced-height facility to the AP600 plant. The *Low-Pressure Integral Systems Test, Facility Scaling Report,* WCAP-14270[2] specified the facility dimensions, resulting flow areas for the breaks, and pressure drops needed to preserve the phenomena expected for the AP600 SBLOCA and long-term cooling transients. The scaling study provides the bridge to relate the *AP600 SPES-2 Test Analysis Report,* WCAP-14254[3] to the similar OSU experiments, and to relate the OSU experiments to the AP600 design.

The following are the specific test objectives of the OSU program:

- To provide data to establish the pedigree of the passive safety system for long-term cooling.
- To provide overlap with the full-pressure, full-height SPES-2 tests[3] so that an assessment of the scaling effects of the OSU tests could be made. Therefore, similar break locations and sizes (scaled) were examined in both facilities and comparisons were made.
- To use the facility to cover the range of phenomena expected for the AP600 LOCA in addition to the long-term cooling period.

1.3 Important SBLOCA and Long-Term Cooling Phenomena

The OSU test matrix was developed to simulate the thermal-hydraulic phenomena expected during SB-LOCA and long-term cooling transients.

1.3.1 SBLOCA

The SBLOCA can be divided into the following four periods that characterize thermal-hydraulic phenomena:

- Blowdown - Initial depressurization from plant operating pressure to the SG secondary-side pressure, after which pressure stabilizes.

- Natural Circulation - The period from the stabilization of primary pressure with secondary-side pressure until ADS-1 is activated. The primary reactor system is cooled by different modes of heat transfer. Each cooling mode is dependent on the system mass inventory. As the mass is lost through the break, cooling proceeds from single-phase natural circulation, to two-phase natural circulation, to reflux condensation cooling.

- ADS 1-4 Blowdown - Once the CMTs drain to their setpoint, the ADS-1 valve opens and the reactor system is depressurized through the ADS flow path in addition to the break. As the CMT continues to drain into the reactor vessel, additional valves are opened on the pressurizer and RCS hot legs to enhance blowdown of the system.

- IRWST Injection - Stable injection from the IRWST indicates the complete depressurization of the primary system down to containment pressure. Also, injection from the IRWST indicates the end of the small-break transient and the beginning of the long-term cooling transient.

Using these different periods, the important thermal-hydraulic phenomena have been identified and ranked in a PIRT (Table 1.3-1). This PIRT has been updated from that which was provided in the *Applicability of the NOTRUMP Computer Code to the AP600 SSAR Small-Break LOCA Analysis,* WCAP-14206.[4] Individual phenomena were emphasized for the ADS system, and other components have been added to the PIRT. The phenomena for each identified phase of the small-break transient relative to the AP600 small-break performance is discussed in the following paragraphs.

The reactor is assumed to be operating at normal full-power, steady-state conditions at the start of the blowdown. The break opens at time zero, and pressurizer pressure begins to fall as mass is lost out the break. This depressurization is largely defined by critical flow through the break. With the break located at the bottom of the cold leg, a mixture flow exits the break for the majority of the transient, since the mixture level stays high in the reactor vessel. Pressurizer pressure falls below the safety signal setpoint, causing the reactor to trip. The safety systems actuation signal (S) follows and results in the opening of the CMT isolation valves. Once the residual fissions decrease, core power is defined

by the decay heat model. The RCPs trip after a short delay. Pump performance, both before and after the trip, is modeled according to the pump characteristic curves. After the pumps coast down, the primary reactor coolant system (RCS) is cooled by natural circulation, with energy removed from the primary system by the SGs via their safety valves and the break. Stored energy from the metal in the reactor vessel and pressurizer is transferred to the coolant. These phenomena are essentially the same for AP600 as for conventional pressurized water reactors (PWRs). Liquid in the upper plenum and upper head (depending on the temperature) will flash, and the upper head will start to drain.

Blowdown phase phenomena unique to the AP600 are those associated with CMT delivery. Once the CMT isolation valves open, the CMT injects borated water by gravity-driven recirculation into the RCS through the DVI lines. The CMT injected volume is replaced with hot liquid via the cold-leg balance line (CLBL); this hot liquid collects at the top of the CMT. The downcomer fluid stays subcooled through the initial blowdown phase.

For the natural circulation phase of the transient, the primary system exists in a quasi-steady-state condition with the secondary side, with decay energy being removed by the SG secondary side as the primary system drains. The SG in the AP600 plays a more limited role in the natural circulation cooling phase than for conventional plants because the generators drain relatively early in the transient. Since PRHR is activated on an S signal during a SBLOCA, the IRWST becomes the primary heat sink for the RCS early in the transient. The PRHR will remove energy from the primary system, causing it to depressurize. The SG secondary side becomes a potential heat source once PRHR reduces primary pressure to that of the secondary side. PRHR is ranked high in the PIRT since it becomes a significant heat removal path, particularly after primary pressure is less than SG pressure. Therefore, condensation in the SG tubes during a SBLOCA ceases early. The requirements for detailed models for condensation heat transfer in the SG tubes are not as significant for AP600 as for a conventional plant. The importance shifts to the PRHR performance and the IRWST heat-sink behavior. The reverse heat transfer path due to secondary heating of the RCS primary system continues until the SGs drain. The CMT continues to deliver in the recirculation mode, but eventually a vapor region forms at the top of the CMT volume, and CMT draindown begins. As the CMT drains while injecting, its level falls to the ADS actuation setpoint, initiating the third phase of the AP600 SBLOCA transient, ADS blowdown. The downcomer and lower plenum are ranked as medium importance in the PIRT since they provide the driving head for natural circulation.

The ADS blowdown phase continues through the actuation of ADS-1, ADS-2, ADS-3, and ADS-4 as the primary system depressurizes to approximately the containment pressure. The PIRT relates AP600-specific components, events, and phenomena that occur during automatic depressurization of the RCS to achieve water injection by gravity from the IRWST. Since ADS-1 creates an opening at the top of the pressurizer, the pressurizer two-phase fluid level increases markedly. Pressurizer tank level and surge-line phenomena are significant factors in the depressurization behavior following ADS actuation. Flashing of fluid in the RCS occurs due to the depressurization caused by the ADS.

Following actuation of ADS-1, the next two stages of ADS, ADS-2 and ADS-3, activate via timers. Once the pressure drops below 700 psia, accumulator injection begins reducing flow delivered from the CMT. CMT flow may even be stopped temporarily due to pressurization of the DVI line by the accumulator. The CMT drain rate, and DVI line and CLBL flow characteristics are significant because ADS-4 actuation is based on the CMT liquid level decreasing below a low-low setpoint value. Condensation of vapor on the CMT walls is of somewhat less importance since recirculation results in heating of the CMT.

Critical flow through the ADS stages is the major factor in determining when the RCS has depressurized to the extent that the gravity injection of water from the IRWST can begin. Fourth-stage ADS performance is affected by the nature of flow in the hot legs. Successful operation of the ADS leads to the IRWST injection cooling phase of the AP600 SBLOCA event.

The final stage of the SBLOCA is IRWST injection. At this point, the primary system is depressurized, and the transient continues into the long-term cooling phase of the accident. By the time of IRWST injection, the CMT is either completely or very nearly empty. CMT phenomena have, therefore, become relatively unimportant, whereas the IRWST gravity-drain rate through the DVI line is important. The hot-leg flow phenomena, together with ADS-4 flow, is also important. Moreover, the break critical flow behavior is now less important than before because all ADS flow paths are open, providing a large area through which to vent steam. Keeping the core covered with liquid or a two-phase mixture becomes a function of the decay heat level and IRWST flow.

The impact of noncondensable gas released when the accumulators empty of liquid during AP600 SBLOCAs is shown to be of low importance in the SBLOCA PIRT because of the large number of vent paths for the gas.

1.3.2 Long-Term Cooling Transient

Long-term cooling is a post-accident phase defined as the period after IRWST injection begins until the plant is recovered. The AP600 passive safety systems are designed to provide post-accident core cooling indefinitely. Steam generated in the core is vented to containment. The steam condenses on the containment shell, and the condensate is directed into the IRWST and sump where it flows into the core through the DVI line. The closed-circuit reflux condensation process insures adequate cooling inventory to maintain the core in a coolable state indefinitely.

When the reactor system is in the long-term cooling mode, the primary system is drained to the hot-leg level. With the SG primary side being filled with stagnate steam, the pressurizer and upper head of the reactor vessel are empty. The CMTs and accumulators have already injected, and the PRHR may or may not be active, depending on whether the IRWST level covers the HX and noncondensable gas is present in the PRHR tubes. Initial injection flow to the vessel comes from the IRWST as long as the IRWST head is larger than the containment sump. If the IRWST has drained to the sump level, there could be injection from both the sump and the IRWST until the IRWST has drained. Flow from

the sump or IRWST is directed to the reactor vessel through the DVI line into the downcomer. The delivery of injection flow is gravity-driven from the elevated sump into the reactor vessel. The driving force for core cooling is the level in the reactor downcomer which provides the elevation head to drive flow through the core and out the hot leg. This gravity-flooding behavior of the core is no different than that in operating plants with the exception that injection flow is driven by a pump and not gravity as in the AP600. The inclusion of a large vent path on the top of the hot leg through the ADS-4 valves provides a low-pressure drop vent path so that ample flow through the core can occur. In operating plants, the downcomer must drive core flow through the SG primary side, superheating the primary fluid, and creating a backpressure that reduces core inlet flow (steam binding). This situation is avoided in the AP600 by using the large vent areas on the top of the hot legs so that very little, if any, flow goes through the SGs. Also, once the IRWST drains, the ADS 1-3 vent path is also available to vent core-generated steam.

Since the primary system is at containment pressure, only the driving heads in the downcomer and the two-phase pressure drop in the core, hot leg, and ADS-4 determine the resulting core flow. If the PIRT is examined, only those items related to the core, downcomer, upper plenum, hot leg, and ADS-4 are highly ranked. While most items indicated on the PIRT for long-term cooling are directly measured in the experiments, the hot-leg flow regime must be inferred from the data. Using the OSU data, the importance of these phenomena can be assessed and used for guidance in validating the AP600 safety analysis computer codes for the long-term cooling period.

TABLE 1.3-1
PIRT FOR AP600 SBLOCA AND LONG-TERM COOLING

Component Phenomenon	Blowdown	Natural Circulation	ADS Blowdown	IRWST Injection Cooling	LCS Recirculation Cooling
Break					
Critical flow	H	H	H	M	L
Subsonic flow	N/A	N/A	N/A	M	L
ADS 1-3					
Critical flow	H (inadvertent ADS)(1)	H (inadvertent ADS)(1)	H	M	L
Two-phase pressure drop	N/A(1)	N/A(1)	H	M	L
Valve loss coefficients	N/A(1)	N/A(1)	H	M	L
Single-phase pressure drop	N/A	N/A	N/A	L	L
Vessel/core					
Decay heat	H	H	H	H	H
Forced convection	M	N/A	N/A	N/A	N/A
Flashing	M	N/A	M	L	N/A
Wall stored energy	M	N/A	M	M	M
Natural circulation flow and heat transfer	M	M	M	M	M
Mixture level mass inventory	H	H	H	H	H
RCP					
RCP performance	M	N/A	N/A	N/A	N/A
Pressurizer					
Pressurizer fluid level	M	M	M	L	L
Wall stored heat	M	M	M	L	L
Pressurizer surge line					
Pressure drop/flow regime	L	L	M	L	L
Downcomer/lower plenum	L	M	M	M	M
Upper head/upper plenum	L	M	M	M	H
Cold legs	L	M	M	M	L

Note:
(1) The ADS is not normally open during these phases unless the transient is an inadvertent ADS; for that case, the ADS phenomena would be ranked as high (H).

TABLE 1.3-1 (Continued)
FIRT FOR AP600 SBLOCA AND LONG-TERM COOLING

Component Phenomenon	Blowdown	Natural Circulation	ADS Blowdown	IRWST Injection Cooling	LCS Recirculation Cooling
Steam generator					
2φ - Natural circulation	L	M	L	L	L
Steam generator heat transfer	L	M	L	L	L
Secondary conditions	L	M	L	L	L
Hot leg					
Flow pattern transition	L	H	H	H	H
ADS 1-4					
Critical flow	N/A	N/A	H	H	H (Stage 4)
Subsonic flow	N/A	N/A	L	H	H (Stage 4)
CMT					
Recirculation injection	M	M	L	L	L
Gravity draining injection	N/A	M	H	L	L
Vapor condensation rate	N/A	M	M	L	L
CMT balance lines					
Pressure drop	M	H	H	L	L
Flow composition	M	H	H	L	L
Accumulators					
Injection flow rate	N/A	M	H	N/A	N/A
Noncondensable gas entrainment	N/A	N/A	L	L	L
IRWST					
Gravity draining injection	N/A	N/A	N/A	H	H
Vapor condensation rate	N/A	N/A	M	L	L
DVI Line					
Pressure drop	M	M	M	M	M
PRHR					
Natural circulation flow and heat transfer	L	H	M	L	L
Sump					
Gravity draining injection					H
Level					H
Temperature					H

1.4 Test Facility Scaling

A detailed component and system scaling analysis was performed for the OSU test facility and is given in the *Facility Scaling Report.*[2] The results of the scaling analysis were used to specify the design of the facility. The primary objective of the scaling analysis was to design a working scale model capable of producing the same types of flow behavior encountered in the AP600 during an SBLOCA, IRWST injection, and long-term cooling.

Various scaling techniques can be applied to the design of a small-scale thermal-hydraulic test facility. The traditional approach has been to use "power to fluid volume" (P/V) scaling. This scaling approach has been successfully applied in various studies such as the *FLECHT SEASET Program Final Report,* NUREG/CR-4167[5] The optimum condition for this scaling approach occurs when the scale model implements the same working fluid as the full-scale system, is built at full height using similar materials, and is operated at full pressure. This generally results in constructing a very tall and thin scale model. Unfortunately, the hydrodynamic behavior in the plenum regions may not be fully represented in the full-height model. A reduced-height, power-to-volume scaled model gives a better representation of multidimensional effects in the plenum and downcomer regions.[6]

The hierarchical two-tiered scaling analysis (H2TS) method has been used to develop the similarity criteria necessary to scale the systems and processes of importance to AP600 integral system and long-term cooling. The H2TS method, developed by the NRC, is fully described in Appendix D of *An Integrated Structure and Scaling Methodology for Severe Accident Technical Issue Resolution,* NUREG/CR-5809,[7] and is referred to as the SASM methodology. There are four basic elements of the H2TS analysis method. The first element consists of system decomposition. Each system can be subdivided into interacting subsystems (or modules), further subdivided into interacting constituents (materials), and further subdivided into interacting phases (liquid, vapor, or solid). Each phase can be characterized by one or more geometric configurations, and each geometric configuration can be described by three field equations (mass, energy, and momentum conservation). Each field equation can be characterized by several processes. This is depicted in Figure 1.4-1.

After identifying the system of interest and decomposing it as in Figure 1.4-1, the next step is to identify the scaling level at which the similarity criteria should be developed. This is determined by the phenomena being considered.

For example, if the phenomenon being considered involves mass, momentum, or energy transport between materials such as water and solid particles, then the scaling analysis should be performed at the constituent level. If the phenomenon of interest involves mass, momentum, or energy transport between vapor and liquid, then the scaling analysis should be performed at the phase level. Therefore, identifying the scaling level will depend on the phenomenon being addressed. Table 1.4-1 presents the system hierarchy implemented in the *Facility Scaling Report.*[2]

Thermal-hydraulic phenomena involving integral system interactions, such as primary system depressurization or loop natural circulation, are examined at the "system" level. Thermal-hydraulic phenomena — such as PRHR decay heat removal, CMT, accumulator, and IRWST passive safety injection, automatic depressurization and LCS recirculation cooling — are examined at the "subsystem" level. Thermal-hydraulic phenomena important to individual components—such as the reactor core, pressurizer, SGs, hot legs, cold legs, coolant pumps, and interconnecting piping—are examined at the "module" level. Specific interaction between the steam-liquid mixture and the stainless steel structure are examined at the "constituent" level.

The OSU scaling study presents scaling analysis performed at different levels. The thermal-hydraulic phenomena of interest, the system level at which the analysis was performed, the control volume for the analysis (i.e., the geometric configuration), the applicable balance equations, and the processes important to the thermal-hydraulic phenomena of interest are discussed and analyzed for the simulated reactor system as well as the major components in the system.

The third element of the H2TS method requires the performance of a "top-down" (system) scaling analysis. The top-down scaling analysis examined the synergistic effects on the system caused by complex interactions between the constituents deemed important by the plausible phenomena identification ranking table (PPIRT). This has been modified as discussed in Section 1.3, and a revised PIRT is presented in Table 1.3-1. The top-down scaling approach used the conservation equations at a given scaling level to obtain characteristic time ratios and similarity criteria, and identified important processes to be addressed in the bottom-up scaling analysis.

The fourth element of the H2TS method required the performance of a "bottom-up" (process) scaling analysis which developed the similarity criteria for specific processes such as flow-pattern transitions, and geometry- and flow-dependent heat transfer. The focus of the bottom-up scaling analysis was to develop similarity criteria to scale individual processes of importance to system behavior identified by the PIRT and develop the design information for the test facility.

The basic objective of the H2TS method was to develop sets of characteristic time ratios for the transfer processes of interest. This can be done by writing the control volume balance equations for each constituent "k" as follows:

$$\frac{dV_k\psi_k}{dt} = \Delta[Q_k\psi_k] \pm \Sigma j_{km} A_{km} \qquad 1.4\text{-}1$$

Defining $\Delta[Q_k\psi_k]$:

$$\Delta[Q_k\psi_k] = [Q_k\psi_k]_{in} - [Q_k\psi_k]_{out} \qquad 1.4\text{-}2$$

where:

ψ_k	=	Conserved property; ρ, ρu, or $\rho\varepsilon$ (mass, momentum, or energy per unit volume)
V_k	=	Control volume
Q_k	=	Volumetric flow rate
j_{km}	=	Flux of property ψ_k transferred from constituent k to n across the transfer area A_{kn}

ψ_k transferred from constituent "k" to "m" across the transfer area A_{km}. Hence, $\Delta[Q_k\psi_k]$ represents the usual mass momentum or energy convection terms, and $\Sigma j_{km}A_{km}$ represents transport process terms such as condensation.

Equation 1.4-1 can be put in dimensionless form by specifying the following dimensionless groups in terms of the constant initial and boundary conditions:

$$V_k^* = \frac{V_k}{V_{k,0}},\ \psi_k^* = \frac{\psi_k}{\psi_{k,0}},\ Q_k^* = \frac{Q_k}{Q_{k,0}},\ j_{km}^* = \frac{j_{km}}{j_{km,0}},\ A_{km}^* = \frac{A_{km}}{A_{km,0}} \qquad 1.4\text{-}3$$

Substituting these groups into Equation 1.4-1 yields:

$$V_{k,0}\psi_{k,0}\frac{dV_k^*\psi_k^*}{dt} = Q_{k,0}\psi_{k,0}\Delta[Q_k^*\psi_k^*] \pm \Sigma(j_{km,0}A_{km,0})j_{km}^*A_{km}^* \qquad 1.4\text{-}4$$

Dividing both sides of this equation by $Q_{k,0}\ \psi_{k,0}$ yields:

$$\tau_k\frac{dV_k^*\psi_k^*}{dt}\Delta[Q_k^*\psi_k^*] \pm \Sigma\prod_{km} j_{km}^*A_{km}^* \qquad 1.4\text{-}5$$

where the residence time of constituent "k" is:

$$\tau_k = \frac{V_{k,0}}{Q_{k,0}} \qquad 1.4\text{-}6$$

and the characteristic time ratio for a transfer process between constituents "k" and "m" is given by:

$$\Pi_{km} = \frac{j_{km,0}A_{km,0}}{Q_{k,0}\psi_{k,0}} \qquad 1.4\text{-}7$$

It is the Π (pi) ratio of the proposed test facility to the plant that are of interest. Important processes can be replicated in the model by fixing the variables that control the process, such as geometry, so that the following criteria is met:

$$\frac{\Pi m}{\Pi p} = 1 \qquad 1.4\text{-}8$$

A deviation from unity indicates the possible deviation of the proposed test design from the plant.

The transients modeled at the OSU facility were SBLOCAs which transition into the long-term cooling mode for the AP600 design. Since the operating pressure for the OSU facility was chosen as 400 psia, a scaling approach was needed to develop the test design so that the most important parameters identified in the PIRT would be preserved.

The small-break scenario shown in Figure 1.4-2 indicates the five periods of interest. After the initial blowdown phase, there are extended periods of single- and two-phase natural circulation as the reactor system drains. Eventually, the ADS valves will open, creating a larger break, which will depressurize the primary system down to containment pressure. This is the ADS operational period. Once IRWST injection begins, there will be a two-phase natural circulation cooling mode with injection from the IRWST and venting from the ADS-4 valves located on the hot legs. This is the IRWST injection period. The long-term cooling period begins as IRWST and sump injection continues for extended times. The long-term cooling mode is with injection from the IRWST or sump and venting through the ADS fourth stage valves.

A top-down scaling analysis was performed using the SASM methodology for both single- and two-phase natural circulation. The objective of the scaling analysis was to scale the steady-state single- and two-phase natural circulation flow rates and the natural circulation heat transfer. A bottom-up scaling was then performed to develop the similarity criteria to specifically scale the core and SG heat transfer regimes, flow regimes and transitions, frictional and form pressure losses, and critical heat flux. To maintain similarity, the Π values developed from the dimensionless conservation equations should be preserved or the ratio of the groups should be unity.

The scaling study requires the user to choose a length scale and an area or diameter scale for the facility to satisfy the system of equations, power requirements, and geometric representation of the facility relative to the plant. Other scaling considerations such as flow regimes in the loop piping must also be considered. Small diameters distort the flow regime and have different transitions between the flow regime compared with the prototype. Small diameter pipes also have different two-phase counter-flow behavior compared with the prototype. Reduced size can also cause manufacturing problems for the core heater simulators.

An evaluation determined that a 1/4-length scale was the most appropriate for the OSU facility since it minimized the power requirements while maximizing the height. A 1/4-scaled facility also had

sufficient volume and size to correctly model the plant pressure drop and possible three-dimensional flow behavior that could occur in the simulated reactor vessel, plenums, and downcomer. To chose a consistent diameter scale, a simple relationship was derived from the one-dimensional momentum equation to relate the length ratio to the diameter ratio. The choice of the diameter ratio was further verified with a bottom-up scaling approach in which the two-phase flow regimes and transitions between flow regimes were examined using the work of Taitel and Dukler.[8] The possible distortions in the flow regimes and their transitions was also examined for the horizontal piping following the approach of Schwartzbeck and Kocamustafaogullari.[9] The flooding review by Bankoff and Lee[10] was also used to verify that the chosen diameter ratio would have minimum surface tension effects if flooding occurred. Using this approach, the facility dimensions could be specified with confidence that the key parameters and phenomena identified in the PIRT would be preserved in the OSU facility so that the resulting data could be used for AP600 safety analysis code validation.

The OSU experiments were designed to start in an all-liquid recirculation mode with the simulated RCPs operating with system pressure at about 400 psia. When a break is initiated, the system begins to depressurize. To preserve the depressurization behavior of the OSU facility, a reference pressure was selected and a scaling rational developed to relate the lower pressure OSU tests to the higher-pressure AP600 transient for the depressurization transients. The results of the scaling approach were used to develop the relationships that led to selection of the OSU facility break areas, ADS valve areas, accumulator gas pressure, and SG secondary-side safety pressures to preserve the scaling relationships between the facility at its reduced pressure and the AP600 plant at its higher pressure. The scaling process used is shown in Figure 1.4-3, in which a top-down scaling approach was used to develop the systems scaling analysis for a simplified control volume of the reactor primary system. A bottom-up approach was then used to develop the fluid property relationships for the depressurization transients. The approach, originally developed by Kocamustafaogullari and Ishii[11] and expanded on by Moskal,[12] was extended to relate the OSU fluid property conditions to the AP600 plant conditions. Moskal defines the property relationship

$$Y = \frac{\Delta\rho}{\rho_g \rho_f h_{fg}} \qquad 1.4\text{-}9$$

as the key property group to be preserved. This particular grouping also appears in the coefficients for the core velocity from the two-phase natural circulation loop scaling analysis previously described. The fluid properties and depressurization approach is to select a reference pressure for both the OSU facility and the AP600 which will capture the important parameters that were identified in the PIRT. Examining Figure 1.4-2, the AP600 primary system pressure will stabilize, after the initial subcooled blowdown, to a near constant value, slightly above the safety valve setpoint for the steam generator secondary side. The primary pressure will remain at this value for a relatively long period, depending upon the break size and when the ADS activates, which will depressurize the primary system to the containment pressure. During this time period, the passive safety systems of the AP600 will be in operation and the phenomena of importance, which are identified in the PIRT, will be present.

Therefore, this pressure was chosen as the reference pressure for the AP600 plant. Note that this ignores the subcooled depressurization portion of the transient which, for a SBLOCA, is a short period compared with the total transient length.

A similar reference pressure can be chosen for the OSU facility where the primary pressure stabilizes above the steam generator pressure, such that:

$$\left[\frac{Y}{Yo}\right]_m = \left[\frac{Y}{Yo}\right]_p \qquad 1.4\text{-}10$$

where:

$Yo]_m$ = OSU reference pressure
$Yo]_p$ = AP600 reference pressure

The top-down and bottom-up pressure scaling must also be consistent with the natural circulation scaling which establishes the facility volume, time, and velocity scaled ratios; given the selection of the length and diameter for the facility.

The bottom-up pressure scaling examined the critical flow through the break and the ADS valves, and developed the relationships for the break areas and the valve areas that were consistent with the fluid property scaling given above. Therefore, given a break size in the AP600, a corresponding break size can be calculated for the OSU facility which will maintain the time, velocity, and volume scaling for a selected length and diameter scale which was chosen from the two-phase natural circulation scaling relationships.

TABLE 1.4-1 GENERAL SYSTEM HIERARCHY: OSU/AP600 SCALING ANALYSIS	
SYSTEM:	Primary loop
SUBSYSTEMS:	PRHR, CMT, IRWST, accumulator, ADS, LCS Recirc System
MODULES:	Reactor core, pressurizer, steam generators, hot legs, cold legs, reactor coolant pumps, interconnecting piping
CONSTITUENTS:	Steam-liquid mixture, stainless steel structure

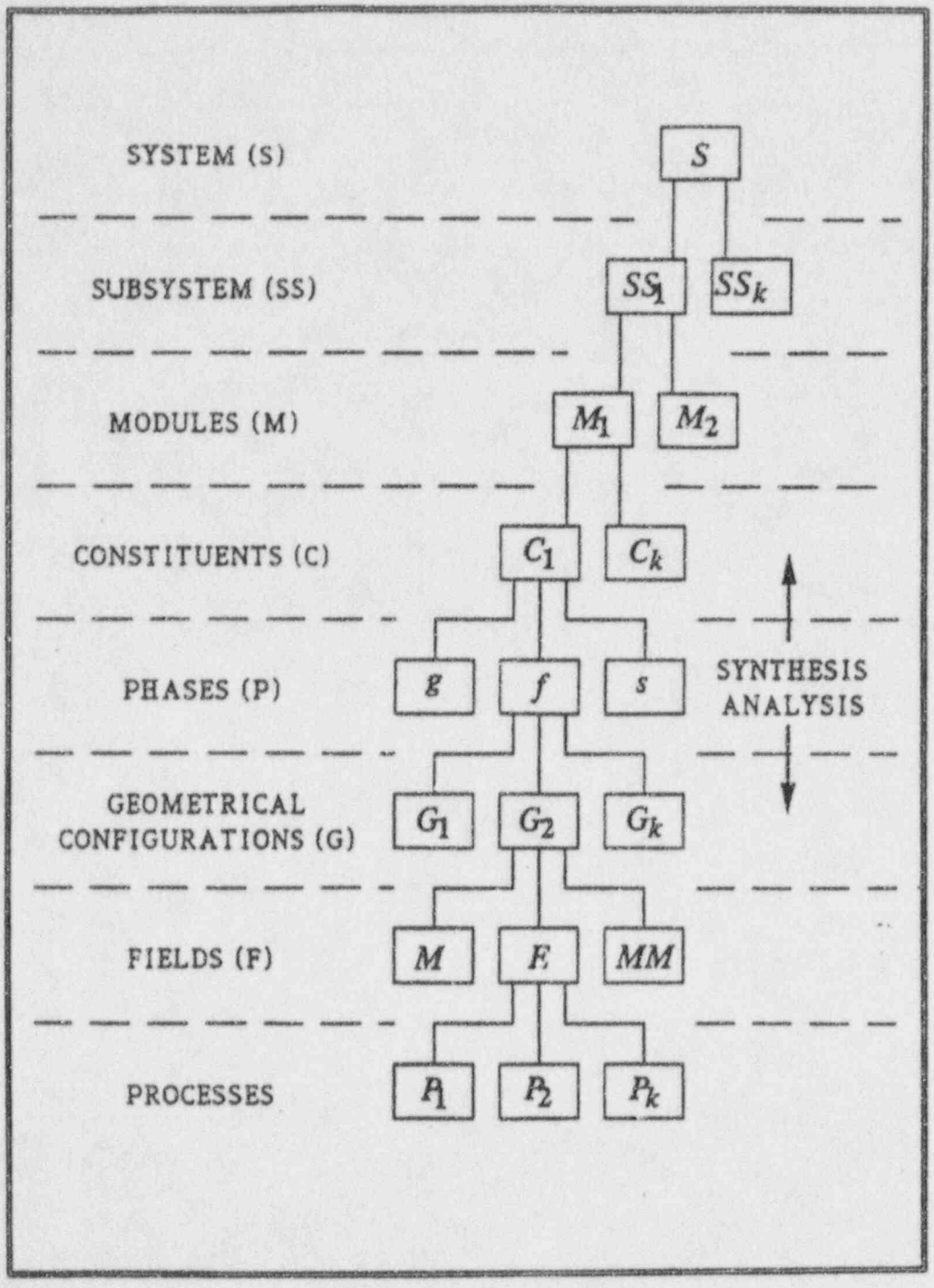

Figure 1.4-1 Decomposition Paradigm and Hierarchy[7]

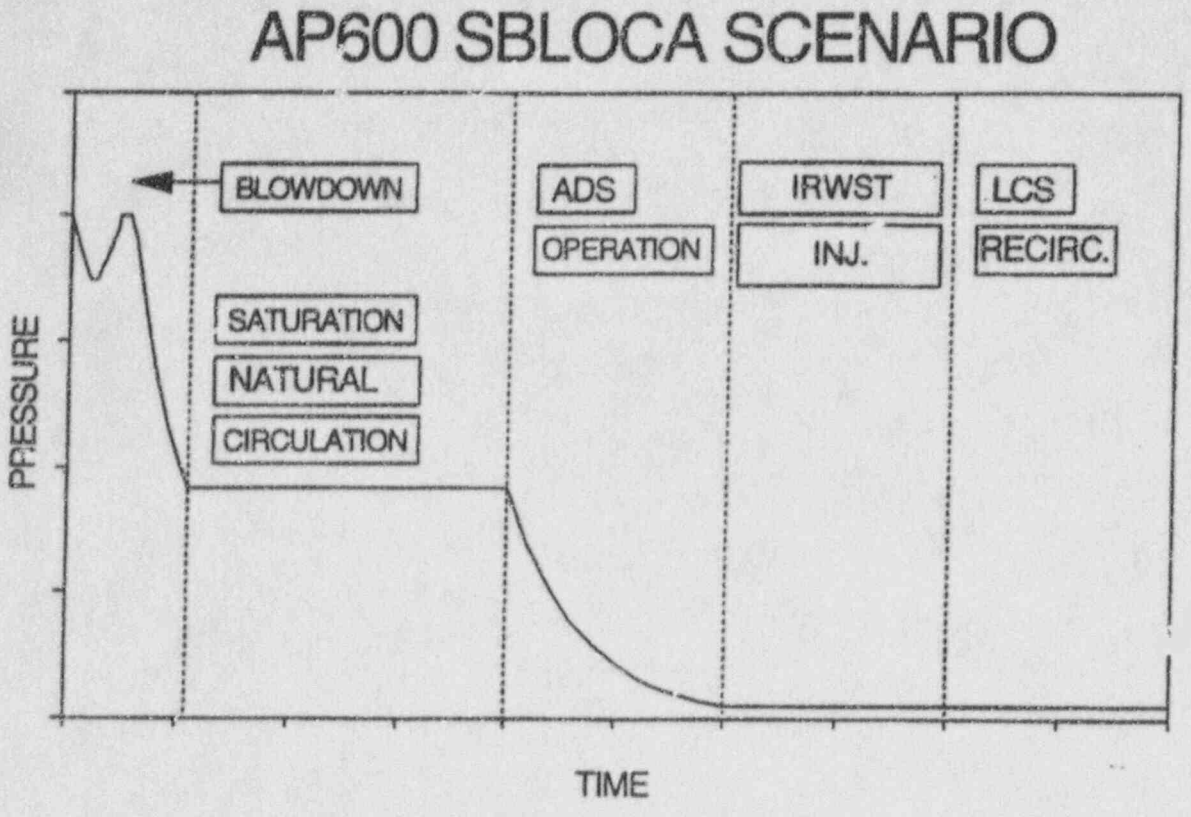

Figure 1.4-2 AP600 SBLOCA Scenario

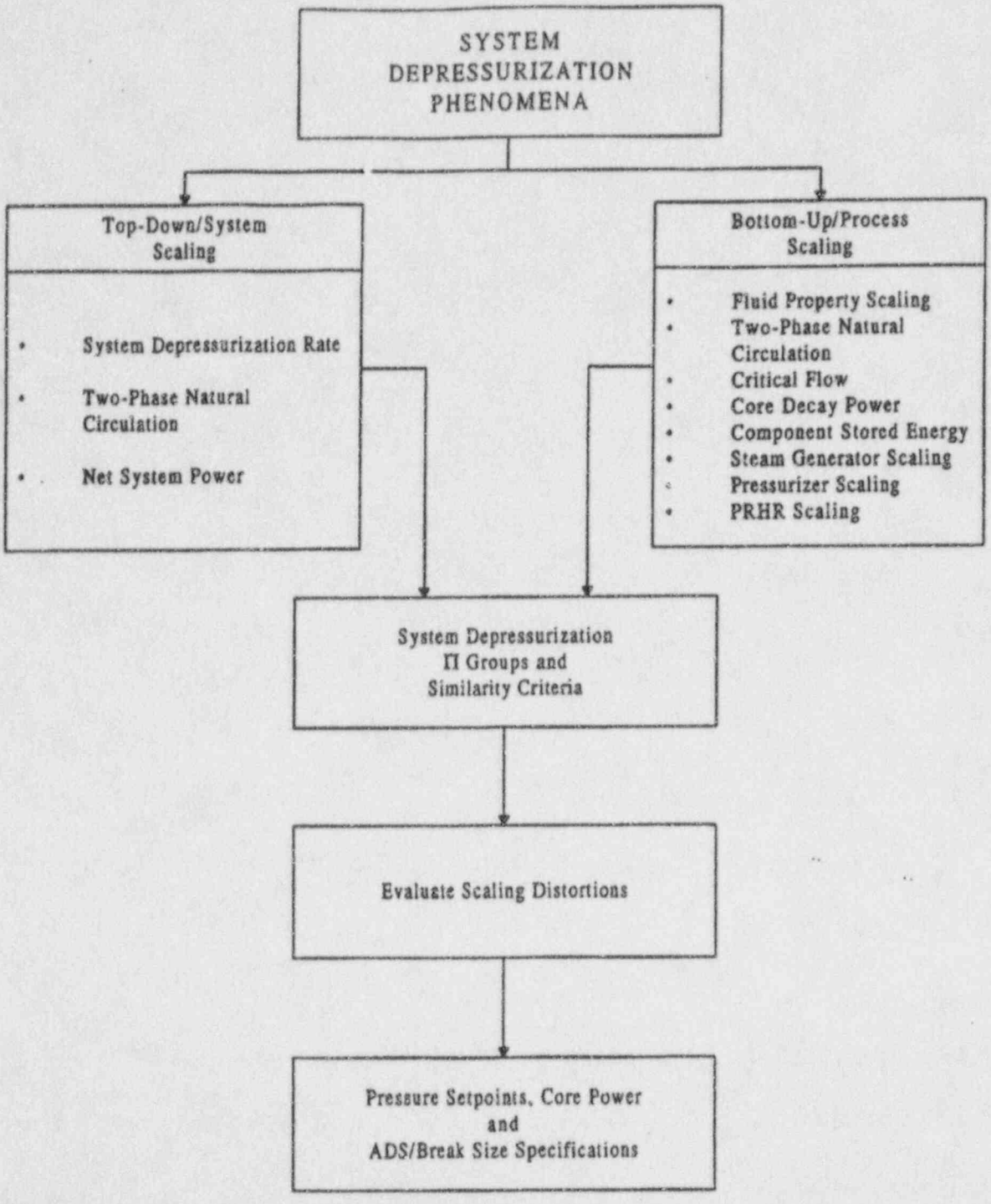

Figure 1.4-3 Scaling Analysis Flow Diagram for System Depressurization

1.5 Test Scaling Assessment and Dimensions

To assess the scaling of the OSU facility, both the proposed scaled facility and the AP600 were modeled using the *NOTRUMP, A Nodal Transient Small-Break and General Network Code*, WCAP-10079-P-A.[13]. The objective of this study was to investigate whether the OSU facility response to a small-break transient would be similar to the response of the AP600. A 2-in. cold-leg break on the CMT-side of the plant was selected. The OSU facility initial conditions for this break are shown in Table 1.5-1. Table 1.5-2 shows the scaling relationships between the plant and the OSU facility, which account for the time scale difference (two-to-one for OSU) and the normalization of flow, pressure, two-phase mixture levels, and total system mass.

Figure 1.5-1 compares the normalized pressure transient for the plant and the OSU test facility and indicates that reasonably good agreement was achieved. The reference pressure chosen is based on when the primary pressure stabilizes above the secondary-side pressure at time, t_o. The normalized CMT levels are shown in Figures 1.5-2 and 1.5-3, and the normalized accumulator levels are shown in Figure 1.5-4 and 1.5-5. These figures are in good agreement and indicate that the scaling correctly preserves the timing of the events for the OSU facility compared with the AP600 when the time scaling logic is applied. ADS 1-3 flow is shown in Figure 1.5-6 and is in reasonable agreement between the test facility and the plant. Break flows are compared in Figure 1.5-7, and a difference between the facility and the plant is indicated. One possible explanation for the difference is that, when scaling the critical flow area for the break, a quality of the flow must be assumed. In reality, the quality of the flow at the break is not a constant and will change with time. Furthermore, exact similitude cannot be simultaneously achieved for both the break energy flow rate and the break mass flow rate with a reduced pressure scale. However, the integrated mass inventory similitude can be preserved. Figure 1.5-8 shows the normalized mass inventory for both the test facility and the plant. Again, agreement between the two calculations is very good, indicating that the scaling approach will yield thermal-hydraulic phenomena similar to the AP600.

In addition to the NOTRUMP code calculations that compared the OSU and the AP600 response, the results from the SPES-2 and OSU tests can be compared to investigate the scaling performance of the OSU facility. Comparisons of a 2-in. cold-leg break from SPES-2 Test S00303[3] have been made with OSU Matrix Test SB01.

The derived OSU scaling factors were applied to the SPES-2 results to compare time, pressure, and flow rates. The OSU time scale was multiplied by a factor of 2. The OSU pressure scale was normalized using the reference pressure (maximum pressure on secondary side). Similarly, the SPES-2 pressure scale was normalized using the reference pressure for the test. The flow rate normalization factor in SPES-2 was the maximum flow rate for the process being examined. For purposes of comparison, the flow rate normalization factor in OSU was the maximum flow rate observed for the identical process in SPES-2 multiplied by the ratio 395/96. Thus, the flow rates can be compared on a similar basis.

A 2-in. cold-leg break was simulated in both the OSU and SPES-2 facilities. The break location for these tests was the bottom of a single cold leg. Each system was at its steady-state initial condition at break initiation. Subsequent depressurization behavior was recorded for each facility, and key data plots are presented for the purpose of comparison. The vertical axis of each graph has been normalized as described previously.

Figure 1.5-9 presents a comparison plot of the SPES-2 and OSU reactor vessel pressure histories and Figure 1.5-10 through 1.5-14 present the data comparisons for the key passive safety systems.

In general, the data comparisons for the 2-in. break case indicate good agreement. The timing of key events, such as ADS valve actuation, were preserved. One difference can be identified in Figure 1.5-14, however, where it is observed that the onset of IRWST injection was delayed in the OSU facility relative to SPES-2.

Similar comparisons were performed for the DEG DVI line break, and the agreement between OSU and SPES-2 was very good. These comparisons of a full-height, full-pressure test facility with the OSU reduced-height, reduced-pressure facility support the scaling logic used in the OSU test design.

As with any scaled experiment, scaling distortions are unavoidable, therefore, the purpose of the PIRT is to identify the most important processes to be scaled so that the system response is most prototypical. In the *Facility Scaling Report,*[2] Section 10.2 specifically discusses scaling distortion for the facility, and an evaluation is made of the scaling distortions on the primary parameters developed from the PIRT. The results are provided in Table 1.5-3. As the table indicates, all of the important pi ratios are within 20 percent.

The depressurization ratio given in the table incorporates the use of the revised depressurization scaling, which uses the system energy and volumetric scaling as a basis. This portion of the scaling was revised after the completion of the Westinghouse tests at OSU. The original scaling for the breaks, which was used for the tests in this report, used the break-dominated depressurization process described in Section 5.4.1 of the *Facility Scaling Report.*[2] This scaling approach was used for all breaks modeled in the OSU tests given in this report as well as the OSU final data report.[1] This scaling process is valid for break sizes of 2 in. or more, but was found to be inaccurate for smaller breaks. Therefore, the 1-in. cold-leg break and the 1/2-in. cold-leg breaks are oversized when considering the system energy and volumetric scaling methodology. The ratio of the break diameter scale factors between the two methods is given in Table 5-6 in the *Facility Scaling Report,*[2] and is 1.5. The break areas used for the Westinghouse tests were greater than the scaled values; therefore, the timing of the events for these tests will be distorted from the properly scaled values, and the events and total transient will be shorter than the revised scaling would predict. Revision of the scaled break diameters is the only significant re-scaling for the OSU test facility. This distortion only affects a few tests; the remaining tests have the properly scaled break diameter. Data for the affected tests are still suitable for the purposes of computer code validation, since the break area used in the experiment can be simulated in the code prediction of the test.

TABLE 1.5-1 INITIAL CONDITIONS FOR OSU TEST FACILITY TO MODEL A 2-IN. COLD-LEG BREAK	
Reactor Cooling System	
Core power	0.700 MWt
Core flow	116.7 lb/sec.
Pressurizer pressure	400 psia
Core inlet temperature	410.4°F
Core outlet temperature	415.6°F
Secondary	
Steam generator temperature	407.6°F
Break size simulated	2-in. cold-leg break

TABLE 1.5-2 SCALE FACTORS TO RELATE THE AP600 PLANT TO OSU NOTRUMP CALCULATIONS		
	AP600	**OSU**
Time	$t-t_o$ [1]	$2*(t-t_o)$
Pressure	P/1080	P/320
Flow	W/96	W

Note:

[1] t_o is the reference time when the primary pressure stabilizes above the secondary-side pressure.

TABLE 1.5-3
DISTORTION FACTORS FOR THE AP600 DOMINANT PROCESSES IDENTIFIED USING THE H2TS METHODOLOGY

Characteristic Time Ratio	Distortion Factor (DF) (%)	Operational Mode
Π_{R_i}	0	• 1ϕ Natural circulation
Π_F	0	• 1ϕ/2ϕ Natural circulation
Π_b	0	• 2ϕ Natural circulation with fluid property similitude/LCS recirculation
Π_b	(Not scaled)	• 2ϕ Natural circulation pressured scaled - core void fraction preserved instead of Π_b
Π_Γ/ε_o	0	• Depressurization - 1-in. cold-leg break (energy dominated)
$\Pi_{\Gamma,CMT}$	17.4	• CMT draining with hot walls
Π_{cond}	2.8	• CMT draining with cold walls
$\Pi_{HC,Head}$	6.3	• CMT draining with cold walls
$\Pi_{m,IRWST}$	0	• IRWST draining (property similitude)
$\Pi_{b,IRWST}$	0	• IRWST draining (property similitude)
$\Pi_{m,IRWST}$	-9.5	• IRWST heat up (pressure scaled)
$\Pi_{b,IRWST}$	19.1	• IRWST heat up (pressure scaled)
$\Pi_{q,DC}$	-16.7	• Downcomer heat transfer during Accumulator injection
$\Pi_{m,sump}$	TBD*	• Sump filling and recirculation AP600 data not available

*TBD— To be determined

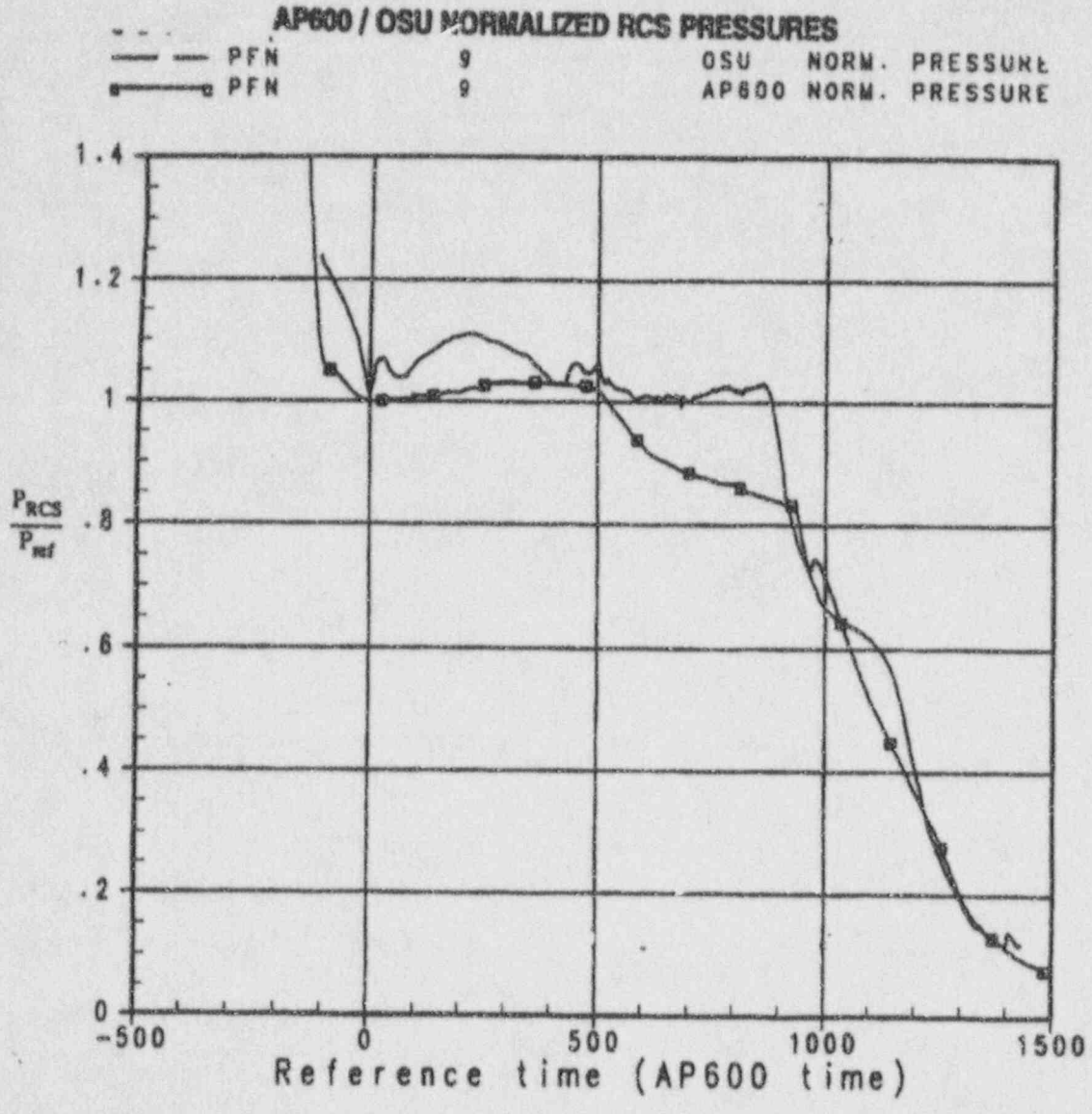

Figure 1.5-1 Normalized Pressure Comparisons between AP600 and OSU Facility

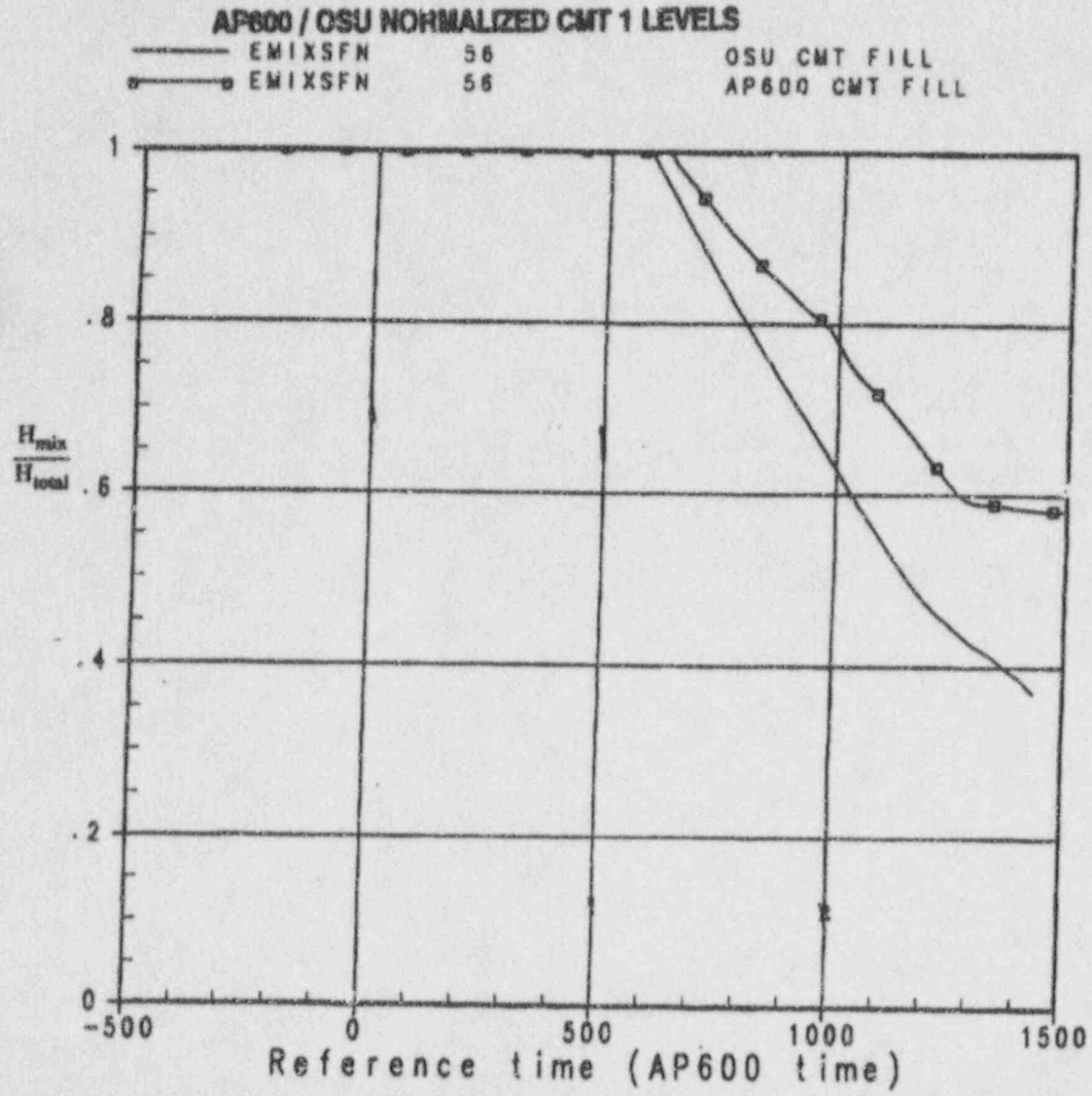

Figure 1.5-2 Normalized CMT-1 Level for AP600 and OSU Facility

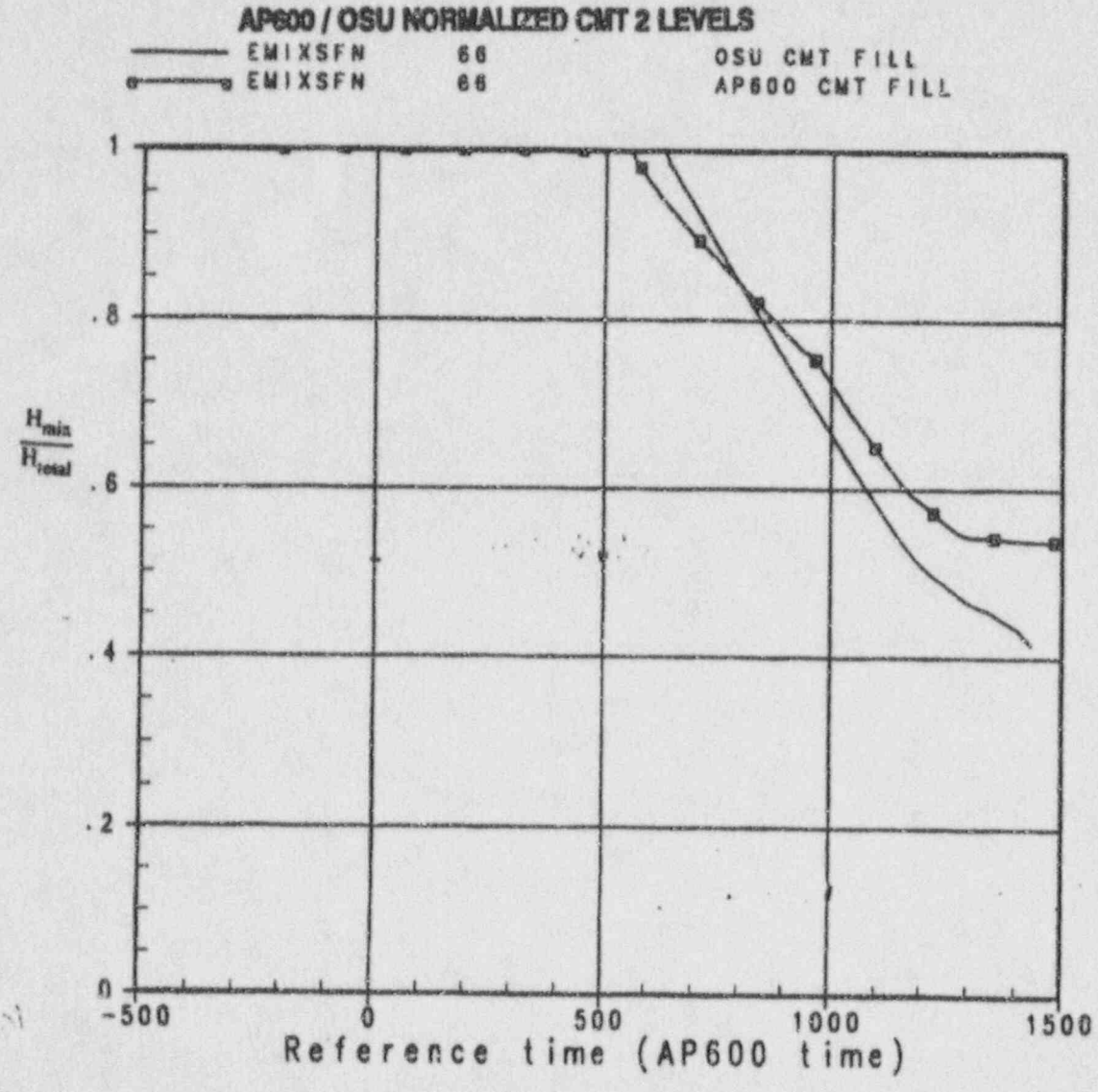

Figure 1.5-3 Normalized CMT-2 Level for AP600 and OSU Facility

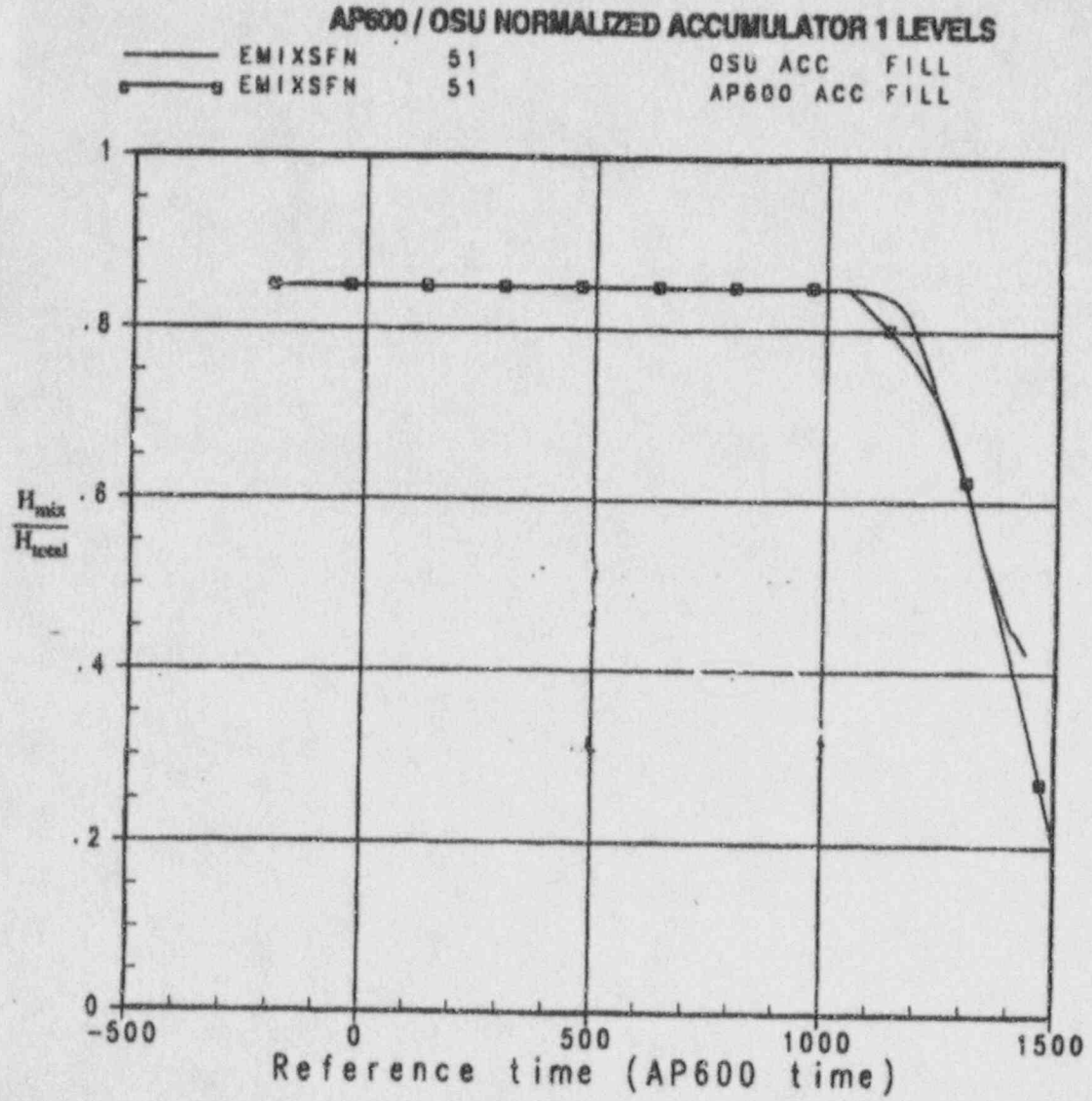

Figure 1.5-4 Normalized ACC-1 Level for AP600 and OSU Facility

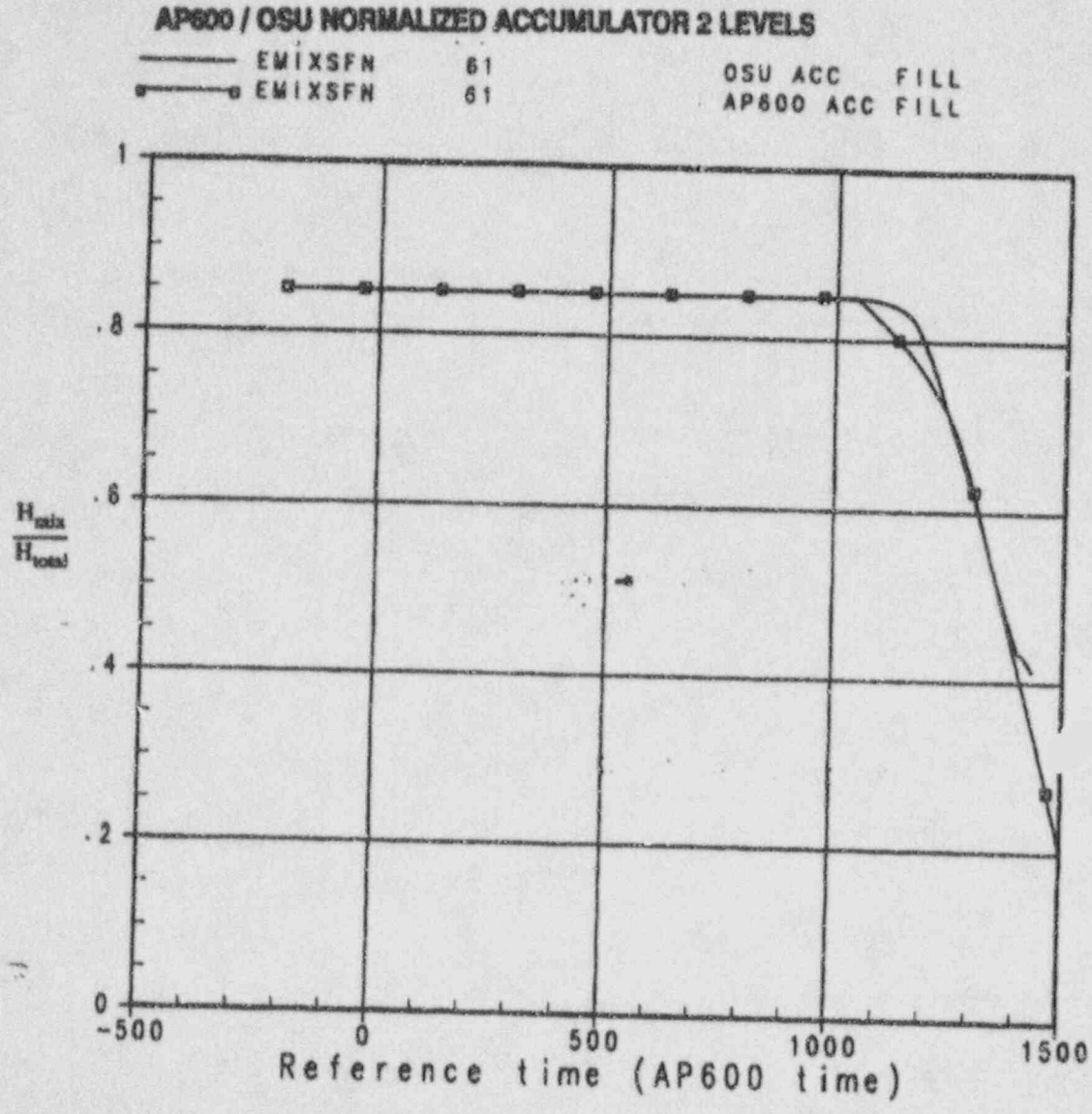

Figure 1.5-5 Normalized ACC-2 Level for AP600 and OSU Facility

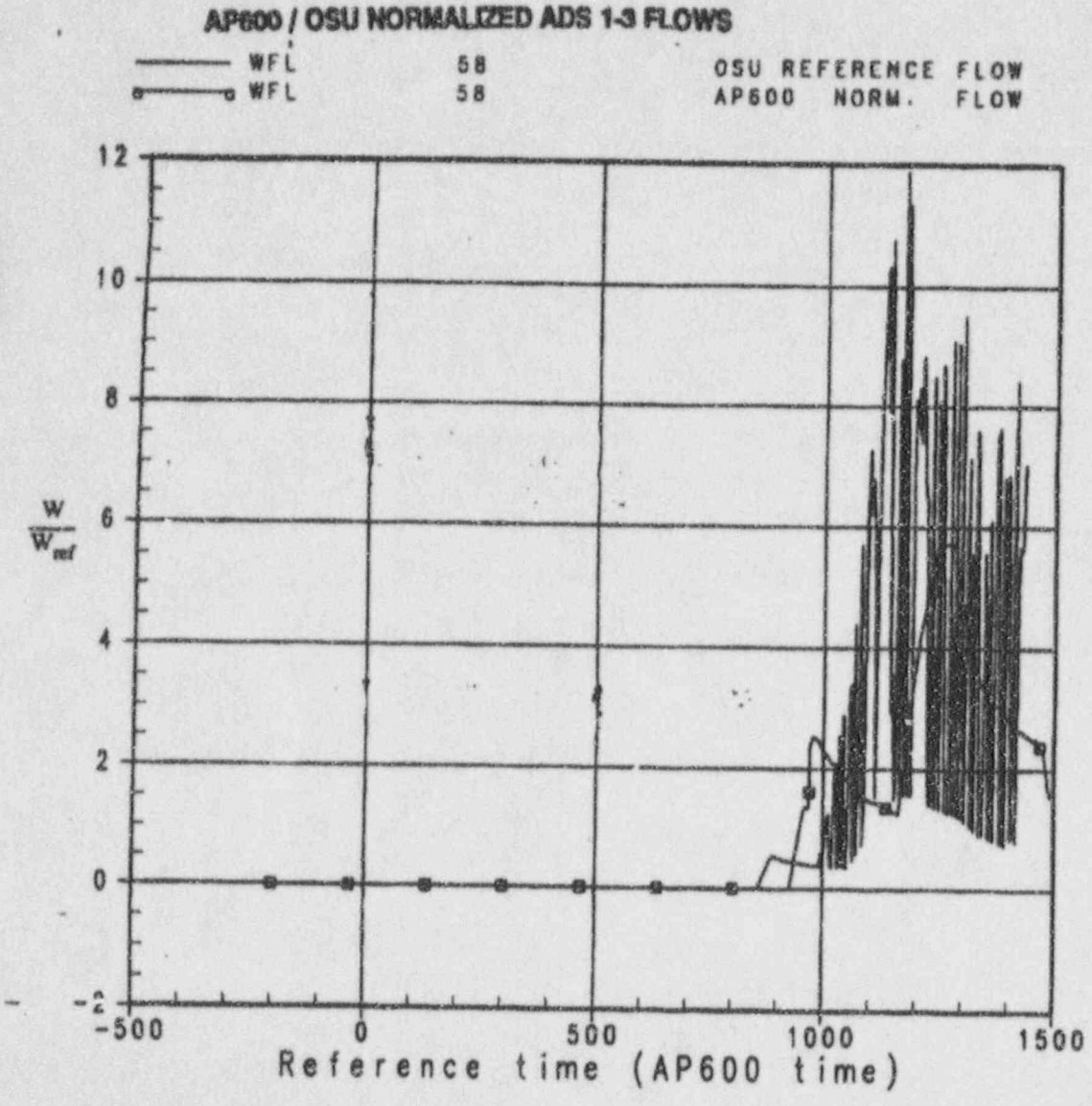

Figure 1.5-6 Normalized ADS 1-3 Flows for AP600 and OSU Facility

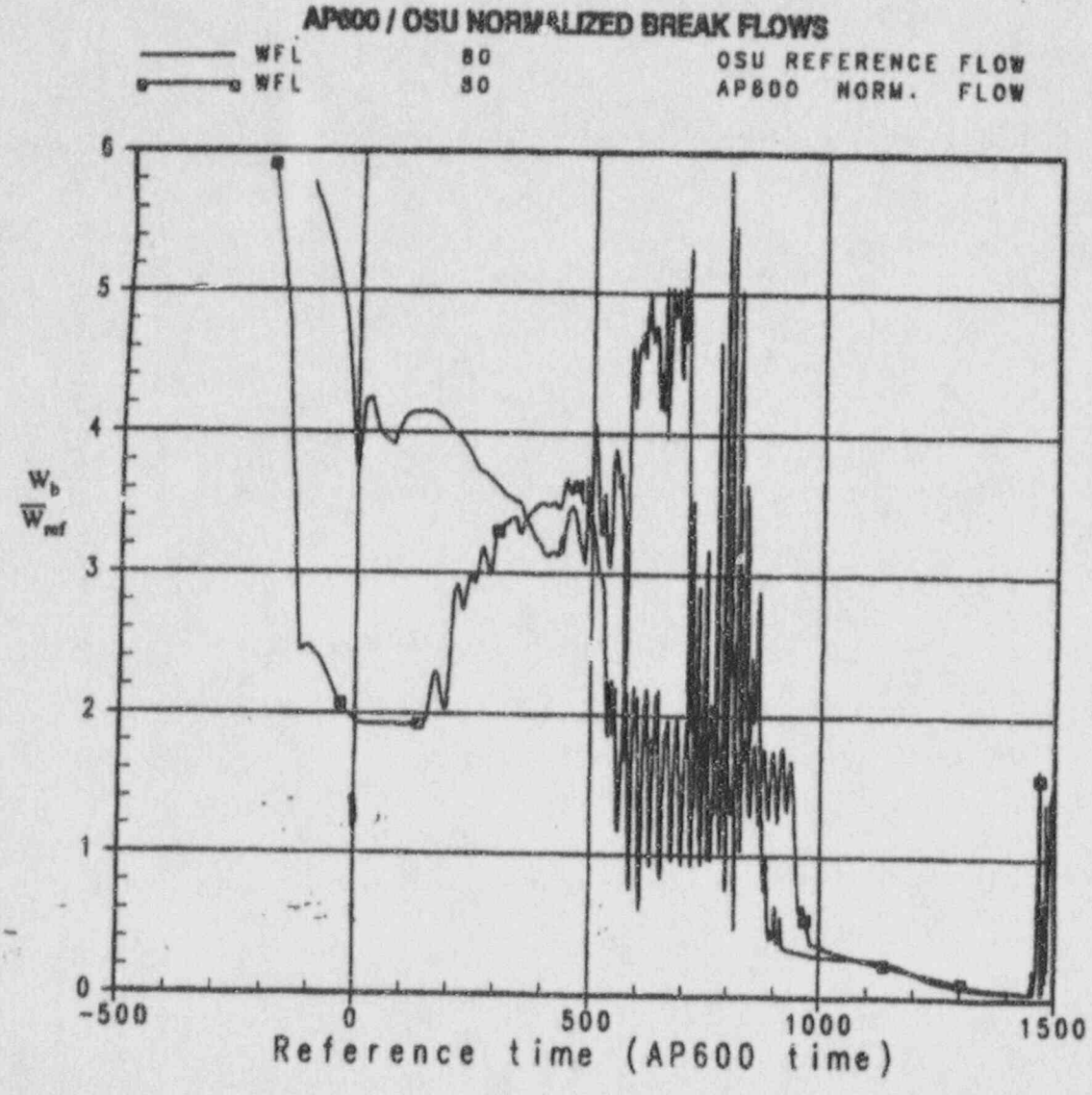

Figure 1.5-7 Normalized Break Flow for AP600 and OSU Facility

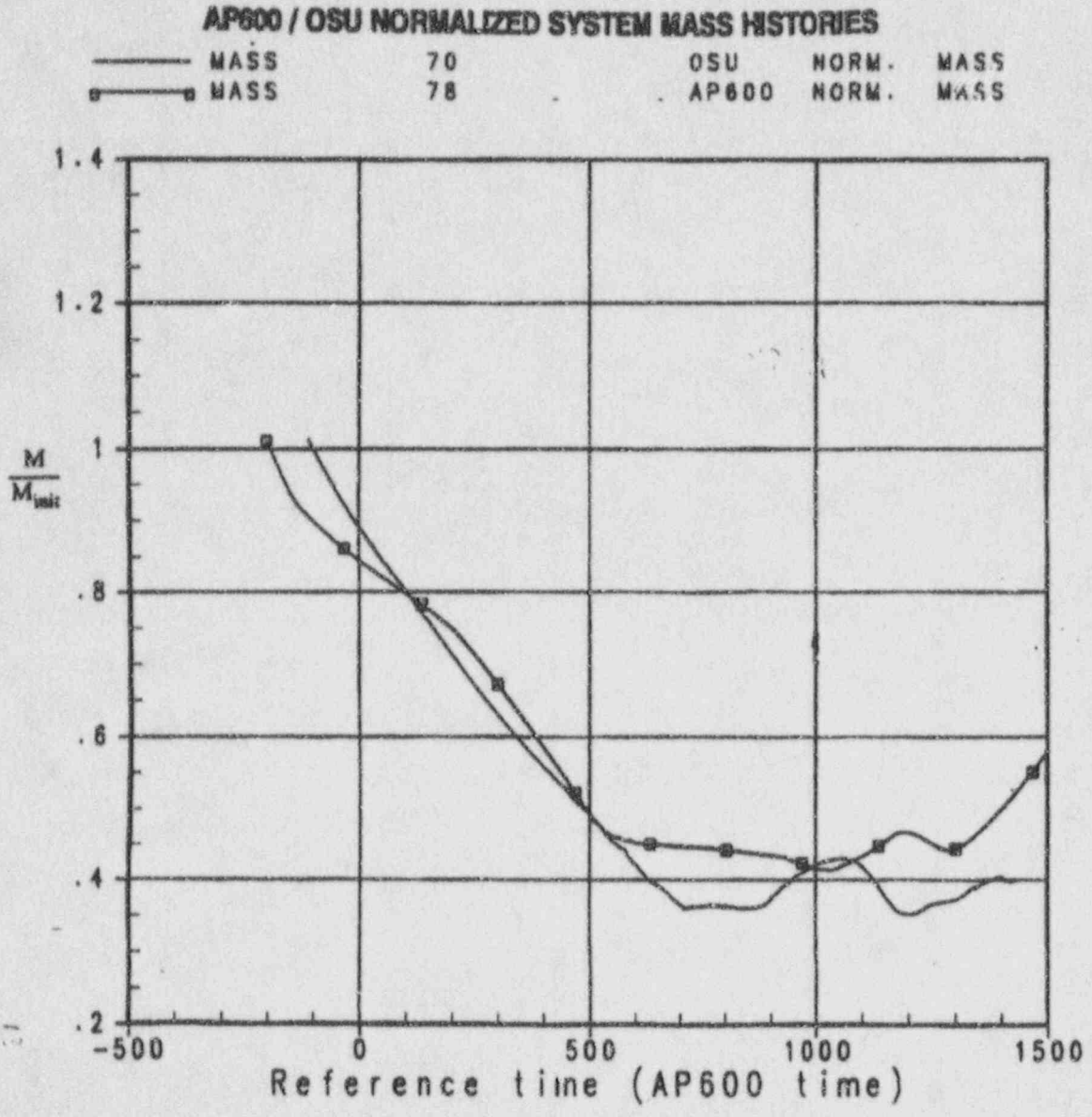

Figure 1.5-8 Normalized System Mass for AP600 and OSU Facility

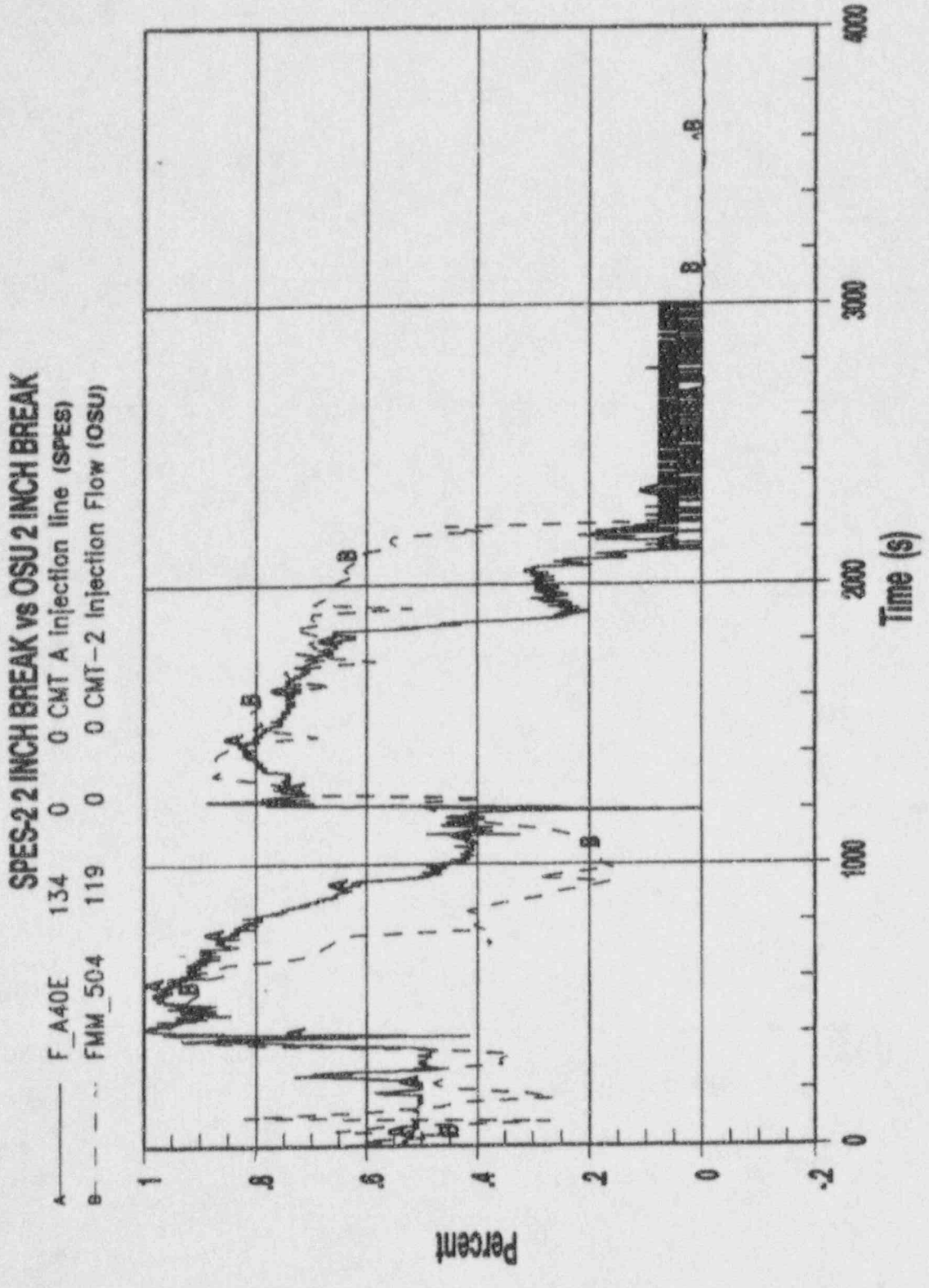

Figure 1.5-9 Comparison of OSU and SPES-2 CMT-1 Injection Flow Rate

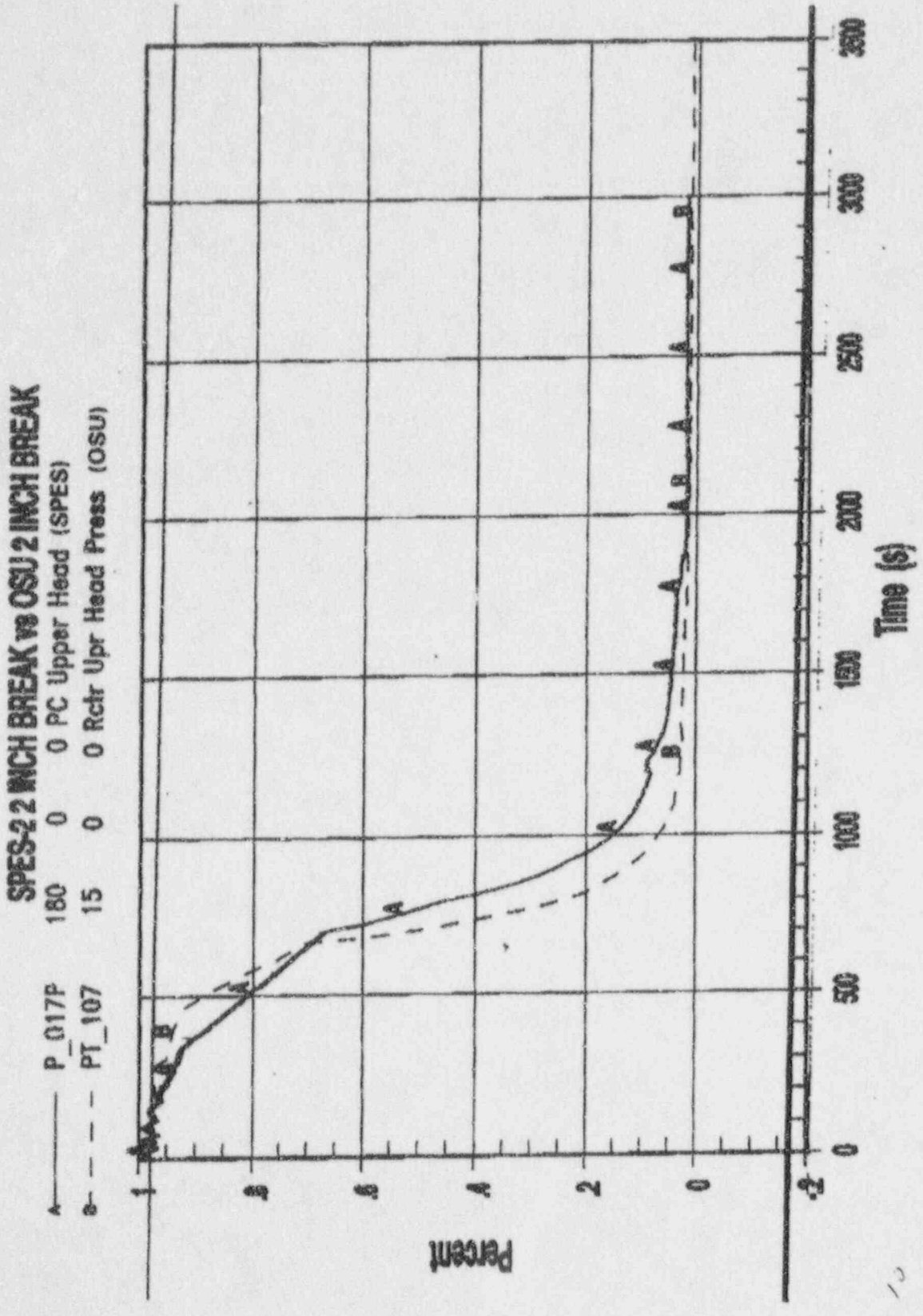

Figure 1.5-10 Comparison of OSU and SPES-2 2-In. Break Pressure Histories

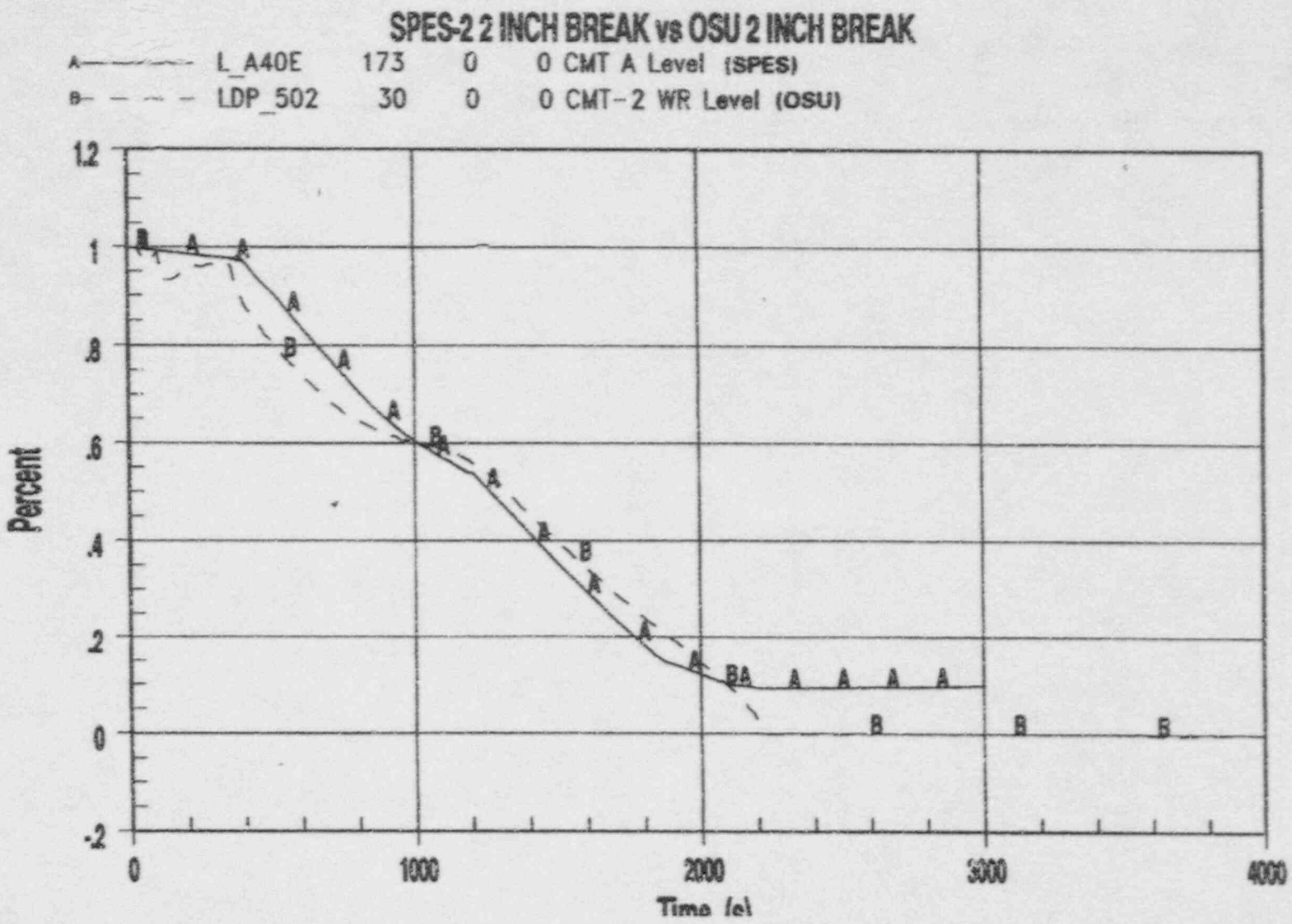

Figure 1.5-11 Comparison of OSU and SPES-2 CMT-1 Liquid Level Histories

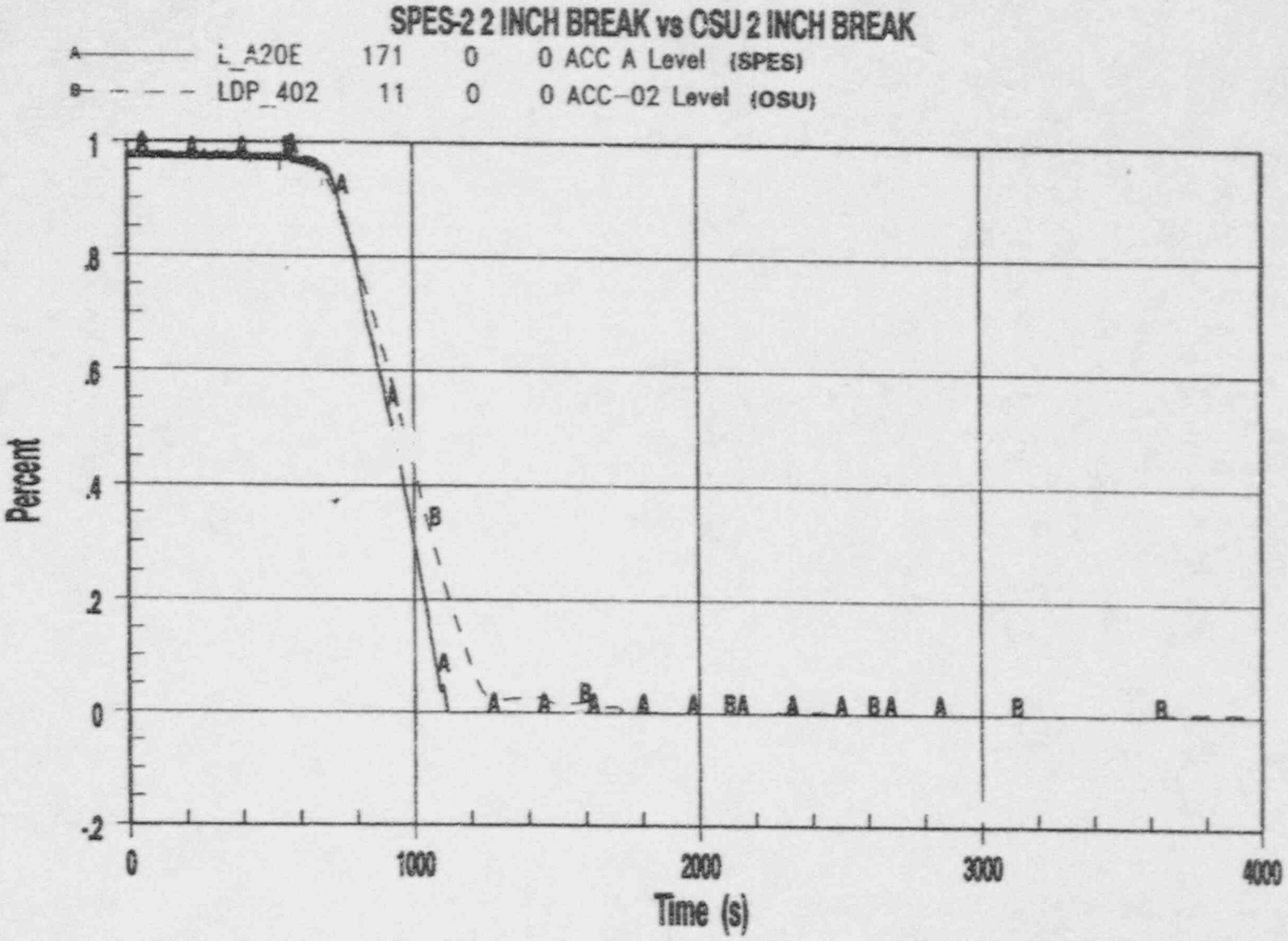

Figure 1.5-12 Comparison of OSU and SPES-2 ACC-1 Liquid Level Histories

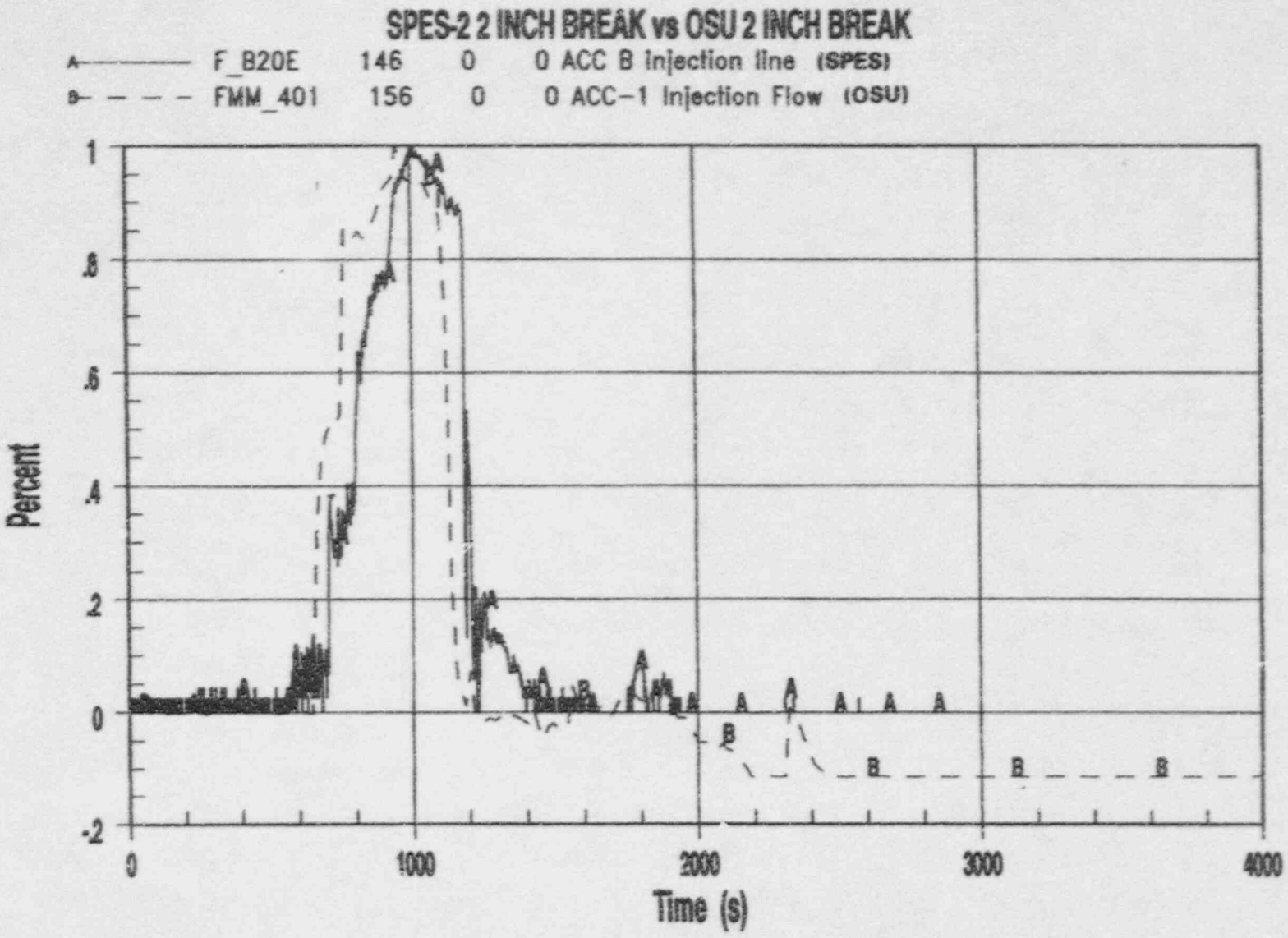

Figure 1.5-13 Comparison of OSU and SPES-2 ACC-1 Injection Flow Rate

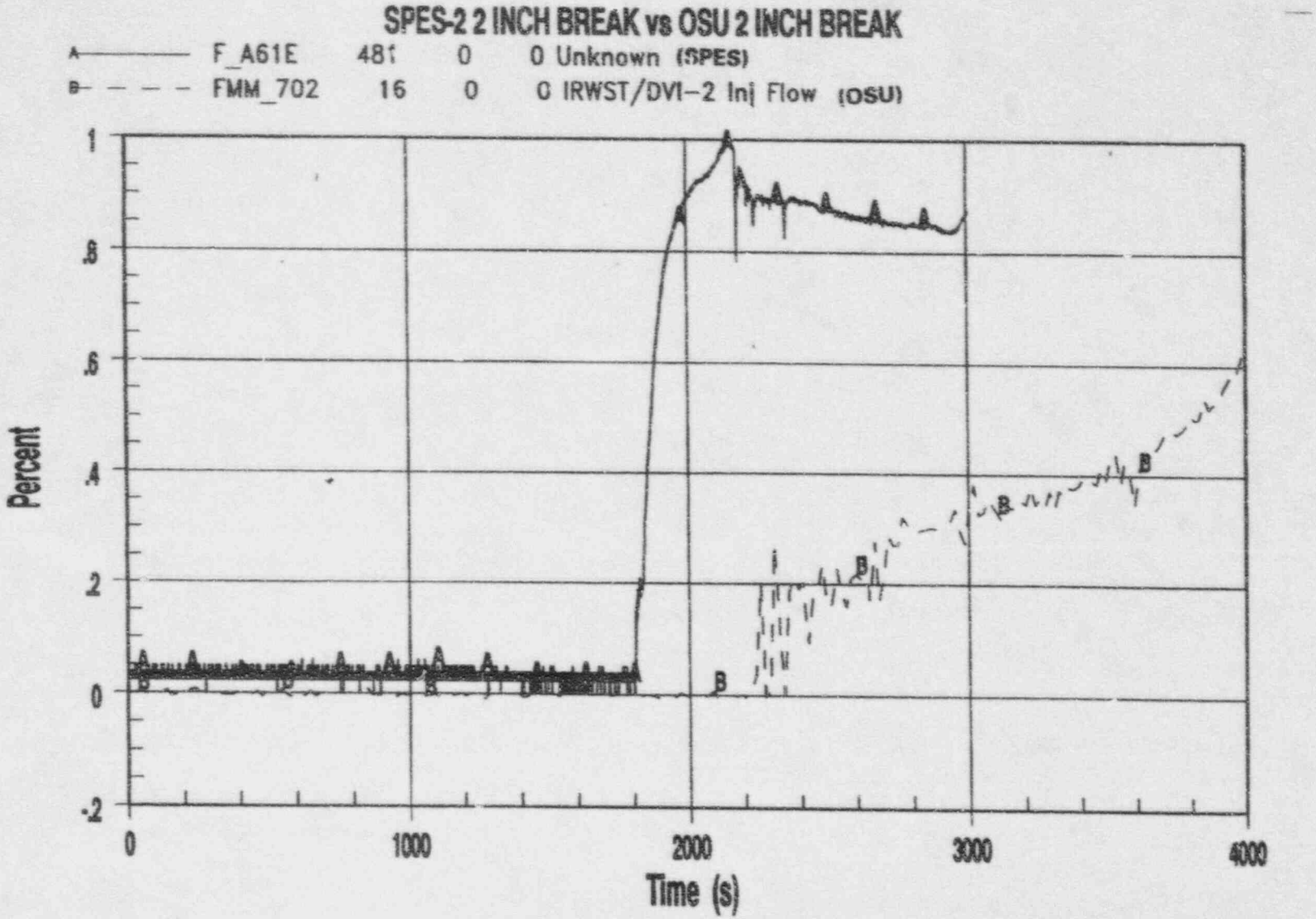

Figure 1.5-14 Comparison of OSU and SPES-2 IRWST-1 Flow Rate

2.0 FACILITY DESCRIPTION SUMMARY

The Oregon State University (OSU) low-pressure integral systems effect test facility is a scaled representation of the AP600. The design operating conditions for the facility are 400 psig at 450°F. The facility includes all the passive safety injection systems that appear in the AP600 design, as well as nonsafety injection systems such as the normal residual heat removal system (RNS) and chemical and volume control system (CVS).

The test facility operated in a steady-state fashion with a maximum electrical power of 660 kW, using four primary system recirculation pumps and two steam generators. Small-break loss-of-coolant accidents (SBLOCA) are simulated using break spool pieces. The break can be located on the hot legs, cold legs, direct vessel injection (DVI) lines, or cold-leg balance line. The test facility is designed to simulate the scaled decay power of AP600.

2.1 Overall Facility Description

The OSU test facility is a scaled model of the AP600 reactor coolant system (RCS), steam generator system (SGS), passive core cooling system (PXS), automatic depressurization system (ADS), lower containment sump (LCS), chemical and volume control system (CVS), and normal residual heat removal system (RNS). In addition, the facility is capable of simulating the AP600 passive containment cooling system (PCS) condensate return process. Figure 2.1-1 is an isometric drawing of the test facility, and Figure 2.1-2 is a simplified flow diagram of the test facility. The facility reflects the scaled AP600 geometry, including the piping routings. All components and piping are fabricated from austenitic stainless steel. The relative locations of all tanks and vessels—such as the in-containment refueling water storage tank (IRWST), core makeup tanks (CMTs), and accumulators were maintained as determined by the scaling approach. The facility uses a unique break and ADS measurement system (BAMS) to measure two-phase break and ADS flow.

The RCS is composed of a reactor vessel, which has electrically heated rods to simulate the decay heat in the reactor core, and two primary loops. Each primary loop consists of two cold-leg pipes and one hot-leg pipe connecting a steam generator (SG) to the reactor vessel. A reactor coolant pump (RCP) on each cold leg takes suction from the SG channel head (downstream of the SG U-tubes) and discharges it into the downcomer region of the reactor vessel. A pressurizer with an electric heater is connected to one of the two hot legs through surge-line piping. The top of the pressurizer is connected to the ADS 1-3 line. An ADS-4 line is connected to each hot leg.

The reactor vessel contains two direct vessel injection (DVI) nozzles that connect to the DVI lines of the PXS. A flow venturi is incorporated in each DVI nozzle to limit the loss of inventory from the reactor vessel in the event of a double-ended DVI line break.

This test facility models the primary and secondary side of the SGs with one generator per primary loop. A simulated feedwater line is used for each loop to maintain proper secondary water level. The steam produced in each generator is measured and exhausted to the atmosphere through a common diffuser and stack.

The test control logic simulates the response of the AP600 by providing an S signal at a fixed time following a break.

The passive safety injection systems consist of two CMTs, two accumulators, one IRWST, and one passive residual heat removal heat exchanger (PRHR HX). The test facility simulates the AP600 IRWST with a cylindrical tank with scaled water volume and height. The IRWST is located above the reactor core; two injection lines connect to the two DVI lines. Each IRWST injection line also connects to the sump tank with interconnecting piping and isolation valves. The PRHR HX is located inside the IRWST, using IRWST water as the heat sink. The inlet of the PRHR HX is connected to the pressurizer-side hot leg via a tee at the ADS-4 line, and the outlet is connected to the SG channel head at the cold-leg side. Since the inlet is hot and the outlet is cold, water is circulated through this

system by natural convection. The water volume and elevation of each CMT are scaled and modeled. They are elevated above the reactor vessel and the DVI lines. A line connecting the top of each CMT to its cold leg provides pressure balance between the RCS and the CMT. Therefore, the CMT injects cooling water by its own elevation head. The accumulators are also modeled with scaled volume and height. However, they are pressurized and, therefore, inject when RCS pressure is below the preselected scaled accumulator pressure.

The AP600 uses four stages of valves to depressurize the RCS. The first three stages of the ADS are provided through connections to the pressurizer. These three stages are arranged in parallel, with each stage containing two lines with each line containing an isolation and control valve. The fourth stage of the ADS contains four separate lines.

The OSU test facility uses only one set of valves to model the ADS 1-3 stages for AP600. This is done using removable flow nozzles to match the scaled flow characteristics of either one or two lines of valves. The first-, second-, and third-stage lines of the ADS split into parallel lines from one connection off the pressurizer.

The discharge lines from the ADS 1-3 valves are joined into one line connected to the ADS 1-3 separator. This two-phase flow is separated using a swirl-vane separator. The liquid and vapor flows are measured to obtain the ADS total flow for mass and energy balance analysis. The separated flow streams are then recombined and discharged into the IRWST through a sparger.

The OSU test facility uses one ADS-4 line connected to the top of each hot leg. Each line contains a pneumatically operated, full port ball valve acting as the ADS-4 isolation valve and a flow nozzle simulating the flow area in the AP600. Two sets of flow nozzles are used in the test: one simulates 100-percent flow area and the other simulates 50-percent flow area. In the test facility, ADS-4 discharge flows to the ADS-4 separators, where the steam and liquid flows are separated and measured. Steam flow is measured and exhausted to the atmosphere.

The lower containment sump in the AP600 consists of two volumes: normally flooded and normally nonflooded. The normally flooded volume consists of those compartments which collect liquid break flow and ADS flow. The normally flooded volume is modeled in OSU with a cylindrical tank, identified as the primary sump tank. The normally nonflooded volume includes those compartments which do not collect any liquid flow. The normally nonflooded volume is modeled in OSU with a cylindrical tank, identified as the secondary sump tank. These two tanks are connected with a line at a level simulating the curb level in the AP600.

In the AP600, the RNS is used to provide nonsafety cooling water injection to the reactor core. The RNS pump takes suction from the IRWST and discharges it into the DVI lines. The test facility RNS pump takes suction from the IRWST at the scaled location and elevation and discharges equal flow to both DVI lines at scaled locations.

BAMS is uniquely designed for the test facility to indirectly measure two-phase flow and energy leaving the break and ADS location. This system separates two-phase flow into single-phase liquid and single-phase steam flows for direct flow rate and temperature measurements. The BAMS consists of steam-liquid separators and the interconnecting pipes and valves to the various break sources, the primary sump tank, the ADS 1-3 lines, and the main steam header.

Two-phase flow (steam and water) from the ADS 1-3 lines enters the ADS 1-3 separator, where the steam is separated from the mixture. Steam flows out of one outlet while liquid drains down the other. These two lines recombine at some distance downstream and discharge into the IRWST via the sparger located inside the IRWST. Therefore, the mass and energy from ADS 1-3 is transferred to the IRWST as in the AP600.

Two ADS-4 separators are used, one for each ADS-4 line. Each ADS-4 separator separates two-phase flow into single-phase steam and single-phase liquid for flow rate, pressure, and temperature measurements. The steam line connects to a common steam header, and the liquid line connects to the primary sump tank. These connections simulate the ADS-4 operation process in the AP600, where the steam flow rises to the containment wall and liquid drains to the sump.

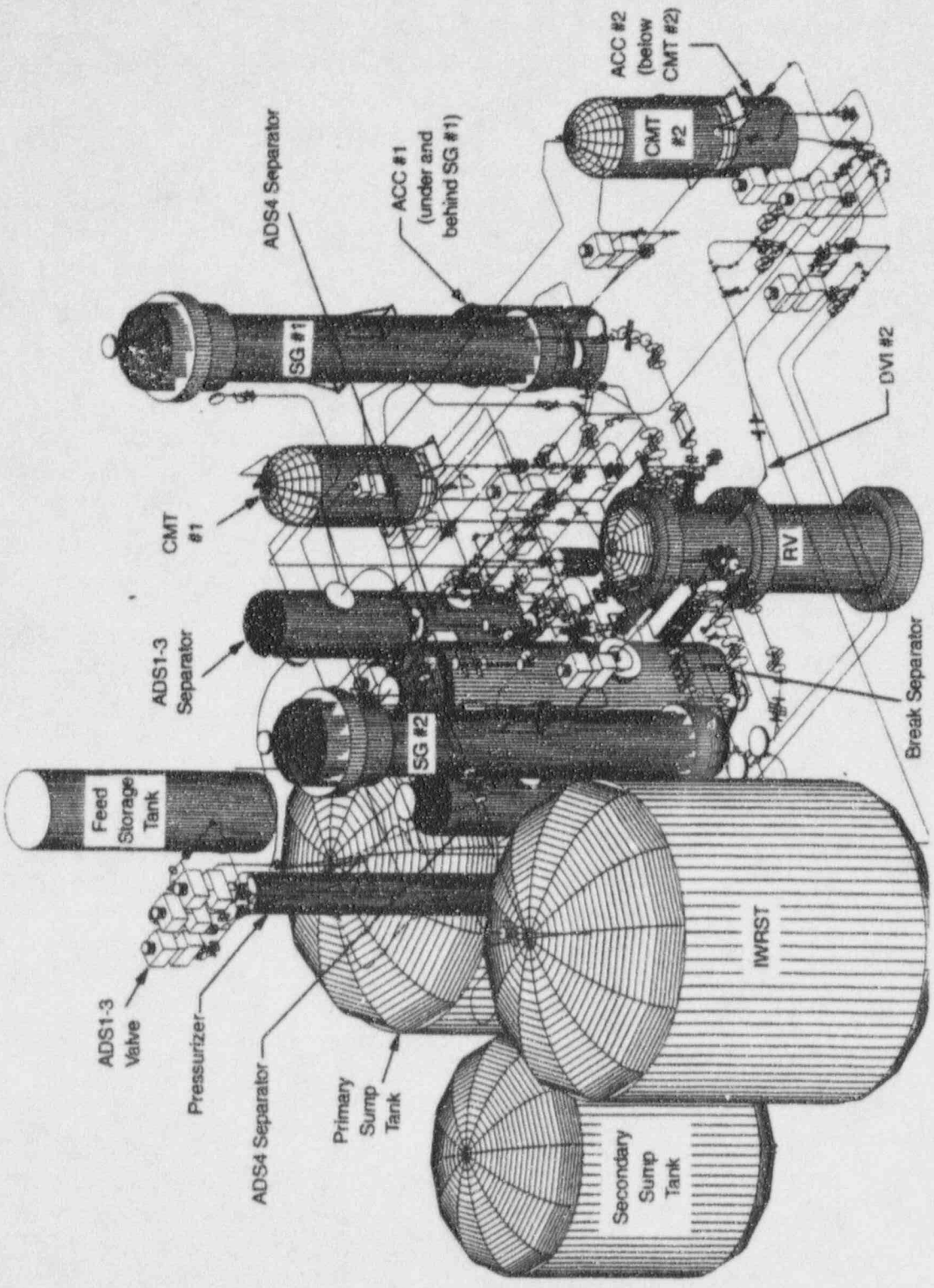

Figure 2.1-1 Isometric Drawing of the OSU Test Facility

2.2 Facility Instrumentation

OSU used standard instrumentation to indicate mass, flow, temperature, and pressure in the system and components. The instrumentation plan was specifically designed to provide a transient mass and energy balance on the components and for the entire system. Details of the instrumentation and its performance can be found in the *Final Data Report*[1]. The function of each of the instruments is discussed below. The use of the instruments for the mass and energy balances is provided in Section 4.

2.2.1 Differential Pressure Transmitters (FDP, LDP, DP)

Differential pressure transmitters measure the flow (FDP), or the level (LDP), in the system.

The only application of FDPs is to measure differential pressure across the flow orifices in the ADS-1, ADS-2, and ADS-3 lines (FDP-604, FDP-605, and FDP-606, respectively).

The level (LDP) transmitters measure levels in the facility tanks, the RCS hot-leg and cold-leg pipes, SG tubes, and PRHR HX tubes. The LDPs were designed to measure level (mass) in a component and were calibrated at ambient temperature. The level data recorded by the facility's data acquisition system (DAS) were uncompensated for temperature. The resulting signals were temperature compensated for the mass and energy balance calculations.

2.2.2 Pressure Transmitters

Pressure transmitters (PTs) are identical to differential pressure transmitters except that the low-pressure side of the transmitter senses atmospheric pressure.

Foxboro™ magnetic flow meters (FMMs) were used to measure liquid flow, in the different liquid solid lines. The FMMs are not designed to accurately measure steam or two-phase flow, and the data from the transmitters are invalid when either of these are measured.

Heated phase switches (HPSs) manufactured by Reotherm™ were used to indicate fluid phase in different components. There are 12 switches: one each on the cold and hot legs, CMT balance lines, PRHR HX inlet, and ADS 1-3 header. In addition, two switches are installed in the pressurizer surge line. The HPSs were usually used in conjunction with an LDP to indicate a separate level in a component.

Heat flux meters (HFMs) were used to measure heat flux through pipe or tank walls to indicate heat loss. The small, wafer-thin instruments are glued to a pipe or tank surface. Three thermocouples are imbedded into each HFM. Two thermocouples measure temperature on either side of the HFM. The thermocouple signals are measured by the DAS, and their temperature difference is converted to a heat

flux using coefficients provided by the vendor. The third thermocouple measures the temperature of the surface.

Fourteen Foxboro™ vortex flow meters (FVMs) were used to measure steam flow in the test facility. The FVMs measure steam flow from the ADS 1-3, ADS 4-1, ADS 4-2, and break separators. In addition, they measure steam flow from the primary sump, the IRWST, and the BAMS header. These meters are known to have a manufacturer's warranted cutoff of 141 actual cfm (acfm) which means they may not detect flaws below 0.088 lbm/sec. at ambient conditions.

The mass of water in the IRWST, primary sump, and secondary sump was measured by load cells mounted under the four supports of each tank. After the transmitter load cell was calibrated, it measured only the weight of water in the tank. The transmitter also provided local indication of weight in the tank for use by test personnel. The load cells were found to be sensitive to variations in ambient conditions, and thus, are not used for absolute measurements. Their readings are valid for tracing short time scale variations in mass.

Thermocouples are assigned one of four instrument designations, depending on the thermocouple's application. A TF thermocouple inserted through the wall of a pipe or tank is mounted on a thermocouple rod. TW thermocouples are mounted on the inside or outside walls of a tank or pipe. TR thermocouples, unique to the reactor vessel, are mounted on vertical thermocouple rods installed in the reactor vessel. TH thermocouples are mounted on the heaters for the reactor vessel and the pressurizer. Thermocouple type and diameter are specified in Appendix C of the *Final Data Report.*[1]

The reactor vessel contains TH thermocouples to measure temperatures of selected heaters. Selected heater thermocouples are used as inputs to the safety shutdown of the reactor heaters to detect abnormally high temperatures.

Thermocouples mounted in hollow rods (TR thermocouples) are unique to the reactor vessel. Five thermocouple rods are installed in the reactor vessel to provide radial and axial fluid temperature distributions in the heated section of the reactor vessel. Each rod contains thermocouples mounted along its entire length. Thermocouples protrude from the hollow rod and are sealed from the outside with silver solder.

The CMTs are instrumented with numerous fluid and wall thermocouples to measure the CMT wall heat flux and temperature, as indicated in Appendix G, Dwg. OSU 600501 and 600502 of the *Final Data Report.*[1] Each CMT contains one long and two short thermocouple rods instrumented with thermocouples along its entire length. In addition, inside and outside wall thermocouples, fluid thermocouples installed 1 in. from the inside wall, and tank centerline thermocouples are installed at the same elevation to measure the temperature of the fluid and walls at that elevation.

The IRWST also contains two thermocouple rods to measure the energy gain in the IRWST as shown in Appendix G, Dwg. OSU 600701 of the *Final Data Report.*[1]

One long and one short tube of each SG are instrumented with shell-side (secondary-side) wall thermocouples and tube-side (primary or RCS-side) fluid thermocouples as shown in Appendix G, Dwg. OSU 600301 of the *Final Data Report*.[1]

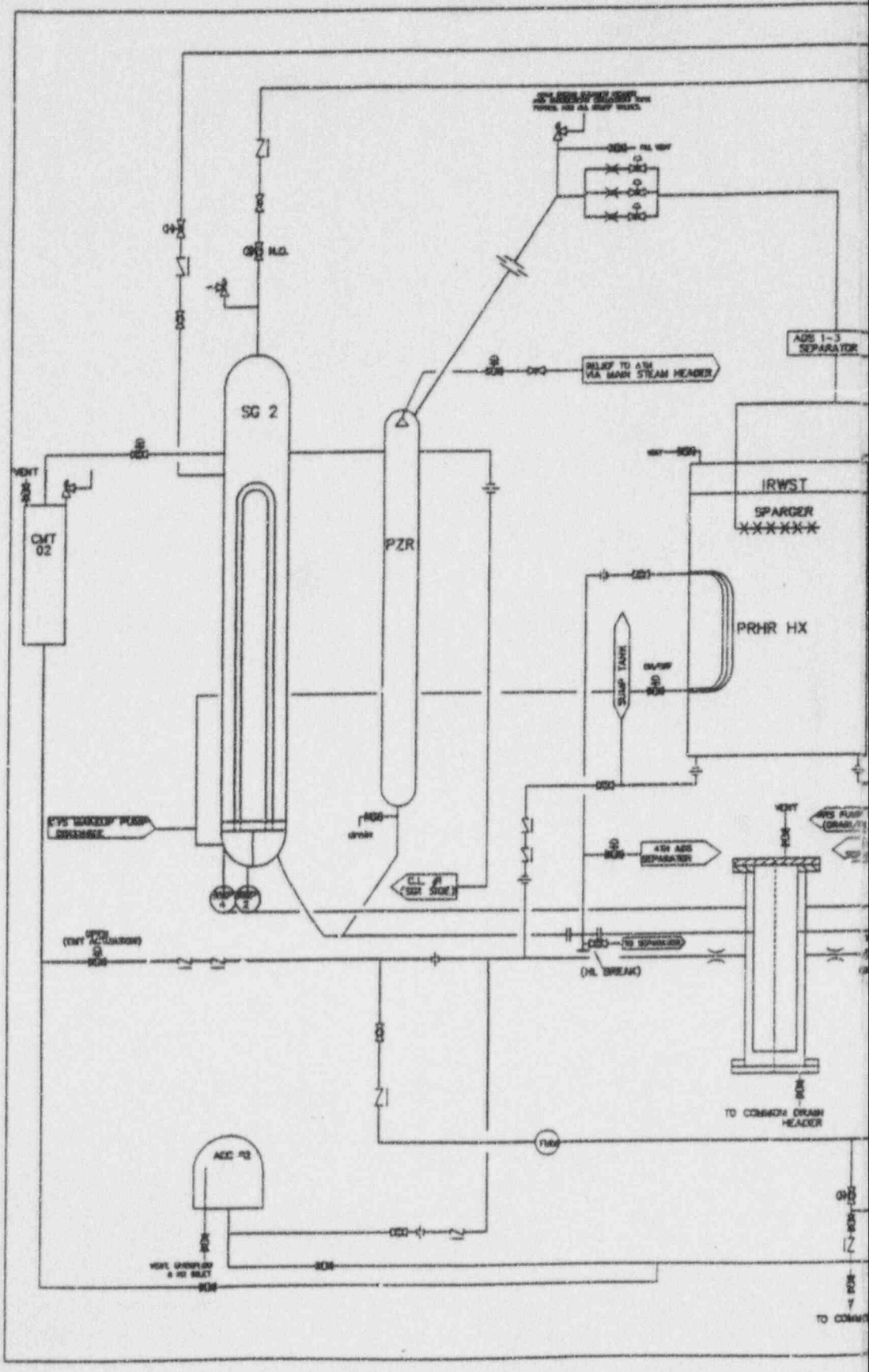
SG 2
PZR
CMT 02
IRWST
SPARGER
PRHR HX
ADS 1-3 SEPARATOR
4TH ADS SEPARATOR
RELIEF TO GTM VIA MAIN STEAM HEADER
(HL BREAK)
TO COMMON DRAIN HEADER
ACC #2
VENT

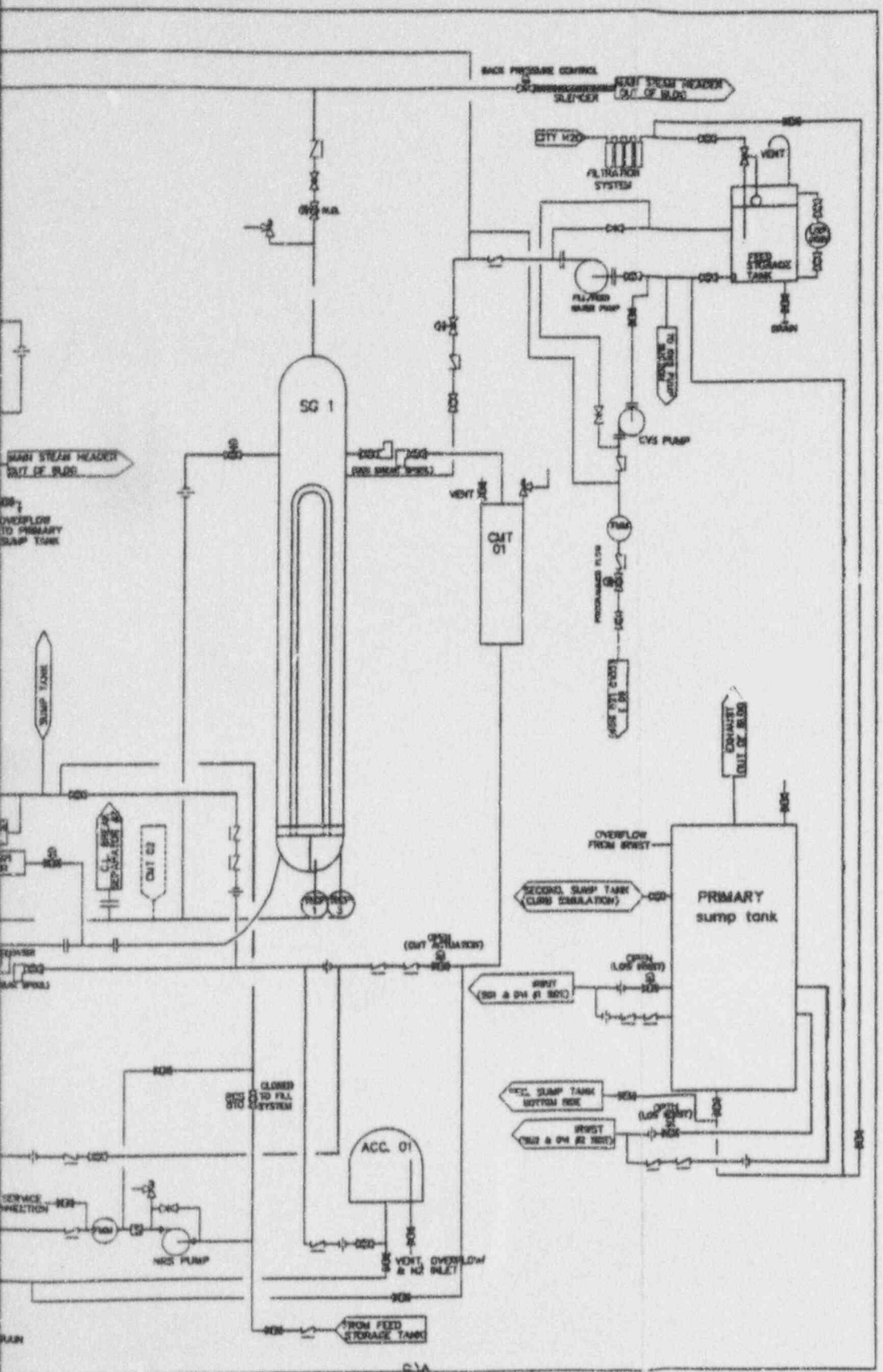

Figure 2.1-2 Simplified Flow Diagram of the OSU Test Facility

3.0 TEST SUMMARY

The following sections describe the test matrix and the data validation processes used for the low-pressure integral systems tests performed at Oregon State University (OSU). The initial test validation process was based on specific instruments that were required to function or selected backup instruments that were available. The *AP600 Low-Pressure Integral Systems Test at Oregon State University, Final Data Report*, WCAP-14252[1] describes the instrumentation from the tests and assesses their performance and reliability. The Test Analysis Report utilized the valid instrumentation to interpret the data.

3.1 Test Validation

As described in the *Final Data Report*[1] the OSU test facility data were reviewed and validated using a three-step process. The first step was performed at the OSU test facility. Immediately following each test, the data were recorded on a compact disc as a read-only file (CD-R), and documented in a Day-of-Test Report. The Day-of-Test Report evaluated the test from a very basic standpoint, including operability of key instruments and deviations from specified initial conditions. The Day-of-Test Report also documented any facility modifications or onsite test observations. The Day-of-Test Report assessed whether the test needed to be rerun because of some significant problem observed during the performance of the test.

The overall test acceptance criteria are shown in Table 3.1-1. Although not an explicit part of the pre-test acceptance criteria, an overall facility mass balance objective of 10 percent was established. The critical instruments were the minimum set of instruments required to perform a transient, component-by-component mass and energy balance.

The second step in the data validation process was performed by the test engineering personnel at the Westinghouse Energy Center in Monroeville, Pennsylvania. This step was performed after receiving the Day-of-Test Report and processing the CD-R. This data validation was documented in the Quick Look Report (QLR). The QLR provided a preliminary validation of all test data. The key purpose of the QLR was to issue some "pedigree" of the data, without specifically evaluating the data for code validation purposes (reviewed, but not yet validated, data) shortly after the test was performed.

The third step was a detailed review of the transient progression, facility and component performance, and cross-test comparisons as reported in the *Final Data Report*.[1]

The Test Analysis Report utilizes the insight derived from the instrumentation performance, and the transient progression gained in the *Final Data Report*,[1] to determine and understand the thermal-hydraulic behavior of the facility during each test. The objective of the analysis is to provide the explanation of the test facility response.

TABLE 3.1-1
OVERALL ACCEPTANCE CRITERIA

- Test initial conditions shall be achieved in a specified tolerance.
- Setpoints shall be achieved in an acceptable tolerance band.
- Sufficient instrumentation shall be operational before the test (exceptions shall be approved by the Westinghouse test engineer).
- Critical instruments not operating shall be identified to the Westinghouse test engineer before the tests. These instruments must be operational before and during the test, or exceptions should be approved.
- A zero check of LDPs, DPs, and FDPs shall be in acceptable tolerances.

  The zero check was eliminated from the acceptance criteria for Category III tests. The earlier pre-test and post-test checks of zero shift showed acceptable variation in the readings of these instruments. Performing these checks required that each instrument be manually isolated and then returned to service. Based on the consistency of the readings from earlier tests and the large number of manual operations, it was decided that the risk of an instrument remaining isolated after the check was greater than an instrument having a zero shift.

3.2 Test Matrix

Before the test matrix was initiated, a series of pre-operational tests were performed to provide an understanding of facility control and operating characteristics, to confirm design features essential to scaling, and to check that the instruments and the data acquisition system (DAS) were performing as expected. Tests were conducted while the facility was in cold conditions to measure system pressure drops and volume of the components. Pressure drops in the test facility were adjusted to the desired scaled AP600 values by using orifice plates. Pre-operational testing was also performed in the hot condition to characterize system heat losses. Results of the pre-operational tests are presented in Section 4, of the *Final Data Report*.[1]

System volume determination tests were performed for the accumulators, core makeup tanks (CMTs), pressurizer, in-containment refueling water storage tank (IRWST), sumps, steam generator (SG) secondary sides, and reactor vessel to compare the actual volumes with the calculated volumes for the facility used in the safety analysis computer codes.

Line resistance determination tests were performed to measure line resistance for the accumulator lines, IRWST lines, and sump injection lines for a given flow rate. The pressure drop in CMT injection and automatic depressurization system (ADS) 1-3 lines was measured over a range of flows. Resistance of the normal residual heat removal system (RNS) injection lines was measured to demonstrate that the pressure drops were within 10 percent of each other. The reactor coolant pump (RCP) head was measured for full flow and pump coastdown conditions. The line resistances also provided data for the computer models of the test facility.

Three separate hot functional tests were performed. The objectives of the tests were to demonstrate proper operation of the equipment prior to the formal matrix test program and to provide data necessary to document temperature characteristics of the system. The first hot functional test measured the steady-state heat loss, natural-circulation flow, and forced-flow characteristics. These tests verified the calculations used to help size the test facility. OSU-HS01 was performed to determine surface heat losses from the system at 100°, 200°, 300°, and 400°F; characterize passive residual heat removal (PRHR) under natural circulation and forced cooling; characterize the primary cooling system at 100, 300, 500, and 600 kW; and characterize the CMT natural-convection characteristics. The objective of the second test (OSU-HS02) was to verify the measuring capability of the break and ADS measurement system (BAMS) and the control of the ADS. The third hot functional test was an inadvertent ADS-1 actuation, and was used as a rehearsal for the formal matrix test program.

The formal test matrix summary given in Table 3.2-1 was designed to provide a wide range of test data on the performance of the passive emergency core cooling systems used in the AP600. The tests were intended to provide overlap with the full height, full pressure SPES-2 experiments[3] as well as the AP600 plant SSAR calculations. The test parameters investigated were:

- Cold-leg break sizes of 1/2, 1, 2, 4 (bottom of cold leg), and 4 in. (top and bottom of cold leg)

- Break locations of cold leg with CMTs, cold leg without CMTs, top of pipe, bottom of pipe, balance line breaks, direct vessel injection (DVI) line breaks, and no breaks with inadvertent ADS actuation
- Different single failures, one of four ADS-4 valves, ADS-1 valves, and ADS-3 valves
- Beyond design-basis experiments with multiple failures
- Spurious S signal (no break)

The break-size range and location, as well as the different assumed single-failure disruptions, provide a thorough and comprehensive set of integral systems data for code validation.

TABLE 3.2-1
OSU MATRIX TEST SUMMARY

Test No.	Break Size and Location	PRHR HX	CVS Pump	RNS Pump	ADS 4-1 (HL-1)	ADS 4-2 (HL-2)	Comments
SB01	2-in. CL-3 bottom of cold leg (CMT side)	On	Off	Off	50-percent flow area in AP600	100-percent flow area in AP600	Failure of one of two lines in ADS 4-1; reference cold-leg break case
SB04	2-in. CL-3 bottom of cold leg (CMT side)	On	On	On	50-percent flow area in AP600	100-percent flow area in AP600	Same as SB01 except safety and nonsafety system interaction
SB05	1-in. CL-3 bottom of cold leg (CMT side)	On	Off	Off	50-percent flow area in AP600	100-percent flow area in AP600	Same as SB01 except break size change
SB09	2-in. CL-3 to CMT-1 balance line	On	Off	Off	50-percent flow area in AP600	100-percent flow Area in AP600	Same as SB01 except different break location; asymmetric behavior of CMTs
SB10	DEG CL-3 to CMT-1 balance line	On	Off	Off	50-percent flow area in AP600	100-percent flow area in AP600	Limiting break on balance line; asymmetric behavior of CMTs; failure of one of two lines in ADS 4-1
SB12	DEG DVI-1 line break	On	Off	Off	100-percent flow area in AP600	100-percent flow area in AP600	Limiting break on DVI line; failure of one of two lines of ADS-1 and ADS-3
SB13	2-in. DVI-1 line break	On	Off	Off	50-percent flow area in AP600	100-percent flow area in AP600	Same as SB01 except different break location
SB14	Inadvertent ADS (no break)	On	Off	Off	50-percent flow area in AP600	100-percent flow area in AP600	No-break case with one failure of two lines in ADS 4-1
SB15	2-in. HL-2 bottom of pipe	On	Off	Off	50-percent flow area in AP600	100-percent flow area in AP600	Same as SB01 except break location

TABLE 3.2-1 (Continued)
OSU MATRIX TEST SUMMARY

Test No.	Break Size and Location	PRHR HX	CVS Pump	RNS Pump	ADS 4-1 (HL-1)	ADS 4-2 (HL-2)	Comments
SB18	2-in. CL-3 bottom of cold leg (CMT side)	On	Off	Off	50-percent flow area in AP600	100-percent flow area in AP600	Repeat test of SB01; confirm behavior of system and instrumentation
SB19	2-in. CL-3 bottom of cold leg (CMT side)	On	Off	Off	50-percent flow area in AP600	100-percent flow area in AP600	Same as SB01 except containment backpressure simulated
SB21	4-in. top of and 4-in. bottom of CL-3 (CMT side)	On	Off	Off	50-percent flow area in AP600	100-percent flow area in AP600	Same as SB01 except larger break size; largest break size simulated in matrix tests
SB23	1/2-in. CL-3 bottom of cold leg (CMT side)	On	Off	Off	50-percent flow area in AP600	100-percent flow area in AP600	Same as SB01 except smaller break size
SB24	1/2-in. CL-3 bottom of cold leg (CMT side)	On	On	On	50-percent flow area in AP600	100-percent flow area in AP600	Safety and nonsafety system interaction; single failure
SB26	Inadvertent ADS with multiple failures (no break)	Off	Off	Off	N/A isolate this line	N/A isolate this line	No-break PRA case with ADS-1 isolated and failure of one of two lines of ADS 4-1; PRHR HX isolated
SB28	DEG DVI-1 line break	Off	Off	Off	N/A isolate this line	N/A isolate this line	Limited break on DVI line with ADS 4-1, ADS 4-2, ACC-1, and PRHX HX isolated.
SB31	Spurious S signal (no break)	On	Off	Off	50-percent flow area in AP600	100-percent flow area in AP600	Failure of one of two lines in ADS 4-1

Note:
DEG -- double-ended guillotine
PRA -- probabilistic risk assessment

4.0 DATA REDUCTION METHODOLOGY

The AP600 incorporates and takes advantage of passive safety systems features, i.e., flows are driven by differences in temperature (natural convection) and elevation heads (gravity). The Oregon State University (OSU) test facility is a scaled model of the systems and components of the AP600 design important to the accident mitigation capability of the AP600 design. Data collected from the OSU test program is used to demonstrate that the safety analysis codes used for design-basis accidents can accurately and reliably predict the performance of the passive safety systems.

Computer software has been developed to reduce the experimental data collected from the OSU test facility into engineering parameters against which code predictions may be directly compared. The data analysis software performs calculations and generates plot files that contain these calculated engineering parameters. The calculations performed by this software include mass and energy balance calculations for the system.

This section describes the equations, and inputs to those equations, used to reduce the experimental data. The system of equations for each component/system are presented in separate subsections.

Ambient pressure and temperature for the laboratory environment were monitored during each test. The ambient pressure data channel was used to convert data from units of psig to units of psia for subsequent calculations, as opposed to using the constant 14.7. Ambient temperatures were used to evaluate heat loss from the test facility to the ambient. The ambient laboratory environment was monitored by the following data channels:

Channel ID	Function
PT-003	ambient pressure
TF-005	ambient temperature, lower elevation of test facility.
TF-006	ambient temperature, middle elevation of test facility
TF-007	ambient temperature, top elevation of test facility

4.1 LDP Compensation Function

Level transducers measure the variation in density of a vertical span relative to a reference. When the reference and the measured span are not at the same temperature, the effect of density differences need be accounted for to obtain a "true" level. The method of applying a compensation to level transducer outputs to account for differences in fluid density between the measured region and the reference leg is described below.

First, an average temperature for the column of water being monitored was calculated:

$$T_{AVG} = \frac{\sum_{i=1}^{n} T_i \, h_i}{\sum_{i=1}^{n} h_i} \qquad 4.1\text{-}1$$

where:

T	=	Temperature, °F
h	=	Span along the column that a temperature measurement was applied, in.

and the subscripts:

i	=	Index of data and time arrays
n	=	Total number of fluid temperature measurements in a column of water
AVG	=	Span-weighted average fluid temperature in the monitored water column

The fluid density in the monitored water column was then calculated as:

$$P_{AVG} = \rho \, (P, \min T_{AVG}, T_{SAT}) \qquad 4.1\text{-}2$$

where:

ρ	=	Density, lbm/ft.^{3}
P	=	Local pressure, psia

and the subscript:

SAT	=	Saturation temperature at local pressure

All other variables and subscripts are as previously defined.

The corrected fluid level of the monitored water column (that is, the compensated LDP reading denoted as LDP_{COMP}) was calculated as:

$$LDP_{COMP} = \frac{62.303}{\rho_{AVG}} LDP_{READING} \qquad 4.1\text{-}3$$

where:

62.303	=	Reference density of water, lbm/ft.^{3}
LDP	=	Reading from a level transducer, in.

and the subscripts:

COMP	=	Density-compensated value
READING	=	Data as recorded by the data acquisition system (DAS)

All level transducer data used in the calculation of mass inventories, energy of fluid volumes, and inferred flows were density-compensated prior to being used in such calculations.

4.2 Selected Level Compensations

A number of level transducer readings were density-compensated, the majority of which are calculated as part of the normal mass and energy calculations performed to support analysis of the data. However, a number of other compensated LDPs were calculated to support the *AP600 Low-Pressure Integral Systems Test at Oregon State University, Final Data Report*, WCAP-14252.[1] The list of these compensated LDPs, together with the pressures and temperatures used to compensate them, are listed in Table 4.2-1.

Note that, since these LDPs are not directly used in the mass and energy calculations performed as part of the analysis, no minimum or maximum range information is applied to the compensated LDP. Also, where more than one temperature data channel is listed for a level transducer, a straight numeric average on all the data channels is used. This is in contrast to the calculation modules, where, typically, only the subset of submerged channels is used.

TABLE 4.2-1 PRESSURES AND TEMPERATURES FOR COMPENSATED LDPs		
Name	**Pressure**	**Temperature(s)**
CLDP-104	PT-102	TF-166, TF-164, TF-165, TF-167, TF-147, TF-148, TF-149, TF-150
CLDP-109	PT-108	TR-001-1, TR-001-2, TR-001-3, TR-303-1, TR-303-2, TR-303-3, TR-313-1, TR-313-2, TR-313-3, TR-308-1
CLDP-110	PT-108	TR-001-4, TR-001-5, TR-001-6, TR-303-4, TR-303-5, TR-303-6, TR-313-4, TR-313-5, TR-313-6, TR-308-2, TR-308-3, TR-318-1, TR-318-2
CLDP-112	LDP-115 DP-114 LDP-113(1)	TF-169
CLDP-113	LDP-115 DP-114(2)	TF-169
CLDP-115	PT-107	TF-171
CLDP-116	PT-111	TF-126, TF-127, TF-162, TF-163, TF-164, TF-165, TF-155, TF-156, TF-130, TF-131, TF-147, TF-148
CLDP-127	PT-107	TF-126, TF-127, TF-162, TF-163, TF-164, TF-165, TF-155, TF-156, TF-130, TF-131, TF-147, TF-148
CLDP-138	PT-108	TR-001-1, TR-001-2, TR-001-3, TR-303-1, TR-303-2, TR-303-3, TR-313-1, TR-313-2, TR-313-3, TR-308-1, TR-001-4, TR-001-5, TR-001-6, TR-303-4, TR-303-5, TR-303-6, TR-313-4, TR-313-5, TR-313-6, TR-308-2, TR-308-3, TR-318-1, TR-318-2
CLDP-139	PT-107	TF-169
CLDP-140	PT-111	TF-126, TF-127, TF-162, TF-163, TF-164, TF-165, TF-155, TF-156, TF-130, TF-131, TF-147, TF-148
CLDP-801	PT-202	TF-803

Note:

(1) These three levels were converted to inches of water.

(2) These two levels were converted to inches of water.

4.3 Accumulators

4.3.1 Fluid Mass Conservation Equations

Each of the two accumulators consists of a tank with a fluid flow path at the bottom connected to the direct vessel injection line. The general fluid (H_2O) mass conservation equation, which relates the change in stored fluid mass with respect to time (the fluid-mass time derivative) to the mass flow rates in and out, reduces to the following for each of the two accumulators, ACC_i, where i = 1,2:

$$\frac{dM_{H_2O,ACC_i}}{dt} = - W_{out\ H_2O,ACC_i} \qquad 4.3\text{-}1$$

Due to the fact that no steam is present in the accumulators, the fluid mass conservation equation further simplifies to:

$$\frac{dM_{water,ACC_i}}{dt} = - W_{out\ water,ACC_i} \qquad 4.3\text{-}2$$

From this point on in the discussions of the mass conservation calculations, the expressions will be in their reduced, water-only form.

The left-hand side of the water mass conservation equation is approximated from the value of the water mass at two consecutive time points as follows, where i = 1,2:

$$\frac{dM_{water,ACC_i}}{dt} \approx \frac{\Delta M_{water,ACC_i}}{\Delta t} = \frac{M^{n}_{water,ACC_i} - M^{n-1}_{water,ACC_i}}{t^{n} - t^{n-1}} \qquad 4.3\text{-}3$$

The water mass calculations are based on measured water level. In general, the water mass may be expressed as follows, where i = 1,2:

$$M_{water,ACC_i} = \rho_{water,ACC_i} \times V_{water,ACC_i} \times C_3 \qquad 4.3\text{-}4$$

where:

C_3 = Conversion constant, 1 ft.^{3}/1728 in.^{3}

Due to the cylindrical shape of the accumulator tanks, the water volume is calculated as follows, where i = 1,2:

$$V_{water,ACC_i} = L_{water,ACC_i} \times A_{ACC_i} \qquad 4.3\text{-}5$$

Thus, the water mass expression becomes, where i = 1,2:

$$M_{water,ACC_i} = \rho_{water,ACC_i} \times L_{water,ACC_i} \times A_{ACC_i} \times C_3 \qquad 4.3\text{-}6$$

Rather than using the LDP compensation method to calculate the actual water level from the measured water level as is done for many other plant components, an equivalent approach is employed. Using the concept of head and recalling that measured water levels (LDPs) are applicable (calibrated) at a reference density, the following is true:

$$\Delta P \text{ [psi]} = \rho_{actual} \times L_{actual} \times \left(\frac{g}{g_c}\right) \times C_3 = \rho_{ref} \times LDP \times \left(\frac{g}{g_c}\right) \times C_3 \qquad 4.3\text{-}7$$

so that, in the case of the accumulators, for i = 1,2:

$$\rho_{water,ACC_i} \times L_{water,ACC_i} = \rho_{ref,ACC_i} \times LDP\text{-}XXX_{ACC_i} \qquad 4.3\text{-}8$$

Thus, the water mass expression becomes, where i = 1,2:

$$M_{water,ACC_i} = \rho_{ref,ACC_i} \times LDP\text{-}XXX_{ACC_i} \times A_{ACC_i} \times C_3 \qquad 4.3\text{-}9$$

It was discovered that the measured water level for the accumulators in certain OSU tests was incorrect due to air in the sense line. For those tests in question, the following correction was developed, where i = 1,2:

$$LDP_{corr,ACC_i} = C_{ACC_i} \times F_{ACC_i} \times LDP\text{-}XXX_{ACC_i} \qquad 4.3\text{-}10$$

$C_{ACC\,i}$ is the following constant based on initial conditions:

$$C_{ACC_i} = \left[\frac{span_{ACC_i}}{(LDP\text{-}XXX_{ACC_i})_{initial}}\right] \times \left[\frac{(P_{ACC_i} \times v_{air,ACC_i}/Z_{air,ACC_i})_{initial}}{(P_{ambient} \times v_{air,ambient}/Z_{air,ambient})_{initial}}\right] \qquad 4.3\text{-}11$$

$F_{ACC\,i}$ is given by the following:

$$F_{ACC_i} = \left[\frac{(P_{ambient} \times v_{air,ambient}/Z_{air,ambient})_{initial}}{(P_{ACC_i} \times v_{air,ACC_i}/Z_{air,ACC_i})_{transient}}\right] \qquad 4.3\text{-}12$$

In the previous equation, the specific volume ($ft.^3$/lbm) and compressibility factor of air are given by the following functions of pressure (psia), respectively:

$$v_{air} = 301.39 \times P^{-1.0788}$$

$$Z_{air} = 1.0\times10^{-8} \times P^2 + 3.0\times10^{-5} \times P + 1.0002 \qquad 4.3\text{-}13$$

In the tests without air in the sense line, the factors $C_{ACC\,i}$ and $F_{ACC\,i}$ are both set to 1.0 to "deactivate" the LDP correction.

Thus, the final expression for the water mass is as follows, where i = 1,2:

$$M_{water,ACC_i} = \rho_{ref,ACC_i} \times LDP_{corr,ACC_i} \times A_{ACC_i} \times C_3 \qquad 4.3\text{-}14$$

This completes the discussion of the calculations related to the left-hand side of the water mass conservation equation.

On the right-hand side of the water mass conservation equation, the calculation of the outlet water mass flow rate is performed directly from the liquid volumetric flow rate (FMM) measurement as follows, where i = 1,2:

$$W_{out\ water,ACC_i} = \max(0., FMM\text{-}XXX_{ACC_i}) \times \rho_{water,ACC_i} \times C_1 \qquad 4.3\text{-}15$$

where:

C_1 = Conversion constant, 1 ft.^{3}/sec./448.86 gpm

The water density is simply the reciprocal of the water-specific volume, where i = 1,2:

$$\rho_{water,ACC_i} = \frac{1.0}{v_{water,ACC_i}} \qquad 4.3\text{-}16$$

The water-specific volume is calculated from the ASME steam table function VCL as follows, where i = 1,2:

$$v_{water,ACC_i} = VCL(P_{ACC_i}, T_{water,ACC_i}) \qquad 4.3\text{-}17$$

The water temperature is given by the fluid thermocouple measurement. Care is taken to insure that the water temperature value employed is at or below the saturation temperature. Thus, for i = 1,2:

$$T_{water,ACC_i} = \min(TF\text{-}XXX_{ACC_i}, T_{sat,ACC_i}) \qquad 4.3\text{-}18$$

The saturation temperature is calculated from the ASME steam table function TSL as follows, where i = 1,2:

$$T_{sat,ACC_i} = TSL(P_{ACC_i}) \qquad 4.3\text{-}19$$

In all of the above, accumulator pressure, $P_{ACC\,i}$, is set equal to the value from the corresponding $PT\text{-}XXX_{ACC\,i}$ measurement after conversion from gauge (psig) to absolute (psia) pressure.

This completes the discussion of the calculations related to the right-hand side of the water mass conservation equation.

Note that in the case of the accumulators, it is possible to calculate all quantities on both the left-hand side and right-hand side of the fluid mass conservation equation. This information can then be used to check the fluid mass conservation equation.

Finally, a complete list of the applicable data for both accumulators appears in Table 4.3-1, including the level instrument channel ID (LDP-$XXX_{ACC\,i}$), the pressure measurement ID (PT-$XXX_{ACC\,i}$), the fluid thermocouple measurement ID (TF-$XXX_{ACC\,i}$), the outlet liquid volumetric flow rate measurement ID (FMM-$XXX_{ACC\,i}$), the water reference density, the water level span, and the tank cylindrical area.

4.3.2 Fluid Energy Conservation Equations

The general fluid (H_2O) energy conservation equation, which relates the change in stored fluid energy with respect to time (the fluid-energy time derivative) to the energy rates in and out (due to the connected flow paths) and the energy addition rate due to other external devices, reduces to the following for each of the two accumulator, ACC_i, where i = 1,2:

$$\frac{d[M \times c_p \times (T-T_{ref})]_{H_2O,ACC_i}}{dt} = - Q_{out\ H_2O,ACC_i} + Q_{[metal \Rightarrow H_2O],ACC_i} \qquad 4.3\text{-}20$$

Due to the fact that no steam is present in the accumulators, the fluid energy conservation equation further simplifies to:

$$\frac{d[M \times c_p \times (T-T_{ref})]_{water,ACC_i}}{dt} = - Q_{out\ water,ACC_i} + Q_{[metal \Rightarrow water],ACC_i} \qquad 4.3\text{-}21$$

From this point on in the discussions of the energy conservation calculations, the expressions will be in their reduced, water-only form.

The left-hand side of the water energy conservation equation is approximated as follows, where i = 1,2:

$$\frac{d[M \times c_p \times (T-T_{ref})]_{water,ACC_i}}{dt} \approx \frac{\Delta[M \times c_p \times (T-T_{ref})]_{water,ACC_i}}{\Delta t} \qquad 4.3\text{-}22$$

and

$$\frac{\Delta[M \times c_p \times (T-T_{ref})]_{water,ACC_i}}{\Delta t} \approx c_{p_{water,ACC_i}} \times \left[\frac{\Delta[M \times (T-T_{ref})]_{water,ACC_i}}{\Delta t}\right]$$

$$\approx c_{p_{water,ACC_i}} \times (T_{water,ACC_i}-T_{ref}) \times \left[\frac{M^{n}_{water,ACC_i} - M^{n-1}_{water,ACC_i}}{t^{n}-t^{n-1}}\right] \quad 4.3\text{-}23$$

$$+ c_{p_{water,ACC_i}} \times M_{water,ACC_i} \times \left[\frac{T^{n}_{water,ACC_i} - T^{n-1}_{water,ACC_i}}{t^{n}-t^{n-1}}\right]$$

The water-specific heat capacity at constant pressure is calculated from the ASME steam table function CPL as follows, where i = 1,2:

$$c_{p_{water,ACC_i}} = CPL(P_{ACC_i}, T_{water,ACC_i}) \quad 4.3\text{-}24$$

This completes the discussion of the calculations related to the left-hand side of the water energy conservation equation.

On the right-hand side of the water energy conservation equation, the calculation of the outlet water energy transport rate is given by the following, where i = 1,2:

$$Q_{out\ water,ACC_i} = W_{out\ water,ACC_i} \times h_{water,ACC_i} \quad 4.3\text{-}25$$

The water-specific enthalpy is calculated from the ASME steam table function HCL as follows:

$$h_{water,ACC_i} = HCL(P_{ACC_i}, T_{water,ACC_i}, S_{water,ACC_i}) \quad 4.3\text{-}26$$

Due to the fact that the heat transfer from the accumulator metal to the fluid is insignificant, the energy addition rate from the metal is neglected. Thus, for i = 1,2:

$$Q_{(metal \Rightarrow water),ACC_i} = 0.0 \qquad 4.3\text{-}27$$

This completes the discussion of the calculations related to the right-hand side of the water energy conservation equation.

Note that, in the case of the accumulators, it is possible to calculate all quantities on both the left-hand side and right-hand side of the fluid energy conservation equation. This information can then be used to check the fluid energy conservation equation.

TABLE 4.3-1 INSTRUMENTATION EMPLOYED FOR ACC FLUID CALCULATIONS		
Description	**ACC-1**	**ACC-2**
Level ID (in.)	LDP-401	LDP-402
Pressure ID (psig)	PT-401	PT-402
Water temp ID (°F)	TF-401	TF-402
Outlet flow ID (gpm)	FMM-401	FMM-402
Ref water ρ ($lbm/ft.^3$)	62.40	62.40
Water level span (in.)	36.75	37.00
Tank area (cylin) ($in.^2$)	416.6208	417.1392

4.4 Core Make-Up Tanks and Cold-Leg Balance Lines

4.4.1 Mass Conservation Equations

Each of the two core makeup tanks (CMTs) consists of a tank with a fluid flow path at the top for the cold-leg balance line (CLBL) connection and a fluid flow path at the bottom for the direct vessel injection line (DVI) connection. The general fluid (H_2O) mass conservation equation, which relates the change in stored mass with respect to time (the mass-time derivative) to the mass flow rates in and out, reduces to the following for each of the two CMTs, CMT_i, where i = 1,2:

$$\frac{dM_{H_2O,CMT_i}}{dt} = W_{in\ (from\ CLBL_i)\ H_2O,CMT_i} - W_{out\ (to\ DVI_i)\ H_2O,CMT_i} \qquad 4.4\text{-}1$$

The left-hand side of the fluid mass conservation equation is approximated from the value of the fluid mass at two consecutive time points as follows, where i = 1,2:

$$\frac{dM_{H_2O,CMT_i}}{dt} \approx \frac{\Delta M_{H_2O,CMT_i}}{\Delta t} = \frac{M^{n}_{H_2O,CMT_i} - M^{n-1}_{H_2O,CMT_i}}{t^{n} - t^{n-1}} \qquad 4.4\text{-}2$$

The H_2O fluid mass is the sum of the water and steam masses, where i = 1,2:

$$M_{H_2O,CMT_i} = M_{water,CMT_i} + M_{steam,CMT_i} \qquad 4.4\text{-}3$$

The water and steam mass calculations are based upon the measured tank water level. A list of the level (LDP-XXX) instrument channel IDs for both CMTs appears in Table 4.4-1. To span the entire tank, either the main LDP, or a sum of the three alternate LDPs, is employed for the indicated water level, which is then corrected for temperature effects using the LDP compensation method. As is generally assumed for each plant component, pure water is modeled below the compensated water level, and pure steam is modeled above the compensated water level.

To utilize the measurements from the numerous tank fluid thermocouples available, each CMT is divided into a number of axial fluid property zones for the calculation of various fluid conditions. Table 4.4-1 contains a list of the fluid thermocouples employed (ten per tank), along with their elevations. Axial fluid property zone boundaries are arbitrarily taken at the vertical midpoint between consecutive fluid thermocouples, which yields ten zones per tank. Figures 4.4-1 and 4.4-2 illustrate the location of the fluid thermocouples and axial fluid property zones for CMT-1 and CMT-2, respectively.

In general, the tank water and steam masses are given by, where i = 1,2:

$$M_{water,CMT_i} = \sum_{j=1}^{N_{zone,CMT_i}} M_{water,CMT_{ij}}$$

$$M_{steam,CMT_i} = \sum_{j=1}^{N_{zone,CMT_i}} M_{steam,CMT_{ij}} \qquad 4.4\text{-}4$$

For zones j below those containing the compensated water level (which contain all water), the zone j water and steam masses are given by, where i = 1,2 and j = 1,...,levzone-1:

$$M_{water,CMT_{ij}} = \rho_{water,CMT_{ij}} \times V_{zone,CMT_{ij}} \times C_3$$

$$M_{steam,CMT_{ij}} = 0. \qquad 4.4\text{-}5$$

For the zone j containing the compensated water level, the zone j water and steam masses are given by, where i = 1,2 and j = levzone:

$$M_{water,CMT_{ij}} = \rho_{water,CMT_{ij}} \times V_{water,zone,CMT_{ij}} \times C_3$$

$$M_{steam,CMT_{ij}} = \rho_{steam,CMT_{ij}} \times V_{steam,zone,CMT_{ij}} \times C_3 \qquad 4.4\text{-}6$$

For zones j above those containing the compensated water level, which contain all steam, the zone j water and steam masses are given by, where i = 1,2 and j = levzone+1,...,$N_{zone,CMT\,i}$:

$$M_{water,CMT_{ij}} = 0.$$

$$M_{steam,CMT_{ij}} = \rho_{steam,CMT_{ij}} \times V_{zone,CMT_{ij}} \times C_3 \qquad 4.4\text{-}7$$

The tank fluid volumes are calculated as a function of level from the volume versus height tabular data listed in Table 4.4-2, via linear interpolation within the table. No extrapolation at either end is performed; the first and last table points define the applicable range (the first point is [hmin (= 0.), Vmin (= 0.)], and the last point is [hmax, Vmax].

During initialization, the volume versus height data/function is employed to calculate the total volume of each zone j as follows, where i = 1,2:

for j=1:

$$V_{zone,CMT_{ij}} = V_{function}(E_{top,CMT_{ij}})$$

4.4-8

for $j=2,\ldots,N_{zone,CMT_i}$:

$$V_{zone,CMT_{ij}} = V_{function}(E_{top,CMT_{ij}}) - \sum_{k=1}^{j-1} V_{zone,CMT_{ik}}$$

The zone j top elevations are determined from the elevations of the fluid thermocouples (or the elevation of the top of the tank in the case of the top zone) as depicted in Figures 4.4-1 and 4.4-2.

During the transient calculations, the volume versus height data/function is employed to calculate the water volume of the zone containing the compensated water level, j = levzone, as follows, where i = 1,2:

if j(=levzone)=1:

$$V_{water,zone,CMT_{ij}} = V_{function} \times (L_{water,CMT_i})$$

4.4-9

if j(=levzone)>1:

$$V_{water,zone,CMT_{ij}} = V_{function} \times (L_{water,CMT_i}) - \sum_{k=1}^{j-1} V_{zone,CMT_{ik}}$$

The steam volume of the zone containing the compensated water level, j = levzone, is then simply the following, where i = 1,2:

$$V_{steam,zone,CMT_i} = V_{zone,CMT_i} - V_{water,zone,CMT_i} \qquad 4.4\text{-}10$$

The zone j water and steam densities are simply the reciprocal of the water- and steam-specific volumes, respectively, where i = 1,2:

$$\rho_{water,CMT_i} = \frac{1.}{V_{water,CMT_i}}$$
$$\rho_{steam,CMT_i} = \frac{1.}{V_{steam,CMT_i}} \qquad 4.4\text{-}11$$

The zone j water-specific volume is calculated from the ASME steam table function VCL as follows, where i = 1,2:

$$v_{water,CMT_i} = VCL(P_{zone,CMT_i}, T_{water,CMT_i}) \qquad 4.4\text{-}12$$

The zone j steam-specific volume is calculated from the ASME steam table function HSS as follows, where i = 1,2:

$$h_{steam,CMT_i} = HSS(P_{zone,CMT_i}, T_{steam,CMT_i}, V_{steam,CMT_i}) \qquad 4.4\text{-}13$$

The zone j water and steam temperatures are simply given by the zone temperatures, which are the fluid thermocouple measurements TF-XXX (see Table 4.4-1, in conjunction with Figures 4.4-1 and 4.4-2). Care is taken to insure that the water temperature value employed is at or below the saturation temperature, and that the steam temperature value employed is at or above the saturation temperature. Thus, for i = 1,2:

$$T_{water,CMT_i} = \min(T_{zone,CMT_i}, T_{sat,CMT_i})$$
$$T_{steam,CMT_i} = \max(T_{zone,CMT_i}, T_{sat,CMT_i}) \qquad 4.4\text{-}14$$

where:

$$T_{zone,\ CMT_i} = TF\text{-}XXX_{CMT_i}$$

The zone j saturation temperature is calculated from the ASME steam table function TSL as follows, where i = 1,2:

$$T_{sat,CMT_{ij}} = TSL(P_{zone,CMT_{ij}}) \qquad 4.4\text{-}15$$

The pressure of the top zone is set equal to the value from the $PT\text{-}XXX_{CMT\ i}$ measurement (see Table 4.4-1 for list) (after conversion from gauge [psig] to absolute [psia] pressure). For the zones below, the pressure is adjusted for hydrostatic effects (to account for the density differences which occur from zone to zone throughout the tank).

This completes the discussion of the calculations related to the left-hand side of the fluid mass conservation equation.

On the right-hand side of the fluid mass conservation equation, the CMT inlet fluid mass flow rate is simply equal to the CLBL outlet fluid mass flow rate (which appears on the right-hand side of the CLBL mass conservation equation), where i = 1,2:

$$W_{in\ (from\ CLBL_i)\ H_2O,CMT_i} = W_{out\ (to\ CMT_i)\ H_2O,CLBL_i} \qquad 4.4\text{-}16$$

Although a liquid volumetric flow rate measurement (FMM) is available for this line, it cannot be relied on for accurate mass flow rate calculations due to the two-phase flow which exists. Thus, the total mass flow rate must be inferred from a combination of the CMT and CLBL mass conservation equations.

Regarding the CMT outlet fluid mass flow rate to the DVI line, the calculation may be performed directly from the liquid volumetric flow rate measurement (FMM-XXX), due to the fact that the water flowing in the line remains subcooled (see Table 4.4-1 for the instrument channel IDs). Thus, for i = 1,2:

$$W_{out\ (to\ DVIL_i)\ H_2O,CMT_i} = W_{out\ (to\ DVIL_i)\ water,CMT_i}$$

$$= \max(0., FMM\text{-}XXX_{CMT/DVIL_i}) \times \rho_{water,CMT/DVIL_i} \times C_1 \qquad 4.4\text{-}17$$

The outlet line water density is simply the reciprocal of the outlet line water-specific volume, where i = 1,2:

$$\rho_{water,CMT/DVIL_i} = \frac{1}{v_{water,CMT/DVIL_i}} \qquad 4.4\text{-}18$$

The outlet line water-specific volume is calculated from the ASME steam table function VCL as follows, where i = 1,2:

$$v_{water,CMT/DVIL_i} = VCL(P_{CMT/DVIL_i}, T_{water,CMT/DVIL_i}) \qquad 4.4\text{-}19$$

The outlet line water temperature is simply given by the outlet line fluid thermocouple measurement TF-XXX (see Table 4.4-1). Care is taken to insure that the water temperature value employed is at or below the saturation temperature. Thus, for i = 1,2:

$$T_{water,CMT/DVIL_i} = \min(TF\text{-}XXX_{CMT/DVIL_i}, T_{sat,CMT/DVIL_i}) \qquad 4.4\text{-}20$$

The outlet line saturation temperature is calculated from the ASME steam table function TSL as follows, where i = 1,2:

$$T_{sat,CMT/DVIL_i} = TSL(P_{CMT/DVIL_i}) \qquad 4.4\text{-}21$$

The pressure in the outlet line is equal to the pressure at the bottom of the tank.

This completes the discussion of the calculations related to the right-hand side of the fluid mass conservation equation.

4.4.2 Energy Conservation Equations

The general fluid (H_2O) energy conservation equation, which relates the change in stored energy with respect to time (the energy time derivative) to the energy rates in and out (due to the connected flow paths) and the energy addition rate due to other external devices, reduces to the following for each of the two CMTs, CMT_i, where i = 1,2:

$$\frac{d[M \times c_p \times (T-T_{ref})]_{H_2O,CMT_i}}{dt} = Q_{in\ (from\ CLBL_i)\ H_2O,CMT_i} - Q_{out\ (to\ DVIL_i)\ H_2O,CMT_i} + Q_{[metal \Rightarrow H_2O],CMT_i} \qquad 4.4\text{-}22$$

The left-hand side of the energy conservation equation is approximated as follows, where i = 1,2:

$$\frac{d[M \times c_p \times (T-T_{ref})]_{H_2O,CMT_i}}{dt} \approx \sum_{j=1}^{N_{water,CMT_i}} \frac{\Delta[M \times c_p \times (T-T_{ref})]_{water,CMT_{ij}}}{\Delta t} + \sum_{j=1}^{N_{steam,CMT_i}} \frac{\Delta[M \times c_p \times (T-T_{ref})]_{steam,CMT_{ij}}}{\Delta t} \qquad 4.4\text{-}23$$

where:

$$\frac{\Delta[M \times c_p \times (T-T_{ref})]_{water,CMT_{ij}}}{\Delta t} \approx c_{p_{water,CMT_{ij}}} \times \left[\frac{\Delta[M \times (T-T_{ref})]_{water,CMT_{ij}}}{\Delta t}\right]$$

$$\approx c_{p_{water,CMT_{ij}}} \times (T_{water,CMT_{ij}} - T_{ref}) \times \left[\frac{M^{n}_{water,CMT_{ij}} - M^{n-1}_{water,CMT_{ij}}}{t^{n} - t^{n-1}}\right] + c_{p_{water,CMT_{ij}}} \times M_{water,CMT_{ij}} \times \left[\frac{T^{n}_{water,CMT_{ij}} - T^{n-1}_{water,CMT_{ij}}}{t^{n} - t^{n-1}}\right] \qquad 4.4\text{-}24$$

and

$$\frac{\Delta[M \times c_p \times (T-T_{ref})]_{steam,CMT_{ij}}}{\Delta t} = c_{p_{steam,CMT_{ij}}} \times \left[\frac{\Delta[M \times (T-T_{ref})]_{steam,CMT_{ij}}}{\Delta t}\right]$$

$$= c_{p_{steam,CMT_{ij}}} \times (T_{steam,CMT_{ij}}-T_{ref}) \times \left[\frac{M^{n}_{steam,CMT_{ij}} - M^{n-1}_{steam,CMT_{ij}}}{t^{n}-t^{n-1}}\right] \quad 4.4\text{-}25$$

$$+ c_{p_{steam,CMT_{ij}}} \times M_{steam,CMT_{ij}} \times \left[\frac{T^{n}_{steam,CMT_{ij}} - T^{n-1}_{steam,CMT_{ij}}}{t^{n}-t^{n-1}}\right]$$

The zone j water-specific heat capacity at constant pressure is calculated from the ASME steam table function CPL as follows, where i = 1,2:

$$c_{p_{water,CMT_{ij}}} = CPL(P_{zone,CMT_{ij}}, T_{water,CMT_{ij}}) \quad 4.4\text{-}26$$

The zone j steam-specific heat capacity at constant pressure is calculated from the ASME steam table function CPV as follows, where i = 1,2:

$$c_{p_{steam,CMT_{ij}}} = CPV(P_{zone,CMT_{ij}}, T_{steam,CMT_{ij}}, v_{steam,CMT_{ij}}) \quad 4.4\text{-}27$$

This completes the discussion of the calculations related to the left-hand side of the fluid energy conservation equation.

On the right-hand side of the fluid energy conservation equation, the CMT inlet fluid energy transport rate is simply equal to the CLBL outlet fluid energy transport rate (which appears in the CLBL energy conservation equation), where i = 1,2:

$$Q_{in\ (from\ CLBL_i)\ H_2O,CMT_i} = Q_{out\ (to\ CMT_i)\ H_2O,CLBL_i} \quad 4.4\text{-}28$$

In a manner analogous to that performed for the corresponding term on the right-hand side of the fluid mass conservation equation, the above CMT inlet fluid energy transport rate term must be inferred from a combination of the CMT and CLBL energy conservation equations, due to the two-phase flow which exists.

The CMT outlet fluid energy transport rate to the DVI line is given by the following, where i = 1,2:

$$Q_{out\ (to\ DVIL_i)\ H_2O,CMT_i} = Q_{out\ (to\ DVIL_i)\ water,CMT_i} \qquad 4.4\text{-}29$$

$$= W_{out\ (to\ DVIL_i)\ water,CMT_i} \times h_{water,CMT/DVIL_i}$$

The outlet line water-specific enthalpy is calculated from the ASME steam table function HCL as follows, where i = 1,2:

$$h_{water,CMT/DVIL_i} = HCL(P_{CMT/DVIL_i}, T_{water,CMT/DVIL_i}, S_{water,CMT/DVIL_i}) \qquad 4.4\text{-}30$$

For the detailed analyses of the heat transfer between the fluid and the metal wall in each of the two CMTs, the CONTRA inverse heat conduction solution is employed to calculate the transient inner surface heat fluxes and temperatures, given the transient temperature data collected from thermocouples imbedded in the walls of the CMTs. The CONTRA inverse heat conduction calculational method[14] models a wall as a one-dimensional cylinder in radial coordinates, and applies to each axial position at which wall thermocouples are located in the OSU CMTs. Table 4.4-3 lists the wall thermocouple channel IDs used for each metal segment of both CMTs. A stand-alone pre-processor code ("osucontra", the OSU CONTRA driver software) employs the CONTRA inverse heat conduction solution on the transient wall thermocouple temperature data for the modeled metal segments of each of the two CMTs and calculates the transient inner surface heat flux and temperature for each of these metal segments.

Therefore, the energy addition rate to the fluid due to heat transfer from the CMT metal is given by the following, where i = 1,2:

$$Q_{[metal \Rightarrow H_2O],CMT_i} = \frac{\sum_{m=1}^{N_{metal,CMT_i}} Q_{flux\ [metal \Rightarrow H_2O],CMT_{i,m}} \times A_{metal\ inner\ surf,\ CMT_{i,m}}}{C_4} \qquad 4.4\text{-}31$$

where:

C_4 = Conversion constant, 3600 sec./1 hr.

This completes the discussion of the calculations related to the right-hand side of the fluid energy conservation equation.

4.4.3 Fluid Mass Conservation Equations

Each of the two CLBL consists of a series of connected pipes with a fluid flow path at the bottom for the inlet connection from the cold leg and a fluid flow path at the top for the outlet connection to the CMT. The general fluid (H_2O) mass conservation equation, which relates the change in stored fluid mass with respect to time (the fluid mass time derivative) to the mass flow rates in and out, reduces to the following for each of the two CLBL, $CLBL_i$, where i = 1,2:

$$\frac{dM_{H_2O,CLBL_i}}{dt} = W_{in\ (from\ CL)\ H_2O,CLBL_i} - W_{out\ (to\ CMT)\ H_2O,CLBL_i} \qquad 4.4\text{-}32$$

The left-hand side of the fluid mass conservation equation is approximated from the value of the fluid mass at two consecutive time points as follows, where i = 1,2:

$$\frac{dM_{H_2O,CLBL_i}}{dt} \approx \frac{\Delta M_{H_2O,CLBL_i}}{\Delta t} = \frac{M^{n}_{H_2O,CLBL_i} - M^{n-1}_{H_2O,CLBL_i}}{t^{n} - t^{n-1}} \qquad 4.4\text{-}33$$

The H_2O fluid mass is simply the sum of the water and steam masses, where i = 1,2:

$$M_{H_2O,CLBL_i} = M_{water,CLBL_i} + M_{steam,CLBL_i} \qquad 4.4\text{-}34$$

The water and steam mass calculations are based upon the measured water level. A list of the level (LDP-XXX) instrument channel IDs for both CLBLs appears in Table 4.4-4. These LDPs are corrected for temperature effects using the LDP compensation method. As is generally assumed for each plant component, pure water is modeled below the compensated water level, and pure steam is modeled above the compensated water level.

For the fluid property calculations, the measurements from the two fluid thermocouples available in each CLBL are utilized. Table 4.4-4 contains a list of these fluid thermocouples; one is located at the very bottom of the line and one is located at the very top of the line. If the line is completely filled with water (water level at top), an average of the two fluid thermocouple temperatures is employed for the water properties. If the line consists of all steam (water level at bottom), an average of the two fluid thermocouple temperatures is employed for the steam properties. Otherwise (water level in between top and bottom), the bottom fluid thermocouple temperature is employed for the water properties, and the top fluid thermocouple temperature is employed for the steam properties.

In general, the water and steam masses are given by, where i = 1,2:

$$M_{water,CLBL_i} = \rho_{water,CLBL_i} \times V_{water,CLBL_i} \times C_3$$
$$M_{steam,CLBL_i} = \rho_{steam,CLBL_i} \times V_{steam,CLBL_i} \times C_3 \qquad 4.4\text{-}35$$

The water volume is calculated as a function of compensated water level from the volume versus height tabular data listed in Table 4.4-5, via linear interpolation within the table. No extrapolation at either end is performed; the first and last table points define the applicable range (the first point is $[h_{min} (= 0.), V_{min} (= 0.)]$, and the last point is $[h_{max}, V_{max}]$. Thus, for i = 1,2:

$$V_{water,CLBL_i} = V_{function}(L_{water,CLBL_i}) \qquad 4.4\text{-}36$$

The steam volume is then simply the following, where i = 1,2:

$$V_{steam,CLBL_i} = V_{CLBL_i} - V_{water,CLBL_i} \qquad 4.4\text{-}37$$

In the above, the CLBL total volume, $V_{CLBL,i}$, is simply given by the last point (V_{max}) in the aforementioned volume versus height table.

The water and steam densities are simply the reciprocal of the water- and steam-specific volumes, respectively, where i = 1,2:

$$\rho_{water,CLBL_i} = \frac{1.0}{V_{water,CLBL_i}}$$
$$\rho_{steam,CLBL_i} = \frac{1.0}{V_{steam,CLBL_i}} \qquad 4.4\text{-}38$$

The water-specific volume is calculated from the ASME steam table function VCL as follows, where i = 1,2:

$$V_{water,CLBL_i} = VCL(P_{CLBL_i}, T_{water,CLBL_i}) \qquad 4.4\text{-}39$$

The steam-specific volume is calculated from the ASME steam table function HSS as follows, where i = 1,2:

$$h_{steam,CLBL_i} = HSS(P_{CLBL_i}, T_{steam,CLBL_i}, S_{steam,CLBL_i}, v_{steam,CLBL_i}) \qquad 4.4\text{-}40$$

As stated above, the water and steam temperatures are given by the fluid thermocouple measurements TF-XXX (see Table 4.4-4). Care is taken to insure that the water temperature value employed is at or below the saturation temperature, and that the steam temperature value employed is at or above the saturation temperature. Thus, for i = 1,2:

$$\begin{aligned} T_{water,CLBL_i} &= \min(T_{water,CLBL_i}, T_{sat,CLBL_i}) \\ T_{steam,CLBL_i} &= \max(T_{steam,CLBL_i}, T_{sat,CLBL_i}) \end{aligned} \qquad 4.4\text{-}41$$

The saturation temperature is calculated from the ASME steam table function TSL as follows, where i = 1,2:

$$T_{sat,CLBL_i} = TSL(P_{CLBL_i}) \qquad 4.4\text{-}42$$

In all of the above, the CLBL pressure, $P_{CLBL\,i}$, is set equal to the value from the corresponding CMT PT-$XXX_{CMT\,i}$ measurement (see Table 4.4-4 for list) (after conversion from gauge [psig] to absolute [psia] pressure).

This completes the discussion of the calculations related to the left-hand side of the fluid mass conservation equation.

Although a liquid volumetric flow rate measurement (FMM) is available for each CLBL, they cannot be relied on for accurate mass flow rate calculations due to the two-phase flow which exists. Thus, the total mass flow rates on the right-hand side of the CLBL fluid mass conservation equation must be inferred from a combination of the CMT and CLBL fluid mass conservation equations.

This completes the discussion of the calculations related to the right-hand side of the fluid mass conservation equation.

4.4.4 Fluid Energy Conservation Equations

The general fluid (H_2O) energy conservation equation, which relates the change in stored fluid energy with respect to time (the fluid-energy time derivative) to the energy rates in and out (due to the

connected flow paths) and the energy addition rate due to other external devices, reduces to the following for each of the two CLBLs, $CLBL_i$, where i = 1,2:

$$\frac{d[M \times c_p \times (T-T_{ref})]_{H_2O,CLBL_i}}{dt} = Q_{in\ (from\ CL_j)\ H_2O,CLBL_i} - Q_{out\ (to\ CMT)\ H_2O,CLBL_i} + Q_{[metal \Rightarrow H_2O],CLBL_i} \qquad 4.4\text{-}43$$

The left-hand side of the fluid energy conservation equation is approximated as follows, where i = 1,2:

$$\frac{d[M \times c_p \times (T-T_{ref})]_{H_2O,CLBL_i}}{dt} \approx \frac{\Delta[M \times c_p \times (T-T_{ref})]_{water,CLBL_i}}{\Delta t} + \frac{\Delta[M \times c_p \times (T-T_{ref})]_{steam,CLBL_i}}{\Delta t} \qquad 4.4\text{-}44$$

where:

$$\frac{\Delta[M \times c_p \times (T-T_{ref})]_{water,CLBL_i}}{\Delta t} \approx c_{p_{water,CLBL_i}} \times \left[\frac{\Delta[M \times (T-T_{ref})]_{water,CLBL_i}}{\Delta t}\right]$$

$$\approx c_{p_{water,CLBL_i}} \times (T_{water,CLBL_i}-T_{ref}) \times \left[\frac{M^{n}_{water,CLBL_i} - M^{n-1}_{water,CLBL_i}}{t^{n}-t^{n-1}}\right] + c_{p_{water,CLBL_i}} \times M_{water,CLBL_i} \times \left[\frac{T^{n}_{water,CLBL_i} - T^{n-1}_{water,CLBL_i}}{t^{n}-t^{n-1}}\right] \qquad 4.4\text{-}45$$

and

$$\frac{\Delta[M \times c_p \times (T-T_{ref})]_{steam,CLBL_i}}{\Delta t} \approx c_{p_{steam,CLBL_i}} \times \left[\frac{\Delta[M \times (T-T_{ref})]_{steam,CLBL_i}}{\Delta t}\right]$$

$$\approx c_{p_{steam,CLBL_i}} \times (T_{steam,CLBL_i}-T_{ref}) \times \left[\frac{M^{n}_{steam,CLBL_i} - M^{n-1}_{steam,CLBL_i}}{t^{n}-t^{n-1}}\right] \quad 4.4\text{-}46$$

$$+ c_{p_{steam,CLBL_i}} \times M_{steam,CLBL_i} \times \left[\frac{T^{n}_{steam,CLBL_i} - T^{n-1}_{steam,CLBL_i}}{t^{n}-t^{n-1}}\right]$$

The water-specific heat capacity at constant pressure is calculated from the ASME steam table function CPL as follows, where i = 1,2:

$$c_{p_{water,CLBL_i}} = CPL(P_{CLBL_i}, T_{water,CLBL_i}) \quad 4.4\text{-}47$$

The steam-specific heat capacity at constant pressure is calculated from the ASME steam table function CPV as follows, where i = 1,2:

$$c_{p_{steam,CLBL_i}} = CPV(P_{CLBL_i}, T_{steam,CLBL_i}, v_{steam,CLBL_i}) \quad 4.4\text{-}48$$

This completes the discussion of the calculations related to the left-hand side of the fluid energy conservation equation.

On the right-hand side of the CLBL fluid energy conservation equation, the energy addition rate to the fluid due to heat transfer from the CLBL metal is calculated from the CLBL metal energy conservation equation, which is discussed below.

Once the metal-to-fluid heat transfer rate is known, the fluid energy transport rates on the right-hand side of the CLBL fluid energy conservation equation are inferred from a combination of the CMT and CLBL fluid energy conservation equations, in a manner analogous to that performed for the mass flow rates on the right-hand side of the fluid mass conservation equation.

This completes the discussion of the calculations related to the right-hand side of the fluid energy conservation equation.

4.4.5 Metal Energy Conservation Equations

The general metal energy conservation equation, which relates the change in stored metal energy with respect to time (the metal-energy time derivative) to the energy rates in and out (due to heat transfer), reduces to the following for each of the two CLBLs, $CLBL_i$, where i = 1,2:

$$\frac{d[M \times c_p \times (T-T_{ref})]_{metal,CLBL_i}}{dt} = - Q_{[metal \Rightarrow H_2O],CLBL_i} - Q_{[metal \Rightarrow ambient],CLBL_i} \qquad 4.4\text{-}49$$

Due to the fact that no metal thermocouple instrumentation exists in the CLBLs, fluid thermocouples are employed to obtain pseudo-metal temperatures. Each CLBL is divided into two metal segments. Table 4.4-6 lists the following data required in the metal energy calculations for each metal segment: fluid thermocouple channel ID for the pseudo-metal temperature, metal mass, outer surface area, and mean surface area. In addition, Table 4.4-7 lists the following data required in the metal energy calculations (which are not on a segment basis): ambient temperature channel ID, insulation thickness, and insulation mean thermal conductivity.

The left-hand side of the metal energy conservation equation is approximated as follows, where i = 1,2:

$$\frac{d[M \times c_p \times (T-T_{ref})]_{metal,CLBL_i}}{dt} \approx \frac{\Delta[M \times c_p \times (T-T_{ref})]_{metal,CLBL_i}}{\Delta t} \qquad 4.4\text{-}50$$

where:

$$\frac{\Delta[M \times c_p \times (T-T_{ref})]_{metal,CLBL_i}}{\Delta t} \approx \sum_{m=1}^{N_{metal,CLBL_i}} M_{metal,CLBL_{i,m}} \times c_{p_{metal,CLBL_{i,m}}} \times \left[\frac{T^{n}_{metal,CLBL_{i,m}} - T^{n-1}_{metal,CLBL_{i,m}}}{t^{n} - t^{n-1}} \right] \qquad 4.4\text{-}51$$

The metal segment specific heat capacity at constant pressure is calculated as a function of the metal segment temperature from the metal c_p versus temperature tabular data listed in Table 4.4-8, via linear interpolation within the table. No extrapolation at either end is performed; the first and last table points define the applicable range (the first point is $[T_{min}, c_{p,min}]$, and the last point is $[T_{max}, c_{p,max}]$.

This completes the discussion of the calculations related to the left-hand side of the metal energy conservation equation.

On the right-hand side of the metal energy conservation equation, the total metal-to-ambient heat transfer rate is equal to the sum of the individual metal segment metal-to-ambient heat transfer rates, where i = 1,2:

$$Q_{\{metal \Rightarrow ambient\},CLBL_i} = \sum_{m=1}^{N_{metal,CLBL_i}} Q_{\{metal \Rightarrow ambient\},CLBL_{i,m}} \qquad 4.4\text{-}52$$

The metal segment m metal-to-ambient heat transfer rate is given by the following, where i = 1,2:

$$Q_{\{metal \Rightarrow ambient\},CLBL_{i,m}} = \frac{(T_{metal,CLBL_{i,m}} - T_{ambient})}{(R_{outer\_surf\_metal,CLBL_{i,m}} + R_{insul\_metal,CLBL_{i,m}}) \times C_4} \qquad 4.4\text{-}53$$

The metal segment m outer surface heat transfer resistance is given by the following, where i = 1,2:

$$R_{outer\_surf\_metal,CLBL_{i,m}} = \frac{1.0}{A_{outer\_metal,CLBL_{i,m}} \times (U_{outer\_conv\_metal,CLBL_{i,m}} + U_{outer\_rad\_metal,CLBL_{i,m}})} \qquad 4.4\text{-}54$$

In the above, the metal segment m outer surface heat transfer coefficient due to convection is given by the following, where i = 1,2:

$$U_{outer\_conv\_metal,CLBL_{i,m}} = 0.17 \times (|T_{metal,CLBL_{i,m}} - T_{ambient}|)^{1/3} \qquad 4.4\text{-}55$$

and, the metal segment m outer surface heat transfer coefficient due to radiation is given by the following, where i = 1,2:

$$U_{outer\_rad\_metal,CLBL_{i,m}} = 1.3704 \times 10^{-9} \times [T^2_{insul\_metal,CLBL_{i,m}} + (T_{ambient} + C_5)^2] \times [T_{insul\_metal,CLBL_{i,m}} + (T_{ambient} + C_5)] \qquad 4.4\text{-}56$$

where:

C_5 = Conversion constant, 459.6 (°F to °R)

The insulation temperature for metal segment m is approximated by the following, where i = 1,2:

$$T_{insul\_metal,CLBL_{i,m}} = 0.1 \times T_{metal,CLBL_{i,m}} + T_{ambient} + C_5 \qquad 4.4\text{-}57$$

The metal segment m insulation heat transfer resistance is given by the following, where i = 1,2:

$$R_{insul\_metal,CLBL_{i,m}} = \frac{\Delta x_{insul\_metal,CLBL_i}}{A_{mean\_metal,CLBL_{i,m}} \times k_{insul\_metal,CLBL_i}} \qquad 4.4\text{-}58$$

Finally, having calculated both the change in stored metal energy (from the left-hand side) and the metal-to-ambient heat transfer rate (from the right-hand side), the metal energy conservation equation is rearranged to solve for the metal-to-fluid heat transfer rate. Recall that the latter is used in the fluid energy conservation equation calculations which were described earlier.

This completes the discussion of the calculations related to the right-hand side of the metal energy conservation equation.

TABLE 4.4-1 INSTRUMENTATION EMPLOYED FOR CMT FLUID CALCULATIONS				
Description	**CMT-1**		**CMT-2**	
Levels – main	LDP-507		LDP-502	
– alternate	LDP-501		LDP-504	
	LDP-503		LDP-506	
	LDP-505		LDP-508	
Top pressure	PT-501		PT-502	
Temperatures/elev (in.)	TF-501	0.300	TF-504	0.300
(Bottom to top)	TF-507	21.170	TF-510	21.170
	TF-509	37.191	TF-512	37.191
	TF-513	40.891	TF-516	40.891
	TF-515	43.711	TF-518	43.711
	TF-519	46.531	TF-522	46.531
	TF-523	49.351	TF-526	49.351
	TF-527	52.171	TF-530	52.171
	TF-547	54.541	TF-548	54.541
	TF-529	56.911	TF-532	56.911
DVI line – flow out bottom	FMM-501		FMM-504	
– temperature	TF-549		TF-550	

TABLE 4.4-2
VOLUME VERSUS HEIGHT TABLES FOR CMT FLUID VOLUME CALCULATIONS

CMT-1		CMT-2	
Height (in.)	**Volume ($in.^3$)**	**Height (in.)**	**Volume ($in.^3$)**
0.00	0.0	0.00	0.0
3.25	122.0	0.50	69.0
6.25	394.0	3.50	293.0
9.25	1103.0	6.50	1080.0
12.25	2009.0	10.50	1956.0
15.25	3006.0	13.50	2942.0
17.00	3599.0	15.00	3455.0
31.50	8888.0	30.00	8957.0
36.75	10786.0	35.00	10763.0
44.25	13484.0	42.50	13450.0
48.75	15105.0	46.625	14960.0
51.75	16130.0	50.00	16049.0
54.75	17036.0	53.00	17060.0
57.75	17704.0	56.00	17706.0
58.90	17945.0	59.00	17911.0

TABLE 4.4-3 CMT METAL WALL THERMOCOUPLE INSTRUMENTATION		
Metal Segment	**CMT-1**	**CMT-2**
1	TW-503, TW-501	TW-504, TW-502
2	TW-507, TW-505	TW-508, TW-506
3	TW-511, TW-509	TW-512, TW-510
4	TW-515, TW-513	TW-516, TW-514
5	TW-521, TW-519, TW-517	TW-522, TW-520, TW-518
6	TW-525, TW-523	TW-526, TW-524
7	TW-529, TW-527	TW-530, TW-528
8	TW-533, TW-531	TW-534, TW-532
9	TW-535, TW-537	TW-538, TW-536
10	TW-541, TW-539	TW-542, TW-540
11	TW-545, TW-543	TW-546, TW-544
12	TW-551, TW-549, TW-547	TW-552, TW-550, TW-548
13	TW-555, TW-553	TW-556, TW-554

Note:
Thermocouples for each metal segment are listed in the following order: inside surface, centerline (if applicable; only if three thermocouples are listed), outside surface.

TABLE 4.4-4 INSTRUMENTATION EMPLOYED FOR CLBL FLUID CALCULATIONS		
Description	**CLBL-1**	**CLBL-2**
Level	LDP-509	LDP-510
Temperatures: bottom	TF-533	HPS201-3
top	TF-531	TF-546
Pressure	PT-501	PT-502

TABLE 4.4-5 VOLUME VERSUS HEIGHT TABLES FOR CLBL FLUID VOLUME CALCULATIONS			
CLBL-1		**CLBL-2**	
Height (in.)	**Volume ($in.^3$)**	**Height (in.)**	**Volume ($in.^3$)**
0.000	0.000	0.000	0.000
11.000	16.453	9.000	13.461
44.440	49.398	38.440	42.465
45.560	66.147	39.560	55.765
47.375	85.687	41.500	75.316
50.815	108.477	44.000	90.298
51.935	158.539	48.191	124.537
75.250	181.449	49.309	147.629
78.693	218.059	74.500	172.387
80.000	257.284	77.000	196.405
		78.949	209.478
		80.000	225.046

TABLE 4.4-6 DATA FOR CLBL METAL ENERGY CALCULATIONS (PER SEGMENT)				
CLBL-1 Metal Segments				
Metal Segment	Pseudo-Metal Temperature ID (°F)	Metal Mass (lbm)	Outer Surface Area ($ft.^2$)	Mean Surface Area ($ft.^2$)
1	TF-533	42.9	9.03	5.82
2	TF-531	42.9	9.03	5.82
CLBL 2 Metal Segments				
Metal Segment	Pseudo-Metal Temperature ID (°F)	Metal Mass (lbm)	Outer Surface Area ($ft.^2$)	Mean Surface Area ($ft.^2$)
1	HPS201-3	31.9	6.00	5.16
2	TF-546	31.9	6.00	5.16

TABLE 4.4-7 DATA FOR CLBL METAL ENERGY CALCULATIONS		
Description	CLBL-1	CLBL-2
Ambient temperature ID (°F)	TF-006	TF-006
Insulation thickness (in.)	1.0	1.0
Insulation mean thermal conductivity [(Btu-in.)/(hr.-$ft.^2$-°F)]	0.31	0.31

TABLE 4.4-8 SPECIFIC HEAT CAPACITY VERSUS TEMPERATURE TABLE FOR CLBL METAL ENERGY CALCULATIONS	
Metal c_p [Btu/(lbm-°F)]	**Metal Temperature (°F)**
0.1085	70
0.1109	100
0.1175	200
0.1223	300
0.1256	400
0.1279	500
0.1297	600

4.5 In-Containment Refueling Water Storage Tank

For the AP600, the in-containment refueling water storage tank (IRWST) is a reservoir of coolant held inside containment at ambient containment pressure. Once the reactor coolant system (RCS) has been depressurized by actuation of all four stages of the automatic depressurization system (ADS), the IRWST inventory flows to the core by gravity through piping and valves connecting the IRWST to the direct vessel injection (DVI) lines. The IRWST injection phase continues until the IRWST inventory is depleted, and recirculation of the containment sump inventory through the RCS is initiated.

The OSU test simulated the IRWST with a tank and associated piping. In addition to piping and valves connecting the IRWST to the DVI lines, the IRWST simulation accounted for the following AP600 features:

- A sparger to distribute flow from ADS 1-3 to the IRWST
- A submersed heat exchanger to simulate the operation of passive residual heat removal (PRHR) during simulated events
- An overflow line between the IRWST and the containment sump tank to simulate the interaction of the IRWST directly with the sump

The operation of each of these features is accounted for in the mass and energy balance performed for the IRWST simulation.

4.5.1 General Mass and Energy Balance Formulation

The general mass balance equation for the IRWST is expressed as:

$$\frac{dM_{IRWST}}{dt} = \dot{M}_{ADS} - \dot{M}_{STM\ VENT} - \dot{M}_{OVRFLW} - \dot{M}_{IRWST\ INJ} \qquad 4.5\text{-}1$$

where:

M	=	Mass, lbm
$\dot{M}$	=	Mass flow rate, lbm/sec.
t	=	Time, sec.

and the subscripts:

ADS	=	Mass flow rate, both vapor and liquid, from automatic depressurization system (ADS) 1-3 separator

STM VENT	=	Vapor mass flow rate exhausted fro n IRWST through FVM-701
OVRFLW	=	Liquid mass flow rate through IRV ST overflow line measured by FMM-703
IRWST INJ	=	Total mass flow rate injected from IRWST through both injection lines

Similarly, the general energy balance on the IRWST is written as:

$$\frac{\sum M_j c_p dT_j}{dt} = Q_{PRHR} + \dot{M}_{ADS} h_{ADS} - \dot{M}_{STM\ VENT} h_g - \dot{M}_{OVRFLW} h_f - \dot{M}_{IRWST\ INJ} h_{IRWST\ INJ} \qquad 4.5\text{-}2$$

where:

c_p	=	Specific heat of water, Btu/(lbm-°F)
T	=	Local liquid temperature, °F
h_f	=	Enthalpy of water (liquid), Btu/lbm
h_g	=	Enthalpy of steam (vapor), Btu/lbm
Q_{PRHR}	=	Heat addition rate from PRHR, Btu/sec.

and the subscript:

j	=	Control volume within the IRWST associated with axial thermocouple locations

All other parameters and subscripts are as previously defined. The IRWST simulation may experience four modes of operation:

Case 1: IRWST inventory is subcooled; ADS has not been actuated; there is no overflow of IRWST inventory.

Case 2: At least some portion of the IRWST inventory is saturated (due to actuation of PRHR); ADS has not been actuated; there may be overflow from the IRWST.

Case 3: At least some portion of the IRWST inventory is saturated; ADS has been actuated; both PRHR and ADS energy is added to the IRWST.

Case 4: After ADS actuation, IRWST inventory is injected into the primary system.

The simplification of the general mass and energy balance equations for the four cases identified above follow.

4.5.2 Case 1

For this case, there is no liquid or vapor flow out of the IRWST, implying the following:

- No injection flow from the IRWST
- No liquid swell (due to heating) that provides for liquid flow through the overflow lines
- No steam generation and, therefore, the bulk liquid temperature of the IRWST inventory is lower than its saturation temperature ($T_f < T_{SAT}$)

According to the first two items, measured flow from the IRWST is given as:

$$\dot{M}_{FMM-701} = \dot{M}_{FMM-702} = \dot{M}_{PMM-703} = \dot{M}_{FVM-701} = 0 \qquad 4.5\text{-}3$$

where the subscripts:

FMM-701 = Flow meters in lines containing both liquid and vapor flow from the IRWST
FMM-702
FMM-703
FVM-701

All other parameters are as previously defined.

With no mass entering or leaving the IRWST, it follows that the time rate of change in mass of the IRWST is defined as:

$$\frac{dM_{IRWST}}{dt} \equiv 0 \qquad 4.5\text{-}4$$

Under these conditions, the energy balance on the IRWST is expressed as:

$$\frac{\sum M_j \, c_p \, dT_j}{dt} = Q_{PRHR} \qquad 4.5\text{-}5$$

The fluid thermocouples used in calculating the mass inventory of the IRWST and their respective elevations referenced to the top of the ceramic filler in the IRWST are given in Table 4.5-1. The difference form of the preceding equation is:

$$\sum M_j c_p \Delta T_j = Q_{PRHR} \Delta t \qquad 4.5\text{-}6$$

Liquid mass inventory of the IRWST is then calculated as follows:

Step 1: Calculate a temperature-compensated water level in the IRWST using outputs from level transducer LDP-701 and the thermocouples identified in Table 4.5-1 as input to the subroutine developed to perform this calculation.

Step 2: Calculate a pressure and density gradient for the water inventory in the IRWST using outputs from total pressure transducer PT-701, the compensated level measurement, and the thermocouples identified in Table 4.5-1. This is accomplished as follows:

First, the IRWST tank is divided into regions. Located in the middle of each region is one of the thermocouples identified in Table 4.5-1. The boundary between adjacent regions is defined as the midpoint between adjacent thermocouples. The bottom boundary of the region at the bottom of the IRWST is the top surface of the ceramic filler. The top boundary of the region at the top of the IRWST is the top of the IRWST.

Next, water column in the IRWST is partitioned into the regions defined above. In the event that the water level resides in a region, but is below the thermocouple in that region, then the height of water in that region is applied to the adjacent region.

Then, the pressure recorded by instrument PT-701 is applied to the top surface of the IRWST inventory and assumed to be representative of the pressure in that region. The liquid density in the first region is calculated as:

$$\rho_1 = \rho(P_1, T_1) \qquad 4.5\text{-}7$$

where P_1 is the pressure measurement of instrument PT-701 and T_1 is the first thermocouple below the surface of the compensated water level. The pressure at the top of the next lowest region is then calculated as:

$$P_j = P_{j-1} + \frac{g}{g_c} \rho_{j-1} \Delta z_{j-1} \qquad 4.5\text{-}8$$

where:

P	=	Pressure, psia
g	=	Gravitational acceleration, 32.2 ft./sec.^{2}
g_C	=	Conversion constant, 32.2 (lbm-ft.)/(lb_F-sec.^{2})
Δz	=	Height of water in a region, ft.

The subscript j is as previously defined.

The calculations defined in Equations 4.5-8 and 4.5-9 are repeated for each of the regions in the IRWST that are below the compensated level indicated by LDP-701.

Step 3: Liquid mass in the IRWST is then calculated as the sum of the masses of each region:

$$M_{IRWST} = \sum \rho_j V(z) \qquad 4.5\text{-}9$$

where:

V(z)	=	Volume of the IRWST as a function of height from the top surface of the ceramic fill in the bottom of the tank

All other parameters and subscripts are as previously defined.

4.5.3 Case 2

In this case, the IRWST liquid inventory is warmed sufficiently due to PRHR so that the liquid volume has swelled above the overflow line. The temperature of the IRWST inventory at or near the top of the IRWST is expected to be at or near saturation. Thus, there may be both liquid and vapor flow out of the IRWST. This situation may be described as:

- There is no injection flow from the IRWST.
- Liquid flow may occur through the overflow line, measured by FMM-703, due to volume swelling resulting from heating.
- There may be steam generation, measured by FVM-701.

From these three conditions, the mass balance on the IRWST given by Equation 4.5-1 is simplified as:

$$\frac{dM_{IRWST}}{dt} = -\dot{M}_{FVM-701} - \dot{M}_{FMM-703} \qquad 4.5\text{-}10$$

All variables and subscripts are as previously defined.

Noting that the left-hand side of the previous equation may be approximated as a difference:

$$\frac{dM_{IRWST}}{dt} \approx \frac{M_{IRWST,i} - M_{IRWST,i-1}}{t_i - t_{i-1}} \qquad 4.5\text{-}11$$

where the subscript:

i = Index of data and time arrays

The mass depletion of the IRWST may now be written as:

$$M_{IRWST,\,i} = M_{IRWST,\,i-1} - \dot{M}_{FVM-701,\,i}\,\Delta t - \dot{M}_{FMM-702,}\,\Delta t \qquad 4.5\text{-}12$$

$\Delta t = t_i - t_{i-1}$ and all other parameters are as previously defined. Density and enthalpy of vapor and liquid flow are evaluated using the outputs from the following instruments:

	Pressure	Temperature
Vapor (steam)	PT-701	TF-722
Liquid (overflow)	PT-701	TF-723

The units of measurement for the vapor and liquid flow meters are $ft.^3$/sec. and gpm, respectively. The vapor mass flow is calculated as:

$$\dot{M}_{FVM-701} = \rho_{(PT-701,\,TF-722)}\,\dot{M}_{(FVM-701,\,INST)} \qquad 4.5\text{-}13$$

where the subscript:

INST = Instrument reading

All other variables and subscripts are as previously defined.

Similarly, the liquid mass flow rate is calculated as:

$$\dot{M}_{FMM-703} = C_1\,\rho_{(PT-701,\,TF-723)}\,\dot{M}_{(FMM-703,\,INST)} \qquad 4.5\text{-}14$$

where:

C_1 = Conversion constant, 1 ft.^{3}/sec./448.86 gpm

The rate of energy transfer associated with the IRWST inventory is simplified from Equation 4.5-2 and expressed as:

$$\frac{\sum M_j c_p dT_j}{dt} = Q_{PRHR} - \dot{M}_{FVM-701} h_g - \dot{M}_{FMM-703} h_f \qquad 4.5\text{-}15$$

The difference form of the previous equation is written as:

$$\sum M_j c_p \Delta T_j = Q_{PRHR} \Delta t - \dot{M}_{FVM-701} h_g \Delta t - \dot{M}_{FMM-703} h_f \Delta t \qquad 4.5\text{-}16$$

4.5.4 Case 3

In this case, the operation of the ADS increases the mass in the IRWST. Also, operation of PRHR and the ADS may heat up the IRWST inventory. The combination of added mass and inventory heatup may cause the IRWST liquid volume to swell to above the overflow line. The temperature of the IRWST inventory is expected to be at or near saturation, and not all ADS flow may be condensed. Thus, there may be both liquid and vapor flow out of the IRWST, implying the following:

- There is no injection flow from the IRWST to the DVI line.
- ADS flow, possibly both steam and water, is being exhausted into the IRWST.
- Liquid flow may occur through the overflow line, measured by FMM-703, due to volume swelling resulting from heating.
- There may be steam generation, measured by FVM-701.

From these four conditions, the mass balance on the IRWST is given as:

$$\frac{dM_{IRWST}}{dt} = \dot{M}_{ADS} - \dot{M}_{FVM-701} - \dot{M}_{FMM-703} \qquad 4.5\text{-}17$$

The ADS flow may consist of both vapor and liquid components:

$$\dot{M}_{ADS} = \dot{M}_{FVM-601} + \dot{M}_{FMM-601} \qquad 4.5\text{-}18$$

where:

FVM-601	=	Vapor flow meter downstream of ADS 1-3 separator
FMM-601	=	Liquid flow meter downstream of ADS 1-3 separator

Expressing the left-hand side of Equation 4.5-18 as a difference and expanding, the liquid mass inventory of the IRWST is calculated as:

$$M_{IRWST,\,i} = M_{IRWST,\,i-1} + \dot{M}_{FVM-601,\,i}\,\Delta t + \dot{M}_{FMM-601,\,i}\,\Delta t - \dot{M}_{FVM-701,\,i}\,\Delta t - \dot{M}_{FMM-703,\,i}\,\Delta t \qquad 4.5\text{-}19$$

All parameters and subscripts are as previously defined. Similarly, the energy balance for this case may be written as:

$$\frac{\sum M_j\, c_p\, dT_j}{dt} = \dot{M}_{FVM-601}\, h_g + \dot{M}_{FMM-601}\, h_f - \dot{M}_{FVM-701}\, h_g - \dot{M}_{FMM-703}\, h_f \qquad 4.5\text{-}20$$

The enthalpy of the vapor and liquid components of the ADS flow, measured by FVM-601 and FMM-601, respectively, is evaluated using the ASME steam table routines and data from the following instruments:

	Pressure	Temperature
Vapor phase	PT-605	TF-617
Liquid phase	PT-605	TF-616

The difference form of the energy equation is written as:

$$\sum M_j\, c_p\, \Delta T_j = \dot{M}_{FVM-601}\, h_g\, \Delta t - \dot{M}_{FMM-601}\, h_f\, \Delta t - \dot{M}_{FVM-701}\, h_g\, \Delta t - \dot{M}_{FMM-703}\, h_f\, \Delta t \qquad 4.5\text{-}21$$

4.5.5 Case 4

This case occurs late in the transient; PRHR is no longer active and ADS 1-3, while open, have low flow. While there may be some steam venting of the IRWST volume, there is most likely no liquid overflow. At this time, the IRWST may be injecting into the DVI lines. The mass balance on the IRWST is given by Equation 4.5-1 where:

$$\dot{M}_{IRWST\ INJ} = \dot{M}_{FMM-701} + \dot{M}_{FMM-702} \qquad 4.5\text{-}22$$

The mass balance for this case is expressed as:

$$M_{IRWST,\,i} = M_{IRWST,\,i-1} + \dot{M}_{FVM-601,\,i}\Delta t + \dot{M}_{FMM-601,\,i}\Delta t - \dot{M}_{FVM-701,\,i}\Delta t - \dot{M}_{FMM-703,\,i}\Delta t$$

$$- \dot{M}_{FMM-701,\,i}\Delta t - \dot{M}_{FMM-702,\,i}\Delta t \qquad 4.5\text{-}23$$

Similarly, the energy balance is written as:

$$\frac{\sum M_j c_p dT_j}{dt} = \dot{M}_{FVM-601} h_g + \dot{M}_{FMM-601} h_f - \dot{M}_{FVM-701} h_g - \dot{M}_{FMM-703} h_f$$

$$- \dot{M}_{FMM-701} h_f - \dot{M}_{FMM-702} h_f \qquad 4.5\text{-}24$$

Expressing the preceding equation in its difference form:

$$\sum M_j c_p \Delta T_j = (\dot{M}_{FVM-601} h_g + \dot{M}_{FMM-601} h_f - \dot{M}_{FVM-701} h_g$$

$$- \dot{M}_{FMM-703} h_f - \dot{M}_{FMM-701} h_f - \dot{M}_{FMM-702} h_f)\,\Delta t \qquad 4.5\text{-}25$$

TABLE 4.5-1 IRWST MASS AND ENERGY CALCULATIONS IDENTIFICATION OF FLUID THERMOCOUPLES AND ELEVATION		
Index	**Thermocouple ID**	**Elevation[1] (in.)**
1	TF-701	1.00
2	TF-702	8.99
3	TF-703	16.97
4	TF-704	26.85
5	TF-705	36.73
6	TF-706	46.61
7	TF-707	56.49
8	TF-708	66.36
9	TF-709	76.24
10	TF-710	87.36
11	TF-711	98.47
12	TF-712	109.59

Note:
(1) Elevations referenced from top surface of plate in bottom of IRWST tank and run vertically upwards.

4.6 ADS 1-3 Separator

The ADS of the AP600 design provides a means of depressurizing the RCS in a controlled, staggered manner through the use of four pairs of valves, with each valve pair sequenced to open at different primary system pressures. The first three pairs of valves, called ADS stages 1, 2, and 3 (ADS 1-3), are located in parallel piping paths running from the top of the pressurizer to the IRWST. This portion of the ADS system operates independently of the fourth and final stage of the ADS.

The ADS 1-3 flow path was simulated in the OSU test facility by three valves (one valve each having a scaled stage 1, stage 2, and stage 3 flow area), a steam/water separator tank, a vortex (vapor) flow meter, a magnetic (liquid) flow meter, and associated piping. During testing, flow through the ADS 1-3 flow path was measured by separating the vapor and liquid components of the flow, measuring the flow rate of the component flows, recombining the flows, then directing the total metered flow to a sparger located in the IRWST.

Flow through ADS 1-3 of the test may be calculated as:

$$\dot{M}_{ADS\ 1-3} = \dot{M}_{ADS\ 1-3,\ f} + \dot{M}_{ADS\ 1-3,\ g} + \frac{dM_{ADS\ 1-3\ SEP}}{dt} \qquad 4.6\text{-}1$$

where:

M	=	Mass, lbm
$\dot{M}$	=	Mass flow rate, lbm/sec.
t	=	Time, sec.

and the subscripts:

f	=	Liquid phase of water
g	=	Gaseous phase of water
ADS 1-3	=	Stages 1 through 3 of the ADS system
SEP	=	Steam water separation tank for ADS 1-3

Energy is transported out of the primary system by both the vapor and liquid flows. Also, the stored energy of the ADS 1-3 separator inventory may change due to changes in the amount of liquid and vapor in the separator, changes in temperature and pressure of the liquid or vapor inventory in the

separator, or a change in the temperature of the separator tank metal mass. Accounting for these terms, the energy rate equation for ADS 1-3 flow may be expressed as:

$$Q_{ADS\ 1\text{-}3} = Q_{ADS\ 1\text{-}3,\ f} + Q_{ADS\ 1\text{-}3,\ g} + c_p \frac{d(M_{ADS\ 1\text{-}3\ SEP}\ T)}{dt}$$

$$- Q_{ADS\ 1\text{-}3,\ METAL} - Q_{ADS\ 1\text{-}3,\ AMB} \qquad 4.6\text{-}2$$

where:

c_p	=	Specific heat, Btu/(lbm-°F)
Q	=	Rate of energy transfer or transport, Btu/sec.
T	=	Temperature, °F

and the subscripts:

METAL	=	Metal mass of the ADS 1-3 separator tank and associated piping
AMB	=	Energy loss to ambient environment

All other variables and subscripts are as previously defined.

4.6.1 ADS 1-3 Separator Liquid Inventory

The ADS 1-3 separator is, in its simplest form, a tank. Liquid inventory in the ADS 1-3 separator is monitored by a level transducer. The functional steps and associated system of equations for operating on the output from the ADS 1-3 separator level transducers to calculate liquid mass in the ADS 1-3 steam/water separator tank follows:

Step 1: Compensate the readings from the ADS 1-3 separator level transducer listed in Table 4.6-1 to account for temperature differences between fluid in the separator tank and fluid in the reference leg of the instrument line. The local pressure and fluid temperatures to be used to accomplish the compensation are also identified in Table 4.6-1.

Step 2: The local pressures and temperatures identified in Table 4.6-1 are used as inputs to the ASME steam tables to calculate the density of the liquid and vapor in the ADS 1-3 separator:

$$\rho_{ADS\ 1\text{-}3,\ f} = \rho_f\ (PT\text{-}605,\ TF\text{-}616)$$

$$\rho_{ADS\ 1\text{-}3,\ g} = \rho_g\ (PT\text{-}605,\ TF\text{-}617) \qquad 4.6\text{-}3$$

where:

ρ	=	Density, lbm/ft.^{3}
PT-605	=	Data channel ID for local pressure measurement in the ADS 1-3 separator tank
TF-616	=	Data channel ID for local liquid temperature measurement, °F
TF-617	=	Data channel ID for local vapor temperature measurement, °F

All subscripts are as previously defined.

As identified previously, both liquid and vapor flow meters have an associated local fluid temperature used to evaluate the thermodynamic properties of the liquid and vapor phases in the ADS 1-3 separator.

Step 3: Using the compensated liquid level and the ADS 1-3 separator volume as a function of height, determine the volume of liquid in the ADS 1-3 separator as:

$$V_{ADS\ 1\text{-}3\ SEP,\ f} = V(l)_{ADS\ 1\text{-}3\ SEP} \times LDP\text{-}610_{COMP} \qquad 4.6\text{-}4$$

where:

V	=	Volume, ft.^{3}
V(l)	=	Volume of the ADS 1-3 separator as a function of elevation, ft.^{3}/ft.
$LDP\text{-}610_{COMP}$	=	Compensated fluid levels data from level transducer LDP-610, ft.

The subscripts f and ADS 1-3 SEP are as previously defined.

Step 4: Liquid mass inventory in the ADS 1-3 separator is now calculated as:

$$M_{ADS\ 1\text{-}3\ SEP,\ f} = \rho_{ADS\ 1\text{-}3,\ f} \times V_{ADS\ 1\text{-}3\ SEP,\ f} \qquad 4.6\text{-}5$$

All parameters and subscripts are as previously defined. Vapor mass in the separator is then calculated as:

$$M_{ADS\ 1\text{-}3\ SEP,\ g} = \rho_{ADS\ 1\text{-}3,\ g} \times (V_{ADS\ 1\text{-}3\ SEP,\ TOT} - V_{ADS\ 1\text{-}3\ SEP,\ f}) \qquad 4.6\text{-}6$$

where the subscript:

TOTAL = Total volume of ADS 1-3 separator, ft.^{3}

All other variables and subscripts are as previously defined.

Step 5: The rate of change in mass inventory of the break separator tank may be approximated by differencing two consecutive calculated values of liquid and vapor mass:

$$\frac{dM_{ADS\ 1\text{-}3\ SEP}}{dt} \approx \frac{\Delta M_{ADS\ 1\text{-}3\ SEP}}{\Delta t} = \frac{M_{ADS\ 1\text{-}3\ SEP,\ f,\ i} - M_{ADS\ 1\text{-}3\ SEP,\ f,\ i\text{-}1}}{t_i - t_{i-1}}$$

$$+ \frac{M_{ADS\ 1\text{-}3\ SEP,\ g,\ i} - M_{ADS\ 1\text{-}3\ SEP,\ g,\ i\text{-}1}}{t_i - t_{i-1}} \qquad 4.6\text{-}7$$

where the subscript:

i = Index of data and time arrays

All other parameters and subscripts are as previously defined.

4.6.2 Steam Flow Rates

The density of steam in the ADS 1-3 exhaust line, evaluated using the pressure and temperature inputs from the data channels identified in Table 4.6-2, is used to calculate the steam mass flow rate through the ADS 1-3 valves as:

$$\dot{M}_{FVM\text{-}601} = C_2 \times \rho_{ADS\ 1\text{-}3,\ g} \times \dddot{M}_{FVM\text{-}601} \qquad 4.6\text{-}8$$

where:

C_2 = Conversion constant, 1 min./60 sec.

$\dddot{M}$ = Volumetric flow, ft.^{3}/min.

and the subscript:

FVM-601 = Instrument channel ID for steam vapor flow meter in line between ADS 1-3 separator and sparger

4.6.3 Liquid Flow Rates

Liquid from ADS 1-3 is ducted from the separator through a magnetic flow meter into a header where it is mixed with steam flow before passing to the sparger in the IRWST. Mass flow from the ADS 1-3 separator to the sparger is calculated as:

$$\dot{M}_{FMM\text{-}601} = C_1 \times \rho_{ADS\ 1\text{-}3,\ f} \times \dddot{M}_{FMM\text{-}601} \qquad 4.6\text{-}9$$

where:

C_1 = Conversion constant, 1 ft.^{3}/sec./448.86 gpm

and the subscript:

FMM-601 = Instrument channel ID for liquid flow meter in line between ADS 1-3 separator and sparger

All parameters are as previously defined but the volumetric liquid flow is in units of gallons per minute (gpm).

The density of the liquid passing through the flow meter is evaluated using data from the pressure and temperature instruments identified in Table 4.6-2.

4.6.4 Total Flow Rate

The total liquid and vapor flows through ADS 1-3 are then calculated as:

$$M_{ADS\ 1\text{-}3,\ f} = \dot{M}_{FMM\text{-}601} + \frac{\Delta M_{ADS\ 1\text{-}3,\ f}}{\Delta t} \qquad 4.6\text{-}10$$

$$M_{ADS\ 1\text{-}3,\ g} = \dot{M}_{FVM\text{-}601} + \frac{\Delta M_{ADS\ 1\text{-}3,\ g}}{\Delta t} \qquad 4.6\text{-}11$$

The total flow through the ADS is then calculated as:

$$\dot{M}_{ADS\ 1\text{-}3} = \dot{M}_{ADS\ 1\text{-}3,\ f} + \dot{M}_{ADS\ 1\text{-}3,\ g} \qquad 4.6\text{-}12$$

The total mass flow rate is integrating step-wise over time to calculate the total mass inventory passed by the ADS 1-3:

$$M_{ADS\ 1\text{-}3} = \sum (\dot{M}_{ADS\ 1\text{-}3,\ TOTAL} \times \Delta t) \qquad 4.6\text{-}13$$

All variables and subscripts are as previously defined. The flow quality of the ADS 1-3 flow is also calculated as:

$$X = \frac{\dot{M}_{ADS\ 1\text{-}3,\ g}}{\dot{M}_{ADS\ 1\text{-}3,\ TOTAL}} \qquad 4.6\text{-}14$$

where:

X = Flow quality

All other variables and subscripts are as previously defined.

4.6.5 Energy Balance

Energy flow through the break separator consists of the following:

- Rate of change in stored energy of the ADS 1-3 separator liquid inventory
- Energy transport rate from the ADS 1-3 separator by exiting steam flow
- Energy transport rate from the ADS 1-3 separator by exiting liquid flow
- Rate of change in stored energy of the ADS 1-3 metal components
- Rate of energy loss from the ADS 1-3 components to the environment

The expressions for evaluating these five energy transfer or transport terms are developed in the following sections.

4.6.5.1 Rate of Change in Stored Energy of the ADS 1-3 Separator Liquid Inventory

The rate of change of energy in the liquid in the ADS 1-3 separator may be expressed as:

$$c_P \frac{d(M_{ADS\ 1\text{-}3\ SEP}\ T)}{dt}$$

$$= c_{P,f}\ T_f \frac{d(M_{ADS\ 1\text{-}3\ SEP,\ f})}{dt} + c_{P,f}\ M_{ADS\ 1\text{-}3\ SEP,\ f} \frac{d(T_f)}{dt}$$

$$+ c_{P,g}\ T_g \frac{d(M_{ADS\ 1\text{-}3\ SEP,\ g})}{dt} + c_{P,g}\ M_{ADS\ 1\text{-}3\ SEP,\ g} \frac{d(T_g)}{dt} \qquad 4.6\text{-}15$$

All variables and subscripts are as previously defined.

Expressing the previous equation as a difference and solving for consecutive data, the rate of change of energy of the fluid in the ADS 1-3 separator is calculated:

$$c_P \frac{\Delta(M_{ADS\ 1\text{-}3\ SEP}\ T)}{\Delta t}$$

$$= c_{P,f}\ T_f \frac{\Delta(M_{ADS\ 1\text{-}3\ SEP,\ f})}{\Delta t} + c_{P,f}\ M_{ADS\ 1\text{-}3\ SEP,\ f} \frac{\Delta(T_f)}{\Delta t}$$

$$+ c_{P,g}\, T_g \frac{\Delta(M_{ADS\ 1\text{-}3\ SEP,\ g})}{\Delta t} + c_{P,g}\, M_{ADS\ 1\text{-}3\ SEP,\ g} \frac{\Delta(T_g)}{\Delta t} \qquad 4.6\text{-}16$$

All variables and subscripts are as previously defined. The specific heats of the liquid and vapor phases, $c_{P,f}$ and $c_{P,g}$ respectively, are evaluated using the outputs of the data channels identified in Table 4.6-2.

4.6.5.2 Energy Transport Rate from the ADS 1-3 Separator by Exiting Steam Flow

The enthalpy of the steam exhaust from the ADS 1-3 separator is determined using the output from the pressure and temperature sensors associated with FVM-601 (Table 4.6-2):

$$h_{FVM\text{-}601,\ g} = h_g\ (PT\text{-}605,\ TF\text{-}617) \qquad 4.6\text{-}17$$

where:

h_g = Enthalpy of steam, Btu/lbm

FVM-601 is the data channel ID for the ADS 1-3 vapor flow meter, and PT-605 and TF-617 denote the vapor pressure and temperatures, respectively, associated with that flow meter.

The rate of energy transport of the ADS 1-3 flow due to the steam component, then, is expressed as:

$$Q_{ADS\ 1\text{-}3,g} = \dot{M}_{ADS\ 1\text{-}3,g} \times h_{FVM\text{-}601,g} \qquad 4.6\text{-}18$$

All parameters and subscripts are as previously defined.

4.6.5.3 Energy Transport Rate from the ADS 1-3 Separator by Exiting Liquid Flow

The enthalpy of ADS liquid flow is determined using the output from the pressure and temperature sensors associated with FMM-601 (Table 4.6-2):

$$h_{FMM\text{-}601,\ f} = h_f\ (PT\text{-}605,\ TF\text{-}616) \qquad 4.6\text{-}19$$

where:

h_f = Enthalpy of liquid, Btu/lbm

FMM-601 is the data channel ID of the ADS 1-3 liquid flow meter, and PT-605 and TF-616 denote the data channel IDs for the liquid pressure and temperatures, respectively, associated with that flow meter.

The rate of energy transport due to ADS 1-3 liquid flow, then, is expressed as:

$$Q_{ADS\ 1\text{-}3,\ f} = \dot{M}_{ADS\ 1\text{-}3,\ f} \times h_{FMM\text{-}601,\ f} \qquad 4.6\text{-}20$$

All parameters and subscripts are as previously defined.

4.6.5.4 Rate of Change in Stored Energy of the ADS 1-3 Metal Components

The change in stored energy of the sump tanks and associated piping may be expressed as:

$$Q_{ADS\ 1\text{-}3\ METAL} = c_{P,\ METAL}\ M_{ADS\ 1\text{-}3\ METAL}\ \frac{d(T_{ADS\ 1\text{-}3\ METAL})}{dt} \qquad 4.6\text{-}21$$

where the subscript:

METAL = Metal mass of steam/water separator tank and all associated piping of ADS 1-3, lbm

All other parameters and subscripts are as previously defined. Temperature data from data channel TW-601 are used to calculate the rate of change of stored energy in the ADS 1-3 separator metal mass.

4.6.5.5 Rate of Energy Loss from the ADS 1-3 Components to the Environment

Piping between the ADS 1-3 valves and the separator, and between the separator and the IRWST were provided with heat tracing. This had the effect of off-setting any energy loss to the ambient environment. Thus, for the purpose of evaluating the rate energy loss from the fluid to the ambient environment (through piping) of the ADS 1-3 piping:

$$QAMB \equiv 0.0 \qquad 4.6\text{-}22$$

TABLE 4.6-1 INSTRUMENTATION TO BE USED FOR ADS 1-3 LEVELS INSTRUMENT CORRECTION				
Location	**Function**	**Level Transducer**	**Pressure Transducer**	**Fluid Temperature**
ADS 1-3 Separator	Density compensation of levels data	LDP-610	PT-605	TF-616

TABLE 4.6-2 ADS 1-3 SEPARATOR STEAM AND LIQUID PRESSURE AND TEMPERATURE INSTRUMENT CHANNELS			
Flow Meter Description	**Flow Meter Channel ID**	**Pressure Channel ID**	**Temperature Channel ID**
ADS 1-3 separator steam flow	FVM-601	PT-605	TF-617
ADS 1-3 separator liquid flow	FMM-601	PT-605	TF-616

4.7 ADS-4 Separators

The ADS of the AP600 design provides a means of depressurizing the RCS in a controlled, staggered manner through the use of four pairs of valves, with each valve pair sequenced to open at different primary system pressures. Mass, flow, and energy calculations associated with the first three pairs of valves, called ADS stage 1, 2, and 3 (ADS 1-3), are described in Section 4.6. A redundant fourth pair of valves, called the ADS-4, are located on each of the two hot legs and exhaust directly to containment atmosphere. The ADS-4 valves are used to complete depressurization of the RCS to near containment pressures.

The ADS-4 flow paths were simulated in the OSU test facility by a valve, a steam/water separator tank, a vortex (vapor) flow meter, a magnetic (liquid) flow meter, and associated piping coming off of each of the two hot legs. During testing, flow through the two ADS-4 flow paths was measured by separating the vapor and liquid components of the flow, measuring the flow rate of the component flows, recombining the flows, then directing the total metered flow to a simulation of the containment sump.

Flow through each of the ADS-4 flow paths may be calculated as:

$$\dot{M}_{ADS\ 4\text{-}X} = \dot{M}_{ADS\ 4\text{-}X\ LIQ} + \dot{M}_{ADS\ 4\text{-}X\ STM} + \frac{dM_{ADS\ 4\text{-}X\ SEP}}{dt} \qquad 4.7\text{-}1$$

where:

M	=	Mass, lbm
$\dot{M}$	=	Mass flow rate, lbm/sec.
t	=	Time, sec.

and the subscripts:

ADS-4	=	Fourth-stage ADS
X	=	Hot leg to which the flow path is connected where: X =1HL-1 2HL-2
LIQ	=	Liquid component of ADS-4 flow
SEP	=	Steam water separation tank for ADS-4
STM	=	Vapor (steam) component of ADS-4 flow

The total ADS-4 flow rate is then calculated as:

$$\dot{M}_{ADS\ 4} = \dot{M}_{ADS\ 4\text{-}1} + \dot{M}_{ADS\ 4\text{-}2} \qquad 4.7\text{-}2$$

All variables and subscripts are as previously defined.

Energy is transported out of the primary system by the ADS-4 vapor and liquid flows. Also, the stored energy of the ADS-4 separator liquid inventory may change due to a change in the amount of liquid in the separator, a change in temperature of the liquid inventory in the separator, or a change in the temperature of the separator tank metal mass. Accounting for these terms, the energy equation for one train of ADS-4 flow may be expressed as:

$$Q_{ADS\ 4\text{-}X} = Q_{ADS\ 4\text{-}X\ LIQ} + Q_{ADS\ 4\text{-}X\ STM} + c_p \frac{d\left(M_{ADS\ 4\text{-}X\ SEP}\ T_l \right)}{dt} - Q_{ADS\ 4\text{-}X\ METAL} - Q_{ADS\ 4\text{-}X\ AMB} \qquad 4.7\text{-}3$$

where:

c_p	=	Specific heat, Btu/(lbm-°F)
Q	=	Rate of energy transfer or transport, Btu/sec.
T	=	Temperature, °F

and the subscripts:

METAL	=	Metal mass of the ADS-4 separator tank and associated piping
AMB	=	Energy loss to ambient environment

All other parameters and subscripts are as previously defined. The total energy associated with the ADS-4 (accounting for both separators) is calculated by summing the terms in the previous equation for each of the two separators.

4.7.1 ADS-4 Separator Liquid Inventory

The ADS-4 separator is, in its simplest form, a tank. Liquid inventory in the ADS-4 separators is monitored by level transducers. The functional steps and associated system of equations for operating

on the output from the ADS-4 separator level transducers to calculate inventory mass in the separator tanks are:

Step 1: Compensate the readings from the ADS-4 separator level transducers listed in Table 4.7-1 to account for temperature differences between fluid in the separator tank and fluid in the reference leg of the instrument line. The local pressure and fluid temperature instruments to be used to accomplish the compensation are also identified in Table 4.7-1.

Step 2: The local pressures and temperatures from the instruments identified in Table 4.7-1 are used to calculate the density of the liquid and vapor in the ADS-4 separator:

$$\rho_{f,\,ADS\,4\text{-}X} = \rho_f\,(PT\text{-}YYY,\ TF\text{-}ZZL)$$
$$\rho_{g,\,ADS\,4\text{-}X} = \rho_g\,(PT\text{-}YYY,\ TF\text{-}ZZV) \qquad 4.7\text{-}4$$

where:

ρ	=	Density, lbm/ft.^{3}
PT-YYY	=	Channel ID for local pressure measurement in ADS-4 separator tank
TF-ZZL, TF-ZZV	=	Channel ID for local temperature measurement of liquid and vapor respectively, exiting ADS-4 separator

and the subscripts:

f	=	Liquid phase of water
g	=	Vapor phase of water

As noted previously, both liquid and vapor flow meters have an associated local fluid temperature used to evaluate the thermodynamic properties of the liquid and vapor phases in the ADS-4 separator.

Step 3: Using the compensated liquid level and the ADS-4 separator volume as a function of height, determine the volume of liquid in the ADS-4 separator as:

$$V_{ADS\,4\text{-}X\,SEP.\,f} = V(l)_{ADS\,4\text{-}X\,SEP} \times LDP\text{-}XXX_{COMP} \qquad 4.7\text{-}5$$

where:

V	=	Volume, $ft.^3$
V(l)	=	Volume of ADS-4 separator as a function of elevation, $ft.^3/ft.$
$LDP\text{-}XXX_{COMP}$	=	Compensated fluid level data from level transducer for ADS-4 separator, ft.
		XXX = 611 ADS 4-1 separator
		= 612 ADS 4-2 separator

The subscripts f, ADS 4, X, and SEP are as previously defined.

Step 4: Liquid mass inventory in the ADS-4 separator is now calculated as:

$$M_{ADS\ 4\text{-}X\ SEP} = \rho_{f,\ ADS\ 4\text{-}X} \times V_{f,\ ADS\ 4\text{-}X\ SEP} \qquad 4.7\text{-}6$$

The vapor mass inventory of an ADS-4 separator is then calculated as:

$$M_{ADS\ 4\text{-}x\ SEP,\ g} = P_g \times (V_{ADS\ 4\text{-}X\ SEP,\ TOTAL} - V_{ADS\ 4\text{-}X\ SEP,\ f}) \qquad 4.7\text{-}7$$

where the subscript:

TOTAL	=	Total volume associated with an ADS-4 separator, $ft.^3$

All other variables and subscripts are as previously defined.

Step 5: The rate of change in mass inventory of an ADS separator tank may be calculated by differencing two consecutive calculated values of the liquid and vapor masses:

$$\frac{dM_{ADS\ 4\text{-}x\ SEP}}{dt} = \frac{\Delta M_{ADS\ 4\text{-}x\ SEP}}{\Delta t}$$

$$= \frac{M_{ADS\ 4\text{-}x\ SEP,\ f,\ i} - M_{ADS\ 4\text{-}x\ SEP,\ f,\ i-1}}{t_i - t_{i-1}} \qquad 4.7\text{-}8$$

$$+ \frac{M_{ADS\ 4\text{-}x\ SEP,\ g,\ i} - M_{ADS\ 4\text{-}x\ SEP,\ g,\ i-1}}{t_i - t_{i-1}}$$

where the subscript:

i = Index of data and time arrays

All other parameters and subscripts are as previously defined.

4.7.2 Steam Flow Rates

The density of steam in the exhaust line from the ADS-4 separator is evaluated using the ASME steam table routines with pressure and temperature inputs from the data channels identified in Table 4.7-2. Using this density, the steam portion of flow through the ADS-4 valves is calculated as:

$$\dot{M}_{ADS\ 4\text{-}X\ STM} = C_2 \times \rho_g \times \dddot{M}_{FVM\text{-}XXX} \qquad 4.7\text{-}9$$

where:

C_2 = Conversion constant, 1 min./60 sec.

$\dddot{M}$ = Volumetric flow

and the subscript:

FVM-XXX = Instrument channel ID for steam vapor flow meter
XXX = 603ADS 4-1 separator
602ADS 4-2 separator

All other variables and subscripts are as previously defined.

4.7.3 Liquid Flow Rates

Liquid from ADS-4 is directed from the separator through a magnetic flow meter into the primary sump tank. Mass flow from the ADS-4 separator to the primary sump is calculated as:

$$\dot{M}_{ADS\ 4\text{-}X\ LIQ} = C_1 \times \rho_{ADS\ 4\text{-}X,\ f} \times \dddot{M}_{FMM\text{-}XXX} \qquad 4.7\text{-}10$$

where:

C_1 = Conversion constant, 1 $ft.^3$/sec./488.86 gpm

and the subscript:

FMM-XXX = Instrument channel ID for liquid flow meter
XXX = 603 ADS 4-1 separator
602 ADS 4-2 separator

All other parameters and subscripts are as previously defined and the volumetric liquid flow is in units of gallons per minute (gpm).

The density of the liquid passing through the flow meter is determined using data from the pressure and temperature instruments identified in Table 4.7-2.

4.7.4 Total Flow Rate

Total liquid and vapor flow through ADS-4 are then calculated as:

$$M_{ADS\ 4\text{-}X,\ f} = \dot{M}_{FMM\text{-}XXX} + \frac{\Delta M_{ADS\ 4\text{-}x,\ f}}{\Delta t} \qquad 4.7\text{-}11$$

$$M_{ADS\ 4\text{-}x,\ g} = \dot{M}_{FVM\text{-}XXX} + \frac{\Delta M_{ADS\ 4\text{-}x,\ g}}{\Delta t} \qquad 4.7\text{-}12$$

Total flow through one ADS-4 flow path is then calculated as:

$$\dot{M}_{ADS\ 4\text{-}x} = \dot{M}_{ADS\ 4\text{-}X,\ f} + \dot{M}_{ADS\ 4\text{-}x,\ g} \qquad 4.7\text{-}13$$

The total ADS-4 flow rate is calculated by summing the total flow rate for each of the two flow paths. The total mass passed by ADS-4 is calculated by integrating step-wise over time:

$$M_{ADS\ 4,\ TOTAL} = \sum \left(\dot{M}_{ADS\ 4\text{-}1,\ TOTAL} + \dot{M}_{ADS\ 4\text{-}2,\ TOTAL} \right) \times \Delta t \qquad 4.7\text{-}14$$

All variables and subscripts are as previously defined. The flow quality of the each of the ADS-4 flow paths is also calculated as:

$$X_{ADS\ 4\text{-}x} = \frac{\dot{M}_{ADS\ 4\text{-}x,\ g}}{\dot{M}_{ADS\ 4\text{-}X,\ TOTAL}} \qquad 4.7\text{-}15$$

where:

X = Flow quality

All other variables and subscripts are as previously defined.

4.7.5 Energy Balance

Energy flow through the ADS-4 separator consists of the following:

- Rate of change in stored energy of the ADS-4 separator fluid inventory
- Energy transport rate from the ADS-4 separator by exiting steam flow
- Energy transport rate from the ADS-4 separator by exiting liquid flow
- Rate of change in stored energy of the ADS-4 metal components
- Rate of energy loss from the ADS-4 components to the environment

The expressions for evaluating these five energy transfer or transport terms are developed in the following sections.

4.7.5.1 Rate of Change in Stored Energy of the ADS-4 Separator Fluid Inventory

The rate of change of energy associated with the fluid (both steam and liquid) inventory of a ADS-4 separator may be expressed as:

$$Q_{ADS\ 4\text{-}X\ LIQ} = c_{P,f} \frac{d\left(M_{ADS\ 4\text{-}X\ SEP}\ T_f\right)}{dt}$$

$$= c_{P,f}\left(T_f - T_{REF}\right) \frac{d\left(M_{ADS\ 4\text{-}X\ SEP,f}\right)}{dt} \qquad 4.7\text{-}16$$

$$+ c_{P,f}\, M_{ADS\ 4\text{-}X\ SEP,f} \frac{d(T_f)}{dt}$$

$$+ c_{P,g}\left(T_g - T_{REF}\right) \frac{d\left(M_{ADS\ 4\text{-}x\ SEP,g}\right)}{\Delta t} + c_{P,g}\, M_{ADS\ 4\text{-}x\ SEP,g} \frac{d\left(T_g\right)}{dt}$$

Expressing the previous equation as a difference:

$$c_{P,f} \frac{d(M_{ADS\ 4\text{-}X\ SEP}\ T_f)}{dt} \approx c_{P,f}\left(T_f - T_{REF}\right) \frac{\Delta M_{ADS\ 4\text{-}X\ SEP,f}}{\Delta t}$$

$$+ c_{P,f}\, M_{ADS\ 4\text{-}X\ SEP,f} \frac{\Delta T_f}{\Delta t} \qquad 4.7\text{-}17$$

$$+ c_{P,g}\left(T_g - T_{REF}\right) \frac{\Delta M_{ADS\ 4\text{-}x\ ,g}}{\Delta t} + c_{P,g}\, M_{ADS\ 4\text{-}x\ sep,g} \frac{\Delta T_g}{\Delta t}$$

All parameters and subscripts are as previously defined. Expanding the terms on the right-hand side of the equation:

$$c_{P,f}\,(T_f - T_{REF})\,\frac{\Delta M_{ADS\ 4\text{-}X\ SEP,\ f}}{\Delta t}$$

$$= c_{P,f}\,(T_{f,i} - T_{REF})\,\frac{M_{ADS\ 4\text{-}X\ SEP,\ f,\ i} - M_{ADS\ 4\text{-}X\ SEP,\ f,\ i-1}}{t_i - t_{i-1}} \qquad 4.7\text{-}18$$

$$c_{P,f}\,M_{ADS\ 4\text{-}X\ SEP,\ f}\,\frac{\Delta T_f}{\Delta t} = c_{P,f}\,M_{ADS\ 4\text{-}X\ SEP,\ f,\ i}\,\frac{T_{f,i} - T_{f,i-1}}{t_i - t_{i-1}}$$

$$c_{P,g}\,(T_g - T_{REF})\,\frac{\Delta M_{ADS\ 4\text{-}X\ SEP,\ g}}{\Delta t}$$

$$= c_{P,g}\,(T_{g,i} - T_{REF})\,\frac{M_{ADS\ 4\text{-}x\ SEP,\ g,\ i} - M_{ADS\ 4\text{-}x\ SEP,\ g,\ i-1}}{t_i - t_{i-1}} \qquad 4.7\text{-}19$$

$$c_{P,g}\,M_{ADS\ 4\text{-}x\ SEP,\ g}\,\frac{\Delta T_f}{\Delta_t} = c_{P,g}\,M_{ADS\ 4\text{-}x\ SEP,\ g,\ i}\,\frac{T_{g,i} - T_{g,i-1}}{t_i - T_{i-1}}$$

where:

i = Index of data and time arrays

All other parameters and subscripts are as previously defined. The specific heat of the liquid, $c_{P,f}$, is evaluated using the pressures and temperatures identified in Table 4.7-2. The total change in energy associated with the change in inventory of the two ADS-4 separators is then calculated as:

$$Q_{ADS\ 4\ LIQ} = Q_{ADS\ 4\text{-}1\ LIQ} + Q_{ADS\ 4\text{-}2\ LIQ} \qquad 4.7\text{-}20$$

4.7.5.2 Energy Transport Rate from the ADS-4 Separator by Exiting Steam Flow

The enthalpy of the steam exhaust from the ADS-4 separator is evaluated using the output from the pressure and temperature sensors associated with vapor flow meters (Table 4.7-2):

$$h_{g,\ FVM\text{-}XXX} = h_g(PT\text{-}XXX,\ TF\text{-}XXX) \qquad 4.7\text{-}21$$

where:

h_g = Enthalpy of steam, Btu/lbm

FVM-XXX is the data channel ID for the ADS-4 vapor flow meter, and PT-XXX and TF-XXX denote the vapor pressure and temperatures, respectively, associated with that flow meter. The rate of energy transport of the ADS-4 flow due to the steam component, then, is expressed as:

$$Q_{ADS\ 4\text{-}X\ STM} = \dot{M}_{ADS\ 4\text{-}X\ STM} \times h_{g,\ FVM\text{-}XXX} \qquad 4.7\text{-}22$$

All parameters and subscripts are as previously defined. The energy transport associated with steam flow from the two ADS-4 separators is then calculated as:

$$Q_{ADS\ 4\ STM} = Q_{ADS\ 4\text{-}1\ STM} + Q_{ADS\ 4\text{-}2\ STM} \qquad 4.7\text{-}23$$

4.7.5.3 Energy Transport Rate from the ADS-4 Separator by Exiting Liquid Flow

The enthalpy of the ADS liquid flow is determined using the output from the pressure and temperature sensors associated with the liquid flow meters as given in Table 4.7-2:

$$h_{f,\ FMM\text{-}XXX} = h_f\ (PT\text{-}XXX,\ TF\text{-}XXX) \qquad 4.7\text{-}24$$

where:

h_f = Enthalpy of liquid, Btu/lbm

FMM-XXX is the data channel ID of the ADS-4 liquid flow meter of interest, and PT-XXX and TF-XXX denote the data channel IDs for the liquid pressure and temperatures, respectively, associated with that flow meter. The rate of energy transport due to liquid flow from the ADS-4 separator, then, is expressed as:

$$Q_{ADS\ 4\text{-}X\ LIQ} = \dot{M}_{ADS\ 4\text{-}X\ LIQ} \times h_{f,\ PMM\text{-}XXX} \qquad 4.7\text{-}25$$

All parameters and subscripts are as previously defined. The total energy transport associated with liquid flow from the two ADS-4 separators is then calculated as:

$$Q_{ADS\ 4\ LIQ} = Q_{ADS\ 4\text{-}1\ LIQ} + Q_{ADS\ 4\text{-}2\ LIQ} \qquad 4.7\text{-}26$$

4.7.5.4 Rate of Change in Stored Energy of the ADS-4 Metal Components

The change in stored energy of the sump tanks and associated piping may be expressed as:

$$Q_{ADS\ 4\text{-}X\ METAL} = c_{P,\ METAL}\, M_{ADS\ 4\text{-}X\ METAL}\, \frac{d(\ T_{ADS\ 4\text{-}X\ METAL}\ )}{dt} \qquad 4.7\text{-}27$$

where the subscript:

METAL = Metal mass of steam/water separator tank and all associated piping of ADS-4 flow path of interest

All other parameters and subscripts are as previously defined. The total energy storage for the ADS-4 is calculated as:

$$Q_{ADS\ 4\ METAL} = Q_{ADS\ 4\text{-}1\ METAL} + Q_{ADS\ 4\text{-}2\ METAL} \qquad 4.7\text{-}28$$

The metal mass of the separator and steam exhaust piping are an input to this calculation. Temperatures from the data channel recording thermocouple TW-905 are used for this calculation.

4.7.5.5 Rate of Energy Loss from the ADS-4 Components to the Environment

The rate of energy loss from the ADS-4 separator and its associated piping to the environment is taken to be zero since the separator and steam exhaust line are trace-heated. Thus, the separator and steam lines are treated as an adiabatic boundary.

TABLE 4.7-1 INSTRUMENTATION TO BE USED FOR ADS-4 SEPARATOR LEVELS INSTRUMENT CORRECTION				
Location	**Function**	**Level Transducer**	**Pressure Transducer**	**Fluid Temperature**
ADS 4-1 Separator	Density compensation of levels data	LDP-611	PT-611	TF-619
ADS 4-2 Separator	Density compensation of levels data	LDP-612	PT-610	TF-618

TABLE 4.7-2 ADS-4 SEPARATOR STEAM AND LIQUID PRESSURE AND TEMPERATURE INSTRUMENT CHANNELS			
Flow Meter Description	**Flow Meter Channel ID**	**Pressure Channel ID**	**Temperature Channel ID**
ADS Separator 4-1 steam flow	FVM-603	PT-611	TF-623
ADS Separator 4-1 liquid flow	FMM-603	PT-610	TF-619
ADS Separator 4-2 steam flow	FVM-602	PT-611	TF-622
ADS Separator 4-2 liquid flow	FMM-602	PT-610	TF-618

4.8 Break Separator

The purpose of the break separator is to separate break flow into liquid and vapor components and to measure the flow rates of the single-phase flow components. Once measured, vapor flow is exhausted to the ambient environment, and liquid is directed to the primary sump simulation of the test facility. The break separator consists of a tank (separator); a vortex (vapor) flow meter; a magnetic (liquid) flow meter; and associated valves, piping, and instrumentation.

The total break flow may be calculated as:

$$\dot{M}_{BREAK} = \dot{M}_{BRK\,LIQ} + \dot{M}_{BRK\,STM} + \frac{dM_{BRK\,SEP}}{dt} \qquad 4.8\text{-}1$$

where:

M	=	Mass, lbm
$\dot{M}$	=	Mass flow rate, lbm/sec.
t	=	Time, sec.

and the subscripts:

BREAK	=	Both the total break flow
BRK LIQ	=	Liquid flow from break separator
BRK SEP	=	Break separator tank
BRK STM	=	Seam exhaust from break separator

Energy is transported out of the primary system by both the vapor and liquid components of break flow. Additionally, the following occurrences cause the stored energy level of the break separator to vary: a change in the fluid inventory held within the separator; a change in temperature of the fluid inventory held within the separator; a change in the temperature of the metal mass of the separator tank or a loss of energy to the ambient. Thus, the energy balance for the break separator, accounting for the change in stored energy of both the liquid inventory of the separator and the separator tank, may be expressed as:

$$Q_{BREAK} = Q_{BRK\,LIQ} + Q_{BRK\,STM} + c_p \frac{d(M_{BRK\,SEP}\,\Delta T)}{dt} + Q_{BLK\,SEP\,METAL} + Q_{BRK\,SEP\,AMB} \qquad 4.8\text{-}2$$

where:

c_p	=	Specific heat, Btu/(lbm-°F)
Q	=	Rate of energy transfer or transport, Btu/sec.
T	=	Temperature, °F

and the subscripts:

METAL	=	Metal mass of break separator tank and associated piping
AMB	=	Energy loss to ambient environment

All other parameters and subscripts are as previously defined.

4.8.1 Break Separator Liquid Inventory

The break separator is, in its simplest form, a tank. Liquid inventory in the break separator is monitored by a level transducer. For all tests, with the exception of double-ended DVI line breaks, an orifice was in place within the span of the level transducer. Therefore, a correction was made to the level indication to adjust for the pressure drop through the orifice. The functional steps and associated system of equations for operating on the output from the break separator level transducers to calculate liquid mass in the sump tanks follows:

Step 1: Calculate the pressure drop through the orifice and add this value to the readings from the break separator level transducer listed in Table 4.8-1 to account for the pressure drop through the orifice. The level channel data is identified in Table 4.8-1. The local pressure, fluid temperatures, and liquid flow rate to be used to calculate the pressure drop are identified in Table 4.8-1.

Step 2: Compensate the adjusted level indication for the break separator level to account for temperature differences between fluid in the separator tank and fluid in the reference leg of the instrument line. The local pressure and fluid temperatures to be used to accomplish the compensation are also identified in Table 4.8-1.

Step 3: The local pressures and temperatures identified in Table 4.8-2 are used to calculate the density of the fluid in the break separator:

$$\rho_{f,\,BRK\,SEP} = \rho_f(PT\text{-}905,\, TF\text{-}912) \qquad 4.8\text{-}3$$

$$\rho_{g,\,BRK\,SEP} = \rho_g(PT\text{-}905,\, TF\text{-}913)$$

where:

ρ	=	Density, lbm/ft.^{3}
PT-905	=	Local pressure in break separator tank
TF-912	=	Local liquid temperature of fluid in break separator tank
TF-913	=	Local vapor temperature of fluid at break separator exhaust

and the subscripts:

f	=	Liquid phase of water
g	=	Vapor phase of water

There is only one liquid temperature measurement instrument for the break separator, located in the drain line to the primary sump just downstream of flow meter FMM-905 and used to evaluate the thermodynamic properties of liquid in the break separators.

Step 4: Using the compensated liquid level and the break separator volume as a function of height, determine the volume of liquid in the break separator as:

$$V_{BRKSEP_f} = V(l)_{BRK\,SEP} \times LDP\text{-}905_{COMP} \qquad 4.8\text{-}4$$

where:

V	=	Volume, $ft.^3$
V(l)	=	Tank (steam/water separator) volume as a function of elevation, $ft.^3/ft.$
$LDP\text{-}905_{COMP}$	=	Compensated fluid levels data from level transducer LDP-905, ft.

The subscripts f and BRK SEP are as previously defined.

Step 5: The liquid mass inventory in the break separator is now calculated as:

$$M_{f,\,BRK\,SEP} = \rho_{f,\,BRK\,SEP} \times V_{f,\,BRK\,SEP} \qquad 4.8\text{-}5$$

All parameters and subscripts are as previously defined.

The vapor mass inventory of the break separator is then calculated as:

$$M_{g,\,BRK\,SEP} = \rho_g \times (V_{BRK\,SEP,\,TOTAL} - V_{f,\,BRK\,SEP}) \qquad 4.8\text{-}6$$

where the subscript:

TOTAL	=	Total volume associated with an ADS-4 separator, $ft.^3$

All other variables and subscripts are as previously defined.

Step 6 The rate of change in mass inventory of the break separator tank may be calculated by differencing two consecutive calculated values of the liquid and vapor masses:

$$\frac{dM_{BRK\ SEP}}{dt} \approx \frac{\Delta M_{BRK\ SEP}}{\Delta t} = \frac{M_{f,\ BRK\ SEP,i} - M_{f,\ BRK\ SEP,\ i-1}}{t_i - T_{i-1}} + \frac{M_{g,\ BRK\ SEP,\ i} - M_{g,\ BRK\ SEP,\ i-1}}{t_i - t_{i-1}} \quad 4.8\text{-}7$$

where the subscript:

i = Index of data and time arrays

All other parameters and subscripts are as previously defined.

4.8.2 Steam Flow Rates

The density of steam in the exhaust line from the break separator is evaluated using the pressure and temperature values recorded from the data channels identified in Table 4.8-2. Using this density, the steam portion of the break flow vented to ambient is calculated as:

$$\dot{M}_{FVM\text{-}XXX} = C_2 \times \rho_g \times \dddot{M}_{FVM\text{-}XXX} \quad 4.8\text{-}8$$

where:

C_2	=	Conversion constant, 1 min./60 sec.
$\dot{M}$	=	Mass flow rate, lbm/sec.
ρ_g	=	Vapor density, lbm/ft.^{3}
$\dddot{M}$	=	Volumetric flow

and the subscript:

FVM-XXX	=	Instrument channel ID where:
XXX	=	905 6-in. line
		906 8-in. common exhaust line

Total break steam flow is calculated as:

$$\dot{M}_{g,BRK} = \dot{M}_{FVM\text{-}905} + \dot{M}_{FVM\text{-}906} + \frac{dM_{g,\ BRKSEP}}{dt} \quad 4.8\text{-}9$$

4.8.3 Liquid Flow Rates

A single line directs liquid flow from the break separator into the primary sump tank. The mass flow from the break separator to the primary sump tank is calculated as:

$$\dot{M}_{FMM\text{-}905} = C_1 \times \rho_{f,\ FMM\text{-}905} \times \dot{\dot{M}}_{FMM\text{-}905} \qquad 4.8\text{-}10$$

and the subscript:

FMM-905 = Instrument channel ID for liquid flow meter in line between break separator and primary sump

All parameters are as previously defined but the volumetric liquid flow is in units of gallons per minute (gpm).

The density of the liquid passing through the flow meters is determined using data from the pressure and temperature instruments identified in Table 4.8-2.

Total liquid break flow rate passed to the sump simulation is calculated as:

$$\dot{M}_{f,\ BRK} = \dot{M}_{FMM\text{-}905} + \frac{dM_{f,\ BRKSEP}}{dt} \qquad 4.8\text{-}11$$

All parameters and subscripts are as previously defined.

4.8.4 Total Flow Rate

The total break flow rate is then calculated as:

$$\dot{M}_{BRK} = \dot{M}_{f,\ BRK} + \dot{M}_{g,\ BRK} \qquad 4.8\text{-}12$$

The total break flow is calculated by integrating the break flow rate step-wise over time:

$$M_{BRK,\ TOTAL} = \sum \left(\dot{M}_{BRK\ SEP} \right) \times \Delta t \qquad 4.8\text{-}13$$

All variables and subscripts are as previously defined. The flow quality of the break flow is also calculated as:

$$X_{BRK} = \frac{\dot{M}_{g,\ BRK}}{\dot{M}_{BRK,\ TOTAL}} \qquad 4.8\text{-}14$$

where:

X = Flow quality

All other variables and subscripts are as previously defined.

4.8.5 Energy Balance

The energy flow through the break separator consists of the following:

- Rate of change in stored energy of the break separator fluid inventory
- Energy transport rate from the break separator by steam exhaust flow
- Energy transport rate from the break separator by liquid flow to the sump
- Rate of change in stored energy of the metal of the break separator tank
- Rate of energy loss to the environment

The expressions evaluating these energy transfer or transport terms are developed in the following sections:

4.8.5.1 Rate of Change in Stored Energy of the Break Separator Fluid Inventory

The rate of change of energy in the break separator fluid may be expressed as:

$$c_P \frac{d(M_f\ \Delta T_f)}{dt} = c_{P,\ f}\ (T_F - T_{REF}) \frac{d(M_{f,\ BRK\ SEP})}{dt} + c_{P,\ f}\ M_{f,\ BRK\ SEP} \frac{d(T_f)}{dt} \qquad 4.8\text{-}15$$

where:

T_{REF} = Reference temperature, 32°F

Expressing the previous equation as a difference:

$$c_{P,\ f} \frac{d(\ M_{f,\ BRK\ SEP}\ T_f\ )}{dt} = c_{P,\ f}\ (T_F - T_{REF}) \frac{\Delta M_{f,\ BRK\ SEP}}{\Delta t} + c_{P,\ f}\ M_{f,\ BRK\ SEP} \frac{\Delta T_f}{\Delta t} \qquad 4.8\text{-}16$$

All parameters and subscripts are as previously defined. Expanding the terms on the right-hand side of the equation:

$$c_{P,f}\,(T_f - T_{REF})\,\frac{\Delta M_{f,\,BRK\,SEP}}{\Delta t} = c_{P,f}\,(T_f - T_{REF})\,\frac{M_{f,BRK\,SEP,\,i} - M_{f,BRK\,SEP,\,i-1}}{t_i - t_{i-1}}$$

$$c_{P,f}\,M_{f,\,BRK\,SEP}\,\frac{\Delta T_f}{\Delta t} = c_{P,f}\,M_{f,\,BRK\,SEP,\,i}\,\frac{T_{f,\,i} - T_{f,\,i+1}}{t_i - t_{i-1}} \qquad 4.8\text{-}17$$

where:

i = Index of data and time array

All other parameters and subscripts are as previously defined. The specific heat of the liquid, $c_{P,f}$, is evaluated using the pressures and temperatures identified in Table 4.8-1.

The rate of change of energy in the steam in the break separator may be expressed as:

$$c_{P,g}\,\frac{d(M_{g,\,BRK\,SEP}\,T_g)}{dt} = c_{P,g}\,(T_g - T_{REF})\,T_g\,\frac{d(M_{g,\,BRK\,SEP})}{dt} + c_{P,g}\,M_{g,\,BRK\,SEP}\,\frac{d(T_g)}{dt} \qquad 4.8\text{-}18$$

Expressing the previous equation as a difference:

$$c_{P,g}\,\frac{d(M_{g,\,BRK\,SEP}\,T_g)}{dt} \approx c_{P,g}\,(T_g - T_{REF})\,T_g\,\frac{\Delta M_{g,\,BRK\,SEP}}{\Delta t} + c_{P,g}\,M_{g,\,BRK\,SEP}\,\frac{\Delta(T_g)}{\Delta t} \qquad 4.8\text{-}19$$

All parameters and subscripts are as previously defined. Expanding the two terms on the right-hand side of the equation:

$$c_{P,g}\,(T_f - T_{REF})\,T_f\,\frac{\Delta M_{g,\,BRK\,SEP}}{\Delta t} = c_{P,g}\,(T_f - T_{REF})\,\frac{M_{g,BRK\,SEP,\,i} - M_{g,BRK\,SEP,\,i-1}}{t_i - t_{i-1}}$$

$$c_{P,g}\,M_{g,\,BRK\,SEP}\,\frac{\Delta(T_g)}{\Delta t} = c_{P,g}\,M_{g,\,BRK\,SEP,\,i}\,\frac{T_{g,\,i} - T_{g,\,i-1}}{t_i - t_{i-1}} \qquad 4.8\text{-}20$$

All variables and subscripts are as previously defined. The specific heat of the steam, $c_{P,f}$, is evaluated using the pressures and temperatures identified in Table 4.8-1.

4.8.5.2 Energy Transport Rate from the Break Separator by Steam Exhaust Flow

The enthalpy of the steam exhaust from the break separator is calculated using the output from the pressure and temperature sensors associated with FVM-905 and FVM-906 (Table 4.8-2):

$$h_{g,\ FVM\text{-}XXX} = h_g(PT\text{-}YYY,\ TF\text{-}ZZZ) \qquad 4.8\text{-}21$$

where:

h_g = Enthalpy of steam, Btu/lbm

FVM-XXX denotes a specific flow meter, and PT-YYY and TF-ZZZ denote the vapor pressure and temperatures associated with that flow meter. The rate of energy transport from the break separator due to exhaust steam, then, is expressed as:

$$Q_{FVM\text{-}XXX} = \dot{M}_{FVM\text{-}XXX} \times h_{g,\ FVM\text{-}XXX} \qquad 4.8\text{-}22$$

where:

$Q_{FVM\text{-}XXX}$ = Rate of energy transport due to steam flow through flow meter FVM-XXX

All subscripts are as previously defined. The total energy transport rate, then, is calculated as:

$$Q_{BRK\ STM} = Q_{FVM\text{-}905} + Q_{FVM\text{-}906} \qquad 4.8\text{-}23$$

4.8.5.3 Energy Transport Rate from the Break Separator by Liquid Flow to the Sump

The enthalpy of liquid flow into the break separator is calculated using the output from the pressure and temperature sensors associated with FMM-905 (Table 4.8-2):

$$h_{f,\ FMM\text{-}905} = h_f\ (PT\text{-}905,\ TF\text{-}912) \qquad 4.8\text{-}24$$

where:

h_f = Enthalpy of liquid, Btu/lbm

FMM-905 denotes the flow meter to which the enthalpy is applicable, and PT-905 and TF-912 denote the liquid pressure and temperatures associated with that flow meter. The rate of energy transport from the break separator due to liquid overflow into the sump, then, is expressed as:

$$Q_{BRK\ LIQ} = \dot{M}_{BRK\ LIQ} \times h_{f,\ FMM-905} \qquad 4.8\text{-}25$$

All parameters and subscripts are as previously defined.

4.8.5.4 Rate of Change in Stored Energy of the Metal of the Break Separator Tank

The change in energy of the break separator tank and associated piping may be expressed as:

$$Q_{BRK\ SEP} = c_{P,\ METAL} \times M_{BRK\ SEP\ METAL} \times \frac{d(T_{BRK\ SEP\ METAL})}{dt} \qquad 4.8\text{-}26$$

where the subscript:

METAL = Metal mass of break separator tank and all associated piping

All other variables and subscripts are as previously defined.

4.8.5.5 Rate of Energy Loss to the Environment

The rate of energy loss from the break separator and its associated piping to the environment is taken to be zero because the separator and the steam exhaust lines are trace-heated. Thus, the separator and steam lines are treated as an adiabatic boundary. Heat loss to the environment from the liquid drain line running from the break separator to the sump is neglected since the run of pipe is small.

TABLE 4.8-1 INSTRUMENTATION TO BE USED FOR SUMP MASS AND ENERGY BALANCE				
Location	**Function**	**Level Transducer**	**Pressure Transducer**	**Fluid Temperature**
Break separator	Density compensation of levels data	LDP-905	PT-905	TF-912

TABLE 4.8-2 BREAK SEPARATOR STEAM EXHAUST AND LIQUID PRESSURE AND TEMPERATURE INSTRUMENT CHANNELS			
Flow Meter Description	**Flow Meter Channel ID**	**Pressure Channel ID**	**Temperature Channel ID**
Break separator steam exhaust flow	FVM-905	PT-905	TF-903
	FVM-906	0.5 x (PT-901 + PT-905)	TF-913
Break separator liquid flow	FMM-905	PT-905	TF-912

4.9 Sumps

In the AP600 plant design, the sump collects all liquid released from the primary system and serves as the source of post-accident long-term cooling water inventory. In the test, the sump is modeled by two tanks: a primary sump tank and a smaller secondary sump tank. These tanks have associated with them piping, vapor and liquid flow meters, and other pressure and temperature measurement instrumentation.

Accounting for all possible flow paths associated with the sump, the general mass balance on that component may be expressed as:

$$\frac{dM_{SUMP}}{dt} = \dot{M}_{f,\ BRK\ SEP} + \dot{M}_{f,\ ADS\ 4\text{-}1\ SEP} + \dot{M}_{f,\ ADS\ 4\text{-}2\ SEP} + \dot{M}_{IRWST} - \dot{M}_{STM\ XHST} - \dot{M}_{SUMP\ INJ} \qquad 4.9\text{-}1$$

where:

M	=	Mass, lbm
$\dot{M}$	=	Mass flow rate, lbm/sec.

and the subscripts:

SUMP	=	Both primary and secondary sump tanks
BRK SEP	=	Liquid flow from break separator through FMM-903
ADS 4-1 SEP	=	Liquid flow from the ADS 4-1 steam/water separator through FMM-603
ADS 4-2 SEP	=	Liquid flow from the ADS 4-2 steam/water separator through FMM-602
IRWST	=	Liquid overflow from IRWST into sump through FMM-703
STM XHST	=	Steam exhaust from sump through FVM-903
SUMP INJ	=	Liquid flow from sump to DVI line through FMM-901 and FMM-902

Energy is transported out of the sump by both the vapor and liquid components of flow associated with the sump. In addition, the stored energy associated with the sump may change due to a change in the liquid inventory held within the sump, a change in temperature of the liquid inventory held within the sump, or a change in the temperature of the metal mass of the sump tanks, or heat loss to the ambient. Thus, the energy balance for the sump, accounting for the change in stored energy of both the liquid inventory of the sump and the sump tank(s) may be expressed as:

$$c_P \frac{d(M_{SUMP}\ T_f)}{dt} = Q_{BRK\ SEP} + Q_{ADS\ 4\text{-}1\ SEP} + Q_{ADS\ 4\text{-}2\ SEP} + Q_{IRWST} - Q_{STM\ XHST} - Q_{SUMP\ INJ} - Q_{SUMP\ METAL} - Q_{SUMP\ AMB} \qquad 4.9\text{-}2$$

where:

c_p	=	Specific heat, Btu/(lbm-°F)
Q	=	Rate of energy transfer or transport, Btu/sec.
T	=	Temperature, °F

and the subscripts:

METAL	=	Metal mass of sump tanks and associated piping
AMB	=	Energy loss to ambient environment

All other parameters and subscripts are as previously defined.

4.9.1 Sump Liquid Inventory

For convenience, liquid mass in the primary and secondary sump tanks are calculated separately, then summed to yield the total liquid mass in the sump. Liquid inventory in the sump tanks are measured by a level transducer. Load cells installed on the two sump tanks are not used to inventory calculations.

4.9.1.1 Use of Levels Measurement for Mass Calculation

The functional steps and associated system of equations for operating on the output of the sump level transducers to calculate liquid mass in the sump tanks follows:

Step 1: Compensate all readings from the primary and secondary sump level transducers to account for temperature differences between fluid in the tanks and fluid in the reference legs of the instrument lines. The two channels of level data to be compensated are identified in Table 4.9-1. The instruments used to measure local pressure and fluid temperatures to be used to accomplish the compensation are also identified in Table 4.9-1.

Step 2: The local pressures and temperatures as recorded from the instrument channels identified in Table 4.9-1 are used to calculate the density of the fluid (liquid and vapor) in the sump tanks:

$$\rho_{\ell,j} = \rho_{\ell,j}(P, T) \qquad 4.9\text{-}3$$

$$\rho_g = \rho_g(P, T) \qquad 4.9\text{-}4$$

where:

ρ	=	Density, lbm/ft.^{3}
$\rho(P, T)$	=	Local pressure in sump tank
T	=	Local temperature of fluid in sump tank

and the subscripts:

f	=	Liquid phase of water
g	=	Vapor phase of water
j	=	Either sump tank
P	=	Primary sump
S	=	Secondary sump

The instrument IDs and the elevation of the instruments for the local fluid temperature measurements to be used in the calculation of fluid densities for both the primary and secondary sumps are given in Table 4.9-1.

Note that there is only one vapor space temperature measurement provided to calculate steam density.

Step 3: Using the compensated liquid level and the sump volume as a function of height, determine the volume of liquid in the sump:

$$V_{f,j} = V(l)_{SUMP_j} \times LDP\text{-}XXX_{COMP} \qquad 4.9\text{-}5$$

where:

V	=	Volume, ft.^{3}
V(l)	=	Volume as a function of elevation, ft.^{3}/ft.
$LDP\text{-}XXX_{COMP}$	=	Compensated fluid levels data from the level transducer identified as
		XXX = 901 primary sump LDP transducer
		902 secondary sump LDP transducer

The subscripts f and j are as previously defined.

Step 4: The liquid mass inventory in the primary and secondary sump is calculated as:

$$M_{f,\,SUMP\,j} = \rho_{f,j} \times V_{f,j} \qquad 4.9\text{-}6$$

All parameters and subscripts are as previously defined.

The total liquid mass inventory in the sump is calculated as:

$$M_{f,\,SUMP} = M_{f,\,SUMP\,P} + M_{f,\,SUMP\,S} \qquad 4.9\text{-}7$$

The vapor mass inventory of the sump is then calculated as:

$$M_{g,\,SUMP} = \rho_g \times (V_{SUMP,\,TOTAL} - V_{f,\,SUMP\,P} - V_{f,\,SUMP\,S}) \qquad 4.9\text{-}8$$

where the subscript:

TOTAL = Total volume associated with an ADS-4 separator, ft.^{3}

All other variables and subscripts are as previously defined.

Step 5: The total fluid mass in the primary and secondary sumps are calculated as:

$$M_{SUMP} = M_{f,\,SUMP} + M_{g,\,SUMP} \qquad 4.9\text{-}9$$

Step 6: The rate of change in mass inventory of the break separator tank may be calculated by differencing two consecutive calculated values of the liquid and vapor masses:

$$\frac{dM_{SUMP}}{dt} \approx \frac{\Delta M_{SUMP}}{\Delta t} = \frac{M_{f,\,SUMP,\,i} - M_{f,\,SUMP,\,i-1}}{t_i - t_{i-1}}$$

$$= \frac{M_{g,\,SUMP,\,i} - M_{g,\,SUMP,\,i-1}}{t_i - t_{i-1}} \qquad 4.9\text{-}10$$

where the subscript:

i = Index of data and time arrays

4.9.2 Sump Steam Exhaust Flow

Steam exhaust from the primary sump may be measured by either of two flow meters: FVM-903 in a 3/4-in. schedule 40 run of piping or FVM-906 in a common 8-in. neader with steam flow from the

break separator. The units of measurement of both vapor flow meters is standard cubic feet per minute (scfm).

4.9.2.1 Steam Flow Rates

The density of steam in the 3/4-in. and 8-in. common header exhaust lines is evaluated using the ASME steam table routines with pressure and temperature inputs from the data channels identified in Table 4.9-3. Using these densities, the steam mass flow is calculated as:

$$\dot{M}_{FVM\text{-}XXX} = C_2 \times \rho_{g,\ FVM\text{-}XXX} \times \dddot{M}_{FVM\text{-}XXX} \qquad 4.9\text{-}11$$

where:

C_2	=	Conversion constant, 1 min./60 sec.
$\dot{M}$	=	Mass flow rate, lbm/sec.
ρ_g	=	Vapor density, lbm/ft.^{3}
$\dddot{M}$	=	Volumetric flow

and the subscript:

FVM-XXX	=	Instrument channel ID where:
	XXX =	903 3/4-in. exhaust line
		906 8-in. common exhaust line

The total steam flow exhausted by the primary sump and the break separator is calculated as:

$$\dot{M}_{STM\ XHST} = \dot{M}_{FVM\text{-}903} + \dot{M}_{FVM\text{-}906} \qquad 4.9\text{-}12$$

4.9.3 Sump Injection

Two lines provide for liquid to flow from the primary sump into the DVI lines and the reactor pressure vessel simulation. Mass flow from the sump through either of the two sump injection lines is calculated as:

$$\dot{M}_{FMM\text{-}XXX} = C_1 \times \rho_{FMM\text{-}XXX} \times \dddot{M}_{FMM\text{-}XXX} \qquad 4.9\text{-}13$$

where the subscript:

C_1	=	Conversion constant (1ft.^{3}/sec.)/448.86 gpm
FMM-XXX	=	Instrument channel ID where:
	XXX	= 901 piping run to DVI-1
		= 902 piping run to DVI-2

All parameters are as previously defined.

The density of the liquid passing through the flow meters is determined using data from the pressure and temperature instruments identified in Table 4.9-2 as input to the ASME steam tables. The total mass flow rate to the DVI lines from the sump is calculated as:

$$\dot{M}_{SUMP\ INJ} = \dot{M}_{FMM-901} + \dot{M}_{FMM-902} \qquad 4.9\text{-}14$$

The total mass injected by each injection line into the DVI line is calculated by integrating the product of the measured mass flow rates and the time interval over which the measurement is taken:

$$M_{FMM-XXX} = \sum (\dot{M}_{FMM-XXX,\,i} \times \Delta t_i) \qquad 4.9\text{-}15$$

All parameters and subscripts are as previously defined. The total liquid mass injected from the sump is calculated as:

$$M_{SUMP\ INJ} = M_{FMM-901} + M_{FMM-902} \qquad 4.9\text{-}16$$

4.9.4 Total Flow Rate Out of the Sump

Total mass flow rate out of the sump is then calculated as:

$$\dot{M}_{SUMP} = \dot{M}_{SUMP\ INJ} + \dot{M}_{STM\ XHST} \qquad 4.9\text{-}17$$

Total mass flow out of the sump is calculated by integrating the mass flow rate step-wise over time:

$$M_{SUMP,\,TOTAL} = \Sigma\ \dot{M}_{SUMP} \times \Delta t \qquad 4.9\text{-}18$$

All variables and subscripts are as previously defined.

4.9.5 Energy Balance

Energy into the sump from the break separator, the two ADS-4 separators, and the IRWST overflow lines are calculated in and obtained from their respective modules. Thus, the calculation of a mass balance on the sump requires that the following parameters be evaluated:

- Rate of change in stored energy of the sump liquid inventory
- Energy removal rate from the sump by steam exhaust flow
- Energy removal rate from the sump by injection flow supplied to the DVI lines
- Rate of change in stored energy of the metal of the sump tanks
- Rate of energy loss to the environment

The expressions for evaluating these five energy transfer or transport terms are developed in the following sections.

4.9.5.1 Rate of Change in Stored Energy of the Sump Liquid Inventory

The rate of change of energy in the liquid in the sump may be expressed as:

$$c_{P,f}\frac{d(M_{f,SUMP}T_f)}{dt} = c_{P,f}(T_f - T_{REF})\frac{d(M_{f,SUMP})}{dt} + c_{P,f}M_{f,SUMP}\frac{d(T_f)}{dt} \qquad 4.9\text{-}19$$

Expressing the previous equation as a difference:

$$c_{P,f}\frac{d(M_{f,SUMP}T_f)}{dt} \approx c_{P,f}(T_f - T_{REF})\frac{\Delta M_{f,SUMP}}{\Delta t} + c_{P,f}M_{f,SUMP}\frac{\Delta T_f}{\Delta t} \qquad 4.9\text{-}20$$

All parameters and subscripts are as previously defined. Expanding the two terms on the right-hand side of the equation:

$$c_{P,f}(T_f - T_{REF})\frac{\Delta M_{f,SUMP}}{\Delta t} = c_{P,f}(T_{f,i} - T_{REF})\frac{M_{f,SUMP,i} - M_{f,SUMP,i-1}}{t_i - t_{i-1}} \qquad 4.9\text{-}21$$

$$c_{P,f}M_{f,SUMP}\frac{\Delta T_f}{\Delta t} = c_{P,f}M_{f,SUMP,i}\frac{T_{f,i} - T_{f,i+1}}{t_i - t_{i-1}}$$

where:

i = Index of data and time arrays

All other parameters and subscripts are as previously defined. Each of the terms on the right-hand side of the previous equation is to be evaluated for both the primary and secondary sump tank inventories. The specific heat of the liquid, $c_{p,f}$, is evaluated using the pressures and temperatures identified in Table 4.9-1. Note that, for the primary sump, the specific heat of the liquid may be evaluated for more than one zone or region, depending on the water level in the sump. A similar set of equations is solved to determine the change in stored energy associated with steam in the sumps.

4.9.5.2 Energy Removal Rate from the Sump by Steam Exhaust Flow

The enthalpy of the steam exhaust from the sump is calculated using the output from the pressure and temperature sensors associated with FVM-903 and FVM-906 (Table 4.9-2):

$$h_{g,\ FVM\text{-}XXX} = h_g(PT\text{-}YYY,\ TF\text{-}ZZZ) \qquad 4.9\text{-}22$$

where:

h_g = Enthalpy of steam, Btu/lbm

FVM-XXX denotes a specific flow meter, and PT-YYY and TF-ZZZ denote the vapor pressure and temperatures associated with that flow meter. The rate of energy transport from the sump due to exhaust steam, then, is expressed as:

$$Q_{FVM\text{-}XXX} = \dot{M}_{FVM\text{-}XXX} \times h_{g,\ FVM\text{-}XXX} \qquad 4.9\text{-}23$$

where:

$Q_{FVM\text{-}XXX}$ = Rate of energy transport due to steam flow through FVM-XXX

All subscripts are as previously defined. The total energy transport rate, then, is calculated as:

$$Q_{sTMXHST} = Q_{FVM\text{-}903} + Q_{FVM\text{-}906} \qquad 4.9\text{-}24$$

4.9.5.3 Energy Removal Rate from the Sump by Injection Flow Supplied to the DVI Lines

The enthalpy of the injected liquid from the sump is determined using the output from the pressure and temperature sensors associated with FMM-901 and FMM-902 (Table 4.9-2) and the ASME steam table routines. Expressed mathematically:

$$h_{f,\ FMM\text{-}XXX} = h_f\ (PT\text{-}YYY,\ TF\text{-}ZZZ) \qquad 4.9\text{-}25$$

where:

h_f = Enthalpy of liquid, Btu/lbm

FMM-XXX denotes a specific flow meter, and PT-YYY and TF-ZZZ denote the liquid pressure and temperatures associated with that flow meter. The rate of energy transport from the sump due to injected liquid, then, is expressed as:

$$Q_{FMM\text{-}XXX} = \dot{M}_{FMM\text{-}XXX} \times h_{f,\ FMM\text{-}XXX} \qquad 4.9\text{-}26$$

where:

$Q_{FMM\text{-}XXX}$ = Rate of energy transport due to liquid flow through FMM-XXX

All subscripts are as previously defined. The total energy transport rate, then, is calculated as:

$$Q_{SUMP\ INJ} = Q_{FMM\text{-}901} + Q_{FMM\text{-}902} \qquad 4.9\text{-}27$$

4.9.5.4 Rate of Change in Stored Energy of the Metal of the Sump Tanks

The change in stored energy of the sump tanks and associated piping may be expressed as:

$$Q_{SUMP\ METAL} = c_{P,\ METAL}\ M_{SUMP\ METAL}\ \frac{d(\ T_{SUMP\ METAL}\ )}{dt} \qquad 4.9\text{-}28$$

where the subscript:

METAL = Metal mass of the primary and secondary tanks and all associated piping, lbm

All other parameters and subscripts are as previously defined.

Two thermocouples are used to characterize the primary and secondary sump metal temperatures: primary sump, TFM-901; secondary sump, TFM-902.

4.9.5.5 Rate of Energy Loss to the Environment

The rate of energy loss from the sump and its associated piping to the environment may be expressed as:

$$Q_{SUMP\ AMB} = U \times A \times \Delta T \qquad 4.9\text{-}29$$

where:

A	=	Effective external surface area of the sump, $ft.^2$
U	=	Overall effective heat transmission coefficient, $Btu/(sec\text{-}ft.^2\text{-}°F)$
ΔT	=	Difference between ambient air temperature and bulk metal temperature, °F

An equivalent heat transfer coefficient, accounting for heat resistance due to any insulation applied to the outside surface of the sump volumes and natural convection from the outside surface to the ambient, is used to evaluate the heat loss to ambient from the metal surfaces of the sump tanks. The same metal surface temperatures used to evaluate metal heat storage of the sumps is used to calculate heat loss to the ambient. Surface areas included in this calculation account for sump tanks and associated piping.

TABLE 4.9-1
INSTRUMENTATION TO BE USED FOR SUMP MASS AND ENERGY BALANCE

Function	Location	Level Transducer	Pressure Transducer	Fluid Temperature
Density compensation of level data	Primary sump	LDP-901	PT-901	TF-901 TF-903 TF-905
	Secondary sump	LDP-902	PT-901	TF-902
Sump vapor temperature	3/4-in. exhaust line		PT-901	TF-906

TABLE 4.9-2
SUMP STEAM EXHAUST AND INJECTION
PRESSURE AND TEMPERATURE INSTRUMENT CHANNELS

Flow Meter Description	Flow Meter Channel ID	Pressure Channel ID	Temperature Channel ID
Sump steam exhaust flow	FVM-903	PT-901	TF-906
	FVM-906	0.5 (PT-901 + PT-905)	TF-918
Sump injection flow	FMM-901	PT-901	TF-909
	FMM-902	PT-901	TF-904

4.10 Passive Residual Heat Removal

4.10.1 Fluid Mass Conservation Equation

The passive residual heat removal heat exchanger (PRHR HX) consists of a number of tubes with a fluid flow path at the top for the inlet connection from hot leg 2 (HL-2) and a fluid flow path at the bottom for the outlet connection to steam generator 2 (SG-2) outlet. The general fluid (H_2O) mass conservation equation, which relates the change in stored fluid mass with respect to time (the fluid-mass time derivative) to the mass flow rates in and out, reduces to the following:

$$\frac{dM_{H_2O,PRHR}}{dt} = W_{in\ (from\ HL_2)\ H_2O,PRHR} - W_{out\ (to\ SG_2)\ H_2O,PRHR} \qquad 4.10\text{-}1$$

The left-hand side of the fluid mass conservation equation is approximated from the value of the fluid mass at two consecutive time points as follows:

$$\frac{dM_{H_2O,PRHR}}{dt} \approx \frac{\Delta M_{H_2O,PRHR}}{\Delta t} = \frac{M^{n}_{H_2O,PRHR} - M^{n-1}_{H_2O,PRHR}}{t^{n} - t^{n-1}} \qquad 4.10\text{-}2$$

The H_2O fluid mass is simply the sum of the water and steam masses:

$$M_{H_2O,PRHR} = M_{water,PRHR} + M_{steam,PRHR} \qquad 4.10\text{-}3$$

The water and steam mass calculations are based on the measured water level. The level (LDP) instrument channel ID for PRHR is listed in Table 4.10-1. This LDP is corrected for temperature effects using the LDP compensation method. As is generally assumed for each plant component, pure water is modeled below the compensated water level, and pure steam is modeled above the compensated water level.

To use the available measurements from the fluid thermocouples, the PRHR HX is divided into five axial fluid property zones for the calculation of various fluid conditions. Table 4.10-1 contains a list of the fluid thermocouples employed for each axial fluid property zone, along with the zone top elevations.

Note that, since LDP-802 (which spans just the tubes) is being employed for the water level of the entire PRHR HX (including the inlet and outlet), instead of the usual method of using the axial fluid property zone temperatures/elevations in the LDP compensation calculations, it is necessary to use an alternate set of temperature channels/elevations for the LDP corrections. Table 4.10-1 contains a list of the fluid thermocouples employed for each LDP compensation region, along with their elevations. The LDP compensation region boundaries are arbitrarily taken at the vertical midpoint between consecutive fluid thermocouples.

In general, the water and steam masses are given by:

$$M_{water,PRHR} = \sum_{j=1}^{N_{zone,PRHR}} M_{water,PRHR_j}$$

$$M_{steam,PRHR} = \sum_{j=1}^{N_{zone,PRHR}} M_{steam,PRHR_j} \qquad 4.10\text{-}4$$

For zones j below those containing the compensated water level (which contain all water), the zone j water and steam masses are given by the following, where j = 1,...,levzone-1:

$$M_{water,PRHR_j} = \rho_{water,PRHR_j} \times V_{zone,PRHR_j} \times C_3$$

$$M_{steam,PRHR_j} = 0. \qquad 4.10\text{-}5$$

where:

C_3 = Conversion constant, 1 ft.^{3}/1728 in.^{3}

For the zone j containing the compensated water level, the zone j water and steam masses are given by the following, where j = levzone:

$$M_{water,PRHR_j} = \rho_{water,PRHR_j} \times V_{water,zone,PRHR_j} \times C_3$$

$$M_{steam,PRHR_j} = \rho_{steam,PRHR_j} \times V_{steam,zone,PRHR_j} \times C_3 \qquad 4.10\text{-}6$$

For zones j above those containing the compensated water level (which contain all steam) the zone j water and steam masses are given by the following, where j = levzone+1,...,$N_{zone,PRHR}$:

$$M_{water,PRHR_j} = 0.$$
$$M_{steam,PRHR_j} = \rho_{steam,PRHR_j} \times V_{zone,PRHR_j} \times C_5 \qquad 4.10\text{-}7$$

The fluid volumes are calculated as a function of level from the volume-versus-height tabular data listed in Table 4.10-2, via linear interpolation within the table. No extrapolation at either end is performed; the first and last table points define the applicable range. The first point is [h_{min} (= 0.), V_{min} (= 0.)], and the last point is [h_{max}, V_{max}].

During initialization, the volume-versus-height data/function is employed to calculate the total volume of each zone j as follows:

for j=1:

$$V_{zone,PRHR_j} = V_{function}(E_{top,PRHR_j}) \qquad 4.10\text{-}8$$

for j=2,...,$N_{zone,PRHR}$:

$$V_{zone,PRHR_j} = V_{function}(E_{top,PRHR_j}) - \sum_{k=1}^{j-1} V_{zone,PRHR_k}$$

During the transient calculations, the volume-versus-height data/function is employed to calculate the water volume of the zone containing the compensated water level, j = levzone, as follows:

if j(=levzone)=1:

$$V_{water,zone,PRHR_j} = V_{function}(L_{water,PRHR}) \qquad 4.10\text{-}9$$

if j(=levzone)>1:

$$V_{water,zone,PRHR_j} = V_{function}(L_{water,PRHR}) - \sum_{k=1}^{j-1} V_{zone,PRHR_k}$$

The steam volume of the zone containing the compensated water level, j = levzone, is then the following:

$$V_{steam,zone,PRHR_j} = V_{zone,PRHR_j} - V_{water,zone,PRHR_j} \qquad 4.10\text{-}10$$

The zone j water and steam densities are simply the reciprocal of the water- and steam-specific volumes, respectively:

$$\rho_{water,PRHR_j} = \frac{1.0}{V_{water,PRHR_j}}$$

$$\rho_{steam,PRHR_j} = \frac{1.0}{V_{steam,PRHR_j}} \qquad 4.10\text{-}11$$

The zone j water-specific volume is calculated from the ASME steam table function VCL as follows:

$$V_{water,PRHR_j} = VCL(P_{PRHR}, T_{water,PRHR_j}) \qquad 4.10\text{-}12$$

The zone j steam-specific volume is calculated from the ASME steam table function HSS as follows:

$$h_{steam,PRHR_j} = HSS(P_{PRHR}, T_{steam,PRHR_j}, S_{steam,PRHR_j}, V_{steam,PRHR_j}) \qquad 4.10\text{-}13$$

The zone j water and steam temperatures are simply given by the zone temperatures, which are the fluid thermocouple measurements TF-XXX (see Table 4.10-1). Care is taken to insure that the water temperature value employed is at or below the saturation temperature and that the steam temperature value employed is at or above the saturation temperature:

$$T_{water,PRHR_j} = \min(T_{zone,PRHR_j}, T_{sat,PRHR})$$

$$T_{steam,PRHR_j} = \max(T_{zone,PRHR_j}, T_{sat,PRHR}) \qquad 4.10\text{-}14$$

where:

$$T_{zone,\ PRHR_i} = TF\text{-}XXX_{PRHR_i} \qquad 4.10\text{-}14$$

The saturation temperature is calculated from the ASME steam table function TSL as follows:

$$T_{sat,PRHR} = TSL(P_{PRHR}) \qquad 4.10\text{-}15$$

The pressure is set equal to the value from the PT-XXX_{PRHR} measurement (see Table 4.10-1) after conversion from gauge (psig) to absolute (psia) pressure.

This completes the discussion of the calculations related to the left-hand side of the fluid mass conservation equation.

On the right-hand side of the fluid mass conservation equation, the calculation of the outlet fluid mass flow rate (to the SG-2 outlet) is performed directly from the liquid volumetric flow rate measurement (FMM-XXX_{PRHR_outlet}), due to the fact that the water flowing in the line remains subcooled (see Table 4.10-1 for the instrument channel ID). Thus:

$$W_{out\ (to\ SG_2)\ H_2O,PRHR} = W_{out\ (to\ SG_2)\ water,PRHR}$$

$$= \max(0.,FMM\text{-}XXX_{PRHR\_outlet}) \times \rho_{water,PRHR_i} \times C_1 \qquad 4.10\text{-}16$$

where:

C_1 = Conversion constant, (1 ft.^{3}/sec.)/448.86 gpm

The water density is given by that from axial fluid property zone 1 (at the bottom).

Although a liquid volumetric flow rate measurement (FMM) is available for the inlet line, it cannot be relied on for accurate mass flow rate calculations due to two-phase flow. Thus, having calculated both the change in stored fluid mass (from the left-hand side) and the outlet fluid mass flow rate (from the right-hand side), the fluid mass conservation equation is rearranged to solve for (infer) the inlet fluid mass flow rate (from the HL-2).

This completes the discussion of the calculations related to the right-hand side of the fluid mass conservation equation.

4.10.2 Fluid Energy Conservation Equation

The general fluid (H_2O) energy conservation equation, which relates the change in stored energy with respect to time (the fluid-energy time derivative) to the energy rates in and out (due to the connected flow paths) and the energy addition rate due to other external devices, reduces to the following:

$$\frac{d[M \times c_p \times (T-T_{ref})]_{H_2O,PRHR}}{dt} = Q_{in\ (from\ HL_2)\ H_2O,PRHR} - Q_{out\ (to\ SG_3)\ H_2O,PRHR} + Q_{[metal \Rightarrow H_2O],PRHR} \qquad 4.10\text{-}17$$

where:

c_p = Specific heat, BTU/(lbm-°F)

The left-hand side of the energy conservation equation is approximated as follows:

$$\frac{d[M \times c_p \times (T-T_{ref})]_{H_2O,PRHR}}{dt} \approx \sum_{j=1}^{N_{sub,PRHR}} \frac{\Delta[M \times c_p \times (T-T_{ref})]_{water,PRHR_j}}{\Delta t} + \sum_{j=1}^{N_{sub,PRHR}} \frac{\Delta[M \times c_p \times (T-T_{ref})]_{steam,PRHR_j}}{\Delta t} \qquad 4.10\text{-}18$$

$$\frac{\Delta[M\times c_p\times(T-T_{ref})]_{water,PRHR_j}}{\Delta t} \approx c_{p_{water,PRHR_j}} \times \left[\frac{\Delta[M\times(T-T_{ref})]_{water,PRHR_j}}{\Delta t}\right]$$

where:

$$\approx c_{p_{water,PRHR_j}} \times (T_{water,PRHR_j}-T_{ref})\times\left[\frac{M^{n}_{water,PRHR_j} - M^{n-1}_{water,PRHR_j}}{t^{n}-t^{n-1}}\right]$$

$$+ c_{p_{water,PRHR_j}} \times M_{water,PRHR_j}\times\left[\frac{T^{n}_{water,PRHR_j} - T^{n-1}_{water,PRHR_j}}{t^{n}-t^{n-1}}\right] \quad 4.10\text{-}19$$

and

$$\frac{\Delta[M\times c_p\times(T-T_{ref})]_{steam,PRHR_j}}{\Delta t} \approx c_{p_{steam,PRHR_j}} \times \left[\frac{\Delta[M\times(T-T_{ref})]_{steam,PRHR_j}}{\Delta t}\right]$$

$$\approx c_{p_{steam,PRHR_j}} \times (T_{steam,PRHR_j}-T_{ref})\times\left[\frac{M^{n}_{steam,PRHR_j} - M^{n-1}_{steam,PRHR_j}}{t^{n}-t^{n-1}}\right] \quad 4.10\text{-}20$$

$$+ c_{p_{steam,PRHR_j}} \times M_{steam,PRHR_j}\times\left[\frac{T^{n}_{steam,PRHR_j} - T^{n-1}_{steam,PRHR_j}}{t^{n}-t^{n-1}}\right]$$

The zone j water-specific heat capacity at constant pressure is calculated from the ASME steam table function CPL as follows:

$$c_{p_{water,PRHR_j}} = CPL(P_{PRHR}, T_{water,PRHR_j}) \quad 4.10\text{-}21$$

The zone j steam-specific heat capacity at constant pressure is calculated from the ASME steam table function CPV as follows:

$$c_{p_{steam,PRHR_j}} = CPV(P_{PRHR}, T_{steam,PRHR_j}, v_{steam,PRHR_j}) \qquad 4.10\text{-}22$$

This completes the discussion of the calculations related to the left-hand side of the fluid energy conservation equation.

On the right-hand side of the fluid energy conservation equation, the calculation of the outlet fluid energy transport rate (to the SG-2 outlet) is given by the following:

$$Q_{out\ (to\ SG_2)\ H_2O,PRHR} = Q_{out\ (to\ SG_2)\ water,PRHR} = W_{out\ (to\ SG_2)\ water,PRHR}\, h_{water,PRHR\_outlet} \qquad 4.10\text{-}23$$

The outlet line water-specific enthalpy is calculated from the ASME steam table function HCL as follows:

$$h_{water,PRHR\_outlet} = HCL(P_{PRHR}, T_{water,PRHR_1}, S_{water,PRHR\_outlet}) \qquad 4.10\text{-}24$$

The water temperature is given by that from axial fluid property zone 1 (at the bottom).

The energy addition rate to the fluid due to heat transfer from the metal is given by:

$$Q_{[metal \Rightarrow H_2O],PRHR} = Q_{[tube\ metal \Rightarrow H_2O],PRHR} + Q_{[inlet\ line\ metal \Rightarrow H_2O],PRHR} + Q_{[outlet\ line\ metal \Rightarrow H_2O],PRHR} \qquad 4.10\text{-}25$$

Due to a lack of metal temperature data for the inlet and outlet lines, their contributions in the previous equation are ignored, i.e.:

$$Q_{[\text{inlet line metal} \Rightarrow H_2O],PRHR} \approx 0.0$$

$$Q_{[\text{outlet line metal} \Rightarrow H_2O],PRHR} \approx 0.0 \qquad 4.10\text{-}26$$

The contribution from the tube metal-to-fluid heat transfer rate is calculated from the tube metal energy conservation equation, which is discussed below.

Finally, having calculated the change in stored fluid energy (from the left-hand side) and the outlet fluid energy transport rate and metal-to-fluid heat transfer rate (from the right-hand side), the fluid energy conservation equation is rearranged to solve for (infer) the inlet fluid energy transport rate (from the HL-2).

This completes the discussion of the calculations related to the right-hand side of the fluid energy conservation equation.

4.10.3 Tube Metal Energy Conservation Equation

The general metal energy conservation equation, which relates the change in stored metal energy with respect to time (the metal-energy time derivative) to the energy rates in and out (due to heat transfer), reduces to the following for the PRHR HX tube metal (note that here, the "ambient" is the IRWST fluid in which the tubes reside):

$$\frac{d[M \times c_p \times (T - T_{ref})]_{\text{tube metal,PRHR}}}{dt} = - Q_{[\text{tube metal} \Rightarrow H_2O],PRHR} - Q_{[\text{tube metal} \Rightarrow \text{IRWST}],PRHR} \qquad 4.10\text{-}27$$

Due to the location of the thermocouple instrumentation, the tube metal is divided into four metal segments. Table 4.10-3 lists the tube metal thermocouple channel ID and tube metal mass data for each tube metal segment, which are required in the tube metal energy calculations.

The left-hand side of the tube metal energy conservation equation is approximated as follows:

$$\frac{d[M \times c_p \times (T - T_{ref})]_{tube\ metal,PRHR}}{dt} \approx \frac{\Delta[M \times c_p \times (T - T_{ref})]_{tube\ metal,PRHR}}{\Delta t} \qquad 4.10\text{-}28$$

where:

$$\frac{\Delta[M \times c_p \times (T - T_{ref})]_{tube\ metal,PRHR}}{\Delta t} \approx \sum_{m=1}^{N_{tube\ metal,PRHR}} M_{tube\ metal,PRHR_m} \times c_{p_{tube\ metal,PRHR_m}} \times \left[\frac{T^{n}_{tube\ metal,PRHR_m} - T^{n-1}_{tube\ metal,PRHR_m}}{t^{n} - t^{n-1}} \right] \qquad 4.10\text{-}29$$

The tube metal segment specific heat capacity at constant pressure is calculated as a function of the tube metal segment temperature from the metal c_p versus temperature tabular data listed in Table 4.10-4, via linear interpolation within the table. No extrapolation at either end is performed; the first and last table points define the applicable range. The first point is (T_{min}, $c_{p,min}$), and the last point is (T_{max}, $c_{p,max}$).

This completes the discussion of the calculations related to the left-hand side of the tube metal energy conservation equation.

On the right-hand side of the tube metal energy conservation equation, the tube metal-to-IRWST heat transfer rate is inferred from the IRWST fluid energy conservation equation, due to a lack of enough detailed information for rigorous heat transfer calculations.

Finally, having calculated both the change in stored tube metal energy (from the left-hand side) and the tube metal-to-IRWST heat transfer rate (from the right-hand side), the tube metal energy conservation equation is rearranged to solve for (infer) the tube metal-to-fluid heat transfer rate.

This completes the discussion of the calculations related to the right-hand side of the tube metal energy conservation equation.

TABLE 4.10-1 INSTRUMENTATION EMPLOYED FOR PRHR FLUID CALCULATIONS	
Description	**Item**
Level (in.)	LDP-802
Pressure (psig)	PT-107
Outlet line liquid flow rate (gpm)	FMM-804
Zone temperature [°F]/Top Elev (in.)	TF-804 4.375
[Bottom (outlet) to Top (inlet)]	TF-805 7.000
	TF-809 50.000
	TF-811 52.875
	TF-803 57.000
LDP Comp region temp (°F)/Elev (in.)	TF-805 0.000
Bottom (outlet) to Top (inlet)	TF-809 29.625
	TF-811 57.000

TABLE 4.10-2 VOLUME VERSUS HEIGHT TABLES FOR PRHR FLUID VOLUME CALCULATIONS	
Height (in.)	**Volume (in^3)**
0.00	0.0
1.75	0.0
7.00	871.3
50.00	1076.7
55.75	1513.4
57.00	1513.4

TABLE 4.10-3 DATA FOR PRHR TUBE METAL ENERGY CALCULATIONS (PER SEGMENT)		
Metal Segment	**Temperature ID (°F)**	**Mass (lbm)**
1 (Bottom horizontal)	TW-801	37.0
2 (Bot 1/2 vertical)	TW-803	40.0
3 (Top 1/2 vertical)	TW-806	40.0
4 (Top horizontal)	TW-808	37.0

TABLE 4.10-4 SPECIFIC HEAT CAPACITY VERSUS TEMPERATURE TABLE FOR PRHR TUBE METAL ENERGY CALCULATIONS	
Metal c_p [Btu/(lbm-°F)]	**Metal Temperature (°F)**
0.1085	70.0
0.1109	100.0
0.1175	200.0
0.1223	300.0
0.1256	400.0
0.1279	500.0
0.1297	600.0

4.11 Reactor Pressure Vessel

The reactor pressure vessel (RPV) model includes the lower plenum, core, upper plenum, and upper head. The vessel analysis includes liquid level and mass, core power, steam production due to core power, and flow quality at the core exit.

The core vessel is shown in Figure 4.11-1. A total of eight regions are modeled. The actual spans and elevations of the lower plenum, core, upper plenum, and upper head are used. Elevations are relative to the inside bottom of the vessel. Volumes for supporting structures are also included so as to support the use of actual elevations and simplify coding algorithms.

Figure 4.11-1 also shows the six axial core heater power steps. Total heater power was varied during the tests; power history data is provided for each test. A top-skewed power distribution was used for all tests.

Fluid thermocouple elevations in the core are shown in Figure 4.11-1. The fifteen locations include all elevations outside of the core region. Where multiple thermocouples are provided at a given elevation, the average was used in all analyses. Two problems were identified with the core fluid thermocouples:

- The core fluid thermocouples are located in instrumented rods, with one rod at the core center and the remainder at the core perimeter. Fluid temperature histories for core center and perimeter thermocouples were found to differ. This was attributed to smaller power-to-flow ratios for the perimeter heater rods than for the center rod due to larger flow areas. In order to best represent the average core temperature associated with the average flow area, the center-rod temperatures were used exclusively.

- The core fluid thermocouple histories were noisy. The noise was investigated and found to be unrelated to core thermal-hydraulic phenomena. A time-history smoothing method was selected to minimize the noise. This smoothing was applied to all core fluid thermocouples.

LDPs available to determine liquid levels are shown in Figure 4.11-2. Level instrumentation problems common to all tests were identified and are summarized below.

Values for LDPs spanning the supporting structures tend to be influenced by flow through the supporting structures. The flow effect tends to bias the LDPs toward higher readings and may cause an LDP to read full during an entire test. Since the bias is a function of flow quality and flow rate, the effect varies during the tests. As a result, DP-111 and DP-114 were not useful; they read either full scale or clearly overstated the liquid levels. These LDPs were not used in any analyses.

LDP-112 generally read full scale. Figure 4.11-3 provides an uncorrected plot of LDP-112 and the adjacent LDP-113 data. LDP-113 is directly above LDP-112. During the period around

1500 seconds, LDP-112 clearly indicated that the level has dropped into the span of LDP-112. LDP-112 failed to respond. LDP-112 was not used in any analyses.

The pressure taps used in the vessel analysis are also shown in Figure 4.11-2. Since the pressure taps (PT-107 and PT-108) are located at the top and bottom of the vessel, the pressures should differ due to the effects of water column density. Some problems were identified via comparison of the pressure gradients of Matrix Tests SB01 and SB18. Figure 4.11-4 shows the pressure gradient ($P_{PT-108} - P_{PT-107}$) for the two tests. The gradients are similar for about the first 2000 seconds, after which the gradient for Matrix Test SB01 deviates to a value inconsistent with the height of the water column. This was found to be due to an error in PT-108 for Matrix Test SB01. To minimize the impact of pressure irregularities, RPV analyses are based on one of the pressure taps, which is selected on a test-by-test basis. PT-107 was used for Matrix Test SB01 and PT-108 was used for Matrix Test SB18.

The pressure tap irregularities were found to be on the order of two psi. The potential impact of a two psi error is related to the importance of the associated change in water and steam properties. For most analyses this effect is relatively unimportant. As discussed in Subsection 4.11.2.1, core steam production calculations may be sensitive to a two psi error.

4.11.1 Core Vessel Model

The core vessel model is shown in Figure 4.11-5. Eight fluid regions and six core heated regions are modeled. The selected level instrumentation is shown. Fifteen temperature zones associated with the fifteen thermocouple elevations are also shown.

The spans of the selected LDPs differ from the fluid regions and temperature zones and are shown in Table 4.11-1.

LDP levels are relative to their lower pressure taps. To be consistent with other elevations, region levels are defined relative to the inside bottom of the vessel. Region liquid levels are related to LDP readings as follows:

- When the LDP reading is empty or less then empty, the region level is set to either the bottom of the region or the bottom of the LDP span, whichever is greater. In cases where the LDP lower tap is above the bottom of the region, as is the case in the upper plenum, this logic results in a minimum calculated liquid level and a void fraction constrained to a value less than 1.

- When the LDP reading is between empty and full, the density-corrected level is used. If this results in a level above the top LDP tap, the next method is used.

- When the LDP reading is full or more than full, the region level is set either to the top of the region and the top of the LDP span, whichever is less. The region is assumed to be full of

liquid; the void fraction is set equal to 0. In cases were the LDP upper tap is below the top of the region, step changes in region void fraction and mass will occur when the LDP readings vary between full and less than full.

The effects of this level and mass methodology are shown in Table 4.11-2.

The fifteen temperature zones bound the thermocouple elevations. The midpoints between the thermocouple elevations define the intermediate zone boundaries. The top and bottom zone boundaries are set equal to the model top and bottom. Fluid and steam properties are assumed constant in each zone. Zone properties are based on the local pressure and temperature. The local pressure is based on the selected pressure tap, the liquid levels, and the density effects of water.

Region liquid masses and volume-based void fractions are determined using lookup tables that relate liquid levels to region volumes. These tables account for axial variations in the region cross-sectional areas.

4.11.2 Core Power and Flow Model

The core is subdivided into six axial heater regions that are 6 in. high. The axial-heater-region power distributions were the same for all tests and were constant during the tests. The core total power and axial power distribution are defined below.

Core total power is defined as:

$$P_T = \frac{1}{2} \sum_{i=1}^{4} P_i \qquad 4.11\text{-}1$$

where:

P_T = Total heater rod power, kW
P_i = Heater rod power data, kW

The heater rod instrument list is provided in Table 4.11-3. The power distribution is provided in Table 4.11-4.

4.11.2.1 Core Steam Production - Tsat Method

Core steam production and saturation line are calculated from core power, core fluid temperature, and local saturation temperature using the following steps:

Step 1: Determine the saturation line by finding the interaction between curves of local saturation temperature and fluid temperature.

Step 2: Determine the power above the saturation line. Power above the saturation line is assumed to generate steam; power below this elevation is assumed to heat water.

Step 3: Determine steam production from power above the saturation line and the enthalpy of vaporization.

Fluid temperatures are defined at the thermocouple elevations. The fluid temperature curve is constructed by linearly interpolating between the elevations. The local pressures are also defined at the thermocouple elevations. The saturation temperature curve is defined by determining the saturation temperature at the local pressure at the thermocouple elevations and linearly interpolating between the elevations. Starting at the bottom and searching in the direction of increasing elevation, the saturation line is found by finding the intersection between the two curves.

The temperature profiles for the entire vessel are used. As a result, the intersection may occur outside of the bounds of the core. If an intersection is not found, or the intersection is not in the core, then:

- If the core fluid temperatures are above the saturation temperature, the intersection elevation is set equal to the bottom of the core.

- If the core fluid temperatures are below the saturation temperature, the intersection elevation is set equal to the top of the core.

Power above and below the saturation line is defined by:

$$P_{ab} = \int_{\text{sat line}}^{\text{top of core}} \frac{P_T}{36''} \, FTP_z \, dz \qquad 4.11\text{-}2$$

$$P_{bl} = P_T - P_{ab}$$

where:

36"	=	Total height of heater region
P_{ab}	=	Power above saturation line
P_{bl}	=	Power below saturation line
FTP_z	=	Fraction of total power for region bounding elevation z

Several methods for calculating steam and flow were investigated. The modeling of the core for steam and flow calculations is shown in Figure 4.11-6. The calculations are based on properties at the three locations shown. Properties at the saturation line are determined from the saturation temperature

calculated by interpolation of the saturation temperature curve. Thermocouple elevations were selected as proxies to the core top and bottom elevations; the corresponding thermocouple temperatures and local pressures were used to calculate associated properties.

The selected method determines steam production directly from power above the saturation line and the enthalpy of vaporization. Steam production from the core is calculated as:

$$\dot{M}_s = \frac{P_{ab}}{h_{fg,si}} \qquad 4.11\text{-}3$$

where:

$\dot{M}_s$	=	Steam production
$h_{fg,si}$	=	Enthalpy of vaporization at saturation line

The viability of this method for determining steam production is dependent on the accuracy of the saturation line calculation. Since the saturation line is the intersection of the fluid and saturation temperature curves, the accuracy of the this elevation is a function of the slope of the two temperature curves. The saturation temperature curve is a function of local pressure and varies only slightly over the span of the core. The fluid temperature gradient varies widely during the transient as shown for Matrix Test SB01 in Figure 4.11-7. The gradient is very small during steady state operation; and is small during the first several hundred seconds of the transient, and during long term cooling. Since the applicability of this method is a function of the fluid temperature gradient, the range of applicability may vary from test to test.

4.11.2.2 Core Steam Production - DVI Line Flow Method

Core steam production and saturation line are calculated from core power, core inlet enthalpy, and the DVI line flow rate using the following steps:

Step 1: The core inlet enthalpy is based on the fluid temperature and local pressure in the lower plenum. Starting with the bottom core heated region, the enthalpy rise for each of the six heated regions is determined from the DVI line flow rate, enthalpy at the bottom of the region, and the core power in the region.

Step 2: The saturation line is identified by locating the first region where the enthalpy exceeds that of saturated liquid and interpolating the enthalpy rise to determine the saturation line elevation in that region. The power above the saturation line is then calculated.

Step 3: Core exit quality is determined using the steam tables and the enthalpy at the top of the core. Steam production is then determined using the quality and DVI line flow rate.

The saturation line is calculated as:

$$(h_{\ell,sl} - h_{\ell,1})\,\dot{M} = \int_{\text{bottom of core}}^{\text{sat line}} \frac{P_T}{36''}\,FTP_z\,dz, \text{ for } \dot{M} > 0 \qquad 4.11\text{-}4$$

where:

sat line = bottom of core, for $\dot{M} = 0$

$\dot{M}$	=	Liquid flow rate into core = DVI line flow
$h_{\ell,sl}$	=	Liquid enthalpy at saturation line
$h_{\ell,1}$	=	Liquid enthalpy at core entrance

Core-exit flow quality and core steam production can be calculated from the liquid flow rate and a core energy balance:

$$h_2 = h_{\ell,1} + \frac{P_T}{\dot{M}} \qquad 4.11\text{-}5$$

$$X_2 = f\,(h_2, P_{TC}) \qquad 4.11\text{-}6$$

$$\dot{M}_s = X_2\,\dot{M} \qquad 4.11\text{-}7$$

$$\alpha_2 = \frac{X_2\rho_{\ell,2}}{X_2\rho_{\ell,2} + (1-X)\rho_{v,2}} \qquad 4.11\text{-}8$$

where:

h_2	=	Mixture enthalpy at core exit
$h_{v,2}$ $h_{\ell,2}$	=	Vapor and liquid enthalpy at core exit, respectively
$\rho_{v,2}$ $\rho_{\ell,2}$	=	Vapor and liquid density at core exit, respectively
X_2	=	Flow quality at core exit
α_2	=	Flow void fraction at core

P_{TC}	=	Pressure at top of the core
f (h, P)	=	Steam table function for quality

The viability of this method for determining steam production is dependent on the assumption that the DVI line flow is representative of the flow into the core from the lower plenum. This assumption clearly does not apply during steady state operation. During the first several hundred seconds of the transient the DVI line flow is not representative due to draining of various components, which includes the steam generators, hot legs, cold legs, and pressurizer. After ~500 seconds, the DVI line flow is a good representation of the core inlet flow.

This method is relatively insensitive to the core temperature gradient. The effects of pressure errors are primarily limited to the change in mixture enthalpy at the top of the core. As a result, this method is well behaved during long term cooling and is preferred over the Tsat Method for this phase of the transient.

TABLE 4.11-1 CORE VESSEL MODEL GEOMETRY					
Region	**Level Instrument**	**Bottom of Region**	**Bottom of LDP**	**Top of Region**	**Top of LDP**
Lower plenum	LDP-106 LDP-107	0	2	6.41	10.22
Lower core plate	LDP-108	6.41	2	9.91	10.22
Core	LDP-138	9.91	10.22	50.86	50.17
Core plenum	LDP-139	50.86	50.17	52.75	74.13
Upper core plate	LDP-139	52.75	50.17	53.5	74.13
Upper plenum	LDP-113	53.5	58.71	74.42	77.83
Upper support plate	LDP-115	74.42	77.83	77.42	97.58
Upper head	LDP-115	77.72	77.83	97.58	97.58

TABLE 4.11-2 MASS METHODOLOGY EFFECTS		
Region	**Minimum Level Effects**	**Maximum Level Effects**
Core	Minimum mass > 0 Maximum void fraction < 1	Small step changes in mass and void fraction when level varies to/from top of LDP span
Upper plenum	Minimum mass >> 0 Maximum void fraction << 1	None
Upper head	Minimum mass > 0 Maximum void fraction < 1	None

TABLE 4.11-3 HEATER ROD INSTRUMENTATION	
Pi	**Instrument Name**
P_1	KW-101
P_2	KW-102
P_3	KW-103
P_4	KW-104

TABLE 4.11-4 POWER DISTRIBUTION	
Axial Heater Region	**Fraction of Total Power in Region**
1, bottom heater region	0.19367
2	0.24293
3	0.22487
4	0.1798
5	0.1172
6, top heater region	0.4153

TABLE 4.11-5
OSU TEST ANALYSIS PLOT PACKAGE FOR SECTION 4.11

Plot Number	Component	Variables	Units	Description
1	Reactor Vessel	N/A	N/A	Reactor Vessel Geometry
2	Reactor Vessel	N/A	N/A	Reactor Vessel Level and Pressure Instrumentation
3	Reactor Vessel	LDP-112 LDP-113	in.	Uncorrected Levels Results of Test SB18
4	Reactor Vessel	Delta-P = PT-108 - PT-107	psi	Pressure Gradients for Tests SB01 and SB18
5	Reactor Vessel	N/A	N/A	Reactor Vessel Model
6	Reactor Vessel	N/A	N/A	Modeling of Core Steam and Flow Calculations
7	Reactor Vessel	Core Temperature Rise	°F	Core Temperature Gradient

Note:

PLOTS 3, 4, AND 7 ARE NOT INCLUDED IN THIS NONPROPRIETARY DOCUMENT.

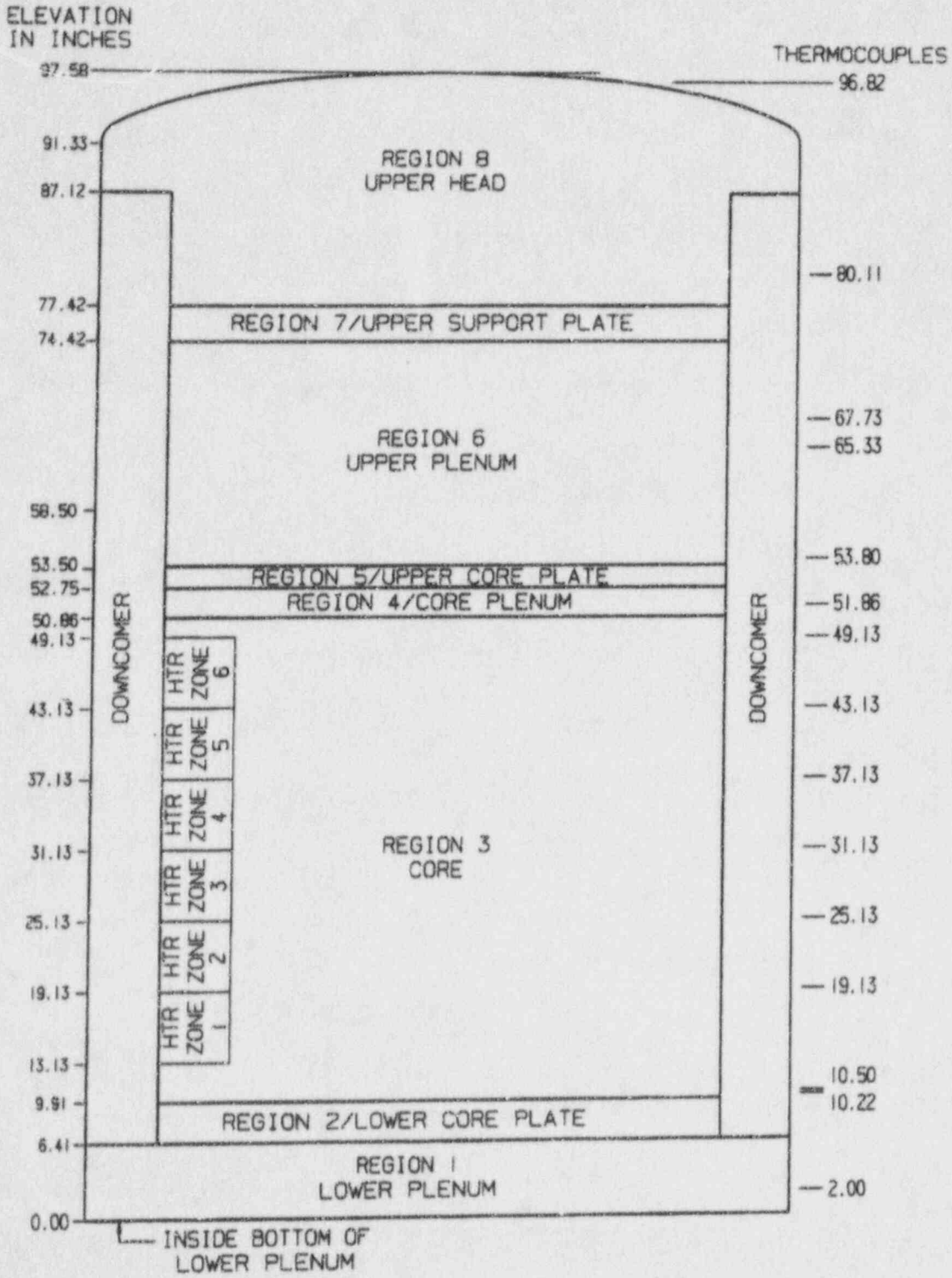

Figure 4.11-1 Reactor Vessel Geometry

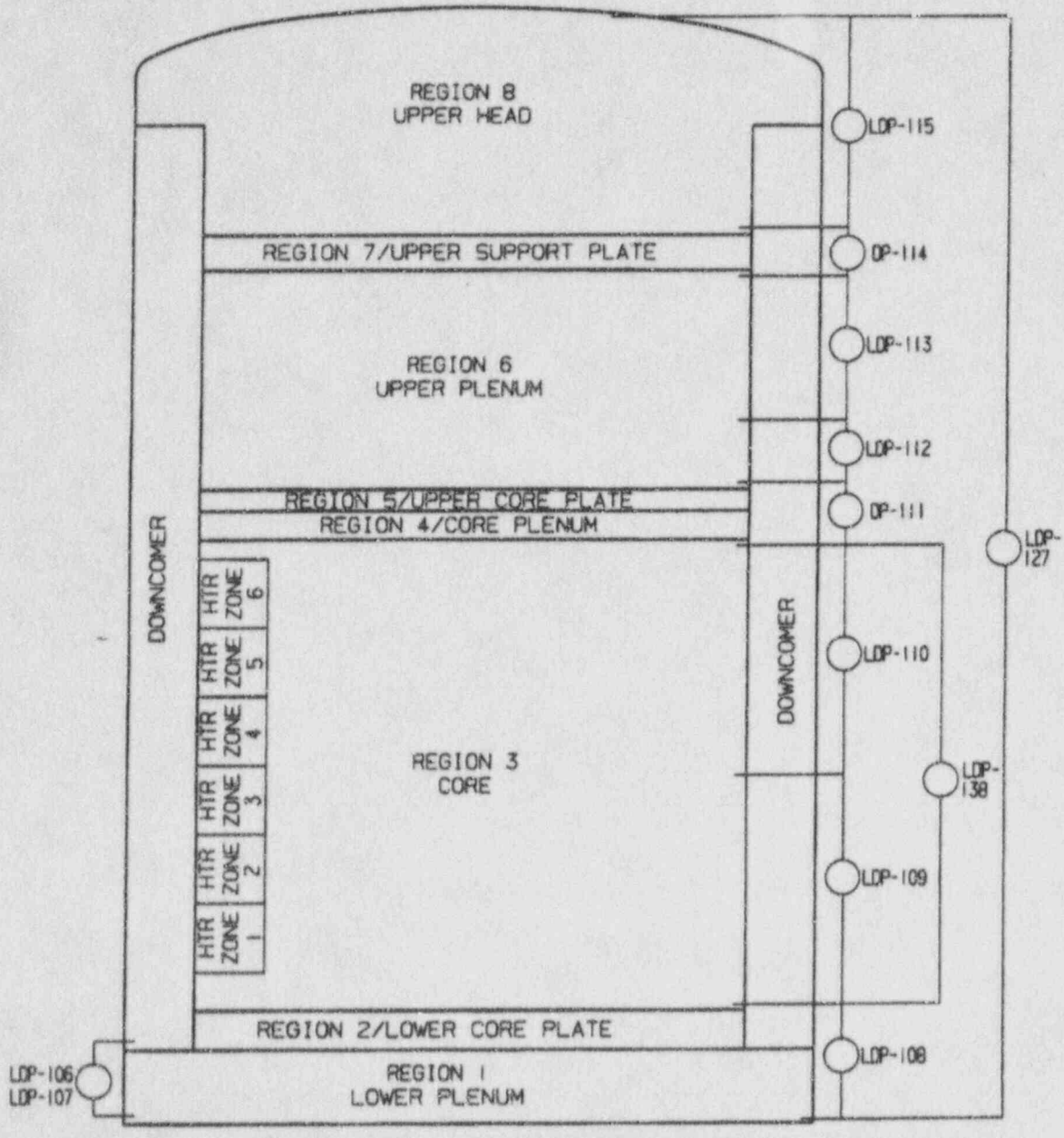

Figure 4.11-2 Reactor Vessel Level Instrumentation

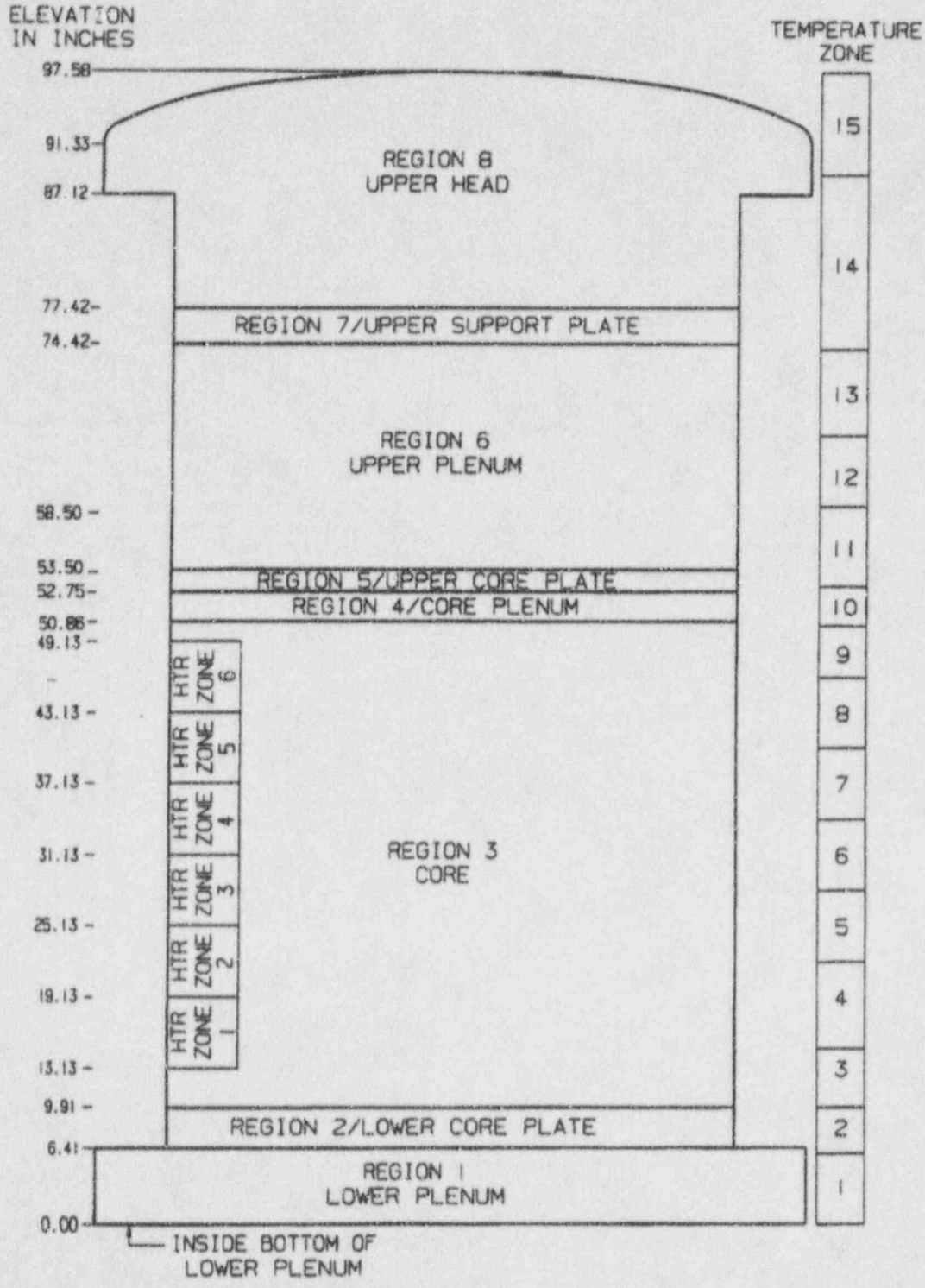

Figure 4.11-5 Reactor Vessel Model

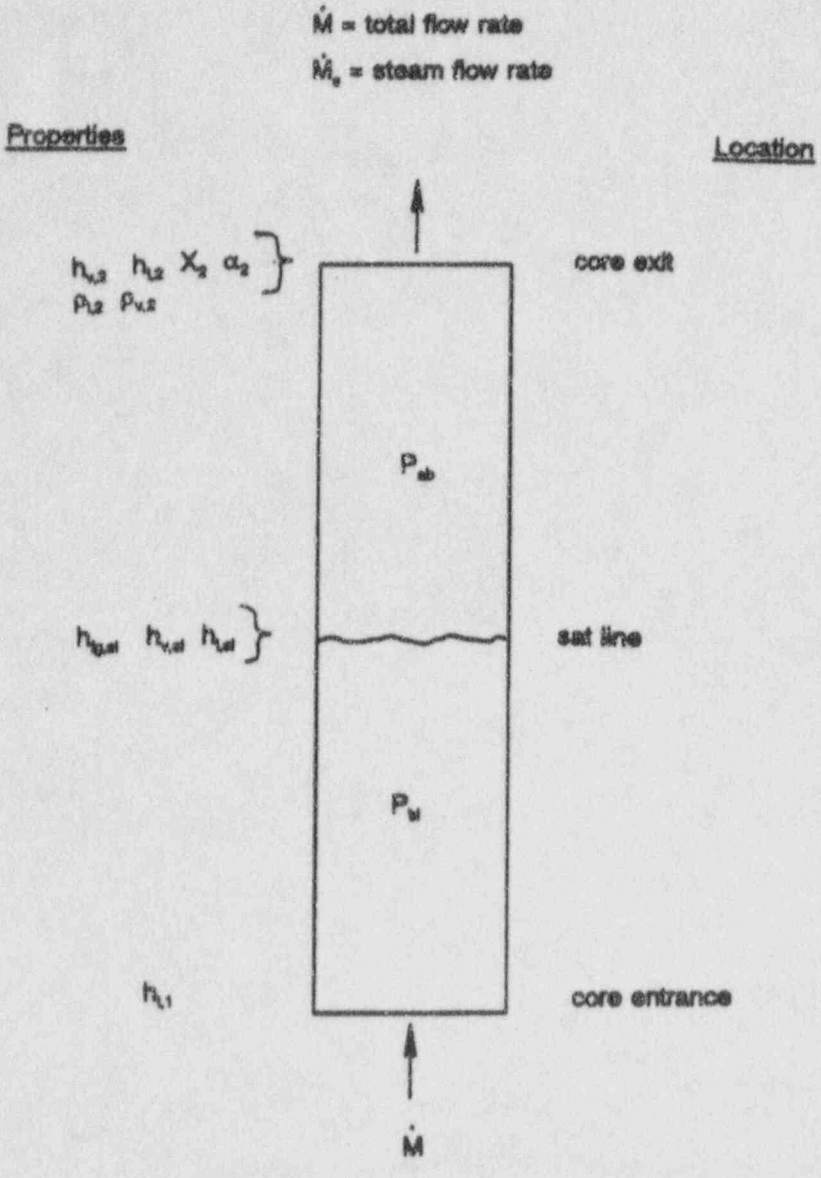

Figure 4.11-6 Modeling of Core Steam and Flow Calculations

4.12 Downcomer

The downcomer consists of the cylindrical volume in the RPV surrounding the core and upper plenum. Its component interfaces include two DVI lines, four cold legs, reactor vessel lower plenum, and reactor vessel upper head bypass gaps. The downcomer is modeled separately from the other reactor vessel regions. Parameters calculated for the downcomer include liquid level, mass, flow from the DVI lines, and flow in the lower plenum.

Downcomer instrumentation used to analyze the test includes two LDPs that measure liquid level, and thermocouples that provide fluid and metal temperatures. The LDPs are positioned at different circumferential locations and span nearly the full height of the downcomer.

4.12.1 Downcomer Level and Mass

The downcomer fluid temperature distribution is defined by dividing the volume into a vertical array of temperature zones. Where multiple thermocouples are provided at a given elevation, the average temperature is used. Axial midpoints between the thermocouple elevations define the intermediate zone boundaries. The top and bottom zone boundaries are set equal to the top and bottom of the downcomer. Fluid and steam properties are assumed to be constant in each temperature zone. Zone properties are based on local pressure and temperature. Local pressure is based on the pressure at the top of the reactor vessel, the liquid levels, and the density effects of water.

The downcomer liquid level is determined by averaging the two LDP readings and applying density corrections for the density difference between the reference leg and the measured water column. Downcomer liquid and vapor mass are determined using lookup tables that relate liquid levels to volumes. These tables account for axial variations in the cross-sectional areas. Mass calculations are done on a temperature-zone basis and employ the temperature-zone densities.

4.12.2 Downcomer Flows

The two DVI lines provide flow to the downcomer from six components: the IRWST, the primary sump, the two CMTs, and the two accumulators. The lines are fully instrumented with liquid flow meters.

Total DVI line flow can be calculated directly from the overall flow meters or by summing up the individual flows. DVI line flows are calculated by:

$$\dot{M}_{DVI\ 1} = \dot{M}_{FMM-205} \qquad 4.12\text{-}1$$

or

$$\dot{M}_{DVI\ 1} = \dot{M}_{FMM-701} + \dot{M}_{FMM-901} + \dot{M}_{FMM-501} + \dot{M}_{FMM-41} \qquad 4.12\text{-}2$$

$$\dot{M}_{DVI\ 2} = \dot{M}_{FMM-206} \qquad 4.12\text{-}3$$

or

$$\dot{M}_{DVI\ 2} = \dot{M}_{FMM-702} + \dot{M}_{FMM-902} + \dot{M}_{FMM-504} + \dot{M}_{FMM-42} \qquad 4.12\text{-}4$$

where:

$\dot{M}_{DVI\ i}$ = DVI line liquid flow rate for DVI line i, lbm/sec.

$\dot{M}_{FMM-xxx}$ = Flow meter liquid flow for FMM-xxx, converted from gpm to lbm/sec. based on thermocouples and pressure taps selected to provide conditions representative of flow meter conditions

Both methods for calculating the DVI line flow are provided; user inputs control the selection of the method used to calculate the DVI line flow into the downcomer. The downcomer calculations in this report are based on readings from overall flow meters FMM-205 and FMM-206.

4.12.3 Cold-Leg Flow

Liquid and vapor flow rates are calculated for the cold leg, as shown in Subsection 4.18. Overall cold-leg flow into the downcomer is calculated by:

$$\dot{M}_{CL} = \sum_{i=1}^{4} \dot{M}_{v,CLi} + \sum_{i=1}^{4} \dot{M}_{\ell,CLi} \qquad 4.12\text{-}5$$

where:

$\dot{M}_{CL}$ = Total mass flow rate into downcomer from cold legs, lbm/sec.

$\dot{M}_{v,CLi}$ = Vapor mass flow rate from cold-leg i, lbm/sec.

$\dot{M}_{\ell,CLi}$ = Liquid mass flow rate from cold-leg i, lbm/sec.

4.12.4 Downcomer Flow into Reactor Lower Plenum

Downcomer flow into the reactor lower plenum is calculated by mass balance:

$$\dot{M}_{DWN} = \dot{M}_{DVI\,1} + \dot{M}_{DVI\,2} + \dot{M}_{CL} - \frac{dM_{DWN}}{dt} \qquad 4.12\text{-}6$$

$$\frac{dM_{DWN}}{dt} = \frac{\Delta M_{\ell,\,DWN} + \Delta M_{v,\,DWN}}{\Delta t} \qquad 4.12\text{-}7$$

where:

$M_{\ell,DWN}$ $M_{v,DWN}$	=	Downcomer liquid and vapor mass, lbm
t	=	Time, sec.
$\dot{M}_{DWN}$	=	Downcomer to lower plenum mass flow rate, lbm/sec.

TABLE 4.12-1 DVI LINE FLOWMETERS		
DVI Line	**Flow Measured for Components**	**Flow Meter**
DVI-1	IRWST	FMM-701
	Primary sump	FMM-901
	CMT-1	FMM-501
	ACC-1	FMM-401
	Overall DVI-1 flow	FMM-205
DVI-2	IRWST	FMM-702
	Primary sump	FMM-902
	CMT-1	FMM-504
	ACC-2	FMM-402
	Overall DVI-2 flow	FMM-206

4.13 Steam Generator Primary Side

The AP600 design includes two steam generators, which under normal operating conditions provide the heat sink for reactor core heat removal and steam source to power the turbine. The OSU test facility incorporates two simulated steam generators (SGs). For the purposes of developing mass and energy balance equations to represent the thermal hydraulic performance of the RCS primary side, the primary side of the simulated steam generators is considered as three interconnected sections:

- Inlet plenum
- Tubes (both *uphill* and *downhill* sides)
- Outlet plenum

The mass and energy balance equations then, will be developed by considering the equations for each of these sections.

4.13.1 Inlet Plenum

A general mass balance equation for the inlet plenums may be written as:

$$\frac{d\,M_{IP}}{dt} = \dot{M}_{HL\,X} - \dot{M}_{IP\text{-}TUBE} \qquad 4.13\text{-}1$$

where:

M	=	Mass of working fluid, lbm
$\dot{M}$	=	Rate of mass flow, lbm/sec.
t	=	Time, sec.

and the subscripts:

HL X	=	Designates a hot leg where: X =1 - SG-1 2 - SG-2
IP	=	SG inlet plenum
IP-TUBE	=	Interface between inlet plenum and tube bundle of SG
SG X	=	Steam generator X =1 - SG-1 2 - SG-2

Similarly, the energy equation for the SG inlet plenum is written as:

$$c_p \frac{d(M\ T)_{SG\ X}}{dt} = \dot{M}_{HL\ X}\ h_{MIX} - \dot{M}_{IP\text{-}TUBE\ SG\ X}\ h_{MIX} - Q_{IP\ SG\ X\ METAL} - Q_{IP\ SG\ X\ AMB} \qquad 4.13\text{-}2$$

where:

c_p	=	Specific heat of working fluid, Btu/lbm-°F
Q	=	Heat loss (gain) rate, Btu/sec.
T	=	Fluid temperature, either vapor or liquid phases, °F

and the subscripts:

AMB	=	Ambient conditions associated with inlet plenum
METAL	=	Metal mass of inlet plenum
MIX	=	Fluid mixture conditions

All other parameters and subscripts are as previously defined.

4.13.1.1 Mass Balance

The mass stored in the steam generator inlet plenums is calculated from level measurements in the plenums. The level measurements must be compensated for temperature differences between the fluid in the plenums and that in the sense lines of the instruments. The data channel IDs of the level, pressure, and temperature instruments to be used in calculating fluid mass in the inlet plenums are listed in Table 4.13-1. The following approach was used in performing the temperature compensation of the level instrument output and calculating the fluid mass in the SG inlet plenums.

Step 1: First, compensate the readings of the inlet plenum level transducers to account for temperature differences between fluid in the plenum and fluid in the reference legs of the instrument lines. As noted above, the channel IDs of the two level transducers to be compensated, one for each SG, are identified in Table 4.13-1. The instruments used to measure local pressure and fluid temperatures to be used to accomplish the compensation are also identified in Table 4.13-1.

Step 2: The local pressures and temperatures measured by the instruments identified in Table 4.13-1 are used as inputs to calculate the thermodynamic properties of the fluid in the inlet plenums:

$$\rho_f = \rho_f(P,T) \qquad \rho_g = \rho_g(P,T)$$
$$h_f = h_f(P,T) \qquad h_g = h_g(P,T) \qquad 4.13\text{-}3$$

where:

h	=	Enthalpy of the fluid, evaluated from ASME steam tables, Btu/lbm
P	=	Local pressure in hot leg associated with steam generator under consideration, psia
T	=	Local temperature of fluid in sump tank, °F
ρ	=	Density, evaluated from ASME steam tables, lbm/ft.^{3}

and the subscripts:

f	=	Liquid phase of water
g	=	Vapor phase of water

Again, the data channel IDs of the instruments to be used in the calculation of the thermodynamic properties of the fluid in the SG inlet plenums are given in Table 4.13-1.

Step 3: Using the compensated liquid level and the inlet plenum volume as a function of height, the volume of liquid in the plenum is calculated:

$$V_{f,\ IP\ SG\ X} = V(l)_{IP\ SG\ X} \times LDP\text{-}XXX_{COMP} \qquad 4.13\text{-}4$$

where:

V	=	Volume, ft.^{3}
V(l)	=	Volume as a function of elevation, ft.^{3}/ft.
$LDP\text{-}XXX_{COMP}$	=	Compensated fluid levels data from level transducer identified as
		XXX = 209 SG-1 inlet plenum (see Table 4.13-1)
		214 SG-2 inlet plenum

The subscripts f, g and SG X are as previously defined.

Step 4: The liquid mass inventory in the primary and secondary sump is calculated as:

$$M_{IP_{SG\ X,f}} = \rho_{f,\ IP\ SG\ X} \times V_{IP\ SG\ X} \qquad 4.13\text{-}5$$

All parameters and subscripts are as previously defined. The mass of vapor in the SG inlet plenum is then calculated as:

$$M_{g,\,IP\,SG\,X} = \rho_{g,\,IP\,SG\,X} \times (V_{TOTAL\,SG\,X} - V_{f,\,IPSG\,X}) \qquad 4.13\text{-}6$$

where:

V_{TOTAL} = Total volume of the SG inlet plenum of interest

All other parameters and subscripts are as previously defined.

Step 5: The total fluid mass in the inlet plenum of the steam generator of interest is then calculated by summing the mass associated with each phase in the plenum:

$$M_{f,\,IP\,SG\,X} = (M_{f,\,IP} + M_{g,\,IP})_{SG\,X} \qquad 4.13\text{-}7$$

Step 6: The rate of change in mass inventory of the of a SG inlet plenum may be approximated by differencing two consecutive calculated values of liquid mass:

$$\frac{dM_{IP\,SG\,X}}{dt} = \frac{\Delta M_{IP\,SG\,X}}{\Delta t} = \frac{(M_{IP\,SG\,X,\,i} - M_{IP\,SG\,X,\,i-1})}{t_i - t_{i-1}} \qquad 4.13\text{-}8$$

where the subscript:

i = Index of the data and time arrays

All other parameters and subscripts are as previously defined.

The total mass flow rate from the hot legs into the SG inlet plenum is calculated in the hot leg calculation module. The general mass balance of Equation 4.13-1 is used to solve for the total mass flow into the tubes of a given SG.

4.13.1.2 Energy Balance

Equation 4.13-2 defines the general form of an energy balance for the steam generator inlet plenum. The plenum may contain both vapor and liquid at the same time. The energy balance must account for both phases of the working fluid. Thus, the left hand side of Equation 4.13-2 may be expanded as:

$$c_p \frac{d(M_{IP\ SG\ X}T)}{dt} = c_{P,f} M_{f,\ IP\ SG\ X} \frac{d(T_f)}{dt} + c_{P,f} (T_f - T_{REF}) \frac{d(M_{f,\ IP\ SG\ X})}{dt}$$
$$+ c_{P,g} M_{g,\ IP\ SG\ X} \frac{d(T_g)}{dt} + c_{P,g} (T_g - T_{REF}) \frac{d(M_{g,\ IP\ SG\ X})}{dt} \qquad 4.13\text{-}9$$

where:

T_{REF} = Reference temperature, 32°F

All other variables and subscripts are as previously defined.

Writing the preceding equation in its difference form, the rate of change of energy associated with the fluid in the SG inlet plenum is calculated:

$$c_p \frac{d\ (M_{IP\ SG\ X})}{dt} = c_{p,f} M_{f,\ IP\ SG\ X} \frac{\Delta T_f}{\Delta t} + c_{p,f} (T_f - T_{REF})$$
$$\frac{\Delta M_{f,\ IP\ SG\ X}}{\Delta t} + c_{p,g} M_{g,\ IP\ SG\ X} \frac{\Delta T_g}{\Delta t} + c_{p,g} (T_f - T_{REF}) \frac{\Delta M_{g,\ IP\ SG\ X}}{\Delta t} \qquad 4.13\text{-}10$$

The data channel IDs of the instruments to be used to evaluate the thermal transport properties for this calculation are listed in Table 4.13-1.

The energy rate of change of the SG inlet plenum is expressed as:

$$Q_{IP\ SG\ X\ METAL} = M_{IP\ SG\ X\ METAL} \times c_{p,\ METAL} \times \frac{dT_{METAL}}{dt} \qquad 4.13\text{-}11$$

All variables and subscripts are as previously defined. Representing the preceding equation in its difference form:

$$Q_{IP\ SG\ X\ METAL} = M_{IP\ SG\ x\ METAL} \times c_{P,\ METAL} \times \frac{\Delta T_{METAL}}{\Delta t} \qquad 4.13\text{-}12$$

For these calculations, the outside surface temperature of the SG inlet plenum will be used to represent the average temperature of all the inlet plenum metal. The specific data channel IDs to be used for these calculations are listed in Table 4.13-1.

The heat loss from the inlet plenum of each steam generator may be represented in the form:

$$Q_{IP\ SG\ X\ AMB} = U_{IP\ SG\ X}\ A_{IP\ SG\ X}\ \frac{dT_{IP\ SG\ X\ SURF}}{dt} \qquad 4.13\text{-}13$$

where:

A	=	Effective area of SG inlet plenum being considered, ft.^{2}
U	=	Overall conductance between SG inlet plena outside surface and ambient, Btu/hr.-ft.^{2}-°F

and the subscript:

SURF	=	Outside surface of SG inlet plenum

All other variables and subscripts are as previously defined.

Rewriting the previous expression in its difference form:

$$Q_{IP\ SG\ X\ AMB} = U_{IP\ SG\ X}\ A_{IP\ SG\ X}\ \frac{\Delta T_{IP\ SG\ X\ SURF}}{\Delta t} \qquad 4.13\text{-}14$$

The rate of energy loss to the ambient may be calculated using data collected from the inlet plenum surface temperature instruments identified in Table 4.13-1.

The rate of energy transport associated with the flow from the hot leg into the steam generator inlet plenum is calculated and available from the Hot Leg calculation module. Thus, the general energy equation, 4.13-2, may now be solved for the product of the total mass flow and enthalpy associated with that mass flow into the SG tubes. From the general mass balance equation, 4.13-1, the total mass

flow into the SG tubes is calculated. Knowing the enthalpy of the liquid and fluid components of the mass flow into the SG tubes, the quality of the flow into the SG tubes may be calculated using the following equation:

$$\dot{M}_{\text{IP-TUBE SG X}}\, h_{MIX} = (1-X)\, \dot{M}_{\text{IP-TUBE SG X}}\, h_f + X\, \dot{M}_{\text{IP-TUBE SG X}}\, h_g \qquad 4.13\text{-}15$$

where:

X = Local volumetric quality

and the subscript:

mix = Liquid-vapor mixture

All other variables and subscripts are as previously defined.

4.13.2 Steam Generator Tubes

The general mass balance equation for the tubes in each steam generator may be written as:

$$\frac{dM_{\text{TUBES SG X}}}{dt} = \dot{M}_{\text{IP-TUBE SG X}} - \dot{M}_{\text{TUBE-OP SG X}} \qquad 4.13\text{-}16$$

where the subscripts:

TUBE = Tube bundle of an SG
TUBE-OP = Interface between tube bundle of SG and SG outlet plenum

All variables and other subscripts are as previously defined. Similarly, the energy balance on the tubes of a steam generator is expressed as:

$$c_P \frac{d(M\,T)_{\text{TUBE SG X}}}{dt} = (\dot{M}\, h_{MIX})_{\text{IP-TUBE SG X}} - (\dot{M}\, h_{MIX})_{\text{TUBE-OP SG X}} - Q_{\text{TUBE SG X, METAL}} - Q_{\text{PRI-SEC}} \qquad 4.13\text{-}17$$

where the subscripts:

MIX	=	Local fluid mixture conditions
PRI-SEC	=	Primary to secondary heat transfer

All variables and other subscripts are as previously defined.

4.13.2.1 Mass Balance

The mass stored in the tubes of each steam generator is calculated from level measurements across the hot leg (up-hill side) and cold leg (down-hill side) of the tubes. Like other level measurements taken with the test facility, these measurements must be compensated for temperature differences between the fluid in the tubes and in the sense lines of the instruments. The data channel IDs of the level, pressure, and temperature instruments to be used in calculating fluid mass in the inlet plenums are listed in Table 4.13-1. The following approach is to be used in performing the temperature compensation of the levels instrument output and calculating the fluid mass in the SG inlet plenum.

Step 1: First, compensate the levels readings associated with the tube level transducers to account for temperature differences between fluid in the tubes and fluid in the reference legs of the instrument lines. As noted above, the channel IDs of the four level transducers to be compensated, two for each SG, are identified in Table 4.13-1. The instruments used to measure local pressure and fluid temperatures to be used to accomplish the compensation are also identified in Table 4.13-1.

Step 2: The local pressures and temperatures identified in Table 4.13-1 are used as inputs to the ASME steam tables to calculate the thermodynamic properties of the fluid in the inlet plenum:

$$\rho_f = \rho_f(P, T) \qquad \rho_g = \rho_g(P, T)_g$$
$$h_f = h_f(P, T) \qquad h_g = h_g(P, T)_g \qquad \text{4.13-18}$$

All variables and subscripts are as previously defined.

Step 3: Using the compensated liquid level and the volume in the SG tubes as a function of height, the volume of liquid in the tubes of a given SG is calculated as:

$$V_{f,\ \text{TUBES XL}} = V(a)_{\text{TUBES XL}} \times \text{LDP-XXX}_{\text{COMP}} \qquad \text{4.13-19}$$

where the subscript:

XL = Side of the tubes of a given SG being considered:
XL = HL - hot-leg side
CL - cold-leg side

All other variables and subscripts are as previously defined. The total volume of liquid in the tubes of a given SG is then calculated as:

$$V_{f,\ TUBES} = V_{f\ TUBES\ CL} + V_{f,\ TUBES\ HL} \qquad 4.13\text{-}20$$

It follows that the volume of vapor in that SG tubes is calculated as:

$$V_{g,\ TUBES} = V_{TUBES\ TOTAL} - V_{F,\ TUBES} \qquad 4.13\text{-}21$$

where the subscript:

TOTAL = Total volume of the tubes bundle of a given SG, $ft.^3$

Step 4: Accounting for a difference in fluid temperature between the hot leg and cold leg sides of the SG tubes, the liquid mass inventory in each side of the SG tubes of interest is calculated as:

$$M_{f,\ TUBES\ XL} = \rho_f \times V_{f,\ TUBES\ XL} \qquad 4.13\text{-}22$$

All variables and subscripts are as previously defined. The total liquid mass in the SG tubes is then calculated as:

$$M_{f,\ TUBES} = M_{f,\ TUBES\ CL} + M_{f,\ TUBES\ HL} \qquad 4.13\text{-}23$$

The mass of vapor in the tubes of the SG of interest is then calculated as:

$$M_{g,\ TUBES} = \rho_{g,\ TUBES} \times (V_{TOTAL} - V_{f,\ TUBES}) \qquad 4.13\text{-}24$$

All parameters and subscripts are as previously defined.

Step 5: The total fluid mass in the tubes of the SG of interest is then calculated by summing the mass associated with each phase in the tubes:

$$M_{TUBES} = (M_{f,\ TUBES} + M_{g,\ TUBES}) \qquad 4.13\text{-}25$$

Step 6: The rate of change in mass inventory of the sump tanks may be approximated by differencing two consecutive calculated values of liquid mass:

$$\frac{dM_{TUBES}}{dt} \approx \frac{\Delta M_{TUBES}}{\Delta t} = \frac{(M_{TUBES,\,i} - M_{TUBES,\,i-1})}{t_i - t_{i-1}} \qquad 4.13\text{-}26$$

where the subscript:

i = Index of the data and time arrays

All other variables and subscripts are as previously defined.

The total mass flow rate from the inlet plenum into the tubes of a given SG is calculated from Equation 4.13-1. With the change in mass storage of the tubes of a given SG calculated from Equation 4.13-26, the terms of the general mass balance on the SG tube bundle, Equation 4.13-16, may be rearranged to solve for the mass flow from the tubes into the outlet plenum of interest.

4.13.2.2 Energy Balance

Equation 4.13-15 defines the general form of an energy balance for the SG tubes. The tubes may contain both vapor and liquid at the same time. The energy balance must account for both phases of the working fluid. Thus, the left-hand side of Equation 4.13-15 may be expanded as:

$$c_p \frac{d(M\,T)_{TUBES}}{dt} = c_{p,\,f}\,T_{f,\,TUBES} - T_{REF}\frac{d\,(M_{f,\,TUBES})}{dt} + c_{p,\,f}\,M_{f,\,TUBES}\frac{d(T_{f,\,TUBES})}{dt} + c_{p,\,g}\,T_{f,\,TUBES} - T_{REF}\frac{d(M_{g,\,TUBES})}{dt} + c_{p,\,g}\,M_{g,\,TUBES}\frac{d(T_{g,\,TUBES})}{dt} \qquad 4.13\text{-}27$$

where:

T_{REF} = Reference temperature; 32°F

All other variables are as previously defined. Equation 4.13-27 may be further expanded to specifically address the liquid volume on the hot leg ("up-hill" side) and cold leg ("down-hill" side) of the SG tubes, and written in its difference form to operate on the data:

$$c_p \frac{d(MT)_{TUBES}}{dt} \approx c_{p,f} M_{f,TUBES} \frac{\Delta T_{f,TUBES}}{\Delta t} c_{p,f} (T_f - T_{REF}) \Delta M_{f,TUBES} + c_{p,g} M_{g,TUBES} \frac{\Delta T_{g,TUBES}}{\Delta t} + c_{p,g} (T_g \quad T_{REF}) \frac{\Delta M_{g,TUBES}}{\Delta t} \qquad 4.13\text{-}28$$

The data channel IDs of the instruments to be used to evaluate the thermal transport properties are listed in Table 4.13-1.

The equation for the rate of change in internal energy of the metal of a tube bundle is written as:

$$Q_{TUBE\ SG\ x\ METAL} = M_{TUBE\ SG\ x\ METAL} \times c_{p,\ METAL} \times \frac{dT_{TUBE\ SG\ x\ METAL}}{dt} \qquad 4.13\text{-}29$$

Representing the rate of change in energy stored by the metal of the tubes of each SG in difference form:

$$Q_{TUBE,\ SG\ x\ METAL} = M_{TUBE,\ SG\ x\ METAL} \times c_{p,\ metal} \times \frac{\Delta T_{TUBE\ SG\ x\ METAL}}{\Delta t} \qquad 4.13\text{-}30$$

All parameters and subscripts are as previously defined. The data channel IDs to be used for the metal energy storage calculations are listed in Table 4.13-1.

The primary to secondary side heat transfer across the tubes of a given SG is calculated in the SG secondary side module.

The rate of energy transport associated with the flow from the inlet plenum into the SG tubes is calculated earlier by solving for that term in Equation 4.13-2. Thus, Equation 4.13-17 may now be solved for the product of the total mass flow and enthalpy associated with that mass flow from the SG tubes into the outlet plenum of a given SG. From Equation 4.13-16, the total mass flow from the SG tubes into the SG outlet plenum is calculated. Knowing the enthalpy of the liquid and fluid components of the mass flow into the SG tubes, the quality of the flow into the outlet plenum is calculated by solving for it in the following equation:

$$\dot{M}_{TUBE\text{-}OP}\ h_{MIX} = (1\text{-}X)\ \dot{M}_{TUBE\text{-}OP,f}\ h + X\ \dot{M}_{TUBE\text{-}OP,g}\ h_g \qquad 4.13\text{-}31$$

where:

X	=	Local volumetric quality

All other variables and subscripts are as previously defined.

4.13.3 Outlet Plenum

A general mass balance equation for the SG outlet plenums may be written as:

$$\frac{d\,M_{OP\ SG\ X}}{dt} = \dot{M}_{TUBE\text{-}OP\ SG\ X} - \dot{M}_{OP\text{-}CL\ X/Y} \qquad 4.13\text{-}32$$

where:

M	=	Mass of working fluid, lbm
$\dot{M}$	=	Rate of mass flow, lbm/sec.
t	=	Time, sec.

and the subscripts:

CL X/Y	=	Designates cold legs where: X/Y = 1/3 - SG-1 2/4 - SG-2
OP	=	SG outlet plenum
TUBE-OP	=	Interface between tube bundle and outlet plenum of a SG

Similarly, the energy equation for the SG inlet plenum is written as:

$$c_P \frac{d(M\ T)_{OP}}{dt} = \dot{M}_{TUBE\text{-}OP}\ h_{MIX} - \dot{M}_{OP\text{-}CL\ X/Y}\ h_{MIX} - Q_{OP\ SGX\ METAL} - Q_{OP\ SG\ x\ AMB} \qquad 4.13\text{-}33$$

All variables and subscripts are as previously defined.

4.13.3.1 Mass Balance

The mass stored in the SG outlet plenum is calculated from a level measurement in the plenum. Like other level measurements taken with the test facility, these measurements must be compensated for temperature differences between the fluid in the plenum and that in the sense lines of the instruments. The data channel IDs of the level, pressure, and temperature instruments to be used in calculating fluid

mass in the inlet plenums are listed in Table 4.13-1. The approach taken to compensate these level readings is identical to that of the inlet plenum and will not be repeated.

Similarly, calculation of fluid mass in the outlet plenum, and mass flow rates into and out of the outlet plenum are the same as those performed for the inlet plenum and are not repeated here.

4.13.3.2 Energy Balance

The calculation of an energy balance for the SG outlet plenums is similar to that performed for the inlet plenums and is not repeated here. The data channels used in the calculation of the energy balance for the outlet plenums are listed in Table 4.13-1. The metal energy and heat loss to ambient calculations are performed using the inlet plenum surface temperature measurements.

TABLE 4.13-1 DATA CHANNEL ID FOR SG INLET PLENUM MASS AND ENERGY CALCULATIONS					
Location		**Data Channel ID for Liquid Levels**	**Data Channel ID for Pressure Transducers**	**Data Channel ID for Fluid Thermocouples**	**Notes**
SG-1 inlet plenum		LDP-209	PT-205	TF-205	Metal Surface TEMP = TFM-301
SG-1 tubes	Hot-leg side	LDP-215	PT-201	TF-205 TF-211 TF-217	
	Cold-leg side	LDP-219	PT-201	TF-217 TF-213 TF-201 TF-203	
SG-1 outlet plenum	CL-1	LDP-213	PT-201	TF-201	Subtract elevation head of water in tubes to calculate local pressure
	CL-3	LDP-211	PT-201	TF-203	
SG-2 inlet plenum		LDP-214	PT-202	TF-206	Metal Surface TEMP = TFM-302
SG-2 tubes	Hot-leg side	LDP-218	PT-204	TF-206 TF-212 TF-218	
	Cold-leg side	LDP-222	PT-204	TF-218 TF-214 TF-202 TF-204	
SG-2 outlet plenum	CL-2	LDP-210	PT-204	TF-202	Subtract elevation head of water in tubes to calculate local pressure
	CL-4	LDP-212	PT-204	TF-204	

4.14 Steam Generator Secondary Side

The design of the AP600 includes two steam generators (SGs), which under normal operating conditions provide the heat sink for reactor core heat removal and steam source to power the turbine. During a transient, when the primary side depressurizes and cools below the temperature of the secondary side, the secondary side then becomes a potential heat source to the primary side.

A general mass balance on the SG secondary side may be expressed as:

$$\frac{dM_{SG\ SS\ X}}{dt} = \dot{M}_{f,\ SG\ SS\ X} - \dot{M}_{g,\ SG\ SS\ X} \qquad 4.14\text{-}1$$

where:

M	=	Mass, lbm
$\dot{M}$	=	Mass flow rate, lbm/sec.
t	=	Time, sec.

and the subscripts:

f	=	Liquid phase of water
SG SS X	=	Secondary side of steam generator X where:
		X = 1 SG-1
		= 2 SG-2
g	=	Vapor phase of water

Similarly, a general energy balance for the SG secondary side may be written as:

$$c_p \frac{d(MT)_{SG\ SS\ X}}{dt} - Q_{f,\ SG\ SS\ X} + Q_{g,\ SG\ SS\ X} - Q_{SG\ SS\ X\ METAL} - Q_{SG\ SS\ X\ AMB} \qquad 4.14\text{-}2$$

where:

c_p	=	Specific heat of the fluid inventory, Btu/lbm-°F
Q	=	Energy transfer or flow rate, Btu/sec
T	=	Local temperature

and the subscripts:

METAL	=	Metal shell of SG being considered
AMB	=	Ambient conditions about SG

All other variables and subscripts are as previously defined.

4.14.1 Mass Balance Calculations

The equations listed below hold for both SG-1 and SG-2; only the data channel names differ.

The fluid mass stored on the SG secondary side is calculated from a wide-range level measurement of that volume. Like other level measurements, these readings must be density compensated. The data channel IDs of the level, pressure, and temperature instruments to be used in calculating the fluid mass of the SG secondary side are listed in Table 4.14-1. The following approach is used in performing the density compensation of the SG secondary side level measurements.

Step 1: There are two fluid temperature measurements associated with the SG secondary side, both measurements are at the same elevation; thus, these measurements are averaged:

$$\bar{T}_{SG\ ss\ X} = \frac{TF\text{-}XXX + TG\text{-}XXY}{2} \qquad 4.14\text{-}3$$

Step 2: Next, compensate the readings of the SG secondary side level transducers to account for temperature differences between fluid in the SG and fluid in the reference legs of the instrument lines. As noted above, the channel IDs of the level transducer to be compensated, are identified in Table 4.14-1. The instrument channels used to measure local pressure and fluid temperatures to be used to accomplish the compensation are also identified in Table 4.14-1.

Step 3: The local pressures and temperatures measured with the instruments identified in Table 4.14-1 are used as inputs to calculate the thermodynamic properties of the fluid on the SG secondary side.

$$\rho_f = \rho_f(P, T) \qquad \rho_g = \rho_g(P, T)$$
$$h_f = h_f(P, T) \qquad h_g = h_g(P,T) \qquad 4.14\text{-}4$$

where:

h	=	Enthalpy of the fluid, evaluated from the ASME steam tables, Btu/lbm
P	=	Local pressure in hot leg associated with SG under consideration, psia
T	=	Local temperature of the fluid in the sump tank, °F
ρ	=	Density, evaluated from the ASME steam tables, lbm/ft.^{3}

and the subscripts:

f	=	Liquid phase of water
g	=	Vapor phase of water

Again, the data channel IDs of the instruments to be used in the calculation of the thermodynamic properties of the fluid in the SG secondary side are given in Table 4.14-1.

Step 4: Using the compensated liquid level and the inlet plenum volume as a function of height, the volume of liquid in the SG secondary side is calculated:

$$V_{SG\ SS\ X} = V(l)_{SG\ SS\ X} \times LDP\text{-}XXX_{COMP} \qquad 4.14\text{-}5$$

where:

V	=	Volume, ft.^{3}
V(l)	=	Volume as a function of elevation, ft.^{3}/ft.
$LDP\text{-}XXX_{COMP}$	=	Compensated fluid levels data from the levels transducer identified as XXX = 301 SG-1 secondary side 302 SG-2 secondary side

The subscripts f, g, and SG SS X are as previously defined.

Step 5: The liquid mass inventory in the SG secondary side is calculated as:

$$M_{f,\ SG\ SS\ X} = \rho_f \times V_{f,\ SG\ SS\ X} \qquad 4.14\text{-}6$$

where all parameters and subscripts are as previously defined. The mass of vapor in the SG secondary side is then calculated as:

$$M_{g,\,SG\,SS\,X} = \rho_g \times V_{SG\,SS\,X,\,TOTAL} - V_{f,\,SG\,SS\,X} \qquad 4.14\text{-}7$$

where the subscript:

TOTAL = Total volume of the SG secondary side of interest

All other variables and subscripts are as previously defined.

Step 6: The total fluid mass in the secondary side of the SG of interest is then calculated by summing the mass associated with each phase:

$$M_{SG\,SS\,X} = (M_{f,\,SG\,SS\,X} + M_{g,\,SG\,SS\,X}) \qquad 4.14\text{-}8$$

Step 7: The rate of change in mass inventory of the of the SG secondary side may be approximated by differencing two consecutive calculated values of liquid mass:

$$\frac{dM_{SG\,SS\,X}}{dt} \approx \frac{\Delta M_{SG\,SS\,X}}{\Delta t} = \frac{M_{SG\,SS\,X,\,i} - M_{SG\,SS\,X,\,i}}{t_i - t_{i-1}} \qquad 4.14\text{-}9$$

where the subscript:

i = Index of data and time arrays

All other variables and subscripts are as previously defined.

The mass flow into the SG secondary side is liquid, simulating feedwater flow. The liquid mass flow rate to the SG secondary side is calculated as:

$$\dot{M}_{f,\,SG\,SS\,X} = \rho_f \times FMM - XXX \qquad 4.14\text{-}10$$

where:

FMM - XXX = Flow meter readings, gpm, where
XXX = 001 SG-1
= 002 SG-2

All other variables and subscripts are as previously defined.

The mass flow out of the SG secondary side is vapor, simulating main steam flow. The vapor mass flow rate from the SG secondary side is calculated as:

$$\dot{M}_{g,\,SG\,SS\,X} = \rho_g \times FVM - XXX \qquad 4.14\text{-}11$$

where:

FVM - XXX = Flow meter readings, cfm, where
XXX = 001 SG-1
= 002 SG-2

All other variables and subscripts are as previously defined.

Note that, on receiving a simulated reactor trip signal, the SG secondary side is isolated. That is, flow paths to and from the SG secondary side are isolated. Thus, once isolated:

$$\dot{M}_{f,\,SG\,SS\,X} = \dot{M}_{g,\,SG\,SS\,X} = 0 \qquad 4.14\text{-}12$$

4.14.2 Energy Balance

The expression for stored energy associated with the fluid inventory on the secondary side of a SG may be expressed as:

$$
\begin{aligned}
& c_p \frac{d(MT)_{SG\ SS\ X}}{dt} \\
& = c_{p,f} \left(M_{f,\ SG\ SS\ X} \frac{d(T_{f,\ SG\ SS\ X})}{dt}\right. \\
& + c_{p,f} \left(\overline{T}_{f,\ SG\ SS\ X} - T_{REF}\right) \frac{d(M_{f,\ SG\ SS\ X})}{dt} \qquad \text{4.14-13} \\
& + c_{p,g} \left(M_{g,\ SG\ SS\ X}\right) \frac{d(\overline{T}_{g,\ SG\ SS\ X})}{dt} \\
& + c_{p,g} \left(\overline{T}_{g,\ SG\ SS\ X} - T_{REF}\right) \frac{d(M_{g,\ SG\ SS\ X})}{dt}
\end{aligned}
$$

All variables and subscripts are as previously defined. Writing the preceding equation in its difference form:

$$
\begin{aligned}
& c_p \frac{d(MT)_{SG\ SS\ X}}{dt} \\
& \approx c_{p,f} \left(M_{f,\ SG\ SS\ X} \frac{\Delta(T_{f,\ SG\ SS\ X})}{\Delta t}\right. \\
& + c_{p,f} \left(T_{f,\ SG\ SS\ X} - T_{REF}\right) \frac{\Delta(M_{f,\ SG\ SS\ X})}{\Delta t} \qquad \text{4.14-14} \\
& + c_{p,g} \left(M_{g,\ SG\ SS\ X}\right) \frac{\Delta(T_{g,\ SG\ SS\ X})}{\Delta t} \\
& + c_{p,g} \left(T_{g,\ SG\ SS\ X} - T_{REF}\right) \frac{\Delta(M_{g,\ SG\ SS\ X})}{\Delta t}
\end{aligned}
$$

Using the average fluid temperatures from Equation 4.14-3 as the liquid temperature (T_f) and the appropriate steam temperature (TF-301 or TF-310), Equation 4.14-14 is used to calculate the range in stored energy of the secondary side fluid inventory.

The internal energy of the feedwater flow is calculated as:

$$Q_{f,\ SG\ SS\ X} = \dot{M}_{f,\ SG\ SS\ X} \times h_{f,\ FMM\text{-}XXX} \qquad 4.14\text{-}15$$

where:

h_f = Enthalpy of liquid, Btu/lbm

All other variables and subscripts are as previously defined. The enthalpy associated with the flow of a given flow meter is evaluated using the temperature and pressure data from the data channels identified in Table 4.14-1.

Similarly, the internal energy of the steam flow is calculated as:

$$Q_{g,\ SG\ SS\ X} = \dot{M}_{g,\ SG\ SS\ X} \times h_{g,\ FVM\text{-}XXX} \qquad 4.14.16$$

where:

h_g = Enthalpy of vapor, Btu/lbm

All other variables and subscripts are as previously defined. The enthalpy of steam associated with a given meter is evaluated using temperatures and pressures from the data channels identified in Table 4.14-1.

A check on the total energy removed by steam from both steam generators can be performed using the output of flow meter FVM-003. Since there is no temperature measurement associated with FVM-003, those associated with FVM-001 and FVM-002 are used to calculate weighted density and enthalpy to use with the FVM-003 reading.

The change in internal energy associated with a SG shell may be expressed as:

$$Q_{SG\ SS\ X\ METAL} = M_{SG\ SS\ X\ METAL} \times c_{P,\ METAL} \times \frac{dT_{SG\ SS\ X\ METAL}}{dt} \qquad 4.14\text{-}17$$

All variables and subscripts are as previously defined. Expressing the preceding equation in its difference form:

$$Q_{SG\ SS\ X\ METAL} = M_{SG\ SS\ X\ METAL} \times c_{P,\ METAL} \times \frac{\Delta T_{SG\ SS\ X\ METAL}}{\Delta t} \qquad 4.14\text{-}18$$

There are two thermocouples on the outside surface of each SG shell. The mass of the SG shell is apportioned between the two readings, then the change in stored energy for each apportioned mass is calculated and summed to determine the total rate of change in energy associated with the SG shell.

The heat loss to the ambient may be expressed as:

$$Q_{SG\ SS\ X\ AMB} = U_{SG\ SS\ X}\ A_{SG\ SS\ X}\ \frac{dT_{SG\ SS\ X\ AMB}}{dt} \qquad 4.14\text{-}19$$

where:

U	=	Overall conductance between the outside diameter of the SG shell and the ambient, Btu/hr.-ft.^{2}-°F
A	=	Surface area of SG shell outside diameter, ft.^{2}

All other variables and subscripts are as previously defined. Again, to facilitate operation on the data, the preceding equation is expressed in its difference form:

$$Q_{SG\ SS\ X\ AMB} = U_{SG\ SS\ X}\ A_{SG\ SS\ X}\ \frac{\Delta T_{SG\ SS\ X\ AMB}}{\Delta t} \qquad 4.14\text{-}20$$

The conductance is evaluated to account for both natural convection to the ambient and conduction applied to the SG shell. As with the stored energy of the metal, the surface area is apportioned between two thermocouple readings on the SG shell, and the heat loss to the ambient is calculated for each apportioned surface area and summed to determine the total rate of heat loss to the ambient.

TABLE 4.14-1 INSTRUMENT CHANNEL IDs FOR SG SECONDARY SIDE MASS AND ENERGY CALCULATIONS					
SG No.	Data Channel IDS				
	Level Transducers	Flow Meter	Pressure Transducer	Fluid Temperature	Metal Shell Temperatures
1	LDP-301(1)		PT-301	TF-305 TF-307	TFM-303 TFM-305
	LDP-303(2)				
		FMM-001	PT-001	TF-311	
		FVM-001	PT-301	TF-301	
2	LDP-302(1)		PT-302	TF-306 TF-308	TFM-304 TFM-305
	LDP-304(2)				
		FMM-002	PT-002	TF-312	
		FVM-002	PT-302	TF-310	
1 and 2		FVM-003	PT-002	TF-301, TF-310	

Note:
(1) Wide-range transducer used in density compensation and fluid inventory calculations
(2) Narrow-range transducer used only in the event that the wide-range transducer is inoperable

4.15 Pressurizer

The pressurizer is a tank-like structure through which, under accident mitigation, mass flows from the primary system to the first three stages of ADS valves. At steady-state, the pressurizer has an initial liquid and steam volume. During a transient, the initial pressurizer and primary side inventory are vented by the ADS through a pipe from the top of the pressurizer to the IRWST.

4.15.1 General Equations

The general mass balance for the pressurizer may be written as:

$$\frac{dM_{PRZR}}{dt} = \dot{M}_{SL\text{-}PRZR} - \dot{M}_{ADS} \qquad 4.15\text{-}1$$

where:

M	=	Mass, lbm
$\dot{M}$	=	Mass flow rate, lbm/sec.
t	=	Time, sec.

and the subscripts:

PRZR	=	Pressurizer
SL-PRZR	=	Connection between pressurizer and surge line
ADS	=	Connection between pressurizer and ADS 1-3

Similarly, a general energy balance on the pressurizer may be expressed as:

$$c_P \frac{d\,(MT)_{PRZR}}{dt} = Q_{SL\text{-}PRZR} - Q_{ADS} - Q_{PRZR\ METAL} - Q_{PRZR\ AMB} \qquad 4.15\text{-}2$$

where:

c_P	=	Specific heat, Btu/(lbm-°F)
Q	=	Rate of energy transfer or transport, Btu/sec.
T	=	Temperature, °F

and the subscripts:

AMB	=	Energy loss to ambient environment
METAL	=	Metal mass of pressurizer

All other parameters and subscripts are as previously defined.

4.15.2 Mass Balance Calculation

Starting at the bottom of the pressurizer, the pressurizer liquid inventory mass is calculated by:

Step 1: Compensate the readings from the pressurizer level transducer listed in Table 4.15-1 to account for temperature differences between fluid in the pressurizer and fluid in the reference leg of the instrument line. The output from local pressure and temperature transducers to be used to accomplish the compensation are also identified in Table 4.15-1.

Step 2: From the collapsed liquid level, calculate the liquid volume in the pressurizer:

$$V_{f,\ PRZR} = V(l)_{PRZR} \times LDP\text{-}601 \qquad 4.15\text{-}3$$

where:

V	=	Volume, $ft.^3$
V(l)	=	Volume as a function of elevation, $ft.^3/ft.$

and the subscripts:

f	=	Liquid phase of water

All other parameters and subscripts are as previously defined.

Step 3: The local pressures and temperatures as measured by the instruments identified in Table 4.15-1 are used as inputs to calculate the density of the liquid and vapor in the pressurizer:

$$\rho_{f,\,PRZR} = \rho(PT\text{-}604,\ TF\text{-}602)$$
$$\rho_{g,\,PRZR} = \rho(PT\text{-}604,\ TF\text{-}605,\ SC\text{-}608) \qquad 4.15\text{-}4$$

where:

ρ	=	Density, lbm/ft.^{3}
PT-604	=	Channel ID for local pressure measurement between pressurizer and header for ADS 1-3
TF-602	=	Channel ID for local temperature measurement of vapor at top of pressurizer
TF-605	=	Channel ID for local temperature measurement of liquid at two locations in the SC-608 pressurizer

and the subscripts:

f	=	Liquid phase of water
g	=	Vapor phase of water

Step 4: Using the thermodynamic properties of water as determined from local pressure and fluid temperature measurements, liquid and vapor masses in the pressurizer are calculated as:

$$M_{f,\,PRZR} = \rho_{f,\,PRZR} \times V_{f,\,PRZR}$$
$$M_{g,\,PRZR} = \rho_{g,\,PRZR} \times (V_{PRZR,TOTAL} - V_{f,\,PRZR}) \qquad 4.15\text{-}5$$

where the subscript:

TOT	=	Total volume of component

All other parameters and subscripts are as previously defined.

Step 5: The rate of change in mass inventory of the pressurizer may be approximated by differencing two consecutive calculated values of the liquid and vapor masses:

$$\frac{dM_{f,\,PRZR}}{dt} \approx \frac{\Delta M_{f,\,PRZR}}{\Delta t} = \frac{M_{f,\,PRZR,\,i+1} - M_{f,\,PRZR,\,i}}{t_{i+1} - t_i}$$

$$\frac{dM_{g,\,PRZR}}{dt} \approx \frac{\Delta M_{g,\,PRZR}}{\Delta t} = \frac{M_{g,\,PRZR,\,i+1} - M_{g,\,PRZR,\,i}}{t_{i+1} - t_i} \qquad 4.15\text{-}6$$

where:

Δ = Difference between two consecutive calculations or data scans

and the subscript:

i = Index of the data and time arrays

All other parameters and subscripts are as previously defined. The total rate of change of the mass inventory of the pressurizer is then calculated as:

$$\frac{dM_{PRZR}}{dt} \approx \frac{\Delta M_{PRZR}}{\Delta t} = \frac{\Delta M_{f,\,PRZR} + \Delta M_{g,\,PRZR}}{\Delta t} \qquad 4.15\text{-}7$$

The mass flow rate through the ADS 1-3 simulation is calculated in the ADS 1-3 module of the software. The rate of flow from the surge line into the pressurizer may now be solved by rearranging Equation 4.15-1 and solving for the rate of flow from the surge line into the pressurizer:

$$\dot{M}_{SL\text{-}PRZR} \approx \frac{\Delta M_{PRZR}}{\Delta t} + \dot{M}_{ADS} \qquad 4.15\text{-}8$$

Thus, mass flow into the pressurizer from the surge line is calculated using the pressurizer mass storage term and the total ADS 1-3 mass flow rate.

4.15.3 Energy Balance

The energy flow associated with the pressurizer consists of the following components:

- Rate of change in stored energy of the pressurizer inventory
- Rate of energy transport to the pressurizer from the surge line
- Rate of energy transport from the pressurizer by way of ADS 1-3

- Rate of change in stored energy of the pressurizer metal
- Rate of energy loss to the environment

Expressions for each of these components are developed in the following sections.

4.15.3.1 Rate of Change in Stored Energy of the Pressurizer Inventory

The stored energy of the pressurizer inventory must account for both the liquid and vapor phases of the inventory. The equations to do this may be written as:

$$c_P \frac{d\,(M\,T)_{PRZR}}{dt} = c_{P,f} \frac{d\,(M_f\,T_f)_{PRZR}}{dt} + c_{P,g} \frac{d\,(M_g\,T_g)_{PRZR}}{dt} \qquad 4.15\text{-}9$$

The equation for energy change associated with the liquid phase of the pressurizer inventory may be expressed as:

$$c_{P,f} \frac{d(\,M_f\,T_f\,)_{PRZR}}{dt} = c_{P,f}\,(T_f - T_{REF}) \frac{d(M_{f,PRZR})}{dt} + c_{P,f}\,M_{f,PRZR} \frac{d(\,T_f\,)}{dt} \qquad 4.15\text{-}10$$

where:

T_{REF} = Reference temperature, 32°F

All other variables and parameters are as previously defined.

Similarly, the energy change associated with the vapor phase of the pressurizer inventory may be expressed as:

$$c_{P,g} \frac{d(\,M_{g,PRZR}\,T_g\,)}{dt} = c_{P,g}\,(T_g - T_{REF}) \frac{d(\,M_{g,PRZR}\,)}{dt} + c_{P,g}\,M_{g,PRZR} \frac{d(\,T_g\,)}{dt} \qquad 4.15\text{-}11$$

All parameters and subscripts are as previously defined. Expressing the previous two equations as differences:

$$c_{P,f}\frac{d(M_{f,PRZR}T_f)}{dt} = c_{P,f}(T_f-T_{REF})\frac{\Delta M_{f,PRZR}}{\Delta t} + c_{P,f}M_{f,PRZR}\frac{\Delta T_f}{\Delta t} \qquad 4.15\text{-}12$$

and

$$c_{P,g}\frac{d(M_{g,PRZR}T_g)}{dt} = c_{P,g}(T_g-T_{REF})-\frac{\Delta M_{g,PRZR}}{\Delta t} + c_{P,g}M_{g,PRZR}\frac{\Delta T_g}{\Delta t} \qquad 4.15\text{-}13$$

All parameters and subscripts are as previously defined. Expanding the two terms on the right-hand side of the previous two equations, the liquid phase expression becomes:

$$c_{P,f}(T_f-T_{REF})\frac{\Delta M_{f,PRZR}}{\Delta t} = c_{P,f}(T_{f,i}-T_{REF})\frac{M_{f,PRZR,i}-M_{f,PRZR,i-1}}{t_i-t_{i-1}} \qquad 4.15\text{-}14$$

$$c_{P,f}M_{f,PRZR}\frac{\Delta T_f}{\Delta t} = c_{P,f}M_{f,PRZR,i}\frac{T_{f,i}-T_{f,i+1}}{t_i-t_{i-1}}$$

The vapor phase expression becomes:

$$c_{P,g}(T_g-T_{REF})\frac{\Delta M_{g,PRZR}}{\Delta t} = c_{P,g}(T_{g,i}-T_{REF})\frac{M_{g,PRZR,i}-M_{g,PRZR,i-1}}{t_i-t_{i-1}} \qquad 4.15\text{-}15$$

$$c_{P,g}M_{g,PRZR}\frac{\Delta T_g}{\Delta t} = c_{P,g}M_{g,PRZR,i}\frac{T_{g,i}-T_{g,i+1}}{t_i-t_{i-1}}$$

where:

i = Index of the data and time arrays

All other parameters and subscripts are as previously defined. The specific heats of the liquid and vapor phases of water, $c_{P,f}$ and $c_{P,g}$ respectively, are evaluated using the values of the data channels identified in Table 4.15-1.

4.15.3.2 Rate of Energy Transport to the Pressurizer from the Surge Line

Equation 4.15-2 may be rewritten to solve for the energy associated with the surge line flow:

$$Q_{SL\text{-}PRZR} = - C_v \frac{d\,(MT)_{PRZR}}{dt} - Q_{ADS} - Q_{PRZR\ METAL} - Q_{PRZR\ AMB} \qquad 4.15\text{-}16$$

Having calculated both the mass and energy flow rates of surge-line flow, and knowing the local fluid pressures and temperatures of surge-line flow, the quality of surge-line flow at the entrance to the pressurizer and at the surge-line/hot leg junction may be calculated.

4.15.3.3 Rate of Energy Transport from the Pressurizer by Way of ADS 1-3

The energy transport associated with flow through ADS by way of ADS 1-3 is calculated in the module for the ADS 1-3 separator.

4.15.3.4 Rate of Change in Stored Energy of the Pressurizer Metal

The change in stored energy of the pressurizer metal may be expressed as:

$$Q_{PRZR} = c_{P,METAL} \times M_{PRZR,METAL} \times \frac{d\,T_{PRZR,METAL}}{dt} \qquad 4.15\text{-}17$$

All variables and subscripts are as previously defined. Writing the preceding equation in its difference form;

$$Q_{PRZR\ METAL} = c_{P,\ METAL}\ M_{PRZR\ METAL} \frac{\Delta\,T_{PRZR\ MF}}{\Delta t} \qquad 4.15\text{-}18$$

There are three surface-mounted thermocouples on the pressurizer simulation of the OSU test as identified in Table 4.15-1. These surface-mounted thermocouples are taken to be representative of the stored internal energy of the pressurizer metal mass. The metal mass of the pressurizer is apportioned into three sections, each section assigned to a surface-mounted thermocouple. Equation 4.15-18 is then solved using the temperature measurements for each apportioned mass and the results summed at each time interval to yield the total change in internal or stored energy associated with the pressurizer metal mass.

4.15.3.5 Rate of Energy Loss to the Environment

The rate of energy loss from the pressurizer to the environment may be expressed as:

$$Q_{PRZR\ AMB} = U_{PRZR\ AMB} \times A_{PRZR\ AMB} \times dT_{PRZR\ AMB} \qquad 4.15\text{-}19$$

All other variables and subscripts are as previously defined. Writing the preceding equation in its difference form:

where:

A	=	Effective external surface area of pressurizer, $ft.^2$
U	=	Overall effective heat transmission coefficient, $Btu/(sec.\text{-}ft.^2\text{-}°F)$

$$Q_{PRZR\ AMB} = U_{PRZR\ AMB} \times A_{PRZR\ AMB} \times \Delta T_{PRZR\ AMB} \qquad 4.15\text{-}20$$

As was done for the pressurizer stored-energy calculations, the surface area of the pressurizer is apportioned among the three surface-mounted thermocouples identified in Table 4.15-1 to perform the heat loss to ambient calculations. An ambient temperature reading was recorded during the test and is used to calculate the temperature difference used in the calculation of the pressurizer heat loss. The overall conductance from the surface of the pressurizer to the ambient, $U_{PRZR\ AMB}$, is evaluated assuming natural convection at the outside surface of the pressurizer and accounting for any insulation that may be installed on the pressurizer. Equation 4.15-20 is solved using the apportioned surface areas and appropriate surface temperatures, and then summing the three values of heat loss, calculate the rate of heat loss at each time during a test.

TABLE 4.15-1
INSTRUMENT CHANNEL IDs FOR PRESSURIZER MASS AND ENERGY BALANCES

Location	Function	Instrument Channel IDs			
		Level Transducer	Pressure Transducer	Fluid Temperature	Heat Flux Meters
Pressurizer liquid space	Density compensation of level transducer output Evaluation of density and specific heat of water	LDP-601	PT-604	TF-605 SC-608	
Pressurizer steam space	Evaluate density and specific heat of steam		PT-604	TF-602	
Pressurizer outside surface	Calculation of stored energy in pressurizer metal				TFM-602 TFM0604 TFM-605 TFM-607
Pressurizer outside surface	Calculation of heat loss to ambient				HFM-602 HFM-604 HFM-605 HFM-607

4.16 Pressurizer Surge Line

The pressurizer surge line is piping that connects the pressurizer to the primary system. During a transient simulation for which the ADS is actuated, the surge line becomes part of the relief path from the primary system to the pressurizer, ADS, and containment.

A mass balance on the pressurizer surge line may be expressed as:

$$\frac{dM_{SL}}{dt} = \dot{M}_{HL-SL} - \dot{M}_{SL-PRZR} \qquad 4.16\text{-}1$$

where:

M	=	Mass in the surge line, lbm
$\dot{M}$	=	Mass flow rate, lbm/sec.
t	=	Time, seconds

and the subscripts:

HL-SL	=	Junction between hot leg and surge line
SL-PRZR	=	Junction between surge line and pressurizer
SL	=	Surge line

Similarly, a general energy balance on the pressurizer surge line may be written as:

$$c_p \frac{d(MT)_{SL}}{dt} = (Mh)_{HL-SL} - (Mh)_{SL-PRZR} - Q_{SL-METAL} - Q_{SL-AMB} \qquad 4.16\text{-}2$$

where:

c_p	=	Specific heat of fluid, Btu/lbm-°F
T	=	Temperature, °F
h	=	Enthalpy of the fluid, Btu/lbm

and the subscripts:

METAL	=	Metal mass of surge line piping
AMB	=	Ambient conditions about surge line piping

All other variables and subscripts are as previously defined.

4.16.1 Mass Balance

The mass of the surge line liquid inventory is calculated by:

Step 1: Compensate the readings from the two surge line level transducers listed in Table 4.16-1 to account for temperature differences between fluid in the surge line and the fluid in the reference leg of instrument lines. The local pressure and temperature transducers to be used to accomplish the compensation are also identified in Table 4.16-1.

Step 2: From the compensated collapsed liquid levels obtained from Step 1 calculate the liquid volume in the surge line:

$$V_{f,\,SL} = V(l)_{PRZR} \times (LDP\text{-}602 + LDP\text{-}606) \qquad 4.16\text{-}3$$

where:

V	=	Volume, $ft.^3$
V(l)	=	Volume as a function of elevation, $ft.^3/ft.$

and the subscript:

f	=	Liquid phase of water

All other parameters and subscripts are as previously defined.

Step 3: The instruments used to measure local pressures and temperatures to calculate the density of the liquid and vapor in the surge line are identified in Table 4.16-1.

$$\rho_{f,\,SL} = \rho_f(P,\ T)$$
$$\rho_{g,\,SL} = \rho_g(P,\ T) \qquad 4.16\text{-}4$$

where:

ρ	=	Density, $lbm/ft.^3$
P	=	Pressure, psia
T	=	Temperature, °F

and the subscripts:

f	=	Liquid phase of water
g	=	Vapor phase of water

The specific pressure and temperature data channels to be used in calculating liquid and vapor densities are identified in Table 4.16-1.

Step 4: Finally, using the local thermodynamic properties of water as determined from local pressure and fluid temperature measurements, the liquid and vapor mass in the surge line is calculated as:

$$M_{f,\,SL} = \rho_{f,\,SL} \times V_{f,\,SL} \qquad 4.16\text{-}5$$

All variables and subscripts are as previously defined. The vapor mass in the surge line is calculated as:

$$M_{g,\,SL} = \rho_{g,\,SL} \times (V_{SL,\,TOTAL} - V_{f,\,SL}) \qquad 4.16\text{-}6$$

where the subscript:

TOTAL	=	Total volume of the surge line

All other variables and subscripts are as previously defined. The total fluid mass in the surge line is then calculated as:

$$M_{SL} = M_{f,\,SL} + M_{g,\,SL} \qquad 4.16\text{-}7$$

Step 5: The rate of change in mass inventory of the surge line may be approximated by differencing two consecutive calculated values of the liquid and vapor masses:

$$\frac{dM_{f,\,SL}}{dt} = \frac{\Delta M_{f,\,SL}}{\Delta t} = \frac{M_{f,\,SL,\,i} - M_{f,\,SL,\,i-1}}{t_i - t_{i-1}}$$

$$\frac{dM_{g,\,SL}}{dt} = \frac{\Delta M_{g,\,SL}}{\Delta t} = \frac{M_{g,\,SL,\,i} - M_{g,\,SL,\,i-1}}{t_i - t_{i-1}} \qquad 4.16\text{-}8$$

where:

Δ = Difference between two consecutive calculations or data scans

and the subscript:

i = Specific value in the time and corresponding data array

All other parameters and subscripts are as previously defined. The total rate of change of the mass inventory of the surge line is then calculated as:

$$\frac{dM_{SL}}{dt} \approx \frac{\Delta M_{SL}}{\Delta t} = \frac{\Delta M_{f,\,SL} + \Delta M_{g,\,SL}}{\Delta t} \qquad 4.16\text{-}9$$

The mass flow rate from the surge line into the pressurizer is calculated from the mass balance on the pressurizer; the ADS 1-3 mass flow rate is measured and the rate of fluid mass stored in or depleted from the pressurizer is calculated. From Equation 4.16-9, the rate that fluid inventory is either stored in or depleted from the surge line is calculated. Therefore, Equation 4.16-1 may be rearranged to solve for the flow from the hot leg into the surge line:

$$\dot{M}_{HL\text{-}SL} = \dot{M}_{SL\text{-}PRZR} + \frac{dM_{SL}}{dt} \qquad 4.16\text{-}10$$

It is noted that the flow from the hot leg into the surge line is calculated starting with the ADS 1-3 flow and working in to the primary system to solve for mass flow rates and fluid mass inventory changes.

4.16.2 Energy Balance

Assuming that the variation of specific heat of both the liquid and vapor phases of water over the range of pressure conditions experienced in the test is negligible, the left-hand side of Equation 4.16-2 equation is expanded as follows:

$$c_P \frac{d(M_{SL}T)}{dt} = c_{P,\,f}\,(T_F - T_{REF})\,\frac{dM_{f,\,SL}}{dt} + M_{f,\,SL}\,c_{P,\,f}\,\frac{dT}{dt} + c_{P,\,g}\,(T_F - T_{REF})\,\frac{dM_{g,\,SL}}{dt} + M_{g,\,SL}\,c_{P,\,g}\,\frac{dT_g}{dt} \qquad 4.16\text{-}11$$

where the subscript:

REF = Reference temperature, 32°F

All other variables and subscripts are as previously defined. Writing the preceding equation in its difference form:

$$c_P \frac{d(MT)_{SL}}{dt} \approx c_{P,f} (T_f - T_{REF}) \frac{\Delta M_{f,SL}}{\Delta t} + M_{f,SL} c_{P,f} \frac{\Delta T_{f,SL}}{\Delta t} \qquad 4.16\text{-}12$$

$$+ c_{P,g} (T_g - T_{REF}) \frac{\Delta M_{g,SL}}{\Delta t} + M_{g,SL} c_{P,g} \frac{\Delta T_{g,SL}}{\Delta t}$$

The specific heat of the liquid and vapor phases of water is calculated using temperature and pressure measurements from the data channels identified in Table 4.16-1. Equation 4.16-12 is used to calculate the change in stored or internal energy of the fluid in the surge line.

The energy carried by the flow from the surge line into the pressurizer is calculated as a consequence of the energy balance on the pressurizer, that is:

$$\dot{M}_{SL\text{-}PRZR} h_{SL\text{-}PRZR} \equiv \text{pressurizer energy balance} \qquad 4.16\text{-}13$$

The change in stored energy of the surge line metal may be expressed as:

$$Q_{SL\text{-}METAL} = c_{P,METAL} \times M_{SL\text{-}METAL} \times \frac{dT_{SL\text{-}METAL}}{dt} \qquad 4.16\text{-}14$$

where the subscript:

METAL = Metal mass of the pressurizer tank, lbm

All other parameters are as previously defined. The preceding equation may be written in its difference form:

$$Q_{SL\text{-}METAL} = c_{P,METAL} \times M_{SL\text{-}METAL} \times \frac{\Delta T_{SL\text{-}METAL}}{\Delta t} \qquad 4.16\text{-}15$$

Taking the temperature data from the surface mounted thermocouple on the surge line as being representative of the piping temperature, the rate of internal or stored energy associated with the surge line is calculated from test data.

The rate of energy loss from the surge line to the environment may be expressed as:

$$Q_{SL-AMB} = U_{SL-AMB} \times A_{SL-AMB} \times dt_{SL-AMB} \qquad 4.16\text{-}16$$

where:

A	=	Effective external surface area of the surge line, $ft.^2$
U	=	Overall conductance from the surge line outside surface to the ambient, $Btu/(sec.\text{-}ft.^2\text{-}°F)$

All other variables and subscripts are as previously defined. Writing the preceding equation in its difference form:

$$Q_{SL-AMB} = U_{SL-AMB} \times A_{SL-AMB} \times \Delta T_{SL-AMB} \qquad 4.16\text{-}17$$

This equation is used to calculate the heat loss from the separator to the ambient. An overall conductance is evaluated that accounts for energy loss by natural convection to the ambient and the resistance of insulation applied to the surge line. Outputs from the surface mounted thermocouple and an ambient temperature measurement are used to calculate the driving temperature for heat loss to the ambient.

Equation 4.16-2 may now be rewritten to solve for the energy associated with the surge line flow.

$$Q_{HL-SL} = c_p \frac{d(MT)_{SL}}{dt} - Q_{SL-PRZR} - Q_{SL-METAL} - Q_{SL-AMB} \qquad 4.16\text{-}18$$

Solving the preceding equation, the energy associated with the flow from the hot leg into the surge line is calculated.

TABLE 4.16-1
PRESSURIZER SURGE LINE DATA CHANNELS TO BE USED TO CALCULATE FLUID PROPERTIES

Situation	Local Fluid Temperature[1] (°F)	Local Fluid Pressure[2] (psia)	Metal Temperature
LDP-602 and LDP-606 indicate the following pressurizer surge line is water solid	T_f = 0.5 (TF-601 + TF-603)	P_f = PT-603 - (LPD-601 + LDP-606 + 0.5 x LDP-602)	
LDP-606 indicates that the upper portion of the surge line is either two-phase or vapor solid; LDP-602 indicates the lower surge line is water solid	T_f = TF-603 T_g = TF-601	P_f = PT-603 - (LPD-601 + LDP-606 + LDP-602) P_g = PT-603 - (LDP-601 + LDP-606)	TFM-603
LDP-606 indicates that the upper portion of the surge line is either two-phase or vapor solid; LDP-602 indicates the lower surge line is a two-phase mixture	T_f = TF-603 T_g = TF-601	P_f = PT-603 - (LPD-601 + LDP-606 + LDP-602) P_g = PT-603 - (LDP-601 + LDP-606)	
Two-phase fluid or all vapor in the hot leg	T_f = TF-603 T_g = 0.5 (TF-603 + TF-601)	P_f = PT-603 - (LDP-601 + LPD-606 + LDP-602) P_g = PT-603 - (LDP-601 + LDP-606 + 0.5 LDP-602)	

Note:
(1) Liquid calculations need not be done for cases with all steam venting through the surge line.
(2) LDP readings are to be density compensated before being used to calculate local pressure.

4.17 Cold Legs

The CMT piping design provides for pressure balance lines for the CMTs to be connected to two of the four of the four cold legs; specifically, the balance line piping is connected to CL-1 and CL-3. CL-2 and CL-4 do not have CMT pressure balance lines associated with them.

4.17.1 Cold Leg with CMT Balance Lines (CL-1 and CL-3)

The mass balance on the cold legs with CMT balance lines, (CL-1 and CL-3), may be written as:

$$\frac{d\ M_{CL\ w\ BL}}{dt} = \dot{M}_{SG\ 1} - \dot{M}_{BL} - \dot{M}_{DC,\ CL\ w\ BL} \qquad 4.17\text{-}1$$

where:

M	=	Mass, lbm
$\dot{M}$	=	Mass flow rate, lbm/sec.

and the subscripts:

BL	=	CMT balance lines
CL w BL	=	Cold legs with balance lines (CL-1 and CL-3)
DC	=	Downcomer
SG 1	=	Steam generator-1

The change in mass inventory in CL-1 and CL-3 given by the left-hand side of Equation 4.17-1 may be expanded to:

$$\frac{dM_{CL\ w\ BL}}{dt} = \frac{dM_{CL\ 1}}{dt} + \frac{dM_{CL\ 3}}{dt} \qquad 4.17\text{-}2$$

where the subscripts:

CL 1	=	Cold leg-1
CL 3	=	Cold leg-3

All other parameters are as previously defined.

Similarly, the combined energy balance for CL-1 and CL-3 is written as:

$$c_{P,f}\frac{d(M_{CL\ w\ BL}\ T_f)}{dt} = \dot{M}_{SG\ 1}\ h_{SG\ 1} - \dot{M}_{BL}\ h_{BL} - \dot{M}_{DC,\ CL\ w\ BL}\ h_{DC,\ CL\ w\ BL} - Q_{CL\ w\ BL,\ METAL} - Q_{CL\ w\ BL,\ AMB} \qquad 4.17\text{-}3$$

where:

c_p	=	Specific heat, Btu/(lbm - °F)
h	=	Enthalpy of the working fluid, Btu/lbm
Q	=	Rate of energy transfer of transport, Btu/sec
T	=	Temperature, °F

and the subscripts:

f	=	Fluid, both liquid and vapor phases, in cold legs
METAL	=	Metal mass of CL-1 and CL-3
AMB	=	Energy loss to environment

The change in energy associated with CL-1 and CL-3 given by the left-hand side of Equation 4.17-3 may be expanded to:

$$c_{P,f}\frac{d(M_{CL\ w\ BL}\ T_f)}{dt} = c_{P,f}\frac{d(M_{CL\ 1}\ T_f)}{dt} + c_{P,f}\frac{d(M_{CL\ 3}\ T_f)}{dt} \qquad 4.17\text{-}4$$

4.17.1.1 Mass Balance

Prior to test initiation, the simulated reactor coolant pumps (RCPs) are operating. Upon initiation of the transient, the RCPs are "tripped." Within about 30 seconds, forced flow goes to zero, and the level transducer outputs may be used to calculate mass inventory of the cold legs.

Prior to the start of testing and until the RCPs coast down, cold-leg flow is a single-phase liquid and may, therefore, be measured with the magnetic flow meters located in CL-1 and CL-3. Also, under these conditions, the rate of change of mass storage in the cold legs is zero. Thus:

$$\frac{d\ M_{CL\ w\ BL}}{dt} = 0 \qquad 4.17\text{-}5$$

and

$$\dot{M}_{SG\ 1} = \dot{M}_{DC,\ CL\ w\ BL} = \dot{M}_{FMM\text{-}201} + \dot{M}_{FMM\text{-}203} \qquad 4.17\text{-}6$$

where the subscripts:

FMM-201 FMM-203	=	Instrument channel IDs for magnetic flow meters in CL-1 and CL-3, respectively

All other parameters and subscripts are as previously defined. The single-phase liquid flow rate is calculated as:

$$\dot{M}_{FMM\text{-}XXX} = FMM\text{-}XXX \times \rho_{LIQ}(P_{FMM\text{-}XXX},\ T_{FMM\text{-}XXX}) \qquad 4.17\text{-}7$$

where:

FMM-XXX	=	Output from flow meter XXX in units of gpm where XXX = 201 CL-1 203 CL-3
P	=	Local pressure at flow meter, psia.
T	=	Local fluid temperature, °F
ρ	=	Local liquid density, lbm/ft.^{3}

Flows for tests with inoperative flow meters may be inferred from the cold leg differential pressure cells.

The local liquid density is calculated from the ASME steam table routines using pressure, differential pressure, and temperature values from the data channels listed in Table 4.17-1. The local pressure used to evaluate local fluid density is calculated as:

$$P_{FMM-XXX} = PT-XXX + DP-YYY \qquad 4.17\text{-}8$$

All parameters and subscripts are as previously defined.

Once flow in the cold legs becomes two-phase, the magnitude of the output from the flow meters is not indicative of the actual flow in those components. The liquid mass in CL-1 and CL-3 is then calculated using local level transducers as follows:

Step 1: Compensate the readings from the downcomer level transducer listed in Table 4.17-2 to account for temperature differences between fluid in the downcomer and fluid in the reference leg of the instrument line. The local pressure and temperature transducers to be used to accomplish the compensation are also identified in Table 4.17-2.

Step 2: From the collapsed liquid level calculated from Step 1, calculate the liquid volume in the pressurizer, $V_{l,CL\,X}$, as follows:

$$V_{l,CL\,X} = V(l)_{CL\,X} \times LDP-YYY \qquad 4.17\text{-}9$$

where:

LDP-YYY = Output from instrument having this data channel ID, where YYY is determined by cold leg being considered (see Table 4.17-1)
V = Volume, $ft.^3$
V(l) = Volume as a function of elevation, $ft.^3/ft.$

and the subscript:

l = Liquid inventory

All other parameters and subscripts are as previously defined.

The elevation of the cold leg relative to the downcomer LDP span extends from 67.7 to 71.248 in. Thus, the table of volume versus elevation for the cold legs is mapped onto the downcomer levels readings such that:

Downcomer-Compensated Water Level (in.)	Water Level in CL-1 and CL-2 (in.)
67.7	0.0
71.248	3.548

The corresponding volumes of CL-1 and CL-3 are as previously calculated.

Step 3: The local pressures and temperatures measured using the instruments identified in Table 4.17-2 are used as inputs to the ASME steam tables to calculate the density of the liquid and vapor in the pressurizer in the cold legs:

$$\rho_{l,\,CL.\,X} = \rho(PT\text{-}XXX,\ TF\text{-}XXX)$$
$$\rho_{g,\,CL.\,X} = \rho(PT\text{-}XXX,\ TF\text{-}ZZZ) \qquad 4.17\text{-}10$$

where:

ρ	=	Density, lbm/ft.^{3}
PT-XXX	=	Channel ID for local pressure measurement in downcomer
TF-XXX	=	Channel ID for local temperature measurement of liquid temperatures
TF-ZZZ	=	Channel ID for local temperature measurement of vapor temperatures

and the subscripts:

l	=	Liquid phase of water
g	=	Vapor phase of water

All other parameters and subscripts are as previously defined.

Step 4: Using the local thermodynamic properties of water as determined from local pressure and fluid temperature measurements, the liquid and vapor mass in the pressurizer is calculated as:

$$M_{l,\,CL\,X} = \rho_{l,\,CL\,X} \times V_{l,\,CL\,X}$$
$$M_{g,\,CL\,X} = \rho_{g,\,CL\,X} \times (V_{TOT,\,CL\,X} - V_{l,\,CL\,X}) \qquad 4.17\text{-}11$$

where the subscript:

TOT = Total volume of component

All other parameters and subscripts are as previously defined.

Step 5: The rate of change in mass inventory of the cold leg may be approximated by differencing two consecutive calculated values of the liquid and vapor masses:

$$\frac{dM_{l,\,CL\,X}}{dt} \approx \frac{\Delta M_{l,\,CL\,X}}{\Delta t} = \frac{M_{l,\,CL\,X,\,i+1} - M_{l,\,CL\,X,\,i}}{t_{i+1} - t_i}$$
$$\frac{dM_{g,\,CL\,X}}{dt} \approx \frac{\Delta M_{g,\,CL\,X}}{\Delta t} = \frac{M_{g,\,CL\,X,\,i+1} - M_{g,\,CL\,X,\,i}}{t_{i+1} - t_i} \qquad 4.17\text{-}12$$

where:

Δ = Difference between two consecutive calculations or data scans

and the subscript:

i = A specific value in the time and corresponding data array

All other parameters and subscripts are as previously defined. The total rate of change of the mass inventory of CL-1 or CL-3 is then calculated as:

$$\frac{dM_{CL\ w\ BL}}{dt} \approx \frac{\Delta M_{CL\ w\ BL}}{\Delta t} = \frac{\Delta M_{l,\ CL\ 1} + \Delta M_{g,\ CL\ 1} + \Delta M_{l,\ CL\ 3} + \Delta M_{g,\ CL\ 3}}{\Delta t} \qquad 4.17\text{-}13$$

Referring to Equation 4.17-1, the total mass flow rate from SG-1 is calculated in the hot leg and steam generator primary modules and assumed to be equally split between CL-1 and CL-3. Also, the mass flow into each of the CMT balance lines is calculated in the CMT balance line module. The rate of flow from CL-1 and CL-3 into the downcomer may be calculated by rearranging Equation 4.17-1 and solving for that term as follows:

$$\dot{M}_{DC,\ CL\ w\ BL} = \dot{M}_{SG\ 1} - \dot{M}_{BL} - \frac{\Delta M_{CL\ w\ BL}}{\Delta t} \qquad 4.17\text{-}14$$

The total mass flow into the downcomer from CL-1 and CL-3 is calculated using the mass storage term for those two components and the flow rate from SG-1.

4.17.1.2 Energy Balance

Equation 4.17-4 defines the change in energy associated with CL-1 and CL-3 as the sum of the energy associated with the fluid in each of the two cold legs. The fluid in these two cold legs may, depending on the time and nature of the test, be in either a liquid or a vapor phase. The energy balance on CL-1 and CL-3 must account for energy associated with both the vapor and liquid phases. Therefore, the energy balance for either CL-1 or CL-3 may be written as:

$$c_{P,\ f}\frac{d(\ M_{CL\ X}\ T_f\ )}{dt} = c_{P,\ l}\ M_{CL\ X,\ l}\frac{d(\ T_l\ )}{dt} + c_{P,\ l}\ T_l\frac{d(\ M_{CL\ X,\ l}\ )}{dt} + c_{P,\ g}\ M_{CL\ X,\ g}\frac{d(\ T_g\ )}{dt} + c_{P,\ g}\ T_g\frac{d(\ M_{CL\ X,\ g}\ )}{dt} \qquad 4.17\text{-}15$$

where the subscript:

g = Vapor or gaseous phase of fluid
l = Liquid phase of fluid

All other parameters are as previously defined. Writing the previous equation in its difference form:

$$c_{P,f}\frac{d(M_{CL\,X}\,T_f)}{dt} = c_{P,l}\,M_{CL\,X,l}\frac{\Delta T_l}{\Delta t} + c_{P,l}\,T_l\frac{\Delta M_{CL\,X,l}}{\Delta t} + c_{P,g}\,M_{CL\,X,g}\frac{\Delta T_g}{\Delta t} + c_{P,g}\,T_g\frac{\Delta M_{CL\,X,g}}{\Delta t} \qquad 4.17\text{-}16$$

All parameters and subscripts are as previously defined. The data channel IDs for the instruments to be used to define the thermal transport properties are identified in Table 4.17-2.

The rate of energy transport associated with SG-1 mass flow rate is calculated from the primary steam generator module.

The rate of energy change of the metal mass for CL-1 and CL-3 is calculated as:

$$Q_{CL\,w\,BL\,METAL} = Q_{CL\,1\,METAL} + Q_{CL\,3\,METAL} \qquad 4.17\text{-}17$$

expanding,

$$Q_{CL\,X\,METAL} = M \times c_P \times \frac{\Delta T_{TFM\text{-}20X}}{\Delta t} \qquad 4.17\text{-}18$$

where the subscript:

TFM-20X = Temperature-sensing element to be used for this calculation:
X = 1 CL-1
X = 3 CL-3

All other parameters and subscripts are as previously defined.

Similarly, the heat flux from the surface of the cold leg is calculated as:

$$Q_{CL\ w\ BL\ AMB} = Q_{CL\ 1\ AMB} + Q_{CL\ 3\ AMB} \qquad 4.17\text{-}19$$

The heat flux for each cold leg is calculated as:

$$Q_{CL\ X\ AMB} = U_{CL\ X\ AMB} \times A_{CL\ X\ AMB} \times (T_{TFM\text{-}20X} - T_{AMB}) \qquad 4.17\text{-}20$$

where:

A	=	Effective external surface area of the cold legs, ft.^{2}
U	=	Overall conductance from the cold leg outside surface to the ambient, BTU/(sec.-ft.^{2}-°F)
T_{AMB}	=	Ambient temperature

All other parameters and subscripts are as previously defined.

The rate of energy transport into the downcomer is solved for by rearranging the terms of Equation 4.17-3 and solving for that term. Note that the liquid and vapor mass flow rates in CL-1 and CL-3 are calculated, as are the enthalpies associated with the vapor and liquid components.

4.17.2 Cold Leg without CMT Balance Lines (CL-2 and CL-4)

The mass balance on the cold legs without CMT balance lines (CL-2 and CL-4) may be written as:

$$\frac{d\ M_{CL\ w/o\ BL}}{dt} = \dot{M}_{SG\ 2} - \dot{M}_{DC,\ CL\ w/o\ BL} \qquad 4.17\text{-}21$$

where:

M	=	Mass, lbm
$\dot{M}$	=	Mass flow rate, lbm/sec.

and the subscripts:

CL w/o BL	=	Cold legs without balance lines (CL-2 and CL-4)
DC	=	Downcomer
SG 2	=	Steam generator-2

The change in mass inventory in CL-2 and CL-4 given by the left hand side of Equation 4.17-21 above may be expanded to:

$$\frac{dM_{CL\ w/o\ BL}}{dt} = \frac{dM_{CL\ 2}}{dt} + \frac{dM_{CL\ 4}}{dt} \qquad 4.17\text{-}22$$

where the subscripts:

CL 2	=	Cold leg-2
CL 4	=	Cold leg-4

All other parameters are as previously defined.

Similarly, the energy balance for CL-2 and CL-4 is written as:

$$c_{P,f} \frac{d(M_{CL\ w/o\ BL}\ T_f)}{dt} = \dot{M}_{SG\ 2}\ h_{SG\ 2} - \dot{M}_{DC,\ CL\ w/o\ BL}\ h_{DC,\ CL\ w/o\ BL} - Q_{CL\ w/o\ BL\ METAL} - Q_{AMB} \qquad 4.17\text{-}23$$

where:

c_P	=	Specific heat, Btu/(lbm - °F)
Q	=	Rate of energy transfer of transport, Btu/sec.
T	=	Temperature, °F
h	=	Enthalpy of the working fluid, Btu/lbm

and the subscripts:

f	=	Fluid, both liquid and vapor phases, in cold legs
METAL	=	Metal mass of CL-2 and CL-4
AMB	=	Energy loss to environment

The change in energy associated with CL-2 and CL-4 given by the left-hand side of Equation 4.17-23 may be expanded to:

$$c_{P,f} \frac{d(M_{CL\ w/o\ BL}\ T_f)}{dt} = c_{P,f} \frac{d(M_{CL\ 2}\ T_f)}{dt} + c_{P,f} \frac{d(M_{CL\ 4}\ T_f)}{dt} \qquad 4.17\text{-}24$$

4.17.2.1 Mass Balance

Prior to test initiation, the RCPs are operating. Upon initiation of the transient, the RCPs are "tripped" and forced flow goes to zero. At this point, the level transducer outputs may be used to calculate mass inventory of the cold legs.

Prior to the start of testing and until the RCPs coast down, cold-leg flow is a single-phase liquid and may, therefore, be measured with the magnetic flow meters located in CL-2 and CL-4. Also, under these conditions, the rate of change of mass storage in the cold legs is zero. Therefore:

$$\frac{d\ M_{CL\ w/o\ BL}}{dt} = 0 \qquad 4.17\text{-}25$$

and

$$\dot{M}_{SG\ 2} = \dot{M}_{DC,\ CL\ w/o\ BL} = \dot{M}_{FMM\text{-}202} + \dot{M}_{FMM\text{-}204} \qquad 4.17\text{-}26$$

where the subscripts:

FMM-202 FMM-204	=	Instrument channel IDs for magnetic flow meters in CL-2 and CL-4, respectively

All other parameters and subscripts are as previously defined. The single-phase liquid flow rate is calculated as:

$$\dot{M}_{FMM\text{-}XXX} = FMM\text{-}XXX \times \rho_{LIQ}(P_{FMM\text{-}XXX},\ T_{FMM\text{-}XXX}) \qquad 4.17\text{-}27$$

where:

FMM-XXX	=	Output from flow meter XXX in units of gpm where XXX = 202 CL-2 204 CL-4
P	=	Local pressure at flow meter, psia
T	=	Local fluid temperature, °F
ρ	=	Local liquid density, lbm/ft.^{3}

Flows for tests with inoperative flow meters may be inferred from cold leg differential pressure cells.

The local liquid density is calculated from the ASME steam table routines using pressure, differential pressure, and temperature values from the data channels listed in Table 4.17-3. The local pressure used to evaluate local fluid density is calculated as:

$$P_{FMM-XXX} = PT-XXX + DP-YYY \qquad 4.17\text{-}28$$

All parameters and subscripts are as previously defined.

Once flow in the cold legs becomes two-phase, the magnitude of the output from the flow meters is not indicative of the actual flow in those components. The liquid mass in CL-2 and CL-4 is then calculated using local level transducers as follows:

Step 1: Compensate the readings from the downcomer level transducer listed in Table 4.17-4 to account for temperature differences between fluid in the downcomer and the fluid in the reference leg of the instrument line. The local pressure and temperature transducers to be used to accomplish the compensation are also identified in Table 4.17-4.

Step 2: From the collapsed liquid level calculated from Step 1, calculate the liquid volume in the pressurizer, $V_{l, CL\ X}$, as follows:

$$V_{l, CL\ X} = V(l)_{CL\ X} \times LDP-YYY \qquad 4.17\text{-}29$$

where:

LDP-YYY	=	Output from instrument having this data channel ID where YYY is determined by cold leg being considered (see Table 4.17-3)
V	=	Volume, $ft.^3$
V(l)	=	Volume as a function of elevation, $ft.^3/ft.$

and the subscripts:

l	=	Liquid inventory

All other parameters and subscripts are as previously defined.

The elevation of the cold leg extends from 67.7 to 71.248 in. The table of volume versus elevation for CL-2 and CL-4 is mapped onto the downcomer levels readings, such that:

Downcomer-Compensated Water Level (in.)	Water Level in CL-2 and CL-4 (in.)
67.7	0.0
71.248	3.548

The corresponding volumes of CL-2 and CL-4 are as previously calculated.

Step 3: The local pressures and temperatures measured using the instruments identified in Table 4.17-4 are used as inputs to the ASME steam tables to calculate the density of the liquid and vapor in the pressurizer in the cold legs:

$$\rho_{l,\,CL\,X} = \rho(PT\text{-}XXX,\ TF\text{-}XXX)$$
$$\rho_{g,\,CL\,X} = \rho(PT\text{-}XXX,\ TF\text{-}ZZZ) \qquad 4.17\text{-}30$$

where:

ρ	=	Density, $lbm/ft.^3$
PT-XXX	=	Channel ID for local pressure measurement in downcomer
TF-XXX	=	Channel ID for local temperature measurement of liquid and vapor temperatures
TF-ZZZ		in cold leg (see Table 4.17-4)

and the subscripts:

l = Liquid phase of water
g = Vapor phase of water

Step 4: Using the local thermodynamic properties of water as determined from local pressure and fluid temperature measurements, the liquid and vapor mass in the pressurizer is calculated as:

$$M_{l,CL\,X} = \rho_{l,CL\,X} \times V_{l,CL\,X}$$
$$M_{g,CL\,X} = \rho_{g,CL\,X} \times (V_{TOT,CL\,X} - V_{l,CL\,X}) \qquad 4.17\text{-}31$$

where the subscript:

TOT = Total volume of component

All other parameters and subscripts are as previously defined.

Step 5: The rate of change in mass inventory of the cold leg may be approximated by differencing two consecutive calculated values of the liquid and vapor masses:

$$\frac{dM_{l,CL\,X}}{dt} \approx \frac{\Delta M_{l,CL\,X}}{\Delta t} = \frac{M_{l,CL\,X,i+1} - M_{l,CL\,X,i}}{t_{i+1} - t_i}$$
$$\frac{dM_{g,CL\,X}}{dt} \approx \frac{\Delta M_{g,CL\,X}}{\Delta t} = \frac{M_{g,CL\,X,i+1} - M_{g,CL\,X,i}}{t_{i+1} - t_i} \qquad 4.17\text{-}32$$

where:

Δ = Difference between two consecutive calculations or data scans

and the subscript:

i = A specific value in the time and corresponding data array

All other parameters and subscripts are as previously defined. The total rate of change of the mass inventory of CL-2 or CL-4 is then calculated as:

$$\frac{dM_{CL\ w/o\ BL}}{dt} = \frac{\Delta M_{CL\ w/o\ BL}}{\Delta t} = \frac{\Delta M_{l,\ CL\ 2} + \Delta M_{g,\ CL\ 2} + \Delta M_{l,\ CL\ 4} + \Delta M_{g,\ CL\ 4}}{\Delta t} \qquad 4.17\text{-}33$$

Referring to Equation 4.17-21, the total mass flow rate from SG-2 is calculated in the hot leg and steam generator primary modules and assumed to be equally split between CL-2 and CL-4. The rate of flow from CL-2 and CL-4 into the downcomer may be calculated by rearranging Equation 4.17-21 and solving for that term as follows:

$$\dot{M}_{DC,\ CL\ w/o\ BL} = \dot{M}_{SG\ 2} - \frac{\Delta M_{CL\ w/o\ BL}}{\Delta t} \qquad 4.17\text{-}34$$

The mass flow into the downcomer from CL-2 and CL-4 is calculated using the mass storage term for those two components and the flow rate from SG-2.

4.17.2.1 Energy Balance

Equation 4.17-24 defines the change in energy associated with CL-2 and CL-4 as the sum of the energy associated with the fluid in each of the two cold legs. The fluid in these two cold legs may, depending on the time and nature of the test, be in either a liquid or a vapor phase. The energy balance on CL-2 and CL-4 must account for energy associated with both the vapor and liquid phases. The energy balance for either CL-2 or CL-4 may be written as:

$$c_{P,f}\frac{d(M_{CL\ X}\ T_f)}{dt} = c_{P,l}\ M_{CL\ X,l}\frac{d(T_l)}{dt} + c_{P,l}\ T_l\frac{d(M_{CL\ X,l})}{dt} + c_{P,g}\ M_{CL\ X,g}\frac{d(T_g)}{dt} + c_{P,g}\ T_g\frac{d(M_{CL\ X,g})}{dt} \qquad 4.17\text{-}35$$

where the subscript:

g = Vapor or gaseous phase of fluid
l = Liquid phase of fluid

All other parameters are as previously defined. Writing the previous equation in its difference form:

$$c_{P,f} \cdot \frac{d(M_{CL\,X}\,T_f)}{dt} = c_{P,1}\,M_{CL\,X,1}\,\frac{\Delta T_1}{\Delta t} + c_{P,1}\,T_1\,\frac{\Delta M_{CL\,X,1}}{\Delta t} + c_{P,g}\,M_{CL\,X,g}\,\frac{\Delta T_g}{\Delta t} + c_{P,g}\,T_g\,\frac{\Delta M_{CL\,X,g}}{\Delta t} \qquad 4.17\text{-}36$$

All parameters and subscripts are as previously defined. The data channel IDs for the instruments to be used to define the thermal transport properties are identified in Table 4.17-4.

The rate of energy transport associated with SG-2 mass flow rate is calculated from the primary steam generator module.

The rate of energy change of the metal mass for CL-2 and CL-4 is calculated as:

$$Q_{CL\ w/o\ BL\ METAL} = Q_{CL\ 2\ METAL} + Q_{CL\ 4\ METAL} \qquad 4.17\text{-}37$$

expanding,

$$Q_{CL\ X\ METAL} = M \times c_P \times \frac{\Delta T_{TFM\text{-}20X}}{\Delta t} \qquad 4.17\text{-}38$$

where the subscript:

TFM-20X = Temperature-sensing element to be used for this calculation:
X = 2 CL - 2
X = 4 CL - 4

All other parameters and subscripts are as previously defined.

Similarly, the heat flux from the surface of the cold leg is calculated as:

$$Q_{CL\ w/o\ BL\ AMB} = Q_{CL\ 2\ AMB} + Q_{CL\ 4\ AMB} \qquad 4.17\text{-}39$$

The heat flux for each cold leg is calculated as:

$$Q_{CL\ X\ AMB} = U_{CL\ X\ AMB} \times A_{CL\ X\ AMB} \times (T_{TFM\text{-}20X} - T_{AMB}) \qquad 4.17\text{-}40$$

where:

A	=	Effective surface area of the cold legs, $ft.^2$
U	=	Overall conductance from the cold leg outside surface to the ambient, Btu/sec.-$ft.^2$-°F
T_{AMB}	=	Ambient temperature

All other parameters and subscripts are as previously defined.

The rate of energy transport into the downcomer is solved for by rearranging the terms of Equation 4.17-23 and solving for that term. Note that the liquid and vapor mass flow rates in CL-2 and CL-4 are calculated, as are the enthalpies associated with the vapor and liquid components.

TABLE 4.17-1 DATA CHANNEL IDs USED TO CALCULATE LOCAL FLUID PROPERTIES FOR FLOW METERS				
Applicable Conditions	**Channel ID for Liquid Flow Meter**	**Data Channel ID for Pressure Transducers**	**Data Channel ID for Differential Pressure Transducers**	**Data Channel ID for Fluid Thermocouples**
Cold leg inventory is all liquid	FMM-201	PT-101	DP-122	TF-105
	FMM-203	PT-103	DP-124	TF-101

TABLE 4.17-2 DATA CHANNEL IDs USED TO CALCULATE FLUID PROPERTIES FOR LEVELS TRANSDUCERS					
Applicable Conditions	**Location**	**Data Channel ID for Liquid Levels**	**Data Channel ID for Local Pressure**	**Data Channel ID for Fluid Temperature**	**Data Channel ID for Energy Balance Calculations**
Compensated water level when water level in downcomer is above bottom of cold leg	Downcomer annulus at ≈ 180°az (≈ 270°az for backup)	LDP-140 LDP-116[1]	PT-111	TF-152 TF-155 TF-158	
Density and enthalpy of liquid in cold legs	CL-1		PT-101	TF-105 (liquid) TF-107 (vapor)	
	CL-3		PT-103	TF-101 (liquid) TF-103 (vapor)	
Change in stored energy of cold legs	CL-1				TFM-201
	CL-3				TFM-203
Heat loss to ambient	CL-1				HFM-201
	CL-3				HFM-203

TABLE 4.17-3 DATA CHANNEL IDs USED TO CALCULATE LOCAL FLUID PROPERTIES FOR FLOW METERS				
Applicable Conditions	**Channel ID for Liquid Flow Meter**	**Data Channel ID for Pressure Transducers**	**Data Channel ID for Differential Pressure Transducers**	**Data Channel ID for Fluid Thermocouples**
Cold leg inventory is all liquid	FMM-202	PT102	DP-122	TF-106
	FMM-204	PT-104	DP-124	TF-102

TABLE 4.17-4 DATA CHANNEL IDs USED TO CALCULATE FLUID PROPERTIES FOR LEVELS TRANSDUCERS					
Applicable Conditions	**Location**	**Data Channel ID for Liquid Levels**	**Data Channel ID for Local Pressure**	**Data Channel ID for Fluid Temperature**	**Data Channel ID for Energy Balance Calculations**
Compensated water level when water level in downcomer is above bottom of cold leg	Downcomer annulus at ≈ 180°az (≈ 270°az for backup)	LDP-140 LDP-116[1]	PT-111	TF-152 TF-155 TF-158	
Density and enthalpy of liquid in cold legs	CL-2		PT-102	TF-106 (liquid) TF-108 (vapor)	
	CL-4		PT-104	TF-102 (liquid) TF-104 (vapor)	
Change in stored energy of cold legs	CL-2				TFM-202
	CL-4				TFM-204
Heat loss to ambient	CL-2				HFM-202
	CL-4				HFM-204

4.18 Hot Legs

The AP600 OSU test facility incorporates the two hot legs of the AP600 design. Each hot leg has an ADS-4 line associated with it. In addition, one hot leg, designated as HL-2, also has the pressurizer surge line and the PRHR feed line associate with it. The pressurizer surge line connection to HL-2 provides a flow path from the primary system to ADS stages 1, 2 and 3. Considering the various flow paths, the mass balance for HL-1 and HL-2, respectively, may be written as:

$$\frac{d\ M_{HL\ 1}}{dt} = \dot{M}_{UP\text{-}HL\ 1} - \dot{M}_{ADS\ 4\text{-}1} - \dot{M}_{SG\ 1} \qquad 4.18\text{-}1$$

and

$$\frac{d\ M_{HL\ 2}}{dt} = \dot{M}_{UP\text{-}HL\ 2} - \dot{M}_{SL} - \dot{M}_{ADS\ 4\text{-}2} - \dot{M}_{PRHR} - \dot{M}_{SG\ 2} \qquad 4.18\text{-}2$$

where:

M	=	Mass, lbm
$\dot{M}$	=	Mass flow rate, lbm/sec.

and the subscripts:

ADS 4-X	=	ADS-4 X = 1,HL-1 = 2,HL-2
HL 1, HL 2	=	HL-1 or HL-2, respectively
SG 1, SG 2	=	Steam generator-1 or steam generator-2, respectively
SL	=	Junction between HL-2 and the pressurizer surge line
UP - HL 1, UP - HL 2	=	Junction between the RPV upper plenum and HL-1 or HL-2, respectively.

Similarly, the energy balance for HL-1 and HL-2, respectively, is written as:

$$c_{P,f}\frac{d(M_{HL\,1}\,T_f)}{dt} = \dot{M}_{UP\text{-}HL\,1}\,h_{HL\,1\,MIX} - \dot{M}_{ADS\,4\text{-}1}\,h_{ADS\,4\text{-}1} - \dot{M}_{SG\,1}\,h_{SG\,1} - Q_{HL\,1\,METAL} - Q_{HL\,1\,AMB} \qquad 4.18\text{-}3$$

and

$$c_{P,f}\frac{d(M_{HL\,2}\,T_f)}{dt} = \dot{M}_{UP\text{-}HL\,2}\,h_{HL\,2\,MIX} - \dot{M}_{SL}\,h_{SL} - \dot{M}_{ADS\,4\text{-}2}\,h_{ADS\,4\text{-}2} - \dot{M}_{PRHR}\,h_{PRHR} - \dot{M}_{SG\,2}\,h_{SG\,2} - Q_{HL\,2\,METAL} - Q_{HL\,2\,AMB} \qquad 4.18\text{-}4$$

where:

c_p	=	Specific heat, Btu/(lbm - °F)
Q	=	Rate of energy transfer of transport, Btu/sec.
T	=	Temperature, °F

and the subscripts:

f	=	Fluid, both liquid and vapor phases, in the cold legs
METAL	=	Metal mass of the hot leg
AMB	=	Energy loss to the environment

All other parameters and subscripts are as previously defined.

4.18.1 Mass Balance

There is no direct measurement of mass flow in the primary system hot legs of the OSU test facility; hot leg flows are inferred by continuity and/or energy balances performed on the system. Also, four distinctly different characteristic modes of operation may be identified for the hot legs; 1) single phase liquid (early in the test), 2) two-phase natural circulation (prior to ADS actuation, 3) after actuation of ADS 1-3, and 4) after actuation of ADS-4. To properly analyze the test data, the development of mass balance equations for the hot legs shall account for these modes of operation.

As a first step, the calculation of the liquid and steam inventory in the hot legs shall be developed.

4.18.1.1 Liquid Mass Storage in the Hot Legs

The hot leg may be in one of three states; liquid solid, vapor solid, or a mixture of liquid and vapor. The output from the appropriate level transducers listed in Table 4.18-1 is used to first calculate the liquid inventory and mass in the hot leg, and then corresponding vapor inventory and mass. This calculation is accomplished as follows:

Step 1: Compensate the readings from HL-1 level transducers listed in Table 4.18-1 to account for temperature differences between fluid in the hot leg and fluid in the reference leg of the instrument line. The instruments used to measure local pressure and fluid temperatures to be used to accomplish the compensation are also identified in Table 4.18-1.

Step 2: The local pressures and temperatures measured by the instruments identified in Table 4.18-1 are used as inputs to the ASME steam tables to calculate the density of the fluid in the hot legs:

$$\rho_{f,\,HL\,X} = \rho_f\,(\text{Pressure, Temperature}) \qquad 4.18\text{-}5$$

where:

ρ	=	Density, lbm/ft^3
Pressure	=	Local pressure representative of that in the hot leg of interest
Temperature	=	Local fluid temperature representative of that in the hot leg of interest

and the subscript:

f	=	Working fluid, water, and includes both vapor and liquid phases

Step 3: Using the compensated liquid level and the appropriate function of hot leg volume as a function of height, determine the volume of liquid in the hot leg:

$$V_{f,\,HL\,1} = V_{TOT,\,HL\,1} \times LDP\text{-}XXX_{COMP} \qquad 4.18\text{-}6$$

where:

V	=	Volume, ft^3
LDP-XXX$_{COMP}$	=	Compensated fluid levels data from appropriate levels transducer, ft.

and the subscripts:

l	=	Liquid volume, $ft.^3$
TOT	=	Total volume of the hot leg

Other parameters and subscripts are as previously defined.

Step 4: The liquid mass inventory in the hot leg is now calculated as:

$$M_{l,\,HL\,X} = \rho_{l,\,HL\,X} \times V_{l,\,HL\,X} \qquad 4.18\text{-}7$$

and the vapor mass is calculated as:

$$M_{g,\,HL\,X} = \rho_{g,\,HL\,X} \times (V_{TOT,\,HL\,X} - V_{l,\,HL\,X}) \qquad 4.18\text{-}8$$

where the subscript:

g	=	Vapor conditions at the local hot leg pressures and temperatures

All parameters and subscripts are as previously defined. The total fluid mass in the hot leg is calculated as:

$$M_{HL\,X} = M_{l,\,HL\,X} + M_{g,\,HL\,X} \qquad 4.18\text{-}9$$

All other parameters and subscripts are as previously defined.

Step 5: The rate of change in mass inventory of the hot leg may be approximated by differencing two consecutive calculated values of liquid mass:

$$\frac{dM_{HL\,X}}{dt} = \frac{\Delta M_{HL\,X}}{\Delta t} = \frac{M_{HL\,X,\,i} - M_{HL\,X\,i-1}}{t_i - t_{i-1}} \qquad 4.18\text{-}10$$

where the subscript:

i	=	Index of the data and time arrays

All other parameters and subscripts are as previously defined.

4.18.2 Mass Flow Rate

4.18.2.1 Hot Legs are Liquid Solid

Prior to test initiation, the simulated reactor coolant pumps (RCPs) are operating and the fluid in the primary system is at a single-phase liquid condition. Upon initiation of the transient, the RCPs are "tripped" and begin a coast-down, allowing the forced flow in the primary loop to go to zero. As long as the hot legs remain water solid, the flow meters in the cold legs may be used to measure the mass flow rate from the upper plenum into the hot legs. Thus, the flow through the steam generator for this time period during the test may be expressed as the sum of the flow through the cold legs:

$$\dot{M}_{SG\ X} = \dot{M}_{CL\ Y} + \dot{M}_{CL\ Z} \qquad 4.18\text{-}11$$

where:

X, Y, Z A hot leg designation and its related cold legs:

Hot Leg = X	Cold Legs = Y Z
1	1 3
2	2 4

In the event that PRHR is operational during the time that the hot legs are water-solid, the PRHR flow is included in the sum of the cold leg flows. That is, for the condition that the hot legs are water-solid:

$$\dot{M}_{PRHR} + \dot{M}_{SG\ 2} = \dot{M}_{CL\ 2} + \dot{M}_{CL\ 4} \qquad 4.18\text{-}12$$

Substituting Equations 4.18-12 and 4.18-13 into Equations 4.18-1 and 4.18-2:

$$\dot{M}_{UP\text{-}HL\ 1} = \dot{M}_{ADS\ 4\text{-}1} + \dot{M}_{CL\ 1} + \dot{M}_{CL\ 3} + \frac{d\ M_{HL\ 1}}{dt} \qquad 4.18\text{-}13$$

and

$$\dot{M}_{UP\text{-}HL\ 2} = \dot{M}_{SL} + \dot{M}_{ADS\ 4\text{-}2} + \dot{M}_{CL\ 2} + \dot{M}_{CL\ 4} + \frac{d\ M_{HL\ 2}}{dt} \qquad 4.18\text{-}14$$

All other parameters and subscripts are as previously defined.

Note: Early in the test, the change in fluid mass stored in the hot leg is expected to be near zero, ADS-4 flow is expected to be zero, and until ADS 1-3 is actuated, flow attributed to that flow path is expected to be zero.

4.18.2.2 Two-Phase and Two-Phase Natural Circulation

This portion of the test begins after the RCPs stop. Typically, at this time, the PRHR is operating, but ADS has not yet actuated.

For this case, it will be assumed that the void fraction in the upper plenum is equal to the void fraction entering the hot legs. First, the reading of data channel LDP-139 is temperature compensated, and an average void fraction in the upper plenum is calculated using the compensated readings from the data channel:

$$\alpha_{UP} = 1 - \frac{LDP\text{-}139_{COMP}}{H_{LDP\text{-}139}} \qquad 4.18\text{-}15$$

where:

H	=	Height of the span of data channel LDP-139, in.
α	=	Average void fraction

and the subscript:

UP	=	RPV upper plenum

The local quality in the upper plenum is calculated as:

$$X_{UP} = S \frac{v_{f,\,UP}}{v_{g,\,UP}} \alpha^2 \qquad 4.18\text{-}16$$

where:

S	=	Slip ratio between liquid and vapor, input value take to be 2
v	=	Specific volume, $ft.^3/lbm$
α	=	Void fraction
X	=	Local quality

and the subscript:

UP = Upper plenum

Using the upper plenum quality and the rate of vapor generation, calculated in the RPV module, the total mass flow rate out of the core region may now be calculated as:

$$\dot{M}_{TOT,\ CORE} = \frac{\dot{M}_{VAPOR}}{X} \qquad 4.18\text{-}17$$

where the subscripts:

TOT, CORE = Total flow rate out of the top of the core, lbm/sec.
VAPOR = Fate of vapor generation calculated from the RPV module, lbm/sec.

All other parameters are as previously defined. It is further assumed that the change in stored mass in the upper plenum and upper head is small during this time. Thus:

$$\dot{M}_{TOT,\ CORE} = \dot{M}_{HL\ 1} + \dot{M}_{HL\ 2} \qquad 4.18\text{-}18$$

All other parameters and subscripts are as previously defined.

Now, assuming that the quality remains constant as fluid is ducted from the upper plenum to the hot legs, the ratio of the flow rates carried by the two hot legs may be expressed as the ratio of the heat loads carried by the hot legs:

$$\gamma = \frac{\dot{M}_{HL\ 2}}{\dot{M}_{HL\ 1}} = \frac{Q_{SG\ 2} + Q_{PRHR}}{Q_{SG\ 1}} \qquad 4.18\text{-}19$$

where:

Q = Total heat load of a component, Btu/sec.
γ = Ratio of mass flows in HL-2 to that in HL-1

and the subscripts:

SG 1, SG 2 = Steam generators 1 and 2, respectively
PRHR = Passive residual heat removal

The heat load terms are calculated and known from analysis of the steam generators and the PRHR; thus, γ is a known, calculated value. Rearranging Equation 4.18-19:

$$\dot{M}_{HL\,2} = \gamma\ \dot{M}_{HL\,1} \qquad 4.18\text{-}20$$

Substituting into Equations 4.18-17 and 4.18-18, the mass flow rate into HL-1 is expressed as:

$$\dot{M}_{HL\,1} = \frac{\dot{M}_V}{X(1+\gamma)} \qquad 4.18\text{-}21$$

The mass flow rate into HL-2, then, is calculated as:

$$\dot{M}_{HL\,2} = \gamma\ \dot{M}_{HL\,1} = \frac{\gamma\ \dot{M}_v}{X\ (1+\gamma)} \qquad 4.18\text{-}22$$

All other parameters and subscripts are as previously defined.

4.18.2.3 Two-Phase Flow with ADS 1-3 Actuated

As the test progresses, ADS Stages 1-3 actuate. The calculation of the mass flow into HL-1 and HL-2 for this case is similar to that of the case without ADS actuation. Equation 4.18-19, which defined the flow spilt between HL-1 and HL-2 is modified to include the energy associated with the flow through the surge line to the ADS Stage 1-3 valves.

$$\gamma = \frac{\dot{M}_{HL\,2}}{\dot{M}_{HL\,1}} = \frac{Q_{SG\,2} + Q_{SL} + Q_{PRHR}}{Q_{SG\,1}} \qquad 4.18\text{-}23$$

All other steps are the same as described above for the two-phase natural circulation condition. That is, Equation 4.18-23 is used to calculate a flow split ration between HL-1 and HL-2 that is then used in Equations 4.18-21 and 4.18-22 to calculate the mass flows into the two hot legs.

4.18.2.4 Two-Phase Flow with ADS 1-3 and ADS-4 Actuated

As the test transitions into its long term cooling simulation, ADS-4 actuates. The calculation of the mass flow into HL-1 and HL-2 for this case is similar to that of the case without ADS actuation. Equation 4.18-23, which was modified from Equation 4.18-19 to calculate the flow spilt between HL-1 and HL-2 with ADS 1-3 actuation, is further modified to account for the flow and associated energy transport through the ADS-4 valves:

$$\gamma = \frac{\dot{M}_{HL\ 2}}{\dot{M}_{HL\ 1}} = \frac{Q_{SG\ 2} + Q_{SL} + Q_{ADS\ 4\text{-}2} + Q_{PRHR}}{Q_{SG\ 1} + Q_{ADS\ 4\text{-}1}} \qquad 4.18\text{-}24$$

and all other steps are the same as described above for the two-phase natural circulation condition. That is, Equation 4.18-24 is used to calculate a flow split ration between HL-1 and HL-2 that is then used in Equations 4.18-21 and 4.18-22 to calculate the mass flows into the two hot legs.

4.18.3 Energy Balance

Equations 4.18-3 and 4.18-4 define the change in energy associated with HL-1 and HL-2. The fluid in the two hot legs may, depending upon the time and nature of the test, be either in a liquid or a vapor phase. Thus, the energy balance for HL-1 and HL-2 must account for energy associated with both the vapor and liquid phases. Thus, the change of energy for the fluid in either HL-1 or HL-2 may be written as:

$$c_{P,f}\frac{d(M_{HL\ X}\ T_f)}{dt} = c_{P,l}\ M_{HL\ X,l}\frac{d(T_l)}{dt} + c_{P,l}\ T_l\frac{d(M_{HL\ X,l})}{dt} + c_{P,g}\ M_{HL\ X,g}\frac{d(T_g)}{dt} + c_{P,g}\ T_g\frac{d(M_{HL\ X,g})}{dt} \qquad 4.18\text{-}25$$

where the subscript:

g	=	Vapor or gaseous phase of fluid
l	=	Liquid phase of fluid

All other parameters are as previously defined. Writing the above equation in its difference form:

$$c_{P,f}\frac{d(M_{HL\,X}\,T_f)}{dt} = c_{P,l}\,M_{HL\,X,l}\frac{\Delta T_l}{\Delta t} + c_{P,l}\,T_l\frac{\Delta M_{HL\,X,l}}{\Delta t} + c_{P,g}\,M_{HL\,X,g}\frac{\Delta T_g}{\Delta t} + c_{P,g}\,T_g\frac{\Delta M_{HL\,X,g}}{\Delta t} \qquad 4.18\text{-}26$$

All other parameters and subscripts are as previously defined. The data channel IDs for the instruments to be used to define the thermal transport properties are identified in Table 4.18-2.

The rate of energy change of the metal mass for HL-1 and HL-2 is calculated as:

$$Q_{HL\,X\,METAL} = M \times c_P \times \frac{\Delta T_{TFM\text{-}20Y}}{\Delta t} \qquad 4.18\text{-}27$$

where the subscript:

TFM-20Y Designates the temperature sensing element to be used for this calculation:
where Y = 5 ⇒ HL-1
6 ⇒ HL-2

All other parameters and subscripts are as previously defined.

Similarly, the heat flux from the surface of the hot legs is calculated using the surface temperature and convection to ambient.

$$Q_{HL\,X\,AMB} = U_{HL\,X\,AMB} \times A_{HL\,X\,AMB} \times (T_{TFM\text{-}20Y} - T_{AMB}) \qquad 4.18\text{-}28$$

where:

A	=	Effective surface area of the hot legs, ft.^{2}
U	=	Overall conductance from the cold leg outside surface to the ambient, Btu/sec.-ft.^{2}-°F
T_{AMB}	=	Ambient temperature

All other variables and subscripts are as previously defined.

For both HL-1 and HL-2, the energy transported from the hot legs by flow ducted from those components by the ADS-4 system is obtained from the respective ADS-4 separator mass and energy calculations.

Similarly, the energy transported from HL-2 by flow ducted from the hot leg by the surge line is obtained from the surge line mass and energy calculation module.

The mass flow to HL-1 and HL-2 has been estimated using a ratio of heat removal rates and quality for various times during a test. A mixture enthalpy is calculated for the total flow as:

$$h_{HL\ X\ MIX} = X\ h_g + (1 - X)\ h_l \qquad 4.18\text{-}29$$

All parameters are as previously defined and the liquid and vapor enthalpies are defined using the values from the temperature and pressure sensors identified in Table 4.18-1. The energy transport into the hot legs from the upper plenum is calculated by multiplying the appropriate estimated hot leg flow by its respective mixture enthalpy.

For HL-2, the energy transport associated with the operation of the PRHR is evaluated in the PRHR module.

All terms in Equations 4.18-3 and 4.18-4 have now been defined, except the energy transport from the hot legs into SG-1 and SG-2, respectively. Thus, these equations are rearranged to solve for the energy transport rate into the steam generators.

TABLE 4.18-1 DATA CHANNEL IDs USED IN HOT-LEG MASS AND ENERGY CALCULATIONS					
Applicable Conditions	**Location**	**Data Channel ID for Liquid Levels**	**Data Channel ID for Local Pressure**	**Data Channel ID for Fluid Temperature**	**Data Channel ID for Energy Balance Calculations**
Fluid conditions in hot leg	HL-1	HPS-205[1]			
	HL-2	HPS-206[1]			
Compensated levels readings in hot legs	HL-1	LDP-207	PT-205	TF-205	
	HL-2	LDP-208	PT-202	TF-206	
Density and enthalpy of liquid in hot legs	HL-1		PT-205	TF-141 (liquid) TF-143 (vapor)	
	HL-2		PT-202	TF-140 (liquid) TF-142 (vapor)	
Change in stored energy of hot legs	HL-1				TFM-205
	HL-2				TFM-206
Heat loss to ambient	HL-1				HFM-205
	HL-2				HFM-206

Note:
(1) Heated phase switch is used to determine state of fluid in hot legs: liquid solid = 100, full scale reading
two-phase = $0 < x < 100$
vapor solid = 0

TABLE 4.18-2 DATA CHANNEL IDs USED TO CALCULATE LOCAL FLUID PROPERTIES FOR FLOW METERS				
Applicable Conditions	**Channel ID for Liquid Flow Meter**	**Data Channel ID for Pressure Transducers**	**Data Channel ID for Differential Pressure Transducers**	**Data Channel ID for Fluid Thermocouples**
Cold leg inventory is all liquid	FMM-202	PT102	DP-122	TF-106
	FMM-204	PT-104	DP-124	TF-102

TABLE 4.18-3 DATA CHANNEL IDs USED TO CALCULATE FLUID PROPERTIES FOR LEVELS TRANSDUCERS					
Applicable Conditions	**Location**	**Data Channel ID for Liquid Levels**	**Data Channel ID for Local Pressure**	**Data Channel ID for Fluid Temperature**	**Data Channel ID for Energy Balance Calculations**
Compensated water level when water level in downcomer is above the bottom of the cold leg	Downcomer Annulus at ≈ 180°azi (≈ 270°az for backup)	LDP-140 LDP-116	PT-111	TF-152 TF-155 TF-158	
Density and enthalpy of liquid in cold legs	CL-2		PT-102	TF-106 (liquid) TF-108 (vapor)	
	CL-4		PT-104	TF-102 (liquid) TF-104 (vapor)	
Change in stored energy of cold legs	CL-2				TFM-202
	CL-4				TFM-204
Heat loss to ambient	CL-2				HFM-202
	CL-4				HFM-204

4.19 Pressure Conversions

A number of input pressures need to be converted from psig to psia and placed onto the results plot file. As with other caiculations involving input pressures in the various modules, the ambient pressure data channel (PT-003) is used for the conversion, as opposed to a constant of 14.7 psi. The units of the resulting pressure values is psia. A list of pressures converted from psig to psia is given in Table 4.19-1.

TABLE 4.19-1 PRESSURE CONVERSIONS	
Data Channel	**Channel Description**
DP-905	Break Separ Ent DP
PT-001	MFP Dischrg Pressure
PT-002	MS Header Pressure
PT-101	CL1 Press @RV Flange
PT-102	CL2 Press @RV Flange
PT-103	CL3 Press @RV Flange
PT-104	CL4 Press @RV Flange
PT-107	RV Upper Head Press
PT-108	RV Bottom Pressure
PT-109	DVI1 Pres @RV Flange
PT-110	DVI2 Pres @RV Flange
PT-111	RV Dwncmer Press-Top
PT-112	RV Dwncmer Press-Bot
PT-113	Rctr Blw Mid Spc Grd
PT-201	SG1 Long Tube Press
PT-202	HL-2 Pressure
PT-203	PR Upstrm of Break-1
PT-204	SG2 Long Tube Press
PT-205	HL-1 Pressure
PT-206	PR Upstrm of Break-2
PT-301	SG1 Sec Steam Press
PT-302	SG2 Sec Steam Press
PT-401	ACC-1 Pressure
PT-402	ACC-2 Pressure
PT-501	CMT-1 Pressure
PT-502	CMT-2 Pressure

TABLE 4.19-1 (Continued) PRESSURE CONVERSIONS	
Data Channel	**Channel Description**
PT-602	PZR NR Pressure
PT-603	PZR NR Pressure
PT-604	PZR WR Pressure
PT-605	ADS1-3 Separtr Press
PT-606	IRWST Sparger Press
PT-610	ADS4-2 Separtr Press
PT-611	ADS4-1 Separtr Press
PT-701	IRWST Pressure
PT-801	CVSP Discharge Press
PT-802	RNSP Discharge Press
PT-901	Primary Sump Press
PT-902	BAMS Header Pressure
PT-905	Break Separatr Press

5.0 ANALYSIS OF OSU TEST DATA

The phenomena identification ranking table (PIRT) for AP600 small-break loss-of-coolant accident (SBLOCA) with long-term cooling provided a guide for the OSU testing (Table 1.3-1). The PIRT was used to identify the instrumentation needed to record specific phenomena and also the manner in which the tests were performed. An initial acceptance evaluation of the tests against meeting the needs documented in the PIRT was performed in the *AP600 Low-Pressure Integral Systems Test at Oregon State University, Final Data Report*, WCAP-14252, which also included an evaluation of critical instruments and the acceptability of the initial conditions.

LOCAs with long-term cooling (LTC) in the OSU test were divided into phases characterized by primary system pressure and thermal-hydraulic phenomena occurring within the primary and safety systems. The following are the phases selected for the purpose of detailed evaluation of the LOCAs:

- Blowdown phase
- Natural circulation phase
- Automatic depressurization (ADS) phase
- In-containment refueling water storage tank (IRWST) injection phase
- Sump injection phase

The analysis of the OSU test data was performed using the test mass and energy balance computer code developed specifically to perform a continuous mass and energy balance for each component of the system (see Section 4.0). The collapsed levels were also computed for the various components, including the power channel. The actual two-phase level was calculated in the power channel to establish the fluid coverage of the heater bundle during the test.

This section provides an analysis of the test data from Matrix Tests SB01 and SB18. A discussion of each test is provided along with a set of standard plots that quantify the performance of the test. Additional plots are included to aid in characterizing the phenomena observed during each test.

Matrix Tests SB01 and SB18 are both 2-in. cold-leg breaks, with the break located at the bottom of cold leg-3 (CL-3). Matrix Test SB18 was a repeat test of Matrix Test SB01 performed to confirm the behavior of the system and to evaluate the repeatability of test results.

5.1 Analysis of Matrix Test SB01

Matrix Test SB01 (OSU Test U0001) modeled a 2-in. cold-leg break LOCA with LTC and without operation of the nonsafety-related systems. The break was located at the bottom of CL-3 on the core makeup tank side of the facility of one of the ADS-4 lines.

The analysis of Matrix Test SB01 is divided into three sections:

- Facility performance
- Short-term transient
- Long-term transient

The facility performance (Subsection 5.1.1) describes the overall response of the system throughout the test. The short-term transient portion (Subsection 5.1.2) provides a discussion of the system behavior from the start of the test through system depressurization and includes the initial system blowdown, the establishment of natural circulation, and the initial portion of IRWST injection cooling. The long-term transient portion (Subsection 5.1.3) discusses the behavior of the test between 8000 seconds and the end of the test and includes the completion of IRWST injection and the establishment of sump injection. The refill and subsequent recirculation of the core makeup tank (CMT) appears as a separate discussion in Subsection 6.1.1. The period between SBLOCA initiation and LTC is not discussed specifically, since the system behaves in a stable manner.

5.1.1 Facility Performance

A flow nozzle simulating one line of flow was installed in the ADS 4-1 line HL-1 to the ADS 4-1 separator) to provide the single-failure simulation. A flow nozzle simulating two lines of flow was installed in the ADS 4-2 line (HL-2 to the ADS 4-2 separator). Additionally, flow nozzles simulating two ADS 1-3 pairs of valves were installed in the ADS 1-3 inlet lines.

The reactor heater control decay algorithm maintained maximum reactor heater power output for 140 seconds, and then power was programmed to begin to decay to simulate the total post-trip energy input of the AP600 nuclear fuel. This test was performed with reactor heater rod HTR-C2-317 removed and replaced with a dummy rod.

Facility performance is divided into separate discussions of the five phases of the test: blowdown, natural circulation, ADS, IRWST injection, and sump injection. The overall performance of the 30,000-second test is shown in Figures 5.1.1-1, 5.1.1-2, and 5.1.1-3. Figure 5.1.1-1 shows the pressurizer pressure throughout the test with the various phases and operating components indicated for each phase. The time scale is cut for clarity between 2000 and 12,000 seconds since there was no change in the operating mode during this period. Figure 5.1.1-2 shows the total injection flow rates into the DVI line from the various systems as a function of time. Figure 5.1.1-3 shows the calculated quantity of steam generated in the core throughout the test.

A comparison of Figures 5.1.1-1 and 5.1.1-2 shows that, as the primary system depressurized, a continuous flow of water into the reactor vessel was provided by the passive safety systems. The passive safety injection systems overlap so that, as one system drained or emptied, another provided flow into the simulated reactor vessel for continuous core cooling.

The flows were large enough that the simulated core exit temperature was saturated or subcooled for significant portions of the transient, and the core steam flow was less than the passive safety system injection flow (Figures 5.1.1-2 and 5.1.1-3). As the system transitioned into LTC, the water injected from the sump was hot since it originated in the primary system. The hotter sump water combined with the lower driving head during the sump injection resulted in continuous steam generation in the heater rod bundle (Figure 5.1.1-3) after 14,900 seconds. This steam was then vented primarily through the ADS-4 valves.

5.1.1.1 Blowdown Phase

The blowdown phase corresponds to the first 80 seconds of Matrix Test SB01 (Figure 5.1.1-1). The test was initiated (0 time) by opening the break valve located at the bottom of CL-3 and was completed when steam pressure reached the steam generator (SG) safety valve setpoint. The hot leg of the reactor coolant system (RCS) was initially at 420°F and 370 psig prior to test initiation. The simulated S signal was generated at 0.5 seconds after the break signal and initiated the following actions.

In the first [ ]^{a,b,c} seconds, the SG safety relief setpoint pressure was raised to [ ]^{a,b,c} psig, and the reactor shifted to power (kW) control mode with a programmed power demand for 600-kW total power. The main feedwater pump tripped and the feedwater was isolated at [ ]^{a,b,c} seconds. The passive residual heat removal heat exchanger (PRHR HX) outlet valve and CMT discharge valves opened at [ ]^{a,b,c} seconds, and the reactor coolant pumps (RCPs) tripped at [ ]^{a,b,c} seconds after the break signal.

Forced flow continued through the PRHR HX and the CMTs until the RCPs stopped at about [ ]^{a,b,c} seconds, at which time flow changed to natural circulation flow. As the RCS depressurized and coolant escaped through the break, the pressurizer level decreased rapidly and steam formation began in the reactor vessel upper head. At about [ ]^{a,b,c} seconds, the level in the reactor vessel indicated the vessel was beginning to lose inventory as the vessel drained and some liquid flashed to steam. The upper plenum volume began to show a collapsed level decrease indicating that there was steam collecting in this volume at about [ ]^{a,b,c} seconds.

As primary system pressure reached near a steady-state condition, the system transitioned into the natural circulation phase once the pumps coasted down and the system reached the SG pressure setpoint at 335 psig at about [ ]^{a,b,c} seconds. During this period, there was initially liquid solid natural circulation in the PRHR and CMT systems. The CMTs provided recirculating flow to the reactor vessel while PRHR removed energy from the primary system.

5.1.1.2 Natural Circulation Phase

The upper head drained to two-thirds empty after [ ]^{a,b,c} seconds. The mass loss through the break caused a rapid decrease in pressurizer level and emptied the pressurizer at about [ ]^{a,b,c} seconds. The pressurizer surge line was completely emptied at about [ ]^{a,b,c} seconds. The primary system was initially at a pressure above the SG secondary-side pressure and continued to remove energy from the primary system. As the system continued to drain, the SG tubes started to drain at [ ]^{a,b,c} seconds, and the generators transitioned into a two-phase recirculation behavior. The cold legs developed a void fraction at about [ ]^{a,b,c} seconds at which time the CMT balance lines began to drain. CMT-1 and CMT-2 levels began to decrease, making the transition from recirculation to draindown at about [ ]^{a,b,c} respectively, and the injection flow from the CMTs increased (Figure 5.1-2). At about [ ]^{a,b,c} seconds, a condensation/depressurization event took place in CMT-1, as indicated by a rapid refill of the CMT-1 balance line as steam from the balance line was condensed in the CMT. Water from the cold leg was drawn up the balance line into the CMT as the balance line filled.

As the system continued to drain, the hot-leg level began to decrease at about [ ]^{a,b,c} seconds, and the steam generation reached its maximum at 270 seconds (0.54 lbm/sec., Figure 5.1-3). The U-tubes of both SGs were completely empty by about [ ]^{a,b,c} seconds and became superheated at about 360 seconds. The horizontal sections of the hot legs started to drain at about [ ]^{a,b,c} seconds. The hot legs remained at saturation temperature and never superheated, even though they

were partially or completely empty due to a small flow of saturated steam from the reactor heater bundle to the SGs.

The collapsed liquid level inside the reactor pressure vessel reached a near-term minimum valve at [ ]^{a,b,c} seconds but the core remained covered with a two-phase mixture during this period. The maximum steam generation rate shown in Figure 5.1-3, also occurred at this time as the flow from the CMT was decreasing.

When the RCS depressurized to about [ ]^{a,b,c} psig at about [ ]^{a,b,c} seconds, accumulator injection into the DVI line began (Figures 5.1-1 and 5.1-2). At [ ]^{a,b,c} seconds, CMT-1 reached the ADS-1 setpoint, and the ADS-1 valve opened, to initiate ADS blowdown.

5.1.1.3 ADS Phase

The ADS flow path, in conjunction with the break, caused RCS pressure to decrease at a more rapid rate, redistributing the mass inventory of the system. The opening of the ADS-1 valve resulted in two-phase flow going through the pressurizer to the ADS 1-3 separator and into the IRWST through the sparger. The opening of the ADS-1 valve, followed by the ADS-2 valve about [ ]^{a,b,c} minute later, caused an increase in the rate of RCS depressurization. As the different ADS stages opened, the primary vent path shifted from the cold-leg break to the ADS valves through the pressurizer.

The accumulators started discharging into the DVI line, which reduced CMT-1 injection flow to zero over the following [ ]^{a,b,c} seconds and CMT-2 injection flow to less than [ ]^{a,b,c} gpm over the following [ ]^{a,b,c} seconds by closing the CMT discharge line check valves until the accumulators were almost empty and depressurized. With the accumulators at their maximum injection rate, the RCS refilled and the surge line and pressurizer began to reflood at about [ ]^{a,b,c} seconds, and the pressurizer attained its maximum level at [ ]^{a,b,c} seconds. Once the accumulators were empty, the pressurizer and surge line drained back down and were completely empty at [ ]^{a,b,c} seconds.

The pressurizer was slightly subcooled at about [ ]^{a,b,c} seconds and remained subcooled until primary sump injection began, then increased to saturation temperature. The pressurizer remained at saturation temperature until about [ ]^{a,b,c} seconds when the temperature began to rise into the superheated range.

When RCS pressure decreased to [ ]^{a,b,c} psig at about [ ]^{a,b,c} seconds, the two IRWST injection valves automatically opened, but IRWST injection could not occur until RCS pressure decreased to near atmospheric. As ACC-1 and ACC-2 completed injection at [ ]^{a,b,c} and [ ]^{a,b,c} seconds, CMT-2 injection flow started to increase at [ ]^{a,b,c} seconds, and CMT-1 injection flow started to increase at [ ]^{a,b,c} seconds. About 50 percent of the nitrogen gas inventory used to pressurize the accumulator was injected into the DVI lines, momentarily cooling the injection lines. The nitrogen caused a momentary decrease in DVI-1 flow of about [ ]^{a,b,c} gpm and a decrease in ACC-1 outlet temperature of

about [ ]^{a,b,c} at [ ]^{a,b,c} seconds. On the ACC-2 side, there was no indicated change in DVI-2 flow, although the ACC-2 outlet temperature decreased [ ]^{a,b,c} at [ ]^{a,b,c} seconds.

During the accumulator injection period, at about [ ]^{a,b,c} seconds, there was sufficient injection of subcooled liquid to suppress boiling in the core region. The downcomer was filled with subcooled liquid which resulted in the collapse of the superheated steam bubble in the upper portion of the reactor vessel downcomer annulus. As pressure decreased in this region, the downcomer fluid accelerated upward and impacted on the bottom of the core barrel flange where the core bypass holes are located. The impact of the downcomer liquid on the solid surface of the core barrel flange was heard during the test.

During accumulator injection, PRHR flow decreased to near zero (<0.2 lb/sec.) and the PRHR level decreased. The majority of the nitrogen was discharged into the DVI at about [ ]^{a,b,c} seconds, respectively with small subsequent periodic outflows marked by spikes in the DVI line flow. The PRHR HX inlet temperature became subcooled while the ADS-4 valves opened at [ ]^{a,b,c} seconds and over the next [ ]^{a,b,c} seconds dropped to and paralleled the outlet temperature. Again, this is an indication that there was no flow through the PRHR HX during this time frame. From [ ]^{a,b,c} seconds, both DVI nozzle temperatures increased from essentially ambient conditions to as high as [ ]^{a,b,c} °F and then returned to ambient condition. The temperature increase was caused by two factors. First, there was rapid heating of the remaining water injected from the CMTs. Second, the reactor vessel downcomer level was at the DVI nozzle level during this period, possibly partially uncovering the nozzles. The temperature transient was terminated when IRWST injection began refilling the reactor vessel at about [ ]^{a,b,c} seconds, and temperatures returned to ambient conditions when the CMTs were empty, terminating hot liquid injection.

Steam generation in the reactor vessel was reestablished at about [ ]^{a,b,c} seconds and the reactor vessel inventory began to decrease. At [ ]^{a,b,c} seconds, the ADS 4-1 and ADS 4-2 valves opened automatically when the CMT-1 level reached its low-low level setpoint. ADS-4 actuation started a decline in RCS inventory that could not be overcome until IRWST injection began. There is initially too much mass in the system to be vented through ADS-4 before IRWST injection can occur. CMT-1 and CMT-2 were completely empty at [ ]^{a,b,c} seconds, respectively.

The collapsed reactor vessel level reached a minimum value of about [ ]^{a,b,c} in. at [ ]^{a,b,c} seconds. Although this level is below the top of the heater rod heated length, the actual level of the top of the two-phase mixture is much higher, as shown in the behavior of the core outlet thermocouples (Figure 5.1.1-4), which do not exceed saturation temperatures.

At about [ ]^{a,b,c} seconds, the RCS was drained sufficiently that system pressure decreased to about [ ]^{a,b,c} psig, which was sufficiently low that the IRWST static head was greater than RCS pressure, and IRWST injection began.

5.1.1.4 IRWST Injection Phase

IRWST injection was split between the two DVI lines beginning at [ ]^{a,b,c} seconds and continually diminished (Figure 5.1-2) as the differential head between the IRWST and the RCS decreased with drainage of the IRWST. IRWST injection was sufficient for the primary system to refill. The pressurizer and pressurizer surge line emptied a second time at about [ ]^{a,b,c} seconds, respectively.

When the pressurizer had a liquid level, ADS 1-3 separator and sparger pressure became negative by as much as [ ]^{a,b,c} psig. These values remained negative from [ ]^{a,b,c} seconds as steam trapped in the ADS lines was condensed in the IRWST. The negative pressure was broken as the level in the IRWST decreased below the sparger nozzles. No vacuum breaker was installed on the sparger line inside the IRWST for this test. A vacuum breaker is included in the AP600 design, and this OSU test response is not typical of the AP600. The surge line then began to reflood almost immediately at [ ]^{a,b,c} seconds and the pressurizer at about [ ]^{a,b,c} seconds. The reflood was caused by RCS levels increasing above the reactor vessel nozzles because IRWST injection exceeded the inventory losses and the condensation in the ADS 1-3 lines. The maximum pressurizer level attained was about [ ]^{a,b,c} in. at [ ]^{a,b,c} seconds, but it immediately began to decrease. The pressurizer was empty at [ ]^{a,b,c} seconds and remained empty for the remainder of the test. The surge line stayed full until [ ]^{a,b,c} seconds when the level decreased to about [ ]^{a,b,c} in. and remained there until [ ]^{a,b,c} seconds. The level again decreased to about [ ]^{a,b,c} in. at [ ]^{a,b,c} seconds and oscillated between about [ ]^{a,b,c} in. for the remainder of the test.

Both CMT balance lines began to refill at about [ ]^{a,b,c} seconds when the IRWST injection increased the reactor vessel level sufficiently covering and refilling the cold legs. At about [ ]^{a,b,c} seconds, when the CMT-2 balance line had completely refilled, CMT-2 began to rapidly refill and reached the [ ]^{a,b,c} in. level (about two-thirds full) at about [ ]^{a,b,c} seconds. The CMT refill is discussed in more detail in Section 6. After the CMTs were partially refilled, there was no injection flow from the CMTs because the higher static head of the IRWST held the CMT discharge line check valves closed.

Steam generation started again at about 8600 seconds and continued for the remainder of the test (Figure 5.1-3). CMT-1 and CMT-2 remained at essentially constant levels for several [ ]^{a,b,c} seconds and then began slow draindowns at about [ ]^{a,b,c} seconds, respectively. The draindown for both CMTs was slow and did not occur until the IRWST relative level was [ ]^{a,b,c} in. below that of the CMTs. Data indicate that the CMTs drained for a while, and then the differential head between the IRWST and the CMTs again closed the CMT discharge check valves, terminating draining until the differential shifted the other way and draining recommenced. Both CMTs were completely empty at about [ ]^{a,b,c} seconds, which coincides closely with the primary sump injection valve opening at [ ]^{a,b,c} seconds. A possible correlation is that when the primary sump valve opened, the IRWST had just reached its minimum level of about [ ]^{a,b,c} in., which is about [ ]^{a,b,c} in. below the instrumented level for the CMTs, and that there was still a slight negative pressure remaining in the CMTs. Also, when the primary sump injection valves opened, there was a short

period in which the IRWST and primary sump levels equalized, causing a decrease in RCS fluid levels and resulting in a rapid drop in CMT levels from about [ ]^{a,b,c} in.

Starting at about [ ]^{a,b,c} seconds, there was a series of pressure, level, and flow oscillations that occurred throughout the components of the facility lasting until about [ ]^{a,b,c} seconds. These oscillations will be discussed in detail in Section 6.

At [ ]^{a,b,c} seconds, the PRHR HX inlet temperature instantly increased from [ ]^{a,b,c} °F to saturation temperature. The temperatures increased at about [ ]^{a,b,c} seconds after pressure, level, and flow oscillations began in the facility and was possibly caused by the inlet line burping and once again allowing the line to fill with saturated steam. Following the burp, all of the PRHR HX temperatures began to slowly approach saturation.

The break separator level began to increase at the same rate as the primary sump at about [ ]^{a,b,c} seconds. This increase occurred when the sump level reached the height of the break separator loop seal. As a result of this increase, the break separator level reached the height of the break in CL-3, causing break flow to reverse and flow from the break separator into the RCS through the break at about [ ]^{a,b,c} seconds. Break flow then remained essentially zero or slightly negative throughout the rest of the test.

5.1.1.5 Sump Injection Phase

Primary sump injection (Figure 5.1-2) began through the check valves around the sump injection valves at about [ ]^{a,b,c} seconds when primary sump and IRWST levels were essentially equal. At [ ]^{a,b,c} seconds, the primary sump injection valves automatically opened when the IRWST reached its low-low level setpoint of [ ]^{a,b,c} in.

In the LTC mode of operation, system inventory was lost through the ADS 4-1 and ADS 4-2 valves to the primary sump. System inventory was made up through primary sump and IRWST injection through the DVI lines and some small flow from the primary sump through the break separator and into the break. The driving force for this flow was the difference between the liquid head in the downcomer and the corresponding head in the simulated core. The two-phase mixture produced in the core flowed out through the hot legs and ADS-4 to the primary sump, and the somewhat cooler fluid in the sump returned from the bottom of the sump to the reactor vessel downcomer via the DVI lines.

When sump injection began, the reactor vessel downcomer fluid temperatures rapidly increased to the sump flow injection temperature. The core steam generation increased (Figure 5.1-3) due to hotter sump fluid. When the primary sump injection valves opened, the DVI flow decreased, and the sump and IRWST levels equalized. During the reduced DVI flow period, there was an upward spike in reactor downcomer temperatures. The upper downcomer fluid temperature, indicated by thermocouples located above the DVI nozzle elevation, increased to saturation at this time and remained at saturation

for the rest of the test because the reactor vessel collapsed level was at the DVI nozzles. Figure 5.1-3 shows a corresponding increase in steam generation rate.

Overflow from the primary sump to the secondary sump started at about [ ]^{a,b,c} seconds. When primary sump injection started through the check valves, flowing around the sump injection valve lines, IRWST injection from each line was about [ ]^{a,b,c} lb./sec. and another [ ]^{a,b,c} lb./sec. from each sump line to each DVI line. With the opening of the primary sump valves [ ]^{a,b,c}, injection flow increased to approximately [ ]^{a,b,c} lb./sec. through each DVI line. About one-third of the flow from sump-1 was diverted back into the IRWST with the remainder flowing to the DVI nozzle due to the smaller pressure drop in the IRWST to sump line (2.5-in. diameter versus 1.5-in. diameter for sump-2). One-fourth of DVI-2 flow was provided by flow from the IRWST and the remainder from the sump-2 line.

The PRHR HX outlet temperature remained subcooled in the range of [ ]^{a,b,c} °F during most of the test, but after sump injection, it began to rise and was just reaching saturation temperature at the end of the test. The PRHR HX was inactive during this phase, since the IRWST had drained.

TABLE 5.1.1-1 OSU TEST ANALYSIS PLOT PACKAGE FOR SECTION 5.1.1				
Plot No.	**Component**	**Variables**	**Units**	**Description**
1	Pressurizer	CPT-604	psia	System pressure and event history
2	Water injection	WWTDVI1+WWTDVI2, WOUTACC1+WOUTACC2, WWTIRWI1+WWTIRWI2, WWTSMPIT	lbm/sec.	Total of CMT, accumulator, IRWST, and sump injection flows
3	Reactor vessel	RPVRXV	lbm/sec.	Steam generation in reactor vessel
4	Reactor vessel	T08RPV, TSAT	°F	Reactor vessel outlet temperature

THE PLOTS (1-4) LISTED IN TABLE 5.1.1 ARE NOT INCLUDED
IN THIS NONPROPRIETARY DOCUMENT

5.1.2 Short-Term Transient

For the 2-in., cold-leg break, Matrix Test SB01, the short-term transient covered the first 3000 seconds. As can be seen from Figures 5.1.2-1 and 5.1.2-2, this period included full depressurization of the facility through all four stages of the ADS together with CMT and accumulator injection plus the initial stages of IRWST injection. The mass and energy distribution for this phase of the transient is discussed here based on the plot package detailed in Table 5.1.2-1. These plots concentrate on the primary system including the accumulators, CMTs, IRWST, sumps, and flow from the primary system via the ADS, break, and IRWST overflow.

5.1.2.1 Reactor Pressure Vessel and Downcomer Mass Distribution

For the short-term transient, the most important criteria was the maintenance of sufficient core inventory to supply adequate cooling of the heated rods. Figure 5.1.2-57 shows that there were no significant excursions in heated rod temperatures and, therefore, sufficient core inventory was maintained through this phase of the transient to remove the decay heat from the rods. However, for significant portions of the transient a two-phase mixture is present in the core and upper plenum regions. The following discussion tracks the variation in water level and mass throughout the reactor vessel and downcomer.

The total fluid mass in the reactor pressure vessel is shown in Figure 5.1.2-40. The initial vessel inventory is [ ]^{a,b,c} lbm. During the course of the short-term transient, the vessel inventory experiences two mass minimums: [ ]^{a,b,c} lbm before accumulator injection and [ ]^{a,b,c} lbm before IRWST injection. Steam generation was near maximum at these times (Figure 5.1.2-55). By the end of the short-term transient, vessel inventory recovered to a steady 515 lbm. Similar variations were seen in the core fluid mass and water level shown in Figures 5.1.2-44 and 5.1.2-45. The minimum core level occurred before IRWST injection. It can be seen from Figure 5.1.2-45 that during this phase of the transient, the collapsed liquid level dropped to [ ]^{a,b,c} in. below the top of the heated rod length. By the end of the short-term transient, the effect of IRWST injection ended all core boiling (Figure 5.1.2-55), and the core was again water-solid.

It was noticed in the analysis of the LOCA simulations on the SPES facility[3] that following the pump trip there were short-period oscillations in primary system flow, temperature, and pressure. A small number of oscillations were also observed in the OSU test response after the end of the initial blowdown (see, for example, the pressure response in Figure 5.1.2-1 and the reactor vessel mass in Figure 5.1.2-40). In the SPES tests, the oscillations were clearly driven by power-to-flow mismatches in the core due to high core power levels, which were needed in SPES to compensate for high ambient losses. The apparent short-term oscillations observed in the OSU results are believed to be a result of pressure oscillations following the initial blowdown.

Fluid mass in the core region is shown in Figure 5.1.2-44. Once again, the two minimums occur prior to accumulator injection and prior to IRWST injection. The minimum core inventory is [ ]^{a,b,c} lbm.

The collapsed liquid level in the upper plenum region spanned by LDP-138 and the associated fluid mass are shown in Figures 5.1.2-49 and 5.1.2-48. It can be seen that, during the period before accumulator injection, the collapsed liquid level in the upper plenum dropped below the hot-leg elevation. During accumulator injection, the steam bubble in the upper plenum partially condensed and the water level briefly rose above the hot legs. Following the end of accumulator injection, flow from the CMTs was not sufficient to maintain the upper plenum level, and this region completely drained of water. IRWST injection caused the upper plenum to refill, and this region became water-solid again at approximately [ ]^{a,b,c} seconds.

The fluid mass and collapsed liquid level for the head region are given in Figures 5.1.2-50 and 5.1.2-51. During the first [ ]^{a,b,c} seconds, the head inventory reaches a minimum of [ ]^{a,b,c} lbm of water. Following the end of accumulator injection, the head region drained. Both accumulator and IRWST injection were sufficient to supply a level of water in the head.

The mass of fluid and collapsed liquid level in the reactor vessel downcomer are shown in Figures 5.1.2-41 and 5.1.2-42. During the blowdown phase of the transient, the level dropped to the elevation of the cold legs. This elevation was maintained until the cold legs were fully drained. Following this point, the collapsed level remained between the DVI and hot-leg elevations until IRWST injection once again raises the level above the cold legs and cold leg refill commences.

5.1.2.2 Loop Mass Distribution

For this discussion the loop was considered to consist of the hot- and cold-leg pipe work, the SG primary side, and the pressurizer plus surge line.

The total fluid mass and water level for the pressurizer are shown in Figures 5.1.2-34 and 5.1.2-35. During the blowdown phase of the transient ([ ]^{a,b,c} seconds), the pressurizer drained rapidly, becoming completely empty of water at about [ ]^{a,b,c} seconds. The pressurizer remained empty until ADS-1 actuation at [ ]^{a,b,c} seconds. At this time, water was drawn back into the pressurizer as steam and water flowed out of the ADS. A fluid inventory of over [ ]^{a,b,c} lbm was maintained until ADS-4 actuation at [ ]^{a,b,c} seconds. This caused an initial outsurge through the surge line, followed by a more gradual draining of the pressurizer as mass flowed out of the hot legs via the ADS-4 valves The pressurizer fully drained at [ ]^{a,b,c} seconds and remained empty for the remainder of the transient.

Mass data for the SG U-tubes and their associated inlet and outlet plena are reproduced in Figures 5.1.2-32 and 5.1.2-31. The SG tubes gradually drained until ADS actuation when all the tubes and plena were empty of water. The SG on the broken loop (loop 1) drained before that on loop 2. Any flow through the SGs ceased once the tubes drained and steam trapped the U-tubes became superheated. Once the SG tubes drained, natural circulation around the primary loop circuit ceased. The SG U-tubes remained empty for the remainder of the short-term transient.

The mass of water and vapor in the hot legs is reproduced in Figures 5.1.2-58 and 5.1.2-59. The water mass calculated for HL-1 is not considered valid for this test. The hot legs maintained their water inventory until [ ]^{a,b,c} seconds into the transient when they started to drain (Figure 5.1.2-58). The hot legs completely drained within [ ]^{a,b,c} seconds. Actuation of ADS-1 caused a rapid increase in void fraction in both hot legs. A larger void fraction was maintained in HL-1 as steam was preferentially removed from HL-2 by PRHR. Figure 5.1.2-59 reveals that, at around [ ]^{a,b,c} seconds, the small amount of steam remaining in HL-2 was removed, and the water level in that hot leg increased as a result of condensation in the PRHR HX drawing a vacuum and raising the level on loop 2.

The liquid and vapor mass for the four cold legs appear in Figures 5.1.2-60 and 5.1.2-61. Following initial blowdown, all four cold legs became two-phase, although there was a greater void fraction in CL-1 and CL-4 compared with CL-2 and CL-3 (Figure 5.1.2-61). The mass variation in all four cold legs appears very similar. The mass variations were derived from levels in the reactor vessel downcomer because the level instruments on the cold legs are unreliable. All the cold legs were completely drained after ADS actuation and refilled at [ ]^{a,b,c} seconds when flow from the IRWST refilled the reactor vessel downcomer to the level of the cold legs (Figure 5.1.2-42). The cold legs did not drain uniformly, but rather, CL-3 (with the break) drained first, followed by CL-1 with CL-2 and CL-4 delayed. Figure 5.1.2-31 shows that the SG outlet plenum on loop 1 drained at about [ ]^{a,b,c} seconds before that on loop 2, confirming the expected asymmetry in cold-leg behavior.

5.1.2.3 Mass Injected to the Primary System

The CMTs transitioned from a recirculation to a mass injection mode at approximately 100 seconds when the cold leg started to drain. Draindown of the CMTs continued until the CMT check valves were closed by flow from the accumulators. CMT draindown restarted at the end of accumulator injection, continuing until IRWST injection began (Figures 5.1.2-5 and 5.1.2-6).

The accumulators drained about 10 seconds before activation of the ADS. The accumulators started discharging into the DVI line when the system pressure dropped below the pressure in each accumulator. Accumulator injection began at approximately [ ]^{a,b,c} seconds and continued until the accumulator emptied at approximately [ ]^{a,b,c} seconds (Figure 5.1.2-23). Complete discharge from the accumulators was indicated by a sharp decrease in the temperature of the fluid exiting each accumulator due to the discharge of expansion-cooled nitrogen cover gas, which was released into the primary system. Once discharged, the accumulators could not be refilled because of a check valve in the line. Flow from the CMTs was significantly reduced during the discharge of the accumulators and increased again once accumulator discharge was completed.

It should be noted that, for Matrix Test SB01, flow from accumulator was not measured correctly. The integrated mass flow has, however, been included in the mass balance as the total cutflow only in error by a small circuit.

The IRWST injection valves opened when the reactor vessel pressure low-low level setpoint was reached. Injection flow only started when the reactor vessel pressure became less than the static head from the IRWST tank. Figure 5.1.2-16 shows that the IRWST injection began at approximately [ ]^{a,b,c} seconds after CMT flow ceased. IRWST flow gradually increased to a peak value of [ ] lb/sec. ([1.38] lbm/sec. per injection line) at [ ]^{a,b,c} seconds before gradually decreasing.

5.1.2.4 Mass Ejected from the Primary System

At time zero in the transient, a 2-in. break was initiated at the bottom of CL-3. The mass flow rate from the primary system through the break is shown in Figures 5.1.2-6 and 5.1.2-68. For the first [ ]^{a,b,c} seconds following the break, [ ]^{a,b,c} lbm of steam and water left the primary system via the break (Figure 5.1.2-62). During this period, the primary system depressurized to around 300 psi (Figure 5.1.2-1). By the onset of ADS actuation, the cold legs drained, and there was almost no water flow out of the break. Between [ ]^{a,b,c} seconds, ADS 1-3 activated and the system depressurized rapidly. Break flow significantly decreased once the ADS activated, since the ADS valve area was significantly larger than the break. At around [ ]^{a,b,c} seconds, ADS-4 was initiated, and the primary circuit depressurized until IRWST injection commenced at [ ]^{a,b,c} seconds.

Actuation of ADS 1-3 rapidly terminated the flow of steam from the break, although this was replaced by steam flow through the ADS 1-3 valves for the next [ ]^{a,b,c} seconds (Figure 5.1.2-63). This steam flow was accompanied by an outflow of water from ADS 1-3 at a peak rate of over 4 lbm/sec. (Figure 5.1.2-66). After [ ]^{a,b,c} seconds into the accident simulation, the mass flowing through ADS 1-3 was composed almost entirely of water. The rate of flow through the ADS continued at a gradually reducing rate until [ ]^{a,b,c} seconds when the ADS-4 valves opened, causing flow through ADS 1-3 to terminate and be replaced by flow through the lower resistance ADS-4 paths. For ADS 4-1, there was a near-steady water loss rate of [ ]^{a,b,c} lbm/sec. from the time of initiation. However, for ADS 4-2, there was an initial outsurge at [ ]^{a,b,c} lbm/sec. followed by a drop to near zero and an increase to over [ ]^{a,b,c} lbm/sec. (Figure 5.1.2-66).

The integrated mass flow out of the primary system via the ADS and the break are shown in Figures 5.1.2-62 to 5.1.2-64. During the first [ ]^{a,b,c} seconds of the transient, over [ ]^{a,b,c} lbm of water left the primary circuit. Of this, the [ ]^{a,b,c} lbm flowing through ADS 1-3 was deposited in the IRWST. The [ ]^{a,b,c} lbm leaving the ADS-4 system and the liquid part of the [ ]^{a,b,c} lbm flowing through the break were added to the liquid overflow from the IRWST and deposited nearly [ ]^{a,b,c} lbm of water into the primary sump (Figure 5.1.2-28). By the end of the short-term transient, the water level in the primary sump reached nearly [ ]^{a,b,c} in. (Figure 5.1.2-29).

At [ ]^{a,b,c} seconds into the transient, the cold legs refilled enough to allow a restart of approximately 0.4 lbm/sec. of water flow through the break, so that the total rate of water loss from the primary system to the sump was approximately 2.5 lbm/sec. At this time, the rate of gain of reactor vessel mass through the DVI lines was approximately 2.5 lbm/sec.

5.1.2.5 Mass Balance

Figure 5.1.2-70 presents the variation in the total system inventory during the short-term transient. Following the initiation of the break, there was an increase in system mass of approximately [ ]^{a,b,c} lbm. By the end of the short-term transient, the system inventory decreased by approximately [ ]^{a,b,c} lbm compared with the post-break value. During this period of the transient, about [ ]^{a,b,c} lbm of water was lost from the primary system as steam (Figure 5.1.2-73).

In addition to the overall reduction in system inventory, some marked reductions and recoveries (dips) were observed. There was a general decrease in system inventory following the initiation of ADS 1-3 until the start of ADS-4 venting (around [ ]^{a,b,c} seconds). Two other marked dips were also observed at around [ ]^{a,b,c} seconds. These two dips resulted from corresponding changes in the primary sump inventory, which have been observed in the level data from which the masses were calculated. The readings on the load cells for the sump did not show corresponding dips, and there were no indications of flow out of the sump at this time. It is, therefore, believed that these resulted from an increase in pressure above the sump water level and lead to an artificially low differential pressure of the sump and a reduced level indication. The necessary pressure increase could have resulted from condensation in the exhaust line causing a build up in steam until the pressure was great enough to drive the venting through the check valve.

A mass balance analysis was been performed on the primary system. Figure 5.1.2-71 plots the measured primary system mass determined by summing the contributions from the reactor vessel, downcomer, hot and cold legs, SG primary side, pressurizer, and surge line plus the PRHR HX. The second curve on Figure 5.1.2-71 provides an alternative primary system mass determined from the mass balance, that is given by:

$$M'_{prim}(t) = M_{prim}(0) + M_{in}(t) - M_{out}(t)$$

where:

$M_{prim}(0)$	=	Measured primary system mass at the start of transient
$M_{in}(t)$	=	Total integrated mass injected from all sources (i.e., accumulators, CMT, IRWST, and sumps) to time t
$M_{out}(t)$	=	Mass lost from primary system to time t via CMT balance lines, ADS 1-3, ADS-4, and break

The difference in the two primary system mass curves is shown in Figure 5.1.2-72 as the mass balance error.

During the short-term transient, there was, in general, an overestimate of the mass in the primary system from the measured data of up to [ ]^{a,b,c} lbm relative to that calculated from the mass balance, although there was an underestimate following ADS 1-3 initiation. There are two main contributions to

this excess mass. First, the measured primary system inventory did not include all of the pipework in the system, and there was approximately [ ]^{a,b,c} lbm of mass missing from the initial inventory. This mass was deposited in and lost from the measured system as pipes drained and refilled. Some of the additional mass was subsequently lost via one of the leakage paths. Second, the instrumentation on the hot legs is believed to have given erroneous level measurements during certain portions of the transient. It can be seen from Figure 5.1.2-58 that, for this test, only one hot leg appears to drain, and this contributes an overestimate of [ ]^{a,b,c} lbm. By the end of the short-term transient, the apparent mass-balance error was approximately [ ]^{a,b,c} lbm.

Figure 5.1.2-73 shows the total integrated mass flow from and to the primary system, together with the water inventory remaining in the sources of cooling water. It can be seen that, during the short-term transient, there was a net loss of water from the primary system of approximately [ ]^{a,b,c} lbm of which only a small quantity was deposited in the sources. As noted previously, of the lost primary system inventory, [ ]^{a,b,c} lbm was lost as steam. The rest has been added to the water stored in the ADS and break separators.

5.1.2.6 Pressure Decay

Figure 5.1.2-1 shows the primary system pressure during the test. Throughout the LOCA portion of this test, the pressure was controlled by the saturation pressure of the hottest fluid in the primary system. At initiation of the break, the controlling fluid volume was the pressurizer and surge line; however, within the first [ ]^{a,b,c} seconds (after the initial blowdown phase), this shifted to the reactor vessel. Figure 5.1.2-3 shows that the temperature of the upper plenum was equal to the saturation temperature corresponding to the primary system pressure measured in the upper head during the natural circulation phase and into the ADS phase. The pressure stabilized at the saturation pressure for the upper plenum and then continued a slow pressure decrease responding to the cooling caused by CMT injection. Figure 5.1.2-1 shows an increase in the pressure decay rate that occurred at approximately [ ]^{a,b,c} seconds when the CMTs transitioned from natural circulation injection to draindown injection, which essentially doubled the injection rate of cold water into the DVI line. The higher injection rate resulted in a more rapid temperature drop in the upper plenum (core exit in Figure 5.1.2-3), which was reflected in a more rapid pressure decay. With the actuation of ADS-1 at approximately [ ]^{a,b,c} seconds, the pressure dropped rapidly due to the increased rate of mass ejected from the system, and the increased flow of cold water into the downcomer and the core (Figure 5.1.2-63). This continued to reduce the power channel inlet plenum temperature and subcool the rods in the core due to the higher flow. Since the reactor vessel outlet plenum became subcooled at about [ ]^{a,b,c} seconds, the hottest fluid in the system was in the pressurizer, the cold legs, and the CMTs, and the pressure was partially supported by the flashing of fluid in one or several of these locations. When accumulator discharge ended at between [ ]^{a,b,c} seconds, the reactor vessel temperature again increased to the saturation temperature and took control of the system pressure for the remainder of the LOCA phase.

5.1.2.7 Energy Inventory

Heat removal from the reactor core follows a sequence similar to pressure decay for SB LOCA tests. Before the reactor trips, nearly all the energy generated in the core is removed by the SGs and out of the break with a small fraction lost to surrounding heat sinks. When the reactor trips, the primary system pumps trip, and flow through the SG tubes is sharply reduced. Coupled with the isolation of the SG secondary side, the effect is to significantly reduce heat removal from the SGs. At that time, the PRHR HX isolation valves open, and energy is removed to the IRWST as well as out of the break.

As the system drains, primary system pressure is reduced, and the sensible heat of the coolant and metal add to the core heat load. The CMTs start to drain, and the ADS is activated. At that time, heat removal is accomplished through ADS flow, and the PRHR HX becomes less effective. Finally, ADS-4 is actuated, the primary system is completely depressurized, and the IRWST is actuated. The LOCA phase of the test is then completed.

The behavior of the components involved in the energy removal is discussed below.

Core

The power output of the core is shown in Figure 5.1.2-2. After reactor trip, the core power is representative of decay heat levels expected in the AP600 core. Flow through the core is shown in Figure 5.1.2-56 and the steam generation rate is given in Figure 5.1.2-55. As discussed in Subsection 4.11, the steam penetration rate has been calculated by two methods, the T_{sat} method and the DVI line flow method.

Figures 5.1.2-53, 5.1.2-54, and 5.1.2-55 reproduce the saturation line elevation power split above the saturation elevation and steam generation rates from the two methods. It can be seen that both methods give similar predictions. It should be noted that neither method gives valid predictions before [ ]^{a,b,c} seconds because of flow oscillations during natural circulation in the primary system.

Both methods for calculating the steam generation predict that the maximum steam generation rate during the LOCA phase will occur at approximately [ ]^{a,b,c} seconds, just prior to IRWST injection. The peak cladding temperature is shown in Figure 5.1.2-57 and indicates that the core is adequately cooled at all times during the test.

SG Heat Transfer

SGs remove most of the heat from the primary system during normal operation; however, heat transfer from the primary-to-secondary side is significantly reduced after the pumps trip. This is due to reduced flow in the tubes, which causes a sharp reduction in the tube-side heat transfer coefficient. In addition, the secondary side is isolated, which causes the temperature and pressure to remain high as primary-side pressure rapidly decreases.

PRHR Heat Transfer

PRHR is designed to remove heat from the primary system from the time when the SGs become thermally isolated due to the initiation of the ADS. One measure of the effectiveness of PRHR is the increase in the fluid internal energy in the IRWST, which serves as the heat sink for PRHR. Figure 5.1.2-20 shows the fluid internal energy in the IRWST during the first 3000 seconds of the test. PRHR began at about [ ]^{a,b,c} seconds when the SG heat removal ended. The heat removal rate was approximately [ ]^{a,b,c} Btu/sec. until [ ]^{a,b,c} seconds when ADS-1 activated. At that time, the heating rate in the IRWST increased to [ ]^{a,b,c} Btu/sec. due to steam condensing from ADS 1-3 and heating from PRHR. PRHR decreased when the accumulators discharged at about [ ]^{a,b,c} seconds as the core became subcooled.

ADS and Break

Energy removal from the ADS and break are shown in Figure 5.1.2-69. Fluid energy exiting the break increased at a constant rate until ADS-1 actuated. For ADS-1, ADS-2, and ADS-3, the energy removal occurred at a somewhat lower rate due to the reduced system pressure. When ADS-4 actuated, energy removal switched from ADS 1-3 to the larger flow path of ADS-4. The ADS effectively reduced the primary system pressure to allow gravity-injection flow from the IRWST. This flow sufficiently subcooled the primary system, ending core boiling, partially collapsing the steam bubble in the upper plenum, and bringing the system to near atmospheric pressure.

5.1.2.8 Energy Balance

Figure 5.1.2-74 shows all the energy components in the heat balance for the system during the LOCA phase (0 to 3000 sec.). Throughout the event, the heated rod bundle power was the dominant heat input to the system, and before the start of the event, the SGs provided the dominant heat removal. At the start of the event, the SG secondary side was isolated, and the RCPs tripped. During this period, heat removal by the SG was reduced as natural circulation flow occurred in the primary system. As the primary system depressurized, the pressure reached the secondary-side pressure, and heat transfer effectively ended.

The steam component of the break flow was lost from the control volume at the start of the event until ADS actuation. Heat loss via this path was nearly [ ]^{a,b,c} Btu/sec., which is far greater than the reactor decay power ([ ]^{a,b,c} Btu/sec.). The remaining energy lost through the break exhaust resulted from a decrease in the fluid internal energy as the primary system depressurized.

After ADS 1-3 actuated, the break flow effectively ended and ADS heat was deposited into the IRWST. Thus, the fluid internal energy in the control volume increased from this time until the end of the LOCA phase as the IRWST water temperature increased. Also at that time, the metal masses in the control volume lost energy as primary system temperatures decreased. This resulted in energy being lost at a rate of nearly [ ]^{a,b,c} Btu/sec. between [ ]^{a,b,c} seconds. After [ ]^{a,b,c} seconds, the

metal masses lost energy at a much lower rate, which is consistent with the primary system fluid temperature decay. Ambient losses were reduced from a maximum of 40 Btu/sec. at full power conditions to 20 Btu/sec. at the end of the LOCA phase.

A large increase was observed in the deficit between the rod bundle power and the various sources of energy dissipation from the control volume after the initiation of ADS 1-3, and again after the initiation of ADS-4 at approximately 1000 seconds. Steam exhaust included steam from the IRWST and the steam portion of the flow from ADS-4. However, little steam was measured by the vapor flow meters. As was discussed in the mass balance, it is likely that the small steam flow from these sources was not being measured by the vapor flow meters, adding to a deficit in the energy balance.

TABLE 5.1.2-1
OSU TEST ANALYSIS STANDARD PLOT PACKAGE FOR SECTION 5.1.2

Plot No.	Component	Variables	Units	Description
1	Pressurizer	CPT-604	psia	System pressure
2	RV	RVPWR	kW	Core power
3	RV	T01RV, T08RV, ST08RV	°F	Core inlet/outlet temperature, saturation temperature
4	Steam generator	CPT-201, CPT-204, CPT-301, CPT-302	psia	Primary and secondary pressures in SG
5	DVI-1	WWTDVIL1, WWTIRWI1, WOUTACC1, WWTIRWI3	lbm/sec.	Total flow in DVI-1 and individual components
6	DVI-2	WWTDVIL2, WWTIRWI2, WOUTACC2, WWTIRWI4	lbm/sec.	Total flow in DVI-2 and individual components
7	CMT	AMCMT1B, AMCMT2B	lbm	Fluid mass in CMTs (excludes balance lines)
8	CMT	CLDP-502, CLDP-507	in.	Collapsed liquid level in CMTs
9	CMT	MIWDVIL1, MIWDVIL2, MIWCLBL1, MIWCLBL2	lbm	Integrated mass into/out of CMTs
10	CMT	WWTDVIL1, WWTDVIL2	lbm/sec.	Flow out of CMTs
11	CMT	WWTCLBL1, WWTCLBL2	lbm/sec.	Flow into CMTs
12	CMT	CLDP-509, CLDP510	in.	Level CL-CMT balance lines
13	CMT	UCMT1, UCMT2	Btu	Fluid energy in CMTs
14	IRWST	IRWST	lbm	Mass of fluid in IRWST
15	IRWST	CLDP-701	in.	Collapsed liquid level in IRWST
16	IRWST	WWTIRWI1, WWTIRWI2	lbm/sec.	Flow from IRWST to DVI lines
17	IRWST	IRWSTOR	lbm/sec.	Overflow from IRWST to sump
18	IRWST	ADS13VR + ADS13LR	lbm/sec.	Total ADS flow into IRWST
19	IRWST	MIIRWI1, MIIRWI2, MIIRWIO	lbm	Integrated mass out of IRWST
20	IRWST	UIRWST	Btu	Fluid energy in IRWST
21	PRHR	CLDP-802	in.	Collapsed liquid level in PRHR HX

TABLE 5.1.2-1 (Continued)
OSU TEST ANALYSIS STANDARD PLOT PACKAGE FOR SECTION 5.1.2

Plot No.	Component	Variables	Units	Description
22	PRHR	WWOTPRHR	lbm/sec.	Measured outlet flow from PRHR tube
23	Accumulator	AMACC1, AMACC2	lbm	Mass of fluid in accumulators
24	Accumulator	CLDP-401, CLDP-402	in.	Collapsed liquid level in accumulators
25	Accumulator	WOUTACC1, WOUTACC2	lbm/sec.	Flow from accumulators
26	Accumulator	MOUTACC1, MOUTACC2	lbm	Integrated mass out of accumulators
27	Accumulator	UACC1, UACC2	Btu	Fluid energy in accumulators
28	Primary sump	AMPSMP	lbm	Primary sump mass
29	Primary sump	CLDP-901	in.	Primary sump level
30	Primary sump	UPSMP	Btu	Primary sump fluid energy
31	Steam generator	MSSGIP1, MSSGIP2, MSSGOP1, MSSGOP2	lbm	Mass of fluid in SG primary side inlet/outlet plena
32	Steam generator	MSSGHT1, MSSGHT2, MSSGCT1, MSSGCT2	lbm	Mass of fluid in SG primary side hot and cold tubes
34	Pressurizer	PZM	lbm	Fluid mass in pressurizer
35	Pressurizer	CLDP-601	in.	Collapsed liquid level in pressurizer
36	Pressurizer	UPZ	Btu	Fluid energy in pressurizer
37	Surge line	PLM	lbm	Fluid mass in surge line
38	Surge line	CLDP-602	in.	Collapsed liquid level in surge line
39	Surge line	UPSL	Btu	Fluid energy in surge line
40	RV	MWRVRV	lbm	Total fluid mass in reactor vessel
41	RV	DCM	lbm	Fluid mass in downcomer
42	RV	LDP01DC	in.	Collapsed liquid level in downcomer compared to various reference elevations
43	RV	WM01RV	lbm	Fluid mass in lower plenum
44	RV	MW03RV	lbm	Fluid mass in core region
45	RV	LDP03RV	in.	Collapsed liquid level in core
46	RV	RVXVFO		Core exit void fraction
47	RV	RVXRQO		Core exit quality
48	RV	MW06RV	lbm	Fluid mass in the upper plenum
49	RV	LDP06RV	in.	Collapsed liquid level in the upper plenum
50	RV	MW08RV	lbm	Fluid mass in the upper head
51	RV	LDP08RV	in.	Collapsed liquid level in the upper head
52	RV	URV	Btu	Total fluid energy in reactor vessel
53	RV	RVXE	ft	Level of Tsat line

TABLE 5.1.2-1 (Continued)
OSU TEST ANALYSIS STANDARD PLOT PACKAGE FOR SECTION 5.1.2

Plot No.	Component	Variables	Units	Description
54	RV	RVPab, RVPbl, RVPWR	kW	Heated rod power above and below Tsat level and total
55	RV	RVRXV	lbm/sec.	Core steam generation rate
56	RV	RVTMRI	lbm/sec.	Calculated core flow
57	RV		°F	Maximum clad temperature, saturation temperature and delta
58	Hot leg	MWHL1, MWHL2	lbm	Water mass in hot legs
59	Hot leg	MVHL1, MVHL2	lbm	Vapor mass in hot legs
60	Cold leg	CL1WMS, CL2WMS, CL3WMS, CL4WMS	lbm	Water mass in cold legs
61	Cold leg	CL1VMS, CL2VMS, CL3VMS, CL4VMS	lbm	Vapor mass in cold legs
62	ADS and break	BRKSTIR, ADS13TIR, ADS41TIR, ADS42TIR	lbm	Total discharged mass for ADS 1-3, ADS-4s, and break
63	ADS and break	BRKTIVF, AD13TIVF, AD41TIVF, AD42TIVF	lbm	Total integrated vapor flow for ADS and break
64	ADS and break	BRKTILF, AD13TILF, AD41TILF, AD42TILF	lbm	Total integrated liquid flow for ADS and break
65	ADS and break	ADS13SLR, ADS41SLR, ADS42SLR	lbm/sec.	Steam flow out ADS 1-3 and ADS-4
66	ADS and break	ADS13SLR, ADS41SLR, ADS42SLR	lbm/sec.	Liquid flow out ADS 1-3 and ADS-4
67	ADS and break	BRKSSLR	lbm/sec.	Steam flow out of break
68	ADS and break	BRKSSLR	lbm/sec.	Liquid flow out of break
69	ADS and break	BRKSPEI, ADS13EI, ADS41EI, ADS42EI	Btu	Integrated fluid energy for ADS 1-3, ADS-4, and break
70	Mass balance	TOTMASS	lbm	Total system mass inventory
71	Mass balance	PRIMMASS, PRIMASS2	lbm	Measured primary system inventory and value from mass balance
72	Mass balance	MERROR	lbm	Mass balance error
73	Mass balance	MIN, MOUT SRCMASS	lbm	Integrated mass flow in and out of primary system and source mass
74	Energy bal.	Various	Btu	Components of energy balance

THE PLOTS (1-74) LISTED IN TABLE 5.1.2 ARE NOT INCLUDED IN THIS NONPROPRIETARY DOCUMENT.

5.1.3 Long-Term Transit

The long-term transient covers the transition from IRWST to sump injection and provides information on the LTC response of the AP600. For the 2-in. cold-leg break, Matrix Test SB01, the long term transient encompasses the time frame of [ ]^{a,b,c} seconds to the end of the test near [ ]^{a,b,c} seconds. The behavior of the test facility during this period of the transient is discussed in this subsection using the plot package detailed in Table 5.1.3-1. These results concentrate on the components of the primary system that remain active during the LTC phase, that is, the RV, the hot legs, ADS-4, the sumps, and the IRWST.

5.1.3.1 Reactor Pressure Vessel and Downcomer Mass Distribution

For the long-term transient, the passive core cooling systems must supply sufficient flow to prevent any overheating of the heated rods. During the time frame of [ ]^{a,b,c} seconds, the decay heat simulation of the heated rods reduced power from 175 to 120 kW (Figure 5.1.3-1). As seen in Figure 5.1.3-38, there were no significant excursions in heated rod temperatures and, therefore, sufficient core flow was maintained throughout the long-term transient.

The mass of water in the reactor pressure vessel is shown in Figure 5.1.3-25. After an initial decline, the reactor vessel water mass settled at an average value of [ ]^{a,b,c} lbm until the sump injection valves opened at around [ ]^{a,b,c} seconds. From [ ]^{a,b,c} seconds, oscillations in vessel inventory were observed. These oscillations can be seen in measurements throughout the primary system, and they are discussed further in Subsection 6.1.3. The onset of sump injection caused a drop in vessel inventory to a constant value of [ ]^{a,b,c} lbm, which is 67 percent of the initial vessel water inventory. At approximately [ ]^{a,b,c} seconds, the water mass increased to [ ]^{a,b,c} lbm in response to a partial collapse of the steam bubble in the head region (Figure 5.1.3-33) and remained at this level during the last [ ]^{a,b,c} seconds of the transient.

Core water mass and the collapsed liquid level are shown in Figures 5.1.3-28 and 5.1.3-29. It can be seen that, from [ ]^{a,b,c} seconds, the core remained near water-solid with only a very low level of boiling (Figure 5.1.3-36); however, after the sump injection valves opened, the increase in core temperature resulting from the influx of hot sump water (Figures 5.1.3-2 to 5.1.3-5) caused the core collapsed liquid level to drop just below the top of the heated rods. At this time, the level at which the core fluid temperatures reached saturation dropped (Figure 5.1.3-34), and the amount of boiling increased along the upper regions of the heated rods. The level of boiling continued at a constant rate until the end of the accident simulation (Figure 5.1.3-36). It should be noted that the long-term transient core steam generation calculation is based only on the DVI line flow method, since the T_{sat} method is very sensitive to small changes in local pressure.

The collapsed liquid level in the upper plenum region is shown in Figure 5.1.3-32. Right before sump injection began, the collapsed liquid level in the upper plenum remained at the top of the hot legs.

Following the influx of hot water from the sumps, the level dropped to the top of the DVI lines and remained there for the remainder of the transient.

The mass of fluid and collapsed liquid level in the reactor vessel downcomer are shown in Figures 5.1.3-26 and 5.1.3-27. Before the start of sump injection, the collapsed liquid level in the downcomer was at the level of the center of the cold legs. The start of sump injection through the injection valves at [ ]^{a,b,c} seconds caused a readjustment of the levels around the primary circuit, and, subsequently, the downcomer level remained at the bottom of the hot legs for the remainder of the transient.

Figure 5.1.3-4 shows the response of the downcomer water temperatures during the LTC phase of the transient. Initial sump injection via the check valves caused a sudden rise in downcomer water temperature as the hotter sump water entered the downcomer. The opening of the main sump injection valve caused a momentary increase in downcomer temperature as DVI flow temporarily decreased (Figures 5.1.3-6 and 5.1.3-7). During the long-term phase of the transient, the downcomer water temperatures increased gradually, but it can be seen that the temperature remained well subcooled. The downcomer, therefore, provides a potential site for steam condensation. Such a process is believed to be involved in driving the oscillations observed between [ ]^{a,b,c} seconds into the transient (Subsection 6.1.3).

5.1.3.2 Loop Mass Distribution

During the LTC phase of the transient, there was a low level of boiling in the upper regions of the core. The following are five potential paths for the steam:

- To the hot legs and out of the ADS-4 valves
- To HL-2, through the pressurizer and ADS 1-3 valves to be deposited in the IRWST
- To HL-2, through the PRHR HX to the SG outlet
- To the hot legs, through the SGs to the cold legs to return to the reactor vessel or flow out of the break
- To the head region and into the downcomer, potentially condensing in the downcomer, or, if the downcomer water level is below the cold legs, venting through the cold legs to the CMTs and break

It can be seen from Figures 5.1.3-39 and 5.1.3-40 that during sump injection, two-phase flow occurred in the hot legs. Figure 5.1.3-25 shows that throughout this phase of the transient, the pressurizer surge line remained filled with water. Figure 5.1.3-21 shows that the inlet plenum on SG-2 also remained plugged with water. It was expected that the inlet plenum on SG-1 also contained a small amount of

water, although for this test, the level measurement was over-ranged and SG-2 results have been used for SG-1. There is no evidence of flow through the PRHR HX during the long term-transient. Therefore, for steam entering the hot legs, the only available flow path was out of the primary loop to the sumps via the ADS-4 valves. However, there was no evidence on the steam vortex meters for vapor flow out of the ADS. It should be noted that the vortex meters have a dead band, and low flow was detected. The expected rate of loss of steam through each ADS-4 valve during the long-term transient is of that order. Examination of the fluid thermocouples in the steam lines from the ADS-4 separator shows the temperature at or above saturation for all of the transient beyond 15,000 seconds, which indicates that steam was leaving the system by this path.

5.1.3.3 Mass Ejected from the Primary System

The integrated mass flow out of the primary system via the ADS and the break are shown in Figure 5.1.3-43. By the end of the accident simulation, approximately [ ]^{a,b,c} lbm of water had flowed out of the primary system. During the LTC phase of the transient, the only significant outflow was through the ADS-4 valves, with a small apparent flow through the break. The apparent break flow does not represent flow out of the primary system, but indicates continued interaction between the break separator and the sump. The most marked manifestation of this interaction is at 14,000 seconds when the primary sump began to flow into the secondary sump causing oscillating flow indications in the liquid flow out of the break separator. This is confirmed by Figures 5.1.3-44 and 5.1.3-45, which show flow through the ADS and the break. During the sump injection phase of the transient, outflow in the form of liquid exited out of the ADS-4 valves. Water flowed through each of these at an average rate of [ ]^{a,b,c} lbm/sec.

During the long-term transient, there was no evidence from the vortex meters for steam flowing out of the primary system via the ADS-4 valves. It is, therefore, not immediately clear where the steam generated in the core was deposited. As discussed in Subsection 6.1.3, there is evidence for steam flowing from the upper head to the downcomer via the bypass holes, but this is not enough to account for all the steam generated in the core. The system mass inventory (Subsection 5.1.3.5) indicates a flow of [ ]^{a,b,c} lbm/sec. and is required to explain the fall in measured system mass inventory. The fluid temperatures in the vapor lines out of the ADS-4 stage separators indicate that steam left the primary system via the ADS.

At approximately [ ]^{a,b,c} seconds into the transient, the level in the primary sump (Figure 5.1.3-14) reached the point at which overflow to the secondary sump occurred. At this time, there was approximately [ ]^{a,b,c} lbm of water collected in the primary sump. From the start of primary sump overflow to the end of the transient, [ ]^{a,b,c} lbm of water was transferred to the secondary sump (Figure 5.1.3-16).

5.1.3.4 Mass Injected to the Primary System

The total DVI line flow, CMT flow, and IRWST flow are shown in Figures 5.1.3-6 and 5.1.3-7; flow from the primary sump is shown in Figure 5.1.3-19. It can be seen that, from around [ ]^{a,b,c} seconds, there was a contribution to the DVI flow from the CMTs as they finished post-refill draindown.

During the presump injection phase of the transient, IRWST flow proceeded at a gradually reducing rate with the effect of the primary system oscillations superimposed. At [ ]^{a,b,c} seconds, flow from the primary sump began through the check valves around the main injection valves. After the initial outsurge, a flow rate of [ ]^{a,b,c} lbm/sec. was achieved. At around [ ]^{a,b,c} seconds, the level in the IRWST fell to [ ]^{a,b,c} in. and the primary sump injection valves opened, allowing additional flow to the primary circuit from the sump with an initial surge of water at a peak rate of [ ]^{a,b,c} lbm/sec. (Figure 5.1.3-19). As the levels in the primary circuit adjusted, flow through the DVI lines ceased temporarily before restarting again. Following the start of sump injection through the main valve, flow through DVI-1 resulted entirely from sump injection (Figure 5.1.3-6) while for DVI-2, flow was mainly from the IRWST (around [ ]^{a,b,c} lbm/sec.) with a small contribution from the primary sump flow (Figure 5.1.3-7). Both DVI lines delivered water to the reactor vessel at a near-constant rate of just under [ ]^{a,b,c} lbm/sec. for the entire period of the transient following the opening of the sump injection valves. It should be noted that IRWST flow rates were based on measured positive flows. During sump injection, there was reverse flow from the primary sump to the IRWST via the DVI-1 line.

During sump injection, [ ]^{a,b,c} lbm of water was delivered from the primary sump to the primary circuit in addition to [ ]^{a,b,c} lbm from the IRWST (Figure 5.1.3-20). During this time, a total of around [ ]^{a,b,c} lbm of water left the primary circuit via the ADS-4 valves. The inventory of water available for injection to the primary circuit was not reduced significantly by the end of the transient (Figure 5.1.3-13).

During the long-term transient, the water level in the break separator was sufficient to allow flow back into the primary system through the break. This is representative of the behavior expected in the AP600 where the level of water in the sump would reach the break elevation.

5.1.3.5 Mass Balance

Figure 5.1.3-46 shows the variation in the total system mass inventory during the entirety of Matrix Test SB01. Following the short-term transient, the total inventory remained between [ ]^{a,b,c} lbm below the initial value. Initially, there was an increase in inventory until [ ]^{a,b,c} seconds when the inventory fell. From [ ]^{a,b,c} seconds to the start of sump injection, the inventory remained essentially constant. After sump injection began, there was an increase in inventory followed by a gradual reduction, so that by the end of the LTC phase of the transient, [ ]^{a,b,c} lbm of water was also lost. This reduction was consistent with a flow rate of steam

out of the system of [ ]^{a,b,c} lbm/sec. It should be noted that the vortex flow meters have a dead band, and thus, the vortex meters would not register the low flow of steam passing through each ADS-4 valve; therefore, this inventory loss was not measured directly.

Figure 5.1.3-46 shows dips of about [ ] lbm superimposed on the general trends in mass inventory. As in the short-term transient, these dips resulted from corresponding changes in the sump inventory, observed in the level data from which the masses were calculated (Figures 5.1.3-13, 5.1.3-14, 5.1.3-16, and 5.1.3-17). The readings on the load cells for the two sumps did not show corresponding dips, and there were no indications of increased flow at this time; thus, the dips are believed to be the result of pressure variations in the differential pressure taps and not mass changes.

The mass balance calculation described in Subsection 5.1.2-5 has been performed for the entirety of the transient, and the results are presented in Figures 5.1.3-47 to 5.1.3-49. During the long-term phase of the transient, the measured water inventory in the primary system remained approximately constant at [ ] lbm. The mass balance calculations produced inconsistent results due to problems in tracking the flow back into the primary circuit from the break separator while allowing for continued interactions between the separator and the sump.

5.1.3.6 Energy Balance

Figure 5.1.3-50 shows all the energy components in the heat balance for the system during the LTC phase. During this phase, the heated rod bundle power was the dominant heat input to the system. The SG heat transfer ended during the LOCA phase and did not contribute to the overall energy balance during the LTC phase. Thus, for the LTC phase, the active components in the overall energy balance were rod bundle power, change in the fluid internal energy, change in the metal internal energy, ambient losses, and steam exhaust from the control volume.

The fluid energy in the control volume increased steadily until sump injection began at (approximately [ ]^{a,b,c} seconds). At that time, fluid throughout the system approached saturated conditions, and the rate of increase was reduced. At the same time, metal mass temperatures increased and the primary system temperature increased in response to the hotter water from the sump. Also, ambient losses increased slightly as the control volume temperatures increased. The sum of these increases is much less than the rod bundle power and must be a result of steam exhausting from the control volume. This assumption is consistent with the mass balance deficit discussed previously.

The steam component of the ADS-4 flow was lost from the control volume from actuation of ADS-4. For the LTC phase, this quantity is essentially zero, as measured by the vapor flow meters. It is concluded that the vapor flow meters in the ADS-4 separators did not measure the relatively small steam flow rates accurately. If the mass balance deficit during the LTC phase of approximately [ ]^{a,b,c} lbm is converted to steam, the energy balance deficit is accounted for.

TABLE 5.1.3-1
OSU TEST ANALYSIS STANDARD PLOT PACKAGE FOR SECTION 5.1.3
LONG-TERM TRANSIENT

Plot No.	Component	Variables	Units	Description
1	RV	RVPWR	kW	Core power
2	Primary sump	TSMPI1, TSMPI2	°F	Sump injection line temperatures
3	DVI	TDVIL1, TDVIL2	°F	DVI line temperatures
4	RV	T01DC, T02DC, T03DC, ST01DC	°F	Water and saturation temperatures in downcomer
5	RV	T01RV, T08RV, ST08RV	°F	Core inlet/outlet temperature, saturation temperature
6	DVI-1	WWTDVIL1, WWTIRWI1, WOUTACC1, WWTIRWI3	lbm/sec.	Total flow in DVI-1 and individual components
7	DVI-2	WWTDVIL2, WWTIRWI2, WOUTACC2, WWTIRWI4	lbm/sec.	Total flow in DVI-2 and individual components
8	CMT	CLDP-502, CLDP-507	in.	Collapsed liquid level in CMTs
9	CMT	CLDP-509, CLDP510	in.	Level CL-CMT balance lines
10	IRWST	IRWST	lbm	Mass of fluid in IRWST
11	IRWST	CLDP-701	in.	Collapsed liquid level in IRWST
12	IRWST	UIRWST	Btu	Fluid energy in IRWST
13	Primary sump	AMPSMP	lbm	Primary sump mass
14	Primary sump	CLDP-901	in.	Primary sump level
15	Primary sump	UPSMP	Btu	Primary sump fluid energy
16	Secondary sump	AMSSMP	lbm	Secondary sump mass
17	Secondary sump	CLDP-902	in.	Secondary sump level
18	Secondary sump	USSMP	Btu	Secondary sump fluid energy
19	Primary sump	WSTSMPET, WWTSMPIT	lbm/sec.	Primary sump steam and liquid injection rate
20	Primary sump	MISMPI1, MISMPI2, MISMPIT	lbm	Integrated primary sump and IRWST flows
21	SG	MSSGIP1, MSSGIP2, MSSGOP1, MSSGOP2	lbm	Mass of fluid in SG side inlet/outlet plena
22	Surge line	PLM	lbm	Fluid mass in surge line
23	Surge line	CLDP-602	in.	Collapsed liquid level in surge line
24	Surge line	UPSL	Btu	Fluid energy in surge line
25	RV	MWRV	lbm	Total fluid mass in reactor vessel

TABLE 5.1.3-1 (Continued)
OSU TEST ANALYSIS STANDARD PLOT PACKAGE FOR SECTION 5.1.3
LONG-TERM TRANSIENT

Plot No.	Component	Variables	Units	Description
26	RV	DCM	lbm	Fluid mass in downcomer
27	RV	LDP01DC	in.	Collapsed liquid level in downcomer compared to various reference elevations
28	RV	MW03RV	lbm	Fluid mass in core region
29	RV	LDP03RV	in.	Collapsed liquid level in core
30	RV	RVXVFO		Core exit void fraction
31	RV	RVXRQO		Core exit quality
32	RV	LDP06RV	in.	Collapsed liquid level in the upper plenum
33	RV	MW08RV	lbm	Fluid mass in the upper head
34	RV	RVXE	ft.	Level of Tsat line
35	RV	RVPab, RVPbl, RVPWR	kW	Heated rod power above and below Tsat level and total
36	RV	RVRXV	lbm/sec.	Core steam generation rate
37	RV	RVTMRI	lbm/sec.	Calculated core flow
38	RV		°F	Maximum clad temperature, saturation temperature and delta
39	Hot leg	MWHL1, MWHL2	lbm	Water mass in hot legs
40	Hot leg	MVHL1, MVHL2	lbm	Vapor mass in hot legs
41	Cold leg	CL1WMS, CL2WMS, CL3WMS, CL4WMS	lbm	Water mass in cold legs
42	Cold leg	CL1VMS, CL2VMS, CL3VMS, CL4VMS	lbm	Vapor mass in cold legs
43	ADS and break	BRKSTIR, ADS13TIR, ADS41TIR, ADS42TIR	lbm	Total discharged mass for ADS 1-3, ADS-4, and break
44	ADS and break	ADS13SLR, ADS41SLR, ADS42SLR	lbm/sec.	Liquid flow out ADS 1-3 and ADS-4
45	ADS and break	BRKSTLR	ibm/sec.	Liquid flow and total flow out of break
46	Mass balance	TOTMASS	lbm	Total system mass inventory
47	Mass balance	PRIMMASS, PRIMASS2	lbm	Measured primary system inventory and valve from mass balances
48	Mass balance	MERROR	lbm	Mass balance error
49	Mass balance	MIN, MOUT SRCMASS	lbm	Integrated mass flow in and out of primary system and source mass
50	Energy balance	Various	Btu	Component of energy balance

THE PLOTS (1-50) LISTED IN TABLE 5.1.3 ARE NOT INCLUDED IN THIS NONPROPRIETARY DOCUMENT

5.2 Analysis of Matrix Test SB18

Matrix Test SB18 (OSU Test U0018) simulated a 2-in. cold-leg (CL) break loss-of-coolant accident (LOCA) with long-term cooling (LTC) and without operation of nonsafety-related systems. Basically, it duplicated Matrix Test SB01. The purpose of performing Matrix Test SB18 was to confirm the ability of the facility to replicate its response to a small-break LOCA (SBLOCA), with the same configuration from the beginning to the end of the test program.

Analysis of Matrix Test SB18 is divided into three sections:

- General facility performance
- SBLOCA
- LTC

The general facility performance (Subsection 5.2.1) describes the overall response of the system throughout the test. The SBLOCA portion (Subsection 5.2.2) provides a discussion of the system behavior from the start of the test, through system depressurization, to approximately 3000 seconds into the transient, and includes the initial system blowdown, the establishment of natural circulation, and the initial portion of the IRWST injection cooling (Figure 5.2-2). The LTC portion (Section 5.2.3) discusses the behavior of the remainder of the test and includes the completion of IRWST injection and the establishment of sump injection. The refill and subsequent recirculation of the CMT is considered as a separate discussion within Subsection 6.1.1. The period between SBLOCA and LTC is not discussed specifically since the system is as behaving in a stable manner.

Matrix Test SB18, the final test performed, duplicated Matrix Test SB01, the first test performed. The purpose of performing Matrix Test SB18 was to confirm the ability of the facility to replicate its response to a SBLOCA with the same configuration from the beginning to the end of the test program.

The main differences for the two matrix tests were:

- A vacuum breaker was installed on the ADS 1-3 sparger line inside the IRWST to eliminate negative pressures in the pressurizer and ADS 1-3 separator.

- Pressurizer heater logic was changed so that the PLC initiated a signal to open the pressurizer heater SCR contactor at [ ]^{a,b,c} seconds after S signal actuation, thereby ensuring de-energization of the heaters.

- CMT balance line isolation valves were closed and opened by the operator one minute after the TEST pushbutton was pressed in Matrix Test SB18 to prevent heating at the top of the CMTs prior to break valve opening.

5.2.1 Facility Performance

Matrix Test SB18 simulated a 2-in. CL-break LOCA with long-term cooling and without operation of nonsafety systems. The break was located at the bottom of CL-3 with a simulated failure of one of the automatic depressurization system-4 (ADS-4) lines. CL-3 is on the core makeup tank (CMT) side of the facility.

A flow nozzle simulating one line of flow was installed in the ADS 4-1 line, hot leg-1 (HL-1) to the ADS 4-1 separator, to provide the single failure simulation. A flow nozzle simulating two lines of flow was installed in the ADS 4-2 line (HL-2 to the ADS 4-2 separator). Additionally, flow nozzles simulating two lines of flow each were installed in the ADS 1-3 inlet lines.

The reactor heater control decay algorithm maintained the maximum reactor heater power output for [ ]^{a,b,c} seconds, and then power was programmed to begin to decay to simulate the total decay energy input of the AP600 nuclear fuel. This test was performed with reactor heater rod HTR-C2-317 electrically disconnected to simulate the heater conditions during the performance of Matrix Test SB01.

The facility performance is divided into separate discussions of the five phases of the test: blowdown, natural circulation, ADS, IRWST injection, and sump injection. The overall performance over the 14,300 second test is shown in Figures 5.2-1, 5.2-2, and 5.2-3. Figure 5.2-1 shows the pressurizer pressure throughout the test, indicating the various phases and operating components. The time scale is split out for clarity between 1600 and 13,000 seconds since there was no change in the operating mode during this period. Figure 5.2-2 shows the total injection flow rates into the DVI line from the various systems as a function of time. Figure 5.2-3 shows the quantity of steam generating in the core throughout the test.

Figures 5.2-1 and 5.2-2 show that as the primary system is depressurizing, a continuous flow of water into the reactor vessel is provided by passive safety systems. The passive safety systems overlap so that as one system drains or empties, another provides flow into the simulated reactor vessel providing continuous core cooling.

The flows are large enough that the simulated core exit temperature is just saturated or subcooled for significant portions of the transient, and the core steam flow is less than the passive safety system injection flow, as seen by comparing Figures 5.2.1-2 and -3 and Figure 5.2-3. As the system transitions into long-term cooling, the water injected from the sump was hot since it originated in the primary system. The hotter injection water temperature after 3000 seconds results in continuous steam generation in the heater rod bundle as seen in Figure 5.1-3. The resulting steam generation is vented primarily through the fourth stage ADS valves.

5.2.1.1 Blowdown Phase

The blowdown phase corresponds to the first 90 seconds of the SB18 test as shown in Figure 5.2-1, and is completed when the steam pressure reaches the steam generator safety valve setpoint. As with Matrix Test SB01, the test initiated (0 time) by opening the break valve. The hot leg of the RCS was initially at the same temperature and pressure (420°F at 372 psig) prior to the initiation of the test as for test SB01. The simulated S signal was generated 0.5 second after the break signal and initiated the following actions.

In the first [ ]^{a,b,c} seconds, the SG pressure setpoint was raised to 335 psig, the reactor shifted to power (kW) control mode with a programmed power demand for 600 kW total power, the main feedwater pump tripped and feedwater was isolated (at 4 seconds), the passive residual heat removal heat exchanger (PRHR HX) outlet valve and CMT discharge valves opened (at [ ]^{a,b,c} seconds), and the reactor coolant pumps (RCPs) tripped at [ ]^{a,b,c} seconds into the event.

Forced flow was continued through the PRHR HX and the CMTs until the RCPs stopped at approximately [ ]^{a,b,c} seconds, at which time the flow changed to natural circulation flow. As the RCS depressurized and coolant escaped through the break, pressurizer level decreased rapidly and steam formation began in the reactor vessel upper head. At about [ ]^{a,b,c} seconds, the level in the upperhead of the reactor vessel indicated the vessel was beginning to lose inventory as the vessel drained and some liquid flashed to steam.

As the primary system pressure reached near steady-state condition, the system transitioned into the natural circulation phase once the pumps coasted down and the system reached the steam generator pressure setpoint at 335 psig at approximately 89 seconds. During this time period, there was initially forced and then liquid-solid natural circulation in the PRHR and CMT systems. The CMTs provided recirculating flow to the reactor vessel while the PRHR removed energy from the primary system.

5.2.1.2 Natural Circulation Phase

The cold legs developed a void fraction at approximately [ ]^{a,b,c} seconds at which time the CMT balance lines began to drain. CMT-1 and CMT-2 levels began to decrease, making the transition from recirculation to draindown at about [ ]^{a,b,c} seconds, respectively, and the injection flow from the CMTs increased (Figure 5.2-2). As the system continued to drain, the steam generator tubes started to drain at [ ]^{a,b,c} seconds and the generators transitioned into a two phase recirculation behavior. The mass loss through the break caused a rapid decrease in pressurizer level and emptied the pressurizer at approximately [ ]^{a,b,c} seconds. At both [ ]^{a,b,c} seconds, a condensation/depressurization event took place in CMT-1 as indicated by a rapid refill of the CMT-1 balance line as steam from the balance line was condensed in the CMT. Water from the cold leg was drawn up the balance line into the CMT tank as the balance line filled.

The upper head continued to drain and was empty at [ ]^{a,b,c} seconds. Steam generation in the reactor vessel reached its maximum (0.56 lbm/sec, Figure 5.2-3) at 260 seconds. The pressurizer surge line was completely emptied at approximately [ ]^{a,b,c} seconds. Primary system was at a pressure above the steam generator secondary side pressure, which continued to remove energy until approximately 330 seconds when the tubes become superheated.

As the system continued to drain, the U-tubes of both SGs were completely empty by approximately [ ]^{a,b,c} seconds and the HL-1 and HL-2 levels began to decrease at about [ ]^{a,b,c} seconds. The horizontal sections of the hot legs started to drain at about [ ]^{a,b,c} seconds. The hot legs remained at saturation temperature and never superheated, even though they were partially or completely empty due to a small flow of saturated steam from the reactor heater bundle to the SGs.

At [ ]^{a,b,c} seconds, CMT-1 reached the ADS-1 setpoint, and the ADS-1 valve opened to initiate ADS blowdown.

5.2.1.3 ADS Phase

The ADS flow path, in conjunction with the break, caused RCS pressure to decrease at a rapid rate, redistributing the mass inventory of the system. The opening of the ADS-1 valve released two-phase flow going through the pressurizer to the ADS 1-3 separator and into the IRWST through the sparger. The opening of the ADS-1 valve, followed by the ADS-2 valve approximately [ ]^{a,b,c} minute later, caused an increase in the rate of RCS depressurization. As the different ADS stages opened, the primary vent path shifted from the cold leg break to the ADS valves through the pressurizer.

The collapsed-liquid level inside the reactor core barrel reached a near-term minimum value at [ ]^{a,b,c} seconds, but the core remained covered during this time period with a two-phase mixture. When the RCS depressurized to approximately [ ]^{a,b,c} psia at about [ ]^{a,b,c} seconds, accumulator injection into the DVI line began (Figures 5.2.1-1 and 5.2.1-2).

The accumulators started discharging into the DVI line which reduced CMT-1 injection flow during accumulator injection by closing off the CMT discharge line check valves until the accumulators were almost empty and depressurized. With the accumulators at their maximum injection rate the RCS refilled and the surge line and pressurizer began to reflood at about [ ]^{a,b,c} seconds, and the pressurizer attained its maximum level at [ ]^{a,b,c} seconds. Once the accumulators were empty, the pressurizer and surge line then drained back down and were completely empty at [ ]^{a,b,c} seconds.

When RCS pressure decreased to [ ]^{a,b,c} psig at approximately [ ]^{a,b,c} seconds, the two IRWST injection valves automatically opened, but IRWST injection could not occur until RCS pressure decreased to near atmospheric pressure. As accumulators completed injection at [ ]^{a,b,c} seconds for ACC-1 and [ ]^{a,b,c} seconds for ACC-2, CMT-1 and CMT-2 injection flow started to increase at [ ]^{a,b,c} seconds. Approximately 50 percent of the nitrogen gas in the accumulator was injected into the DVI lines, momentarily cooling the injection lines at the end of accumulator injection. The

nitrogen caused a decrease in ACC-1 and -2 outlet temperature of about [ ]^{a,b,c} at approximately [ ]^{a,b,c} seconds. There was no indicated change in total DVI flow in either DVI line.

During the accumulator injection period, there was sufficient injection of subcooled liquid to suppress boiling in the core region. The downcomer was filled with subcooled liquid, which resulted in the collapse of the superheated steam bubble in the upper portion of the reactor vessel downcomer annulus. As the pressure decreased in this region, the downcomer fluid accelerated upward and impacted on the bottom of the core barrel flange where the core bypass holes are located. The impact of the downcomer liquid on the solid surface of the core barrel flange was heard during the test.

During accumulator injection, the PRHR and PRHR level decreased. The PRHR HX inlet temperature became subcooled coincident with the ADS-4 valves opening at [ ]^{a,b,c} seconds and over the next [ ]^{a,b,c} seconds dropped to and paralleled the outlet temperature.

From [ ]^{a,b,c} seconds, both DVI nozzle temperatures increased from essentially ambient conditions to as high as [ ]^{a,b,c} as the CMT fluid heated. The temperature transient was terminated when the CMT inventory was exhausted, and the IRWST injection began refilling the reactor vessel at about [ ]^{a,b,c} seconds and temperatures returned to ambient when the CMTs were empty, terminating the hot liquid injection. This temperature transient does not appear to have affected any other facility parameters.

Steam generation in the reactor vessel (RV) was reestablished in the period between about 680 and 300 seconds after accumulator injection ended and the system began to drain again. At [ ]^{a,b,c} seconds, the ADS 4-1 and ADS 4-2 valves opened automatically when CMT-1 level reached its low-low level setpoint. ADS-4 actuation started a decline in RCS inventory that could not be overcome until IRWST injection began. There is initially too much mass in the system which must be vented through ADS-4 before IRWST injection can occur. CMT-1 and CMT-2 were completely empty at [ ]^{a,b,c} seconds, respectively.

The pressurizer was slightly subcooled at about 1000 seconds and remained subcooled until the data acquisition ceased at approximately 14300 seconds.

At about [ ]^{a,b,c} seconds, the RCS was drained sufficiently that system pressure decreased to about [ ]^{a,b,c} psi$_g$, which was sufficiently low that the IRWST static head was greater than RCS pressure, and IRWST injection began.

5.2.1.4 IRWST Injection Phase

IRWST injection started about [ ]^{a,b,c} seconds and proceeded at a continually diminishing rate (Figure 5.2-2) as the differential head between the IRWST and the RCS decreased with the drainage of the IRWST. The IRWST injection was sufficient to begin refilling the primary system. The pressurizer and pressurizer surge line emptied for the second time at approximately [

]^{a,b,c} seconds, respectively. No reflood of the pressurizer occurred because of the vacuum breaker installed on the ADS 1-3 sparger line inside the IRWST.

Both CMT balance lines began to refill at about [ ]^{a,b,c} seconds after the IRWST injection increased the reactor vessel level to cover and refill the cold legs. At about 3300^{a,b,c} seconds, when the CMT-2 balance line had completely refilled, CMT-2 began to rapidly refill and reached the [ ]^{a,b,c} in. level (about 75 percent full) at about 3500^{a,b,c} seconds. The CMT refill will be discussed in more detail in Section 6 of this report. After the CMTs were partially refilled, there was no injection flow from the CMTs because the higher static head of the IRWST held the CMT discharge line check valves closed.

CMT-1 and CMT-2 reflooded at about [ ]^{a,b,c} seconds and the draindown was completed about [ ]^{a,b,c} seconds or about the time that sump injection started through the primary sump injection line check valves.

Steam generation started again about 7800 seconds and continued for the remainder of the test (Figure 5.1-3). CMT-1 and CMT-2 remained at essentially constant levels for several [ ]^{a,b,c} seconds and then began slow draindowns at about [ ]^{a,b,c} seconds, respectively. The draindown for both CMTs was slow and did not occur until IRWST relative level was [ ]^{a,b,c} below that of the CMTs. Data indicate that the CMTs drained for a while, and then the differential head between the IRWST and the CMTs again closed the CMT discharge check valves, terminating draining until the differential shifted the other way and draining recommenced. Both CMTs were completely empty at about [ ]^{a,b,c} seconds, which coincides closely with the primary sump injection valve opening at [ ]^{a,b,c} second. Failure of the DAS from 14,300 seconds until the completion of the test stopped any further description of the test events.

The break separator level began to increase at the same rate as the primary sump at about [ ]^{a,b,c} seconds. This occurred when sump level reached the height of the break separator loop seal. As a result of this level increase, break separator level reached the height of the break in CL-3, causing break flow to reverse and flow from the break separator into the RCS through the break at about [ ]^{a,b,c} seconds. The break flow then remained essentially 0 or slightly negative throughout the rest of the test.

At approximately 9000 seconds, the PRHR inlet temperature starts rising to the saturation temperature while the discharge temperature remains steady at approximately 100°F for the remainder of the data collection period.

5.2.1.5 Sump Injection Phase

Primary sump injection (Figure 5.2-2) started at about [ ]^{a,b,c} seconds, or some [ ]^{a,b,c} seconds earlier in Matrix Test SB18 than in Matrix Test SB01. When sump injection begins, the reactor vessel downcomer fluid temperatures rapidly increased to the sump flow injection temperature. Primary sump injection valves opened at [ ]^{a,b,c} seconds, and the test was stopped 30 minutes later but the

detailed data between 14,312 and the end of the test is missing for one instrument rack and thus this phase of the transient cannot be analyzed.

TABLE 5.2.1-1
OSU TEST ANALYSIS PLOT PACKAGE FOR SECTION 5.2.1

Plot Number	Component	Variables	Units	Description
1	Pressurizer	CPT-604	psia	System pressure and event history
2	Water Injection	WWTDVI1+WWTDVI2, WOUTACC1+WOUTACC2, WWTIRWI1+WWTIRWI2, WWTSMPIT	lbm/sec.	Total of CMT, accumulator, IRWST and sump injection flows
3	Reactor Vessel	RPVRXV	lbm/sec.	Steam generation in reactor vessel
4	Reactor Vessel	T08RPV, TSAT	°F	Reactor vessel outlet temperature

THE PLOTS (1-4) LISTED IN TABLE 5.2.1-1 ARE NOT INCLUDED IN THIS NONPROPRIETARY DOCUMENT

5.2.2 Short-Term Transient

For the 2-inch cold leg break, Test SB18 (a repeat of SB01), the short-term transient encompassed the first 3000 seconds. As can be seen from Figures 5.2.2-1 and 5.2.2-2, this period included the full depressurization of the facility through all four stages of the ADS together with CMT and accumulator injection plus the initial stages of IRWST injection. The mass and energy distribution results for this phase of the transient were based on the plot package detailed in Table 5.2.2-1. These plots concentrate on the primary system including the accumulators, CMTs, IRWST tanks and the sumps and the flows from the primary system via the ADS, break and IRWST overflow.

5.2.2.1 Reactor Pressure Vessel and Downcomer Mass Distribution

For the short-term transient, the most important criteria is the maintenance of sufficient core inventory to supply adequate cooling of the heated rods. Figure 5.2.2-57 shows that there are no significant excursions in heated rod temperatures and, therefore, sufficient core inventory was maintained through this phase of the transient to remove the decay heat from the rods. However, for significant portions of the transient a two-phase mixture will be present in the core and upper plenum regions. The following discussion tracks the variation in water level and mass throughout the RV and downcomer.

The total fluid mass in the reactor pressure vessel is shown in Figure 5.2.2-40. The initial vessel inventory was [ ]^{a,b,c} lbm. During the course of the short term transient the vessel inventory experiences two minima, one of [ ]^{a,b,c} lbm before accumulator injection and one of [ ]^{a,b,c} lbm before IRWST injection. Steam generation was near maximum at these times as shown in Figures 5.2.2-55. By the end of the short-term transient the vessel inventory recovered to a steady [ ]^{a,b,c} lbm. Similar variations were seen in the core fluid mass and water level reproduced in Figures 5.2.2-44 and 5.2.2-45. Minimum core level occurred before IRWST injection. During this phase of the transient, the collapsed liquid level dropped to [ ]^{a,b,c} inches below the top of the heated rod length (see Figure 5.2.2-45). By the end of the short-term transient, the effect of IRWST injection ended all core boiling (see Figure 5.2.2-55), and the core was again water-solid.

In the analysis of the LOCA simulations on the SPES facility (WCAP-14254, SPES Test Analysis Report) following the pump trip, there were short-term oscillations in primary system flow, temperature, and pressure. A small number of oscillations were also observed in the OSU test response at the end of the initial blowdown (see for example the pressure response (Figure 5.2.2-1) and the RV mass (Figure 5.2.2-40)). In the SPES tests, the oscillations were clearly driven by power-to-flow mismatches in the core due to the high core power levels which were needed in SPES to compensate for the high ambient losses. The short-term oscillations observed in OSU results are believed to be a result of pressure oscillations following the initial blowdown.

The fluid mass in the core region is shown in Figure 5.2.2-44. Once again, the two minima occurred prior to accumulator injection, and prior to IRWST injection. The minimum core inventory is [ ]^{a,b,c} lbm.

The collapsed liquid level in the upper plenum region spanned by LDP-138 and the associated fluid mass are shown in Figures 5.2.2-49 and 5.2.2-48. It can be seen that, during the period before accumulator injection, the collapsed liquid level in the upper plenum dropped below the hot-leg elevation. During the accumulator injection, the steam bubble in the upper plenum partially condensed and the water level briefly rose above the hot legs. Following the end of accumulator injection, the flow from the CMTs is not sufficient to maintain the upper plenum level, and this region completely drains of water. The start of IRWST injection causes the upper plenum to refill, and this region became near water-solid again at approximately [ ]^{a,b,c} seconds.

The fluid mass and collapsed liquid level for the head region are given in Figure 5.2.2-50 and 5.2.2-51. During the first [ ]^{a,b,c} seconds, the head inventory drained. Following the end of accumulator injection, the head region also drained. Both accumulator injection and IRWST injection were sufficient to supply a level of water in the head.

The mass of fluid and collapsed liquid level in the RV downcomer are shown in Figures 5.2.2-41 and 5.2.2-42. During the blowdown phase of the transient, the level dropped to the elevation of the cold legs. This elevation was maintained until the cold legs were fully drained. Following this point, the collapsed level remained between the DVI and hot-leg elevations, until IRWST injection once again raised the level above the cold legs and cold-leg refill commenced.

5.2.2.2 Loop Mass Distribution

For this discussion, the loop was considered to consist of the hot- and cold-leg pipe work, the steam generator (SG) primary side, and the pressurizer plus surge line.

The total fluid mass and water level for the pressurizer are shown in Figures 5.2.2-34 and 5.2.2-35. During the blowdown phase of the transient ([ ]^{a,b,c}) seconds, the pressurizer drained rapidly, becoming completely empty of water at about [ ]^{a,b,c} seconds. The pressurizer remained empty until ADS stage 1 actuation at [ ]^{a,b,c} seconds. At that time, water was drawn back into the pressurizer as steam and water flow out of the ADS system. A fluid inventory of over [ ]^{a,b,c} lbm was maintained until ADS-4 actuation at [ ]^{a,b,c} seconds. This caused an initial outsurge through the surge line, followed by a more gradual draining of the pressurizer as mass flowed out of the hot legs via the ADS fourth stage valves. The pressurizer fully drained at [ ]^{a,b,c} seconds and remained empty for the remainder of the transient.

Mass data for the SG U-tubes and their associated inlet and outlet plena are reproduced in Figures 5.2.2-32 and 5.2.2-31. The SG tubes gradually drained until ADS actuation, when all the tubes and plena were empty of water. The SG on the broken loop (loop 1) drained before that on loop 2. Any flow through the SGs ceased once the tubes were drained and the steam trapped within the U-tubes became superheated. Once the SG tubes drained, natural circulation around the primary loop circuit ceased.

The SG U-tubes remained empty for the remainder of the short-term transient. However, both inlet and outlet plena on SG 2 show an influx of water [ ]^{a,b,c} seconds into the transient. This corresponds to the time at which the primary circuit reached atmospheric pressure. It can be seen from Figure 5.2.2-59 that, in approximately [ ]^{a,b,c} seconds, the small amount of steam remaining in hot leg 2 was removed and the water level in that hot leg increased. This is believed to result from condensation in the PRHR drawing a vacuum and raising the level on loop 2.

The mass of water and vapor in the hot legs is reproduced in Figures 5.2.2-58 and 5.2.2-59. The hot legs maintained their water inventory until [ ]^{a,b,c} seconds into the transient, when they started to drain (Figure 5.2.2-58), and were completely drained by [ ]^{a,b,c} seconds. Actuation of ADS-1 caused a rapid increase in void fraction in both hot legs. A larger void fraction was maintained in HL-1 as steam was preferentially removed from HL-2 by the PRHR.

The liquid and vapor mass for the four cold legs are given in Figures 5.2.2-60 and 5.2.2-61. Following the initial blowdown, all four cold legs became two phase although there was a greater void fraction in CL-1 and CL-4 as compared to CL-2 and CL-3 (Figure 5.2.2-61). The mass variation in all four cold legs appears very similar, as these have been derived from levels in the RV downcomer. This is because the level instruments on the cold legs have been found to be unreliable. All the cold legs completely drained after ADS initiation, and refilled at [ ]^{a,b,c} seconds when flow from the IRWST refilled the RV downcomer to the level of the cold legs (Figure 5.2.2-42). The cold legs did not drain uniformly, instead, CL-3 (with the break) drained first, followed by CL-1, with CL-2 and CL-4 delayed. Figure 5.2.2-31 shows that the steam generator outlet plenum on loop 1 drains at [ ]^{a,b,c} seconds a little more than, and before loop 2; therefore, the expected asymmetry in cold leg-behavior did occur.

5.2.2.3 Mass Injected to the Primary System

The CMTs transitioned from a recirculation to a mass injection mode at approximately 100 seconds when the cold leg started to drain. Draindown of the CMTs continued until the CMT check valves were closed by the flow from the accumulators. CMT draindown restarted at the end of accumulator injection, continuing until IRWST injection began.

The accumulators started draining approximately [ ]^{a,b,c} seconds after activation of the ADS. Accumulators start discharging into the DVI line when the system pressure drops below the pressure preset in each accumulator. Accumulator injection began at approximately [ ]^{a,b,c} seconds and continued until the accumulator was empty at approximately [ ]^{a,b,c} seconds (Figure 5.2.2-23). Complete discharge from the accumulators was indicated by a sharp decrease in the temperature of the fluid exiting each accumulator due to the discharge of expansion-cooled, nitrogen-cover gas, which is released into the primary system. Once discharged, the accumulators cannot be refilled because of a check valve in the line. Flow from the CMTs was significantly reduced during the discharge of the accumulators and increased again once accumulator discharge was completed.

The IRWST injection valves were opened when the reactor vessel pressure low-low setpoint was reached. Injection flow only starts when the reactor vessel pressure becomes less than the static head from the IRWST tank. Figure 5.2.2-16 shows that the IRWST injection began at approximately [ ]^{a,b,c} seconds after the CMT flow ceased. The IRWST flow gradually increased to a peak value of 2.75 lb/sec. (1.38 lbm/sec. per injection line) at [ ]^{a,b,c} seconds before gradually decreasing.

5.2.2.4 Mass Ejected from the Primary System

At time zero in the transient, a 2-inch break was initiated at the bottom of CL-3. The rate of flow of mass out of the primary system, via the break, is shown in Figures 5.2.2-66 to 5.2.2-68. For the first [ ]^{a,b,c} seconds following the break, [ ]^{a,b,c} lbm of steam and water escaped from the primary system via the break (Figure 5.2.2-62). During that period, the primary system depressurized to around 300 psi (Figure 5.2.2-1). By the onset of ADS actuation, the cold legs drained, and there was almost no water flow out of the break. Between [ ]^{a,b,c} and [ ]^{a,b,c} seconds, ADS stages 1 to 3 activated, and the system depressurized rapidly. The break flow significantly decreased once ADS activated, since the ADS valve area is significantly larger than the break. At around [ ]^{a,b,c} seconds the ADS 4th stage was initiated and the primary circuit continued to depressurize until IRWST injection commenced at [ ]^{a,b,c} seconds.

The actuation of ADS 1-3 rapidly terminated the flow of steam from the break, although this was replaced by steam flow through the ADS 1-3 valves for the next [ ]^{a,b,c} seconds (Figure 5.2.2-63). This steam flow was accompanied by an outflow of water from the ADS 1-3 at a peak rate of over [ ]^{a,b,c} lbm/sec. (Figure 5.2.2-66). After [ ]^{a,b,c} seconds into the accident/simulation, the mass flowing through ADS 1-3 was composed almost entirely of water. The rate of flow through the ADS continued at a gradually reducing rate until [ ]^{a,b,c} seconds when the ADS stage 4 valves were opened, causing the flow through the ADS stages 1-3 to terminate and be replaced by flow through the lower resistance stage 4 paths. For ADS 4-1, there was a near-steady water loss at a rate of 0.75 lbm/sec. from the time of initiation. However, for stage 4-2 there was an initial outsurge at 2.5 lbm/sec., which was followed by a drop to near zero and an increase to over 1 lbm/sec. (see Figure 5.2.2-66).

The integrated mass flow out of the primary system via the ADS and the break are shown in Figures 5.2.2-62 to 5.2.2-66. During the first [ ]^{a,b,c} seconds of the transient, over 6800 lbm of water escaped from the primary circuit. Of this, the [ ]^{a,b,c} lbm flowing through ADS 1-3 was deposited in the IRWST. The [ ]^{a,b,c} lbm leaving the ADS stage 4 system, and the liquid part of the [ ]^{a,b,c} lbm flowing through the break, were added to the overflow from the IRWST to deposit [ ]^{a,b,c} lbm of water in the primary sump (Figure 5.2.2-28). By the end of the short-term transient, the water level in the primary sump reached nearly [ ]^{a,b,c} inches (Figure 5.2.2-29).

At [ ]^{a,b,c} seconds into the transient, the cold legs refilled enough to allow a restart of water flow through the break site. This proceeded a rate of approximately 0.5 lbm/sec. at the end of the short period transient, so that the total rate of water loss from the primary system to the sump was

approximately 2.5 lbm/sec. At that time the rate of gain of RV mass through the DVI lines was about 2.5 lbm/sec.

5.2.2.5 Mass Balance

Figure 5.2.2-70 presents the variation in the total system inventory during the short-term phase of the transient. It can be seen that, in addition to the random variations associated with the measurement uncertainties and some inventory dips, there is a general reduction in inventory of around 200 to 300 lbm from the initial value. During this phase of the transient, around 300 lbm of steam was lost from the system (see Figure 5.2.3-63).

A mass-balance analysis was performed on the primary system. Figure 5.2.2-71 plots the measured primary system mass determined by summing the contributions from the RV, downcomer, hot and cold legs, SG primary, pressurizer and surge line plus the PRHR. The second curve on Figure 5.2.2-71 provides an alternative primary system mass determined from the mass balance, that is given by:

$$M'_{prim}(t) = M_{prim}(0) + M_{in}(t) - M_{out}(t)$$

where:

$M_{prim}(0)$	is the measured primary system mass at the start of the transient
$M_{in}(t)$	is the total integrated mass injected from all sources (i.e., accumulators, CMT, IRWST and sumps) to time t
$M_{out}(t)$	is the mass lost from the primary system to time t via the CMT balance lines, ADS 1-3, ADS-4 and break

The difference in the two primary system mass curves is shown in Figure 5.2.2-72 as the mass-balance error.

During the short-term transient, there is an apparent systematic overestimate of the mass in the primary system from the measured data of up to 300 lbm relative to that calculated from the mass balance. There are two main contributions to this excess mass. First, the measured primary system inventory does not include all of the pipework in the system and there is about 150 lbm of mass missing from the initial inventory. This mass will be deposited in, and lost from, the measured system as pipes drain and refill. Some of the additional mass is subsequently lost via one of the leakage paths. Second, the instrumentation on the hot legs may be giving erroneous level measurements during certain portions of the transient. It can be seen from Figure 5.2.2-58 that in this test, neither hot leg appears to drain and this contributes an overestimate of some 40 to 60 lbm. By the end of the short-term transient, the apparent mass-balance error is about 60 lbm.

Figure 5.2.2-73 shows the total integrated-mass flow from and to the primary system, together with the water inventory remaining in the sources of cooling water. It can be seen that during the short-term transient, there was a net loss of water from the primary system of approximately [ ]^{a,b,c} lbm of which only a small quantity was deposited in the sources. As noted above, the overall system mass inventory shows that of the lost primary system mass, 200 to 300 lbm has been lost as steam. The rest has been added to the water stored in the ADS and break separators.

5.2.2.6 Pressure Decay

Figure 5.2.2-1 shows the primary system pressure during the test. Throughout the LOCA portion of this test, the pressure was controlled by the saturation pressure of the hottest fluid in the primary system. At initiation of the break, the controlling fluid volume was the pressurizer and surge line; however, within the first 80 seconds, (after the initial blowdown phase) this shifted to the RV. Figure 5.2.2-3 shows that the average temperature of the upper plenum was equal to the saturation temperature corresponding to the primary system pressure measured in the upper head during the natural circulation phase and into the ADS phase. The pressure stabilized at the saturation pressure for the upper plenum, and then continued a slow pressure decay responding to the cooling caused by the CMT injection. Figure 5.2.2-1 shows an increase in the pressure decay rate occurred at about 200 seconds, when the CMTs transitioned from natural circulation injection to draindown injection, which essentially doubled the injection rate of cold water into the DVI line. The higher injection rate resulted in a more rapid temperature drop in the upper plenum (core exit in Figure 5.2.2-3), which was reflected in a more rapid pressure decay. With the actuation of ADS-1 at about 374 seconds, the pressure dropped rapidly due to the increased rate of mass ejected from the system (Figure 5.2.2-56), and the increased flow of cold water injected into the downcomer and flowing through the core. This continued to reduce power channel inlet plenum temperature, and subcooled the heater rods in the core due to the higher flow. Since the RV outlet plenum became subcooled at about [ ]^{a,b,c} seconds, the hottest fluid in the system was in the pressurizer, the cold legs, and the CMTs, and the pressure was partially supported by the flashing of the fluid in one or several of these locations. When the accumulator discharge ended (about [ ]^{a,b,c} seconds), the RV temperature again increased to the saturation temperature and took control of the system pressure for the rest of the LOCA phase. Also at the end of accumulator injection, a large amount of noncondensible gas was injected into the primary system, and could have affected the heat transfer performance of the PRHR and the CMTs.

5.2.2.7 Energy Inventory

Heat removal from the reactor core follows a sequence similar to the pressure decay for the small-break LOCA tests. Before reactor trip, nearly all the energy generated in the core is removed by the SGs and out of the break with a small fraction lost to the surroundings. When the reactor tripped, the primary system pumps tripped, and flow through the SG tubes was sharply reduced. Coupled with the isolation of the SG secondary side, the result was to significantly reduce heat removal from the SGs. At that time, the PRHR isolation valves opened, and energy was removed to the IRWST as well as out of the break.

As the system drained, the primary system pressure was reduced, and the sensible heat of the coolant and metal added to the core heat load. The CMTs started to drain, and the ADS activated. At that time, heat removal was accomplished through the ADS flow, and the PRHR became less effective. Finally, ADS-4 actuated, the primary system completely depressurized, and the IRWST actuated. The LOCA phase of the test was then completed.

The behavior of the components involved in the energy removal is discussed below.

Core

The power output of the core is shown in Figure 5.2.2-2. After reactor trip, the core power is representative of decay heat levels expected in the AP600 core. Flow through the core is shown in Figure 5.2.2-56 and the steam generation rate is given in Figure 5.2.2-55. As discussed in Section 4.0, the steam generation rate has been calculated by two methods, the T_{sat} method and the DVI line flow method.

Figures 5.2.2-53, 5.2.2-54, and 4.1.2-55 reproduce the saturation line elevation, power split above the saturation elevation and stream generation rates from the two methods. It can be seen that both methods give similar predictions. It should be noted that neither method gives valid predictions before [ ]^{a,b,c} seconds because of flow oscillations during natural circulation in the primary system.

The maximum steam generation rate during the LOCA phase occurs at approximately [ ]^{a,b,c} seconds, which is just prior to IRWST injection. The peak cladding temperature is shown in Figure 5.2.1-57, and indicates that the core is adequately cooled at all times during the test.

Steam Generator Heat Transfer

The steam generators remove most of the heat from the primary system during normal operation. However, heat transfer from the primary-to-secondary side is significantly reduced after the pumps trip. This is due to reduced flow in the tubes, which causes a sharp reduction in the tube-side heat transfer coefficient. In addition, the secondary side is isolated, which causes the temperature and pressure to remain high as the primary-side pressure rapidly decreases.

PRHR Heat Transfer

The PRHR is designed to remove heat from the primary system from the time when the steam generators become thermally isolated due to the initiation of the ADS. One measure of the effectiveness of the PRHR is the increase in the fluid internal energy in the IRWST, which serves as the heat sink for the PRHR. Figure 5.2.2-20 shows the fluid internal energy in the IRWST during the first [ ]^{a,b,c} seconds of the test. The PRHR begins operating at about [ ]^{a,b,c} seconds as the SG heat removal ends. The heat removal rate is approximately [ ]^{a,b,c} Btu/sec. until [ ]^{a,b,c} seconds when ADS-1 activates. At that time, the heating rate in the IRWST increases to [ ]^{a,b,c} Btu/sec.

due to steam condensing from the ADS 1-3, and heating from the PRHR. The PRHR heat removal decreases when the accumulators discharge at about [ ]^{a,b,c} seconds as the core becomes subcooled.

ADS and Break

The energy removal from the ADS and break are shown in Figure 5.2.2-69. The fluid energy exiting the break increases at a constant rate until ADS-1 is actuated. For ADS-1, ADS-2, and ADS-3, the energy removal occurs at a somewhat lower rate due to reduced system pressure. When ADS-4 is actuated, energy removal switches from ADS 1-3 to the larger flow path ADS-4. The ADS effectively reduced the primary system pressure to allow gravity injection flow from the IRWST. This flow was sufficient to subcool the primary system, ending core boiling and partially collapsing the steam bubble in the upper plenum and bringing the system to near atmospheric pressure.

5.2.2.8 Energy Balance

Figure 5.2.2-74 shows all the energy components in the heat balance for the system during the LOCA phase (0-3000 sec). Throughout the event, the heated rod bundle power was the dominant heat input to the system, and before the start of the event, the steam generators provided the dominant heat removal. At the start of the event, the SG secondary side is isolated, and the reactor coolant pumps trip. During this period, heat removal by the SG is reduced as natural circulation flow occurs in the primary system. As the primary system depressurizes, the pressure reaches the secondary-side pressure, and heat transfer effectively ends.

From the start of the event, the steam component of the break flow is lost from the control volume until the actuation of ADS. Heat loss via this path is nearly [ ]^{a,b,c} Btu/sec., which is far greater than the reactor decay power [ ]^{a,b,c}. The remaining energy lost through the break exhaust consists of a decrease in the fluid internal energy as the primary system depressurizes.

After ADS stage 1-3 is actuated, the break flow effectively ends, and the ADS heat is deposited into the IRWST. Thus, the fluid internal energy in the control volume increases until the end of the LOCA phase, as the IRWST water temperature increases. Also, at this time, the metal masses in the control volume lose energy as primary system temperature decreases. As a result, energy is deposited at a rate of nearly [ ]^{a,b,c} Btu/sec. between [ ]^{a,b,c} seconds. After [ ]^{a,b,c} seconds, the metal masses lose energy at a much lower rate, which is consistent with the primary system fluid temperature decay. Ambient losses are reduced from a maximum of [ ]^{a,b,c} Btu/sec. at full power conditions to [ ]^{a,b,c} Btu/sec. at the end of the LOCA phase.

A large increase is observed in the deficit between the rod bundle power and the various sources of energy dissipation from the control volume after the initiation of ADS 1-3, and again after the initiation of ADS-4 at approximately [ ]^{a,b,c} seconds. The steam exhaust includes steam from the IRWST and the steam portion of the flow from ADS-4. However, little steam is measured by the vapor flow meters. As was discussed in the mass balance, it is likely that the small steam flows from

these sources is not being measured by the vapor flow meters, resulting in a deficit in the energy balance.

TABLE 5.2.2-1

OSU TEST ANALYSIS STANDARD PLOT PACKAGE FOR SECTION 5.2.2

Plot Number	Component	Variables	Units	Description
1	Pressurizer	CPT-604	psia	System pressure
2	RV	RVPWR	kW	Core power
3	RV	T01RV, T08RV, ST08RV	°F	Core inlet/outlet temperature, saturation temperature
4	Steam Generator	CPT-201, CPT-204, CPT-301, CPT-302	psia	Primary and secondary pressures in steam generator
5	DVI-1	WWTDVIL1, WWTIRWI1, WOUTACC1, WWTIRWI3	lbm/sec.	Total flow in DVI-1 and individual components
6	DVI-2	WWTDVIL2, WWTIRWI2, WOUTACC2, WWTIRWI4	lbm/sec.	Total flow in DVI-2 and individual components
7	CMT	AMCMT1B, AMCMT2B	lbm	Fluid mass in CMTs (excludes balance lines)
8	CMT	CLDP-502, CLDP-507	in.	Collapsed liquid level in CMTs
9	CMT	MIWDVIL1, MIWDVIL2, MIWCLBL1, MIWCLBL2	lbm	Integrated mass it to/out of CMTs
10	CMT	WWTDVIL1, WWTDVIL2	lbm/sec.	Flow out of CMTs
11	CMT	WWTCLBL1, WWTCLBL2	lbm/sec.	Flow into CMTs
12	CMT	CLDP-509, CLDP510	in.	Level CL-CMT balance lines
13	CMT	UCMT1, UCMT2	Btu	Fluid energy in CMTs
14	IRWST	IRWST	lbm	Mass of fluid in IRWST
15	IRWST	CLDP-701	in.	Collapsed liquid level in IRWST
16	IRWST	WWTIRWI1, WWTIRWI2	lbm/sec.	Flow from IRWST Tank to DVI lines
17	IRWST	IRWSTOR	lbm/sec.	Overflow from IRWST to sump
18	IRWST	ADS13VR + ADS13LR	lbm/sec.	Total ADS flow into IRWST
19	IRWST	MIIRWI1, MIIRWI2, MIIRWIO	lbm	Integrated mass out of IRWST
20	IRWST	UIRWST	Btu	Fluid energy in IRWST
21	PRHR	CLDP-802	in.	Collapsed liquid level in PRHR heat exchanger

TABLE 5.2.2-1 (Continued)

OSU TEST ANALYSIS STANDARD PLOT PACKAGE FOR SECTION 5.2.2

Plot Number	Component	Variables	Units	Description
22	PRHR	WWOTPRHR	lbm/sec.	Measured outlet flow from PRHR tube
23	Accumulator	AMACC1, AMACC2	lbm	Mass of fluid in accumulators
24	Accumulator	CLDP-401, CLDP-402	in.	Collapsed liquid level in accumulators
25	Accumulator	WOUTACC1, WOUTACC2	lbm/sec.	Flow from accumulators
26	Accumulator	MOUTACC1, MOUTACC2	lbm	Integrated mass out of accumulators
27	Accumulator	UACC1, UACC2	Btu	Fluid energy in accumulators
28	Primary sump	AMPSMP	lbm	Primary sump mass
29	Primary sump	CLDP-901	in.	Primary sump level
30	Primary sump	UPSMP	Btu	Primary sump fluid energy
31	Steam Generator	MSSGIP1, MSSGIP2, MSSGOP1, MSSGOP2	lbm	Mass of fluid in steam generators - primary side inlet/outlet plena
32	Steam Generator	MSSGHT1, MSSGHT2, MSSGCT1, MSSGCT2	lbm	Mass of fluid in steam generators - primary side hot and cold tubes
34	Pressurizer	PZM	lbm	Fluid mass in pressurizer
35	Pressurizer	CLDP-601	in.	Collapsed liquid level in pressurizer
36	Pressurizer	UPZ	Btu	Fluid energy in pressurizer
37	Surge line	PLM	lbm	Fluid mass in surge line
38	Surge line	CLDP-602	in.	Collapsed liquid level in surge line
39	Surge line	UPSL	Btu	Fluid energy in surge line
40	RV	MWRVRV	lbm	Total fluid mass in RV
41	RV	DCM	lbm	Fluid mass in downcomer
42	RV	LDP01DC	in.	Collapsed liquid level in downcomer compared to various reference elevations
43	RV	WM01RV	lbm	Fluid mass in lower plenum
44	RV	MW03RV	lbm	Fluid mass in core region
45	RV	LDP03RV	in.	Collapsed liquid level in core
46	RV	RVXVFO		Core exit void fraction
47	RV	RVXQO		Core exit quality
48	RV	MW06RV	lbm	Fluid mass in the upper plenum
49	RV	LDP06RV	in.	Collapsed liquid level in the upper plenum
50	RV	MW08RV	lbm	Fluid mass in the upper head
51	RV	LDP08RV	in.	Collapsed liquid level in the upper head

TABLE 5.2.2-1 (Continued)

OSU TEST ANALYSIS STANDARD PLOT PACKAGE FOR SECTION 5.2.2

Plot Number	Component	Variables	Units	Description
52	RV	URV	Btu	Total fluid energy in RV
53	RV	RVXE	ft	Level of Tsat line
54	RV	RVPab, RVPbl, RVPWR	kW	Heated rod power above and below Tsat level and total
55	RV	RVRXV	lbm/sec.	Core steam generation rate
56	RV	RVTMRI	lbm/sec.	Calculated core flow
57	RV		°F	Maximum clad temperature, saturation temperature and delta
58	Hot Leg	MWHL1, MWHL2	lbm	Water mass in hot legs
59	Hot Leg	MVHL1, MVHL2	lbm	Vapor mass in hot legs
60	Cold Leg	CL1WMS, CL2WMS, CL3WMS, CL4WMS	lbm	Water mass in cold legs
61	Cold Leg	CL1VMS, CL2VMS, CL3VMS, CL4VMS	lbm	Vapor mass in cold legs
62	ADS and break	BRKSTIR, ADS13TIR, ADS41TIR, ADS42TIR	lbm	Total discharged mass for ADS 1-3, ADS-4s, and break
63	ADS and break	BRKTIVF, AD13TIVF, AD41TIVF, AD42TIVF	lbm	Total integrated vapor flow for ADS and break
64	ADS and break	BRKTILF, AD13TILF, AD41TILF, AD42TILF	lbm	Total integrated liquid flow for ADS and break
65	ADS and break	ADS13SLR, ADS41SLR, ADS42SLR	lbm/sec.	Steam flow out ADS 1-3 and 4
66	ADS and break	ADS13SLR, ADS41SLR, ADS42SLR	lbm/sec.	Liquid flow out ADS 1-3 and 4
67	ADS and break	BRKSSLR	lbm/sec.	Steam flow out of break
68	ADS and break	BRKSSLR	lbm/sec.	Liquid flow out of break
69	ADS and break	BRKSPEI, ADS13EI, ADS41EI, ADS42EI	Btu	Integrated fluid energy for ADS1-3, ADS4, and the break
70	Mass Balance	TOTMASS	lbm	Total system mass inventory
71	Mass Balance	PRIMMASS, PRIMASS2	lbm	Measured primary system inventory and value from mass balance
72	Mass Balance	MERROR	lbm	Mass Balance Error
73	Mass Balance	MIN. MOUT, SRCMASS	lbm	Integrated mass flow in and out of primary system 2 source mass
74	Energy Balance	VARIOUS	Btu	Components of energy balance

THE PLOTS (1-74) LISTED IN TABLE 5.2.2 ARE NOT
INCLUDED IN THIS NONPROPRIETARY DOCUMENT.

5.2.3 Long-Term Transient

The long-term transient covers the transition from IRWST to sump injection and provides information on the long-term cooling response of the AP600. For the 2-inch cold leg break, Test SB18, there were problems with instrumentation beyond 14,300 seconds which means the sump injection phase cannot be analyzed. In this case, the long-term transient covers the [ ]^{a,b,c} seconds time frame. By this time, the initial stages of flow from the primary sump have begun via the check valves around the main injection valves, but the main sump injection valves have not opened. The behavior of the test facility during this period of the transient is discussed in this subsection using the plot package detailed in Table 5.2.3-1. These results concentrate on the components of the primary system that remain active during the long-term cooling phase, that is the RV, the hot legs, ADS-4, the sumps and the IRWST.

5.2.3.1 Reactor Pressure Vessel and Downcomer Mass Distribution

For the long-term transient, the passive core cooling systems must supply sufficient flow to prevent any overheating of the heated rods. At [ ]^{a,b,c} seconds, the decay heat simulation of the heated rods reduced the power from [ ]^{a,b,c} kW (Figure 5.2.3-1). As seen in Figure 5.2.3-38, there are no significant excursions in heated rod temperatures and therefore sufficient core flow has been maintained throughout the long-term transient.

The mass of water in the reactor pressure vessel is shown in Figure 5.2.3-25. After an initial decline, the reactor vessel water mass settled at an average value of around [ ]^{a,b,c} lbm where it remained until the end of the analysis. From [ ]^{a,b,c} seconds, oscillations in vessel inventory can be observed. These oscillations can be seen in measurements throughout the primary circuit and they are discussed further in Section 6.1.3.

The core water mass and collapsed-liquid level are shown in Figures 5.2.3-28 and 5.2.3-29. During the analysis, the core remained near water-solid with only a low level of boiling (Figure 5.2.3-36). The level at which the core fluid reached saturation temperature was around 45 inches for the period of the analysis (Figure 5.2.3-34). Figure 5.2.3-29 shows that at the end of the analysis, the effect of the hotter water arriving from the sump was detected as a decreased core collapsed liquid level.

The collapsed-liquid level in the upper plenum region is shown in Figure 5.2.3-32. During the period before sump injection began, the collapsed-liquid level in the upper plenum remained at the top of the hot legs. Following the start of the influx of hot water from the sumps, the level dropped to the middle of the hot legs.

The mass of fluid and collapsed-liquid level in the RV downcomer are shown in Figures 5.2.3-26 and 5.2.3-27. Before sump injection begins the collapsed-liquid level in the downcomer is at the level of the center of the cold legs. By the end of the analysis, the effect of the initial stages of sump injection cause the downcomer collapsed-liquid level to fall to the hot leg elevation.

5.2.3.2 Loop Mass Distribution

As discussed, the long-term cooling phase of the transient shows that there is a low level of boiling in the upper regions of the core. However, analysis of the long-term transient is not detailed enough to track the behavior of this steam.

5.2.3.3 Mass Ejected from the Primary System

The integrated-mass flow out of the primary system via the ADS systems and the break are shown in Figure 5.2.3-43. By the end of the analysis, [ ]^{a,b,c} lbm of water has flowed out of the primary system. It can be seen that during the long-term cooling phase of the transient, the only significant out flow is through the ADS stage 4 valves with a small apparent flow through the break. The apparent break flow does not represent a flow out of the primary system, but indicates continued interaction between the break separator and the sump. The most marked manifestation of this interaction is at 1300 seconds when the primary sump begins to overflow into the secondary sump. This causes oscillating flow indications in the liquid flow out of the break separator. This is confirmed by Figures 5.2.3-44 to 5.2.3-45 which show the flows through the ADS and break. During the sump injection phase of the transient, outflow was in the form of liquid out of the ADS stage 4 valves. Water flowed through each of these at an average rate of [ ]^{a,b,c} lbm/sec. There was no measurement recorded from the vortex meters to show steam escaping from the system via ADS-4. However, as discussed in Section 6.1.3, it is believed that steam is leaving the system by this route.

At approximately [ ]^{a,b,c} seconds into the transient, the level in the primary sump (Figure 5.2.3-14) reached the point at which overflow to the secondary sump occurred. At that time, there was [ ]^{a,b,c} lbm of water collected in the primary sump. From the beginning of primary sump overflow to the end of the analysis [ ]^{a,b,c} lbm of water was transferred to the secondary sump.

5.2.3.4 Mass Injected to the Primary System

The total DVI line flow CMT flow and IRWST flows are shown in Figures 5.2.3-6 and 5.2.3-7, and the flow from the primary sump is shown in Figure 5.2.3-19. It can be seen that from around [ ]^{a,b,c} seconds, there is a contribution to the DVI flow from the CMTs, as they finish their post refill draindown.

During the presump injection phase of the transient, the IRWST flow proceeded at a gradually reduced rate, with the effect of the primary system oscillations superimposed. At [ ]^{a,b,c} seconds, flow from the primary sump began through the check valves around the main injection valves. At the end of the analysis, the level in the IRWST tank fell to [ ]^{a,b,c} inches, which is above the level at which the primary sump injection valves open.

5.2.3.5 Mass Balance

Figure 5.2.3-46 shows the variation in the total system mass inventory during the entirety of Test SB18. Following the short-term transient, total inventory increased by [ ]^{a,b,c} lbm to approximately [ ]^{a,b,c} lbm above the initial value at the time sump injection around the main valve started. The initiation of sump injection led to [ ]^{a,b,c} lbm increase in inventory. Due to the loss of instrumentation, analysis of the long-term transient did not continue enough to determine whether any inventory was lost as steam.

The mass-balance calculation described in Section 5.2.2-5 was performed for the entirety of the transient, and the results are presented in Figures 5.2.3-47 to 5.2.3-49. From 3000 to 13,600 seconds the error remained between ± 100 lbm. Following the overflow from the primary to secondary sump the error increases. The complete interaction between the break separator, sumps and cold legs has not been fully investigated at this stage.

5.2.3.6 Energy Balance

Figure 5.2.3-50 shows all the energy components in the heat balance for the system during the long-term cooling (LTC) phase. The LTC phase for this test was abbreviated because of instrumentation problems. During this phase, the heated rod bundle power was the dominant heat input to the system. The steam generator heat transfer ended during the LOCA phase and did not contribute to the overall energy balance during the LTC phase. Thus, for the LTC phase, the active components in the overall energy balance are the rod bundle power, the change in the fluid internal energy, the change in the metal internal energy, and ambient losses, and the steam exhaust from the control volume.

The fluid energy in the control volume increased steadily until sump injection began {(approximately 15,000 sec.)}^{a,b,c}. At that time, the fluid throughout the system approached saturated conditions, and the rate of increase was lower. At the same time, the metal mass temperatures increased as the primary system temperature increased. Also, the ambient losses increased slightly as the control volume temperatures increased.

The steam component of the ADS stage 4 flow was lost from the control volume from the actuation of ADS-4. For times subsequent to the LOCA phase, this quantity is essentially zero, as measured by the vapor flow meters. It is concluded that the vapor flow meters in the ADS-4 separators did not measure the relatively small steam flow rates accurately, and this accounts for the energy balance deficit.

TABLE 5.2.3-1
OSU TEST ANALYSIS PLOT PACKAGE FOR SECTION 5.2.3
LONG-TERM TRANSIENT

Plot No.	Component	Variables	Units	Description
1	RV	RVPWR	kW	Core power
2	Primary sump	TSMPI1, TSMPI2	°F	Sump injection line temperatures
3	DVI	TDVIL1, TDVIL2	°F	DVI line temperatures
4	RV	T01DC, T02DC, T03DC, ST01DC	°F	Water and saturation temperatures in downcomer
5	RV	T01RV, T08RV, ST08RV	°F	Core inlet/outlet temperature, saturation temperature
6	DVI-1	WWTDVIL1, WWTIRWI1, WOUTACC1, WWTIRWI3	lbm/sec.	Total flow in DVI-1 and individual components
7	DVI-2	WWTDVIL2, WWTIRWI2, WOUTACC2, WWTIRWI4	lbm/sec.	Total flow in DVI-2 and individual components
8	CMT	CLDP-502, CLDP-507	in.	Collapsed liquid level in CMTs
9	CMT	CLDP-509, CLDP510	in.	Level CL-CMT balance lines
10	IRWST	IRWST	lbm	Mass of fluid in IRWST
11	IRWST	CLDP-701	in.	Collapsed liquid level in IRWST
12	IRWST	UIRWST	Btu	Fluid energy in IRWST tank
13	Primary sump	AMPSMP	lbm	Primary sump mass
14	Primary sump	CLDP-901	in.	Primary sump level
15	Primary sump	UPSMP	Btu	Primary sump fluid energy
16	Secondary sump	AMSSMP	lbm	Secondary sump mass
17	Secondary sump	CLDP-902	in.	Secondary sump level
18	Secondary sump	USSMP	Btu	Secondary sump fluid energy
19	Primary sump	WSTSMPET, WWTSMPIT	lbm/sec.	Primary sump steam and liquid injection rate
20	Primary sump	MISMPI1, MISMPI2, MISMPIT	lbm	Integrated primary sump and IRWST flows
21	SG	MSSGIP1, MSSGIP2, MSSGOP1, MSSGOP2	lbm	Mass of fluid in SGs - primary side inlet/outlet plena
22	Surge line	PLM	lbm	Fluid mass in surge line

TABLE 5.2.3-1 (Continued)
OSU TEST ANALYSIS PLOT PACKAGE FOR SECTION 5.2.3
LONG-TERM TRANSIENT

Plot No.	Component	Variables	Units	Description
23	Surge line	CLDP-602	in.	Collapsed liquid level in surge line
24	Surge line	UPSL	Btu	Fluid energy in surge line
25	RV	MWRV	lbm	Total fluid mass in RV
26	RV	DCM	lbm	Fluid mass in downcomer
27	RV	LDP01DC	in.	Collapsed liquid level in downcomer compared to various reference elevations
28	RV	MW03RV	lbm	Fluid mass in core region
29	RV	LDP03RV	in.	Collapsed liquid level in core
30	RV	RVXVFO		Core exit void fraction
31	RV	RVXQO		Core exit quality
32	RV	LDP06RV	in.	Collapsed liquid level in the upper plenum
33	RV	MW08RV	lbm	Fluid mass in the upper head
34	RV	RVXE	ft	Level of Tsat line
35	RV	RVPab, RVPbl, RVPWR	kW	Heated rod power above and below Tsat level and total
36	RV	RVRXV	lbm/sec.	Core steam generation rate
37	RV	RVTMRI	lbm/sec.	Calculated core flow
38	RV		°F	Maximum clad temperature, saturation temperature and delta
39	Hot leg	MWHL1, MWHL2	lbm	Water mass in hot legs
40	Hot leg	MVHL1, MVHL2	lbm	Vapor mass in hot legs
41	Cold leg	CL1WMS, CL2WMS, CL3WMS, CL4WMS	lbm	Water mass in cold legs
42	Cold leg	CL1VMS, CL2VMS, CL3VMS, CL4VMS	lbm	Vapor mass in cold legs
43	ADS and break	BRKSTIR, ADS13TIR, ADS41TIR, ADS42TIR	lbm	Total discharged mass for ADS 1-3, ADS-4s, and break
44	ADS and break	ADS13SLR, ADS41SLR, ADS42SLR	lbm/sec.	Liquid flow out ADS 1-3 and 4
45	ADS and break	BRKSSLR	lbm/sec.	Liquid flow and total flow out of break
46	Mass balance	TOTMASS	lbm	Total system mass inventory
47	Mass balance	PRIMMASS, PRIMASS2	lbm	Measured primary system mass and valve from mass balance
48	Mass balance	MERROR	lbm	Mass balance error
49	Mass balance	MIN, MOUT, SRCMASS	lbm	Integrated mass flow in and out of primary system and source mass
50	Energy balance	Various	Btu	Components of energy balance

THE PLOTS (1-50) LISTED IN TABLE 5.2.3 ARE NOT INCLUDED IN THIS NONPROPRIETARY DOCUMENT.

6.0 TEST FACILITY PERFORMANCE

This section discusses the following test analysis issues common to the matrix testing performed at Oregon State University (OSU):

- Observed thermal-hydraulic behavior, including the phenomena associated with core makeup tank (CMT) refill and oscillation in the reactor
- Passive residual heat removal (PRHR) performance
- Results of the mass and energy balance

The repeatability of test data derived from comparisons between Matrix Tests SB01 and SB18, each a 2-in. loss-of-coolant accident (LOCA) in CL-3, is reviewed and evaluated.

Accumulator nitrogen dispersal and recollection will be addressed in the next revision of this report.

6.1 Observed Thermal-Hydraulic Phenomena

The following thermal-hydraulic phenomena, observed during the matrix test program and identified in the *AP600 Low-Pressure Integral Systems Test at Oregon State University, Final Data Report*, WCAP-14242[1] are evaluated:

- CMT refill, which appeared to be the result of condensation in the CMT after initial injection and draindown
- PRHR performance
- Causes of pressure and liquid level oscillations in the reactor

6.1.1 CMT Reflood Response

Upon initiation of CMT draindown, incoming steam from the reactor coolant system (RCS) via the cold-leg balance line heated the CMT inside wall surfaces. Figure 6.1.1-1 represents the average fluid and metal temperatures and inside heat flux for one metal segment in the upper head of CMT-1 based on Matrix Test SB18; Figure 6.1.1-2 represents the same parameters for CMT-2. Given the sign convention used in the OSU data analysis code, the negative heat flux represents heat in the metal CMT walls.

Following initial draindown, the CMTs and respective cold-leg balance lines emptied and contained steam and, possibly, some quantity of noncondensable gas. As the uninsulated CMTs continued to transfer heat to the environment, steam condensed in the CMTs, resulting in a decrease in CMT pressure relative to primary system pressure. This decrease in CMT pressure resulted in a proportional increase in the cold-leg balance line level (Figure 6.1.1-3) which was sufficient to cover and refill the cold legs. When the cold-leg balance line completely refilled, water entered or sprayed into the CMT through the inlet diffuser, resulting in rapid condensation of steam in the CMT and a corresponding rapid additional decrease in CMT pressure (Figure 6.1.1-4). The sudden decrease in pressure resulted in a quick refill of the CMT through the balance line (Figure 6.1.1-5).

Refill of subcooled fluid resulting in a CMT condensation/depressurization event is reflected in the reactor vessel mass (Figure 6.1.1-6). The event is also reflected in the cold-leg water levels (Figure 6.1.1-7).

The CMT reflood event continued until the cold legs uncovered in the reactor vessel downcomer. Figure 6.1.1-8 shows that the end of the reflood event correlates to the downcomer level and, additionally, that this level corresponds to the top of the cold-leg nozzles located at about the 71-in. elevation. The system water inventory, available prior to uncovering the cold legs, was sufficient to refill the CMT to about two-thirds full; therefore, the CMT reflood event was terminated prior to the entire CMT refilling.

CMT refill also resulted in a rapid decrease in CMT internal fluid and metal temperatures, with resultant positive heat fluxes as the energy stored in the heated metal was transferred to the subcooled liquid.

The phenomena that drives the CMT reflood response is identical for both CMT and whichever CMT refills first is random. However, once the reflood event was initiated in a particular CMT, the accompanying depressurization in system levels precluded the event from taking place in the remaining CMT until the first reflood event terminated and the system levels were restored by IRWST injection. This characteristic is illustrated in Figure 6.1.1-9, which shows that the CMT-1 balance line level was depressed as a result of CMT-2 refill. Immediately, following recovery of the downcomer level, the CL-3/CMT-1 balance line began to refill; as soon as the balance line level recovered to completely full, the CMT-1 refill event was initiated.

The CMTs refill with ease in the OSU test because of the facility's one-quarter height scaling. The decrease in CMT pressure, which lifted the liquid up and filled the cold-leg balance line, was only about 3.4 psi (Figure 6.1.1-3). This corresponds to an absolute CMT pressure of about 11.3 psia in the OSU test. In comparison, the pressure decrease in the AP600 plant would have to be about 13.4 psi. Since the reactor system is nearly at containment pressure, about 17 to 19 psia for a small-break LOCA during this period, the CMTs would have to be at an absolute pressure of about 4.6 psia. Other factors that could influence the potential for, as well as the timing of, a CMT refill include: energy stored in the CMT metal, heat loss to the environment, and presence of noncondensables in the CMT.

While it is possible that CMT refill could occur in the AP600, and evidence of the CMT balance line beginning to refill was observed in SPES-2 the ease by which the CMTs refilled in the OSU test is believed to be a result of a scaling distortion. Subsequently, refill of the CMTs would be less likely to occur in the AP600 than in the OSU test.

TABLE 6.1.1-1 OSU TEST ANALYSIS PLOT PACKAGE FOR SECTION 6.1.1				
Plot No.	**Component**	**Variables**	**Units**	**Description**
1	CMT	-	°F Btu/sec.	CMT-1 Average fluid and metal temperatures and upper head heat flux
2	CMT	-	°F Btu/sec.	CMT-2 Average fluid and metal temperatures and upper head heat flux
3	CMT	-	psia in.	Effect of CMT pressure on balance line level
4	CMT	-	lbm/sec. psia	Effect of flow from CMT balance line on CMT pressure
5	CMT	-	psia in.	CMT Refill - response to CMT pressure decrease
6	CMT	-	in. lbm	Effect of CMT refill on RPV mass
7	CMT	-	in.	Effect of CMT refill on cold-leg level
8	CMT	-	in.	Effect of CMT refill on downcomer level
9	CMT	-	in.	Effect of CMT refill on balance line and downcomer levels

THE PLOTS (1-9) LISTED IN TABLE 6.1.1 ARE NOT
INCLUDED IN THIS NONPROPRIETARY DOCUMENT.

6.1.2 PRHR Performance

Passive residual heat removal (PRHR) is designed to remove core decay heat in the event that the active safety systems are not available. The heat exchanger (HX) consists of a series of tubes in the in-containment refueling water storage tank (IRWST) that are connected to the hot leg (inlet) and pump suction (outlet). The tubes enter the tank a few feet below the surface and exit the tank near the bottom. At normal operating conditions, the PRHR HX is isolated from the primary system. In the event of an accident, the isolation valves are opened and natural circulation flow is established, driven by the density difference between the hot fluid entering the PRHR HX and the cold fluid exiting the PRHR HX. Heat is transferred from the tubes to the IRWST water by either subcooled boiling or free convection.

This section will determine the heat transfer characteristics of the OSU representation of the PRHR HX/IRWST. Heat transfer from the PRHR HX tubes to the IRWST is determined by observing the increase in the internal energy of the IRWST water. The PRHR HX is the sole source of energy input into the IRWST until the actuation of the automatic depressurization system (ADS) stages 1-3. After this time, PRHR heat transfer is determined by:

$$Q_{PRHR} = \left(\frac{dU}{dt}\right)_{IRWST} - Q_{ADS13} \qquad 6.1.2\text{-}1$$

where:

Q_{PRHR}	=	Heat transferred from PRHR HX
$(dU/dt)_{IRWST}$	=	Time rate of change of IRWST water internal energy
Q_{ADS13}	=	Heat transferred from ADS 1-3 flow

Equation 6.1.2-1 can be integrated:

$$\int Q_{PRHR}\,dt = (U - U_o)_{IRWST} - \int Q_{ADS13}\,dt \qquad 6.1.2\text{-}2$$

Water temperature in the IRWST was measured at axial locations. By associating a volume with each of these measurements, a total fluid internal energy was calculated for each time step. The difference between this value and the internal energy of the tank at the start of the test is used in Equation 6.1.2-2 to determine the total PRHR energy transferred until the actuation of ADS 1-3. No evaporative heat loss from the IRWST was considered in this calculation.

6.1.2.1 Matrix Test SB01

The calculated PRHR HX performance for Matrix Test SB01 is shown in Figure 6.1.2-1, which indicates that PRHR transferred heat at a rate of about [ ]^{a,b,c} Btu/sec. from the initiation of the event until the actuation of ADS 1-3 ([ ]^{a,b,c} seconds). During this time, the increase in the internal energy of the IRWST water is equivalent to the total PRHR energy transfer. When ADS 1-3 actuated, the PRHR heat transfer dropped rapidly to zero, and the subsequent heating of the IRWST water was due to ADS flow. At about [ ]^{a,b,c} seconds, IRWST draining was initiated, and the heat balance described in Equation 6.1.2-2 is no longer valid.

6.1.2.2 Matrix Test SB18

Similar results were observed for Matrix Test SB18. The calculated PRHR HX performance for Matrix Test SB18 is shown in Figure 6.1.2-2, which indicates that PRHR transferred heat at a rate of about [ ]^{a,b,c} Btu/sec. from the initiation of the event until the actuation of ADS 1-3 ([ ]^{a,b,c} seconds). During this time, the increase in the internal energy of the IRWST water is equivalent to the total PRHR energy transfer. When ADS 1-3 actuated, the PRHR heat transfer dropped rapidly to zero, and the subsequent heating of the IRWST water was due to the ADS flow. At about 1000 seconds, IRWST draining was initiated, and the heat balance described in Equation 6.1.2-2 is no longer valid.

These results indicate that the PRHR HX operated as designed in removing core decay heat from the initiation of the event until ADS actuation. After ADS actuation, the PRHR HX is no longer utilized as a significant energy removal path.

TABLE 6.1.2-1 OSU TEST ANALYSIS PLOT PACKAGE FOR SECTION 6.1.2				
Plot No.	**Component**	**Variables**	**Units**	**Description**
1	PRHR / IRWST	U-U0IRW, UPRHR, ADS13EI	Btu	PRHR Performance for Matrix Test SB0i
2	PRHR / IRWST	U-U0IRW, UPRHR, ADS13EI	Btu	PRHR Performance for Matrix Test SB18

THE PLOTS (1-2) LISTED IN TABLE 6.1.2 ARE NOT INCLUDED IN THIS NONPROPRIETARY DOCUMENT.

6.1.3 Observed Oscillations During Long-Term Cooling

Cyclic flow, pressure, level, and temperature oscillations were observed in most of the matrix tests performed at the OSU test facility. These oscillations occurred during the latter stage of the IRWST injection phase for SBLOCA simulations. Several possible causes of these oscillations, and the extrapolated effect in the AP600 are presented in this section.

The fluid paths in the reactor vessel during IRWST injection are schematically illustrated in Figure 6.1.3-1. Coolant from the IRWST enters the downcomer through two DVI lines located 180 degrees apart. This coolant flows down through the downcomer and up through the core, where the electrical heaters generate steam. The two-phase water/steam mixture exits the core. Liquid (and possibly some steam) is released from the reactor vessel through the hot legs and ADS-4 lines, which are open during this phase. Steam is separated from the liquid in the upper head and flows into the downcomer through a series of ten small holes in the downcomer top plate. The steam condenses on the surface of the colder fluid in the downcomer.

6.1.3.1 Oscillations Observed in Matrix Tests SB01 and SB18

Oscillating behavior of the primary coolant in Matrix Tests SB01 and SB18 is shown in Figures 6.1.3-2 and 6.1.3-3 which correlate the upper plenum level (LDP-113) with time for these tests. The main oscillations started at about 8800 and 9100 seconds, respectively, for these tests and persisted for about 4000 seconds. Oscillations of lower amplitude and higher frequency continued through the end of the tests. These lesser oscillations were probably caused by boiling effects in the upper portion of the core heaters. In Matrix Test SB18, DAS Rack 1, which contained the level channel as well as other data channels pertinent to these oscillations, failed after about 14,500 seconds. However, the failure occurred after the main oscillations had stopped and, therefore, did not affect the availability of data for the evaluation of the main oscillation phenomena.

The key features of the oscillations for these tests are summarized in Table 6.1.3-1. The oscillations exhibited several common characteristics:

- The oscillations began after steam was generated in the core during IRWST injection.
- The oscillations were regular with a period of 136 seconds for Matrix Test SB01 and 100 seconds for Matrix Test SB18.
- The oscillations started gradually and ended gradually.

Although these general characteristics are similar, they differ slightly in detail. The most striking difference is the period of the oscillations: 136 seconds for Matrix Test SB01 and 110 seconds for Matrix Test SB18. Another difference is in the timing: Matrix Test SB01 oscillations began at 9100 seconds and ended at 13,000 seconds, compared with Matrix Test SB18 where the oscillations began

at 8830 seconds and ended at 13,450 seconds. These differences are discussed in the next section after the hypothesized mechanism causing these oscillations is described.

The behaviors of the CMTs are significantly different for these two tests. During Matrix Test SB01, both CMTs partially drained. The water levels were 17 and 34 in., respectively for CMT-1 and CMT-2, when the oscillation terminated. In Matrix Test SB18, CMT-1 drained completely during the oscillation period, while the water level was 10 in. in CMT-2 when the oscillations ended.

Upper plenum temperatures (TF-170) for Matrix Tests SB01 and SB18 are compared during an expanded time span (10,000 to 11,000 seconds) in Figure 6.1.3-4. The average temperatures were about the same at 175° to 177°F, but the range of the temperature oscillations were slightly greater for Matrix Test SB01 (168° to 181°F) than for Matrix Test SB18 (171° to 180°F). These temperatures were less than saturation even though there was boiling in the core because this thermocouple (TF-170) was located near the core barrel and just above the upper core support plate. A relatively stagnant liquid layer along the wall was supported by the two-phase flow exiting through the holes in the upper core support plate. Heat transfer from this water layer to the cooler water in the downcomer resulted in temperatures below saturation in this region. The only two thermocouples in the upper plenum were located in the same region, 180 degrees apart. These temperatures can be used to evaluate the temperature variations during the oscillating period.

Pressure in the upper head (PT-107) for Matrix Tests SB01 and SB18 is shown in Figure 6.1.3-5 during the same expanded period used for the temperature comparison. Average pressure in the upper head was about 1 psig for both tests. Pressure ranged from 0.7 to 1.3 psig for both tests. The difference between the maximum and the minimum pressure during one cycle was slightly greater for Matrix Test SB01 (about 0.6 psi) compared with Matrix Test SB18 (0.4 to 0.5 psi).

Compensated upper plenum levels (LDP-113) for Matrix Tests SB01 and SB18 are compared in Figure 6.1.3-6 during the same expanded period used for the temperature and pressure comparisons. The average collapsed level of Matrix Test SB01 was about 10 in., while the average collapsed level for Matrix Test SB18 was slightly lower, about 9 in. The centerline of the hot legs corresponded to a level of 8-1/2 in. for this measurement. The difference in level per cycle was greater for Matrix Test SB01 (about 5-1/2 in.) compared to Matrix Test SB18 (about 3 in.). This difference was consistent with the larger pressure differences during the oscillations in these tests.

The relationships between pressure/temperature/level near atmospheric pressure are:

$$1 \text{ psi} = 3.3°\text{F} = 28.4 \text{ in.}$$

Therefore, the observed pressure difference of 0.6 psi in Matrix Test SB01 would increase the saturation temperature by 2°F and the level by 17 in. Since level changes less than this were observed, this infers that the pressure in the downcomer was somewhat out-of-phase with the upper head pressure.

6.1.3.2 Proposed Mechanism

Three candidate mechanisms for these oscillations observed during LTC were investigated and are described and evaluated in this section. The observed oscillations may be a combination of all the postulated mechanisms given below. The candidate mechanisms are:

- Level fluctuations in the upper plenum opened and closed the steam vent path at the hot-leg nozzle. Level fluctuations were driven by pressure changes resulting from alternately covering and uncovering the hot-leg nozzle.

- Slug flow in ADS-4 lines caused pressure surges when the steam slugs discharged into the separator, by changing the two-phase flow regime and pressure drop in these lines.

- Pressure fluctuations were driven by changes in condensation rates for steam flowing from the upper head and condensing in the downcomer.

Fluctuating Level About the Hot-Leg Nozzle

In this mechanism, steam pressure in the reactor head increased because all the steam generated in the core was not released with the two-phase flow vented through the ADS-4 lines. As pressure in the reactor head increased, the level in the reactor upper plenum decreased until the hot-leg nozzle became uncovered by the two-phase fluid. When the nozzle became uncovered, steam was vented from the upper plenum and reactor head. As steam was vented, pressure decreased and the fluid level in the upper plenum rose until the hot-leg nozzle was covered. When the hot-leg nozzle became covered, again, pressure started to rise. This cycle continued to repeat until the fluid level in the upper plenum decreased below the hot leg so that steam was continuously vented through the ADS-4 lines. When steam could flow through the hot leg and ADS-4 lines without restriction, steam was not available to accumulate in the reactor head, and the pressure increase/level decrease fluctuations halted.

Figures 6.1.3-1 and 6.1.3-2 show the collapsed levels in the upper plenum for Matrix Tests SB01 and SB18, respectively. For this particular level instrument, the relative position of the hot-leg nozzle is:

Top of hot leg	11.0 in.
Centerline of hot leg	8.5 in.
Bottom of hot leg	6.0 in.

The average collapsed level did not decrease until about 1000 seconds after the oscillations stopped. Therefore, the hot-leg steam venting path did not change significantly when the oscillations stopped.

Based on a pressure change of 0.3 psi in the upper head and the steam generation rate (0.05 lb/sec.), it would require only a net accumulation of 0.2 percent of the steam generated to provide this pressure rise in 50 seconds (one half the period — i.e., the time during a cycle when the pressure was

increasing). The net steam accumulation in the reactor head was the difference between the steam generated less the steam vented through the ADS-4 lines and the steam flowing into the downcomer. It is more likely that this steam accumulation was a large fraction of the steam production based on the flow analysis of the ADS-4 line discussed later. A larger rate of steam accumulation would result in a much smaller period for the oscillations than that which was observed.

Because the oscillations ended before the level changed significantly in the upper plenum, and because of the predicted short period for the range of steam accumulation rates, it appears that level fluctuations about the hot leg nozzle are not a probable mechanism for the observed flow oscillations.

Slug Flow in ADS-4 Lines

Oscillations could be produced if slug flow existed in the ADS-4 lines. When the alternate slugs of vapor and liquid discharge into the separator, pressure pulses that would be propagated through the system could be generated.

To investigate this possibility, several approaches were used. First, the flow regime in the hot legs and ADS-4 lines were estimated using the flow pattern map (Figure 6.1.3-7) published by Baker.[15] Based on the measured liquid flow from the ADS-4 separators, the calculated steam flow through the ADS-4 lines (calculated from the total steam generated in the core less the steam flow to the downcomer calculated from the pressure difference across the flow holes in the downcomer top), and the flow areas of the piping, flow in the 5-in. hot leg and 1 1/2 in. ADS-4 line were in the stratified and slug regime, respectively (Figure 6.1.3-7). The calculated transport time through the hot leg and ADS-4 line based on an average volume for the steam/liquid mixture is about 5 seconds.

Several analyses were performed to determine the flow characteristics in the ADS-4 lines during the long-term oscillations. These analyses are discussed in the following sections.

Steam flow measured downstream of ADS-4 steam/water separator is shown in Figure 6.1.3-8. Figure 6.1.3-8 shows that, before 5000 seconds, there was steam flow in the line. Between 5000 and 8000 seconds, there was no steam flow in the ADS-4 line, because the core did not generate steam. (Figure 6.1.3-10 shows the steam generation rate in the core.) After 8000 seconds, the core did generate steam; however, Figure 6.1.3-8 shows that the steam flow rate in the ADS-4 line was very small, except for a few spikes with very short durations that may have been slugs of steam. Figures 6.1.3-9 and 6.1.3-11 are the enlarged plots of Figures 6.1.3-8 and 6.1.3-10, respectively. Figure 6.1.3-4 shows that a spike of steam flow occurred at 9340 seconds. The magnitude of the spike was smaller than one half of the peak flow rate in Figure 6.1.3-11. That is, the steam flow meter used to measure steam flow in the ADS-4 line was sensitive enough to measure the steam flow rate that would have come from the vessel. Yet Figure 6.1.3-9 shows that the steam flow rate in the ADS-4 line was so small that it was below the flow meter's detection limit for most of the time. Since the duration of steam flow may be less than the 8-second scanning time for the data acquisition system (DAS) during this phase of the test, it is possible that some slugs of steam could have been

undetected. However, the data analyses for transport time confirm that steam flow was intermittent and small, so that transport time was affected.

The transportation time of fluid in the ADS-4 line computed by assuming that flow was single-phase liquid agreed with the time lag between the flow oscillations in the vessel and the downstream of the ADS-4 steam/water separator. The oscillation is a marker that can be used to trace fluid. That is, the time lag between flow oscillations in the vessel and downstream of the ADS-4 steam/water separators should be equal to the transportation time of the fluid between these two locations. Since the vessel flow rate has been computed for steam but not for liquid, the steam flow rate will be used for the vessel, while the liquid flow rate will be used for the ADS-4 line in the oscillation time-lag calculation. Figure 6.1.3-11 shows the oscillation of steam flow in the vessel, and Figure 6.1.3-12 shows the oscillation of liquid flow at the downstream of the ADS 4-1 separator. The time lag between the oscillations was about 38 seconds. On the other hand, assuming that flow in the ADS-4 line and the hot leg were single-phase liquid and that the fluid was travelling at the average flow rate of 0.57 lbm/sec., the transportation time is calculated to be 36 seconds. This time lag is about the same as the time lag between the two oscillations, which was 38 seconds. This indicates that the hot leg flow was primarily single-phase liquid .

Further evidence is that the DP measurement (LDP-112) at the inner barrel wall above the core plate and the temperature (TF-170 as discussed in Section 6.1.3.1) indicated that this region was liquid-solid with an annular liquid region above the upper core plate. Therefore, this liquid is more likely to flow into the hot leg and the ADS-4 line.

The above discussion suggests that the hot-leg flow was primarily liquid and that an occasional vapor bubble flowed down the hot-leg and out of the ADS-4 valve.

Slug Flow

- It is extremely unlikely that the slugs of steam in the two ADS-4 lines would be exactly synchronized so that the period would be as regular as observed.

- The measured time lags for the ADS-4 oscillations agreed with the calculated time lag for single-phase liquid flow.

- Two-phase flow pressure variations would be random and would occur at a shorter period than the observed 100 seconds.

Liquid Flow

- If the flow through the ADS-4 lines were completely liquid, there would be no pressure pulses because of vapor/liquid slugs. The observed flow oscillations would have originated from pressure pulses driven by another source in this case.

Downcomer Condensation/Fluctuations

A large fraction of the steam in the upper head flowed through the ten holes (0.20-in. diameter) in the top of the downcomer, and was condensed on the surface of the coolant in the downcomer. Steam flow into the downcomer has been estimated by the three following methods:

- Pressure drop measurement (DP-130) across the downcomer top plate (i.e., across the flow holes)
- Heat balance based on the temperature rise of flow through the downcomer
- Total steam generation assuming there was no steam flow through the ADS-4 line (based on previous discussion of transport analysis of flow in the ADS-4 line)

The results of these methods provide a range of estimated steam flow into the downcomer as summarized below:

Method	Steam Flow to Downcomer (lb/sec.)
Pressure drop across downcomer top	0.015
Heat balance	0.02
Core heat generation	0.03

During the IRWST injection phase, the temperature of the injection flow into the downcomer slowly increased. This temperature increased with time (Figure 6.1.3-13) because the water in the IRWST had been heated by steam released through the ADS 1-3 lines. Steam production in the core started at about 8100 seconds (Figure 6.1.3-14). The existing steam bubble in the upper head was superheated and was gradually being cooled by heat loss through the reactor head. When steam produced in the core mixed with the superheated steam, the steam temperature in the upper head began to decline. The start of this temperature reduction, which occurred at about 8100 seconds, indicated the initiation of steam production in the core.

The oscillations began about 1000 seconds after the initiation of steam production in the simulated core. Therefore, the initiating event for the oscillations was not simply the onset of boiling in the simulated core. However, the temperature difference between coolant in the downcomer (TF-147) and steam in the downcomer vapor space decreased about 30 percent during the period from the initiation of steam production and the start of the oscillations. The oscillations began when the temperature of the downcomer coolant became so high that condensation could not condense all the steam flowing from the upper plenum to the downcomer. The pressure then increased in the downcomer causing

flow from the upper head to decrease. Since steam continued to be generated, pressure in the upper head increased, raising flow through the ADS-4 line and decreasing IRWST flow. Increased flow in the ADS-4 line reduced steam pressure which decreased steam flow to the downcomer. The level change in the downcomer because of the pressure change also caused some mixing of coolant at the steam/liquid interface, and enhanced the condensation rate. The enhanced condensation tended to reduce pressure in the downcomer and upper head. As the steam-downcomer liquid interface increased in temperature from the collecting condensate, the condensation rate decreased below the rate of steam flowing into the downcomer, and pressure began to rise again. Thus, this cycle was repeated producing the observed oscillations.

It is possible that a layer of saturated liquid formed on the liquid interface and caused condensation to stop completely. If so, it is the increase in steam saturation temperature from the pressure increase, and mixing from the level change that would tend to initiate condensation again. This process would result in the observed oscillating behavior.

The oscillations ceased when the level in the downcomer decreased sufficiently that the cold leg was uncovered, and steam could be released through the cold leg instead of increasing pressure in the downcomer vapor volume and reactor upper head. Since the level changes required to release steam through the cold leg were too small to be determined from the level measurement, the presence of steam in the CMTs was used to indicate initial release of steam through the cold leg. Figure 6.1.3-15 shows a rise in CMT temperature slightly before the oscillations stopped, supports the uncovering of the cold leg as the termination mechanism for the oscillations.

The downcomer condensation model is the most probable explanation for the long-term oscillations. This conclusion is supported by the following observations:

- Both the start and the end of the oscillations were gradual. This is consistent with the slow increase in IRWST temperature at the onset of the oscillations and the gradual decrease in downcomer liquid level at the end of the oscillations.

- The oscillations were regular and smooth, which would result from changes in a process, such as condensation, where a very small driving temperature exists.

- Oscillations stopped when steam was vented through the cold leg to the CMT (and also through the break).

- The level and pressure oscillations were 180 degrees out of phase (Figure 6.1.3-16).

- The heat balance indicated that up to 0.02 lb/sec. of steam was condensed in the downcomer.

- The estimated average heat transfer coefficient for 0.02 lb/sec. of steam flow was about 1200 Btu/hr., ft.^{2}, °F, which is consistent with values for condensation of steam. This was a

bounding estimate using the downcomer liquid temperature (TF-147), which is lower than the temperature of the liquid at the interface.

- Matrix Test SB23 (1/2-cold leg break) was the only test in which the oscillation started and stopped. This is also the only test in which the temperature of the downcomer coolant decreased (Figure 6.1.3-17). The downcomer coolant temperatures at which the oscillations started were nearly identical while the coolant temperature was lower during the nonoscillating period. These data support the role of downcomer coolant temperatures and condensation in producing the observed oscillations.

6.1.3.3 Expected Effect in AP600

The oscillations observed in the OSU test facility during IRWST injection may also occur in the AP600. Timing of the initiation and termination of these oscillations may be different in the AP600 and will depend on the following factors:

- Temperature and flow from the IRWST related to the condensation rate of steam flowing to the downcomer compared with the production rate in the core

- Hydraulic flow characteristics of the steam path from the upper head to the downcomer which determine the steam flow rate

- Liquid level in the downcomer relative to the cold leg will determine when the oscillations begin

Since pressure in AP600 and the OSU test facility will be close to atmospheric pressure during IRWST injection, there is no scaling necessary for the condensation process. Assuming that the power and geometric scaling in the OSU test facility accurately model these characteristics of the AP600, there is no scaling necessary for these parameters. Therefore, the magnitude and frequency of the oscillations in the AP600 should be the same as in the OSU test facility (Table 6.1.3-1). The oscillations will not become unstable, since there is a dual feedback that relieves the pressure increase (i.e., increased flow through the ADS-4 lines and increased condensation because of the mixing of the liquid at the condensing interface).

Therefore, the temperature/pressure/flow oscillations that occurred during IRWST injection at the OSU test facility are expected to occur with the same amplitude and frequency in the AP600 during about the same time in a SBLOCA event.

TABLE 6.1.3-1
SUMMARY OF FLOW OSCILLATION DATA FOR MATRIX TESTS SB01 AND SB18

No.	Break Type	Start Time	End Time	IRWST Level, Start (in.)	IRWST Level, End (in.)	Del P, (ave) psi	Del T, (ave)•F	Del Level (ave), in.	Level, Start (in.)	Level, End (in.)	Period (sec.)
									LDP-127		
SB01	2-in. cold-leg	9100	13,000	37.9	22.2	0.5 to 0.6	6 to 8	5 to 6	67.5	65.0	136
SB18	2-in. cold-leg	8830	13,450	40.2	23.0	0.3 to 0.4	2.5 to 9	4.8 to 5	66.4	66.3	110

TABLE 6.1.3-2
OSU TEST ANALYSIS PLOT PACKAGE FOR SECTION 6.1.3

Plot No.	Component	Variables	Units	Description
-1	RV	N/A	N/A	Reactor vessel/flow paths
-2	RV	CLDP-113	in.	Compensated level, reactor vessel upper plenum SB01
-3	RV	CLDP-113	in.	Compensated level, reactor vessel upper plenum SB18
-4	RV	TF-170	°F	Upper plenum temperatures, SB01, SB18
-5	RV	PT-107	psig	Upper head pressure, SB01 and SB18
-6	RV	CLDP-113	in.	Compensated level, reactor vessel upper plenum, SB01 and SB18, expanded time scale
-7	ADS 4 Lines	N/A	N/A	Flow pattern map
-8	ADS 4-2	FVM-602	CFM	Steam flow in ADS-4-2, SB18
-9	ADS 4-2	FVM-602	CFM	Steam flow in ADS-4-2, SB18, expanded scale
-10	RV	RPVASOUT	lb/sec.	SG in core, SB18
-11	RV	RPVASOUT	lb/sec.	Steam production in core, SB18, expanded scale
-12	ADS 4-1	FMM-603	lb/sec.	ADS 4-1 liquid flow from separator, SB18
-13	RV	TF-147	°F	Downcomer temperatures, SB01
-14	RV	TF-120	°F	Reactor upper head temperature, SB01

TABLE 6.1.3-2 (Continued)
OSU TEST ANALYSIS PLOT PACKAGE FOR SECTION 6.1.3

Plot No.	Component	Variables	Units	Description
-15	CMT-2	TF-524 TF-528 TF-540 TF-542 T_{sat} based on PT-502	°F	CMT-2 temperature, SB01
-16	RV	CLDP-13 PT-107	in. psig	Comparison of pressure and level, SB01
-17	RV	TF-147 TF-168	°F	Temperature in downcomer, SB23

THE PLOTS IN TABLE 6.1.3 ARE NOT INCLUDED IN THIS NONPROPRIETARY DOCUMENT

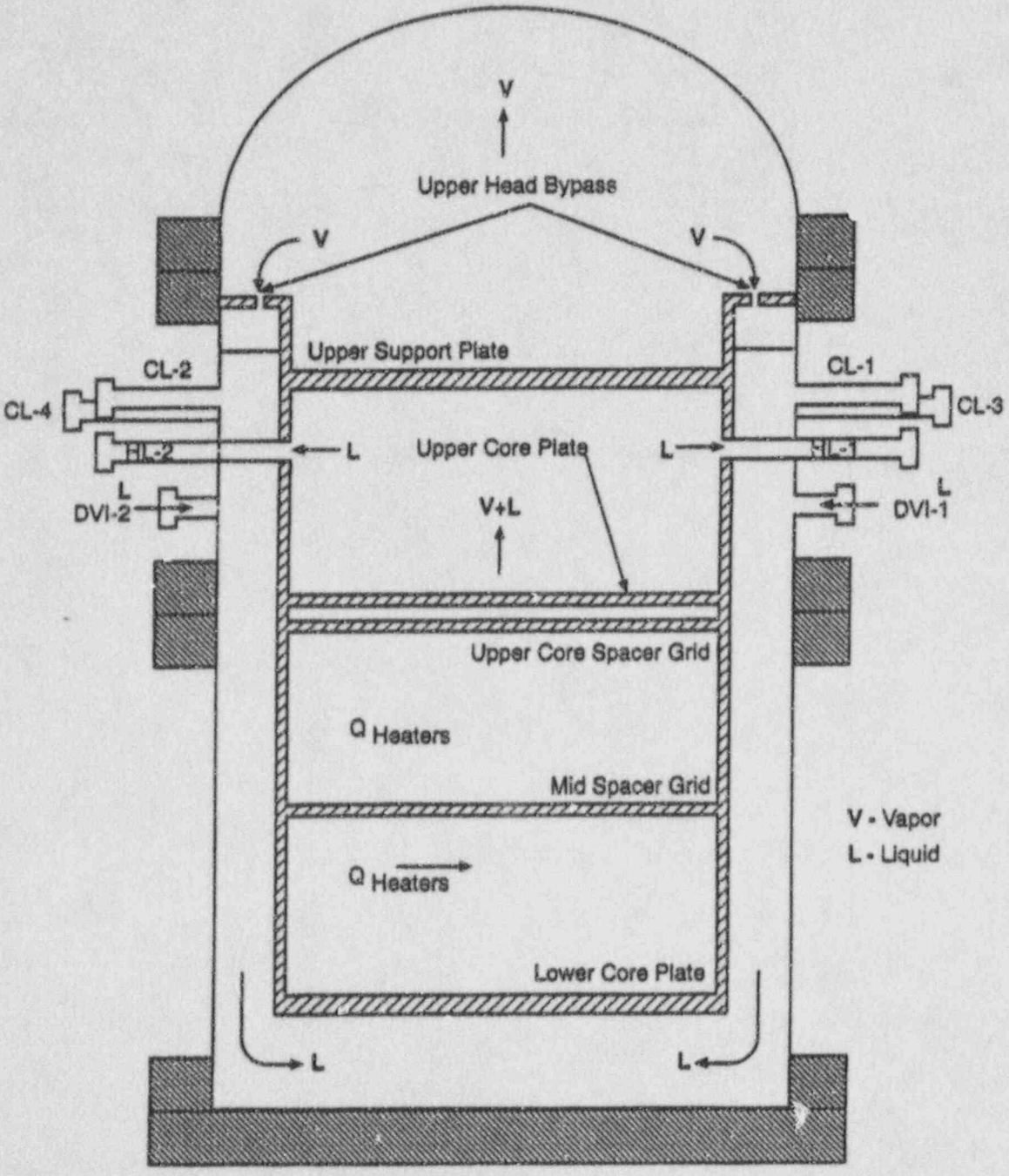

Figure 6.1.3-1 Reactor Flow Paths During IRWST Injection

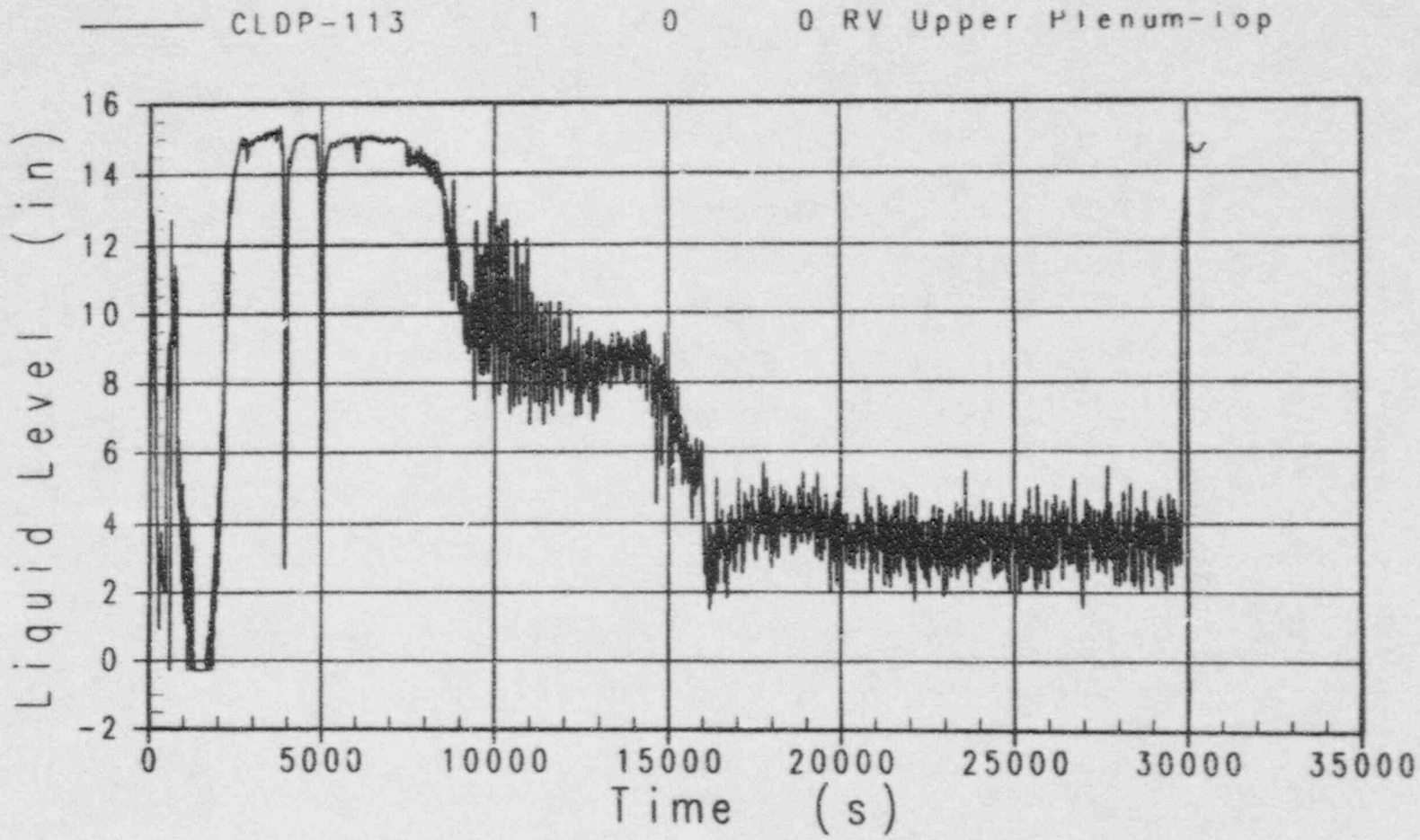

Figure 6.1.3-2 Matrix Test SB01 Upper Plenum Level

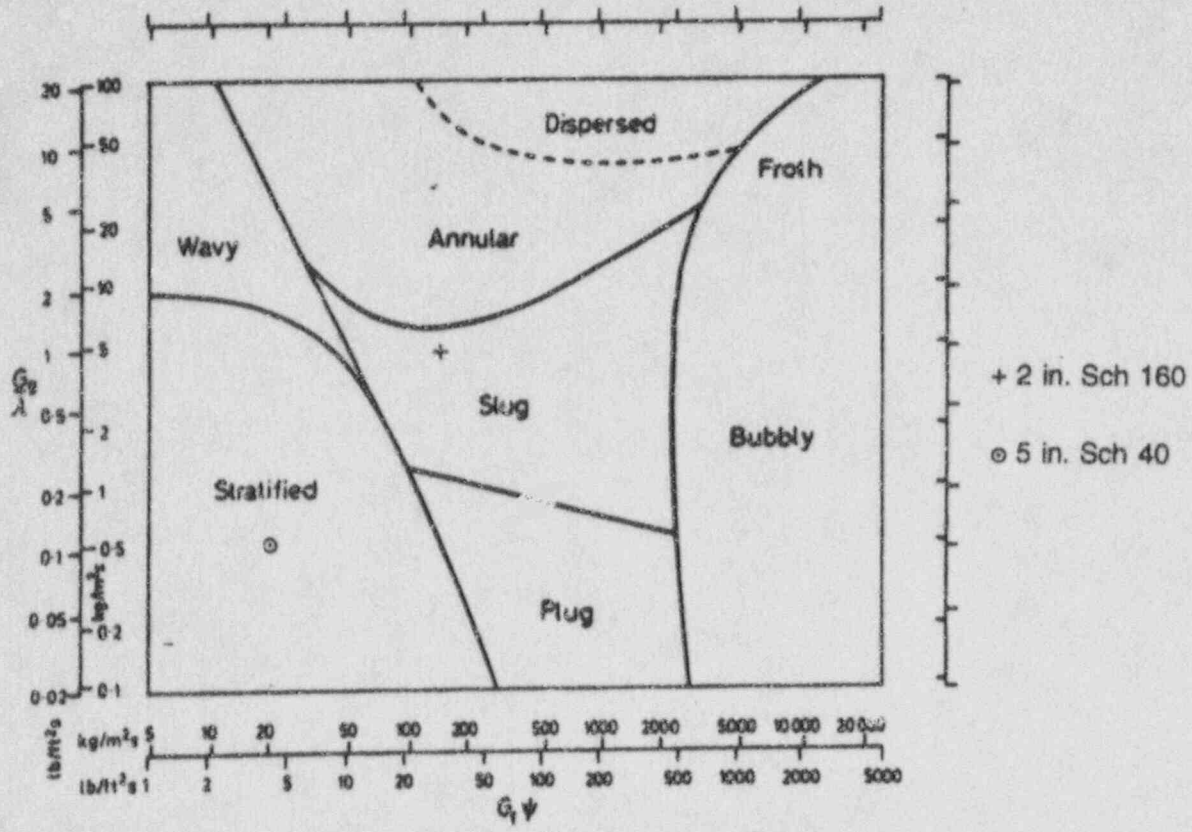

Flow pattern map for horizontal flow (Baker 1954).

Figure 6.1.3-7 Flow Regimes in ADS-4 Lines Matrix Test SB18

Section 7.0 has not been included for this first printing, but it will be added to this report at a later date.

8. REFERENCES

1. Dumsday, C.L., et al, *AP600 Low-Pressure Integral Systems Test at Oregon State University Final Data Report*, WCAP-14252, May 1995.

2. Reyes, J.N., Hochreiter, L.E., Lau, L.K., and A.Y. Lofi, *Low Pressure Integral Systems Test Facility Scaling Report*, WCAP-14270, January 1995.

3. Cunningham J.P., et al., *AP600 SPES-2 Test Analysis Report*, WCAP-14254, May 1995.

4. Kemper, R.M., *Applicability of the NOTRUMP Computer Code to the AP600 SSAR Small-Break LOCA Analysis*, WCAP-14206, November 1994.

5. Hochreiter, L.E., *FLECHT SEASET Program Final Report*, NUREG/CR-4167, EPRI NP-4112, Prepared for the U.S. Nuclear Regulator Commission, November 1985.

6. Modro, S.M., et al., *Evaluation of Scaled Integral Test Facility Concepts for the AP600*, Idaho National Engineering Laboratory, SMM-27-91, Transmitted to U.S. NRC, July 1991.

7. U.S. Nuclear Regulatory Commission, *An Integrated Structure and Scaling Methodology for Severe Accident Technical Issue Resolution*, NUREG-CR-5809, (1991).

8. Taitel, Y. and A.E. Dukler, *A Model for Predicting Flow regime Transitions in Horizontal and Near Horizontal Gas-Liquid Flow*, *AIChE Journal*, Vol. 22, No. 1, pp. 47-54, January 1976.

9. Schwartzbeck, R.K., and G. Kocamustafaogullari, *Similarity Requirements for Two-Phase Flow-Pattern Transitions*, Nuclear Engineering and Design, 116, pp. 135-1457, 1989.

10. Bankoff, S.G., and S.C. Lee, *A Critical Review of Flooding Literature*, NUREG-CR-3060, (1983).

11. Kocamustafaogullari, G. and M. Ishii, *Scaling Criteria for Two-Phase Flow Natural and Forced Convection Loop and Their Application to Conceptual 2x4 Simulation Loop Design*, Argonne National Laboratory, ANL-83-61, NUREG/CR-3420, May 1983.

12. Moskal, Thomas E., *Examination of Scaling Criteria for Nuclear Reactor Thermal-Hydraulic Test Facilities*, Ph.D. Dissertation, Carnegie-Mellon University, Pittsburgh, PA, March 1987.

13. Meyer, P.E., *NOTRUMP, A nodal Transient Small break and General Network Code*, WCAP-10079-P-A, (1985).

14. Cunningham, J. P., et al., *AP600 Core Makeup Tank Test Analysis*, WCAP-14215, December 1994.

15. Baker, O., *Design of Pipe Lines for Simultaneous Flow of Oil and Gas*, Oil and Gas Journal, July 26, 1954.